CONTINUOUS SUGAR BEET PULP PRETREATMENT AND BIOCONVERSION IN A BIOREFINERY CONTEXT

Roberto Chiocchio

A Thesis submitted for the degree of

Engineering Doctorate

To

University College London

The Advanced Centre for Biochemical Engineering

Department of Biochemical Engineering

University College London

Declaration

I, Roberto Chiocchio, confirm that the work presented in this thesis is my own. Where information has been derived from other sources I confirm that this has been indicated in the thesis.

Signature:_____Date:_____

Abstract

Valorisation of agricultural wastes, such as Sugar Beet Pulp (SBP), for production of biofuels and value-added chemicals, has garnered increasing interest in recent years. Through physicochemical means, lignocellulosic material can be pretreated to release monosacharides which can then be upgraded by fermentative and biocatalytic routes. Previous UCL-led research has examined many aspects of utilisation of waste streams from sugar refineries. Vinasse, a glycerol-rich waste product of bioethanol production, was used as a nutrient source for enzyme production. Sugars from SBP, such as D-glucose, L-arabinose and D-galacturonic acid and which make up approximately 25% w/w, 21% w/w, and 20% w/w of the total pulp weight, respectively, were solubilised through operations such as steam explosion pretreatment and depolymerisation of the released polysaccharides. These SBP monosaccharides were then employed in bioconversion reactions using thermostable enzymes.

This Thesis aims to study SBP as a feedstock for the enzymatic production of value added chemicals. It also aims to translate key reactions in the valorisation process from batch mode into a continuous flow process in a scalable, 100 mL, Agitated Cell Reactor (ACR).

Initial Residence Time Distribution characterisation of the ACR showed that it provided excellent plug flow properties, equivalent to 13 stirred reactors in series. The ACR was able to handle SBP slurries over a range of solids loadings (1% w/v – 5% w/v) and residence times (3.8 min – 19.0 min). The SBP suspension was shown to be shear thinning with measured viscosities in the range of 0.0011 Pa.s at 1% w/v and 0.0339 Pa.s at 10% w/v. A set of correlations was developed that enable prediction of the feed viscosity as a function of SBP concentration and shear rate. The SBP particle size distribution ranged from 15.0 µm (D10) to 446 µm (D90) with a median size of 128 µm. Studies on the particle flow through the ACR demonstrated that steady state could be achieved, but that larger particles had longer residence times than smaller particles through the ACR.

Dilute acid pretreatment (DAP) of SBP was investigated as an alternative to previous work on steam explosion as it would be more compatible with continuous operation. DAP using sulfuric acid at concentrations up to 75 mM and 80 °C was performed. These conditions showed good release of polymeric L-arabinose, which increased with higher temperatures and acid concentrations (70% w/w at 75 mM and 80 °C). Cellulose, which is more heat- and acid-resistant than SBP pectin, was only slightly hydrolysed into D-glucose, creating the

potential for selective sugar fractionation. When compared to steam explosion pretreatment, flow DAP in the ACR obtained similar throughputs (3.5 and 3.1 $g_{L\text{-arabinose}}.hr^{-1}$, respectively), but productivity (throughput in terms of reactor volume) was an order of magnitude higher (3.5 and 25.6 $g_{L\text{-arabinose}}.L^{-1}.hr^{-1}$). Monomerisation of the polymeric L-arabinose could be achieved in a continuous flow enzyme-membrane as in previously described work.

Finally, valorisation of the L-arabinose monomers by a continuous-flow, two-step enzymatic process in the ACR was demonstrated. L-gluco-heptulose is a rare ketoheptose which has potential cancer and diabetes treatment applications. The one-pot two-step production of L-gluco-heptulose using a thermostable transaminase (TAm) and transketolase (TK) both isolated from *Deinococcus geothermalis* DSM11300 was also carried out in the ACR. The initial goal was to use immobilized TK and TAm enzymes in order to intensify the bioconversion process. While TK could be successfully immobilized on both Nickel-chelated beads and Epoxymethacrylate resin, the TAm immobilization proved challenging with only low levels of retained activity. Consequently, the flow studies were performed with soluble TK and TAm enzymes. ACR bioconversions compared favourably with well-mixed batch reactions yields using the same reaction time (2 hours). Initial studies demonstrated the conversion of model substrates L-arabinose, L-serine and α-ketoglutaric acid into L-gluco-heptulose. Subsequently it was shown that L-gluco-heptulose could be synthesised equally well using SBP-derived L-arabinose. Concentrations of the intermediate product hydroxypyruvic acid (HPA) and L-gluco-heptulose obtained in continuous mode were 2.62 mM and 0.60 mM, respectively using SBP derived L-arabinose and 1.21 mM and 0.31 mM, respectively, using model solutes. This was equivalent throughputs of 170.5 $\mu M.hr^{-1}$ and 39.0 $\mu M.hr^{-1}$ for the SBP derived L-arabinose and 81.0 $\mu M.hr^{-1}$ and 20.0 $\mu M.hr^{-1}$ for the model solutes. Higher final L-gluco-heptulose concentrations could be obtained by increasing starting L-arabinose concentrations.

The continuous process demonstrated here has clear potential for use within a SBP biorefinery. Future work needs to focus on alternative methods of TAm immobilization to enable process intensification and scale-up to pilot scale in order to demonstrate robust commercial operation.

Impact statement

This work has established a continuous process for the utilisation and valorisation of agricultural waste. This was demonstrated by creating a continuous flow process for the production of pharmaceutically relevant L-gluco-heptulose from pretreated sugar beet pulp. There are several potential benefits arising from this work that may impact academia, industry, the environment and wider society.

From an academic perspective the outcomes of this work will enable future research into scalable, efficient lignocellulosic material pretreatment. They will also facilitate investigation into large scale continuous biocatalytic processes. The results of this work could be written up for publication and dissemination and help the production of teaching material and lectures in the Industrial Biotechnology field.

This research could also benefit the industrial and commercial sectors of society. This work demonstrated the possible applications of a UK-made reactor showcasing its effectiveness and thereby aiding the display of the strengths of the reactor design and engineering sectors. Furthermore, the process studied here could be used by UK-based agricultural operations to turn unutilised or low-value waste streams into valuable product streams, thereby creating wealth and jobs and improving sustainability. The biocatalysis research carried out here could be used as a starting point for the development of similar conversions of other agricultural feedstocks

A further benefit of this research is the potential contribution to the environment and society. Clean, scalable and efficient reactions will reduce the impact of current agricultural and fine chemicals operations. Furthermore, improved production of L-gluco-heptulose could have significant impact in the production of affordable treatments benefiting society.

In conclusion, this research has produced outputs that could benefit academia, industry or the wider society either immediately or in the future. Dissemination of these outputs through conferences, talks and journal papers could accelerate this process.

Acknowledgements

I am not skilled enough to put into words the feelings of gratitude I have for the people who have stood by me (and, at times, pushed from behind!) during this EngD.

I should firstly extend my thanks to my family. To my father and mother, who listened, helped and distracted with food and care packages, I will be forever grateful. To my brother who has always been there for me, and even attended a pilot-plant group meeting I am most thankful. I am indebted to my grandparents who sacrificed so much for the sake of education, and some of them were not able to see me finish this important chapter in my life. I am also grateful to Sarah, without her constant encouragement, spell-checking, and help I would not be writing this today, and more importantly, she made what should be the most stressful and difficult time in a doctorate the most enjoyable.

I am truly indebted to my supervisor, Professor Gary Lye. From the moment I frantically set foot in his office to discuss my Masters' thesis results I knew Gary was a force for good. He has taught me a lot about the value of taking a moment to think. Thanks for the support, the guidance, and the trust.

I am grateful to Dr Max Cardenas-Fernandez for the guidance and help he was always ready to give. My thanks also go out to Dr Michael Sulu, whose help in the fermentation rooms as well as in life were greatly appreciated.

I would like to extend my appreciation to Elaine Briggs, who must have helped me with the ordering a thousand times; and to the professional services team, who were so patient with me.

To the many officemates that I have had over the years, Fer, Asma, Greg, Tom, Billy, Lara, Jaz, Joe, and Fang thank you for providing a little home away from home.

And to the many people I have met during my time in the department, thank you for making this adventure worthwhile!

Table of contents

List of Figures

List of Tables

Abbreviations

Abs504	Absorbance measured at 504 nm
ACR	Agitated Cell Reactor
API	Active Pharmaceutical Ingredient
ATR	Agitated Tube Reactor
BSA	Bovine Serine Albumin
Cf-CCD	centre-faced Central Composite Design
CoGs	Cost of Goods
CSTR	Continuously stirred tank reactors
D10	Size of the particle in the first decile of a size distribution
D50	Median particle size
D90	Size of a particle in the last decile of a size distribution
DAP	Dilute Acid Pretreatment
DO	Dissolved Oxygen
DoE	Design of Experiments
DOT	Dissolved Oxygen Tension
E. coli	Escherichia Coli
ECR	Epoxymethacrylate Resin
H_2SO_4	Sulfuric Acid
HCl	Hydrochloric Acid
HCP	host cell proteins
His-tag	Hexahistidine tag
HP	Heat purification
HPAEC-PAD	High Performance Anion Exchange Chromatography – Pulsed Amperometric Detection
IMAC	Immobilized Metal Affinity Chromatography
IPTG	Isopropyl β-D-1-thiogalactopyranoside
KOH	Potassium Hydroxyde
L-Ara	l-arabinofuranoside
LB	Luria Bertani Broth
LHW	Liquid hot water
Li-HPA	Lithium HydroxyPyruvate
N	Equivalent number of tanks
NaOH	Sodium Hydroxyde
N_H	Number of homogenisation passes
Ni-NTA	Nickel chelated Nitriloacetic acid
OD600 nm	Optical Density measured 600 nm
PFR	Plug Flow Reactor
pI	isoelectric point
PLP	Pyridoxal-5'-phosphate
Pnp	p-nitrophenol
Pnp-l-Ara	para nitrophenyl alpha l-arabinofuranoside
PSD	Particle Size Distribution
Re	Reynolds Number

RTD	Residence Time Distribution
RTR	Rotating Tube Reactor
SBP	Sugar Beet Pulp
SDS-PAGE electrophoresis	Sodium dodecyl sulphate polyacrylamide gel
SEM	Standard Error of the Mean
STR	Stirred tank reactor
TAm	Transaminase
TB	Terrific Broth
TFA	Trifluoroacetic acid
ThDP	Thiaminde Pyrophosphate
TK	Transketolase

1

Introduction and Literature Review

1.1 Introduction

Increasing energy demand and world population, combined with dwindling supplies of cheap petrochemicals, have caused a trend in recent years to make industrial processes more sustainable. The agricultural sector has also been challenged to become more efficient by reducing waste streams. The drive to reduce waste and increase competitiveness of various agricultural operations has led to the appearance of the term Biorefinery. Inspired by refineries that turn fossil fuels into a variety of commercial products; biorefineries take biomass from different renewable sources such as agricultural and forestry wastes and convert it into a range of commodities. Through the use of conventional chemical engineering treatment and separation processes along with novel biochemical and biological routes such as fermentation and biocatalysis a range of products can be made as highlighted in Figure 1.1 (Venkata Mohan *et al.*, 2016).

The large quantities of feed streams handled in various agricultural processes, as well as the large amount of residual biomass waste created, mean that this sector could, in part, help replace the need for petrochemical feedstocks and facilitate the sustainable production of platform chemicals and energy. Additionally, due to the low profit margin of most agricultural products and the reduction of government subsidies, technological advances may provide farmers and businesses with an economic incentive to fully utilise all the chemical diversity present in the biomass they produce. This Thesis explores the potential of sugar beet pulp (SBP), a byproduct of table sugar manufacture, as a renewable feedstock for speciality chemicals production. In particular, it explores the application of biocatalysis and continuous process technologies in order to ensure that the outcomes are environmentally friendly and have high enough productivities to be economically viable.

1.2 Overview of sugar beet and table sugar production

1.2.1 Growing sugar beet

Table sugar, or sucrose (a disaccharide composed of a D-glucose molecule and a D-fructose molecule), is a product derived from two agricultural crops: sugar cane and sugar beet. The former has been used for sugar production for many centuries, particularly in warm climates such as the Caribbean, Brazil, and the southern United States (FAO, 2009).

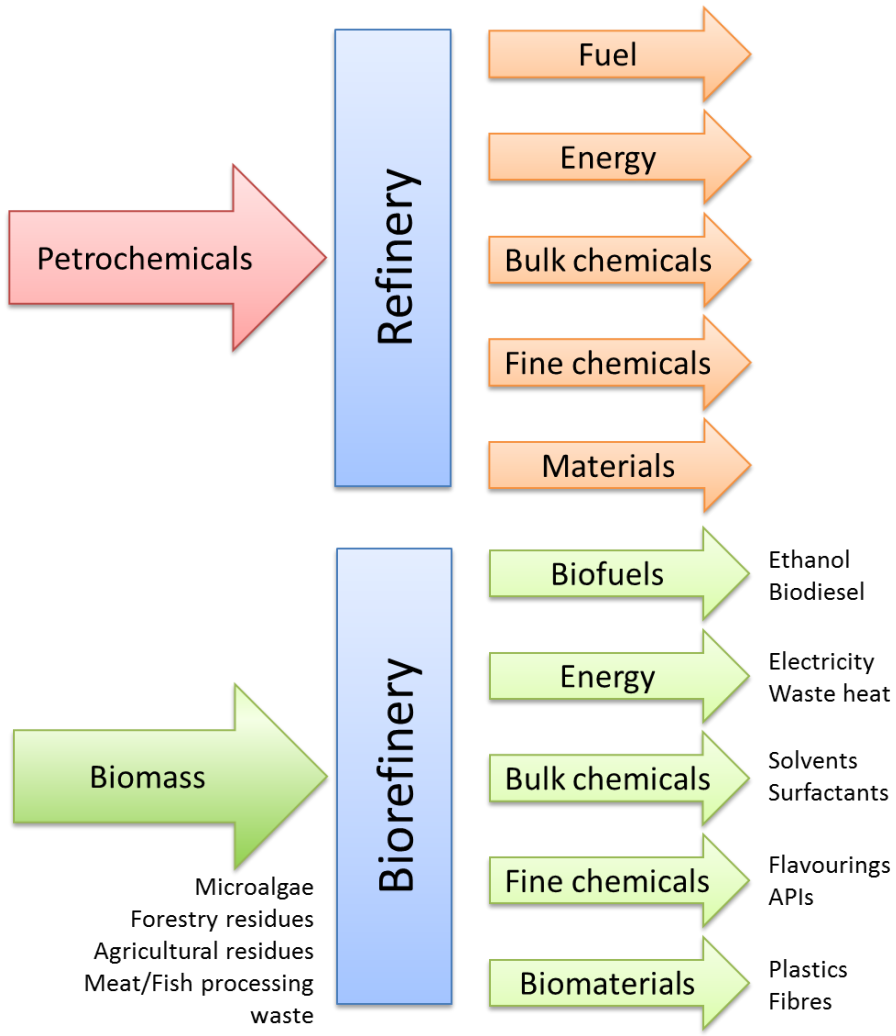

Figure 1.1. Schematic representation of a refinery and a biorefinery. In a biorefinery, different sustainable feedstocks are used to make products with a wide range of applications.

Sugar beet, despite being cultivated by mankind for approximately 2000 years, was not used to produce sugar until the 19th century. *Beta vulgaris*, or sugar beet, is grown in some 50 countries and accounts for approximately a quarter of the world-wide sugar production. Beets are grown mainly in developed countries at temperate climates (Draycott, 2006; FAO, 2009). Some 75% of the world's beet sugar is produced in Europe, and in 2004, 120 million tonnes of beet were processed in the European Union alone. Historically, the countries consuming sugar via this crop would import sugar from tropical colonies where sugar cane was grown. However, agricultural subsidies and incentives to reduce reliance on imported sugar, saw an increase in sugar beet cultivation throughout the 19th and 20th centuries. This, combined with the low profit margins of the final product, has led to a drive for increasing efficiency of the process by utilising waste streams effectively (Draycott, 2006; FAO, 2009; Finkenstadt, 2013).

1.2.2 Sugar beet processing

Sugar beet is generally grown on wet flat land at temperate climates. The plant stores sucrose in the root and then uses it up for growth and the formation of the seeds. To avoid excessive sugar depletion by seed production, plants are typically sown in spring and harvested in autumn. In most sugar beet growing countries, the harvest is done mechanically: a machine cuts the top off the plant and extracts the root from the soil. The tops are usually left in the ground to fertilise the soil in preparation for the next harvest. The beets are either briefly stored near the field in mounds called *clamps*, as shown in Figure 1.2, or transported directly to the sugar refinery (Draycott, 2006).

Figure 1.2 shows a representative flow sheet of an integrated sugar beet biorefinery. At the refinery the sugar beets are first cleaned and separated from any soil and stones that may have been picked up during the harvest. The beets are then sliced into thin strips called *cossettes* and passed through a solid-liquid diffuser. Hot water flows in a counter-current fashion dissolving and extracting the sucrose from the beet. The sugar beet pulp (SBP), made up of the processed *cossettes*, is then pressed to remove excess water that contains sucrose. This water is then re-inserted in the diffuser to increase the sucrose yield. At the end of the diffusion step, a milk of lime is added to the water-sucrose mixture, also called the *raw juice*. This causes some of the impurities such as anions, proteins and pectins to precipitate. Following this, carbon dioxide (CO_2) is bubbled through the raw juice. This causes the calcium hydroxide from the milk of lime to flocculate and precipitate, absorbing and entrapping some

impurities in the process. The flocs are removed in clarifying tanks leaving a solution called *thin juice*. This juice contains the extracted sucrose but is still quite dilute thus requiring further concentration via evaporation and subsequent filtration, yielding a *thick juice*; a viscous solution with approximately 60% w/w sucrose (Duraisam, Salelgn and Berekete, 2017).

At this stage the juice is either processed directly or stored to be processed throughout the year, after the sugar beet campaign has ended. The next step is to crystallise the sucrose present in the juice in vacuum pans. This is achieved by the addition of small sugar crystals that act as the nucleus for sugar crystal formation. The mixture of sugar crystals and liquor is then separated via centrifugation. The liquor, still containing non crystalline sucrose is added to the pans again to continue the reaction. Water is added to the centrifuge to wash the sugar. This wet sugar is then dried using warm air and then placed in storage until it is packaged (FAO, 2009; British Sugar, 2010; Duraisam, Salelgn and Berekete, 2017).

1.2.3 The importance of co-products

The processing of sugar beet is already highly optimised and integrated as shown in Figure 1.2. One ton of sugar beet contains approximately 160 kg of sucrose (16% w/w) and refineries are able to extract approximately 130 kg of refined sugar per ton of sugar beet (>81% w/w yield). High labour costs in developed countries require an efficient utilisation of the refinery's waste streams. This is a way to generate further revenue streams making the plant more competitive (FAO, 2009; Finkenstadt, 2013).

A prime example of this "integrated biorefinery" approach is the Wissington sugar factory near Peterborough, UK. There, sugar is just one of the many products obtained. The soil and stones that are delivered along with the beets are recovered, separated, screened, washed and sold on to garden centres. The pressed SBP is pelleted and often mixed with some of the molasses from the bioethanol unit and sold as animal feed. The flocculated calcium carbonate (the product of the carbonation of milk of lime) is marketed as "LimeX" to farmers to adjust soil alkalinity. The benefit of this is two-fold: plant revenues are increased; and lime extraction from quarries is reduced.

Figure 1.2. Sugar beet storage clamp. Photo credit to Markus Hagenlocher (2005).

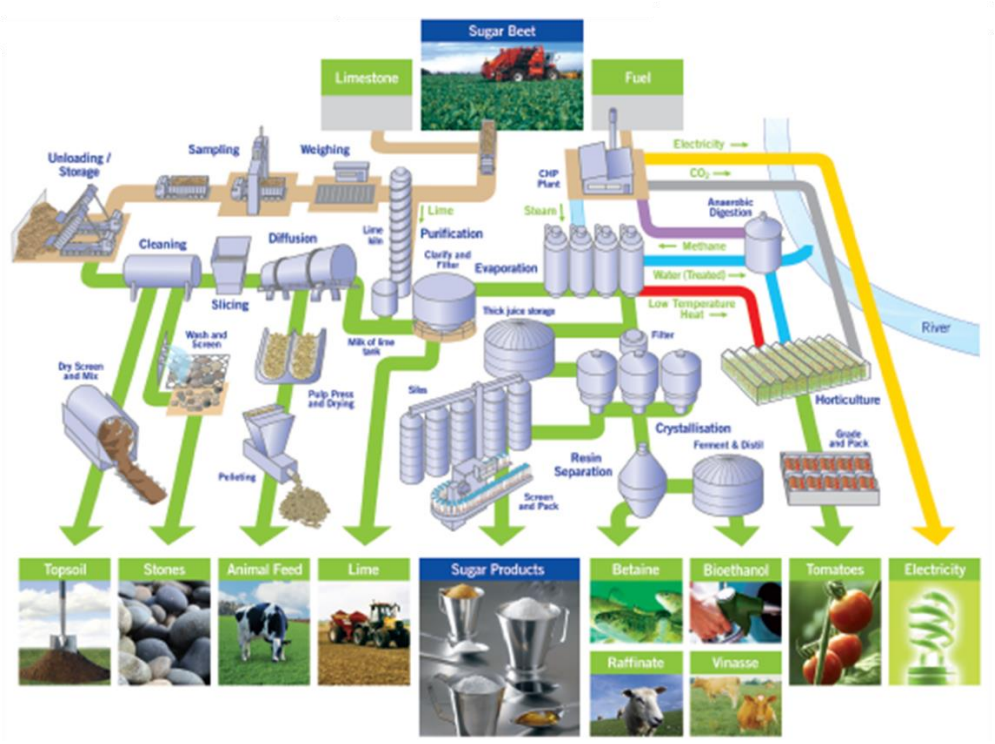

Figure 1.3. Wissington beet sugar refinery plant and process layout. This provides the context for the work presented in this thesis. Image courtesy of British Sugar (British Sugar, 2010)**.**

After the crystallisation step a resin separation step separates the sucrose containing liquor into sugar extract, betaine and raffinate. The sugar extract is used to make bioethanol in what became the United Kingdom's first bioethanol plant, whilst the betaine and raffinate are added to animal feed as they provide useful nutrients. Side-products of the bioethanol production are vinasse, which is sold as a nutrient for farm animals, and CO_2 which is captured, liquefied and sold.

The entirety of the plant requires considerable power and heat. This is obtained via an efficient combined heat and power (CHP) plant. The plant utilises methane gas, a fuel that is naturally abundant in the UK and cleaner than other fossil fuels such as petrol or coal. The plant's heat is used in various processes such as the sucrose concentration stage. The residual low temperature heat is then further used to heat a tomato nursery; this is an 18 hectare glasshouse responsible for the production of some 140 million tomatoes every year. The CO_2 emitted from the CHP plant is also supplied to the tomato nursery. Furthermore, the wastewater from the processes, before being released into the River Wissey, is fed to an anaerobic digester which produces more methane used in the CHP plant. The additional electricity that is not used on the site is sold on and provides energy for some 120,000 people (British Sugar, 2010).

As described above, the complete utilisation of sugar beet is currently possible and can aid in making the whole biorefinery more efficient, generating more revenue streams, whilst simultaneously reducing waste management burdens. However, it can be seen that many of the "new" side-products are low value materials often destined for agricultural use. The materials are composed mainly of organic compounds and could potentially be used to produce higher value products by applying recent advances in synthetic biology and biocatalysis.

A "Sustainable Chemical Feedstocks" project funded by the UK Engineering and Physical Sciences Research Council (EPSRC, EP/K014897/1) focuses on enabling the sustainable, UK-based manufacture of commercially useful chemicals and pharmaceutical intermediates from sugar beet byproducts. The project spans across three universities and a number of industrial partners along the supply chain. The main goal is to use the low value SBP stream as a starting material for production of various value-added chemicals. This can be achieved because SBP consists of approximately 75% w/w cellulose and pectin (Kühnel, Schols and Gruppen, 2011b). Conceptually, the SBP can be treated to firstly separate cellulose and

pectin. These polymers can then be hydrolysed or broken down into the monomeric sugars via addition of acid or alkali or the action of hydrolytic enzymes such as cellulases and pectinases. The individual sugars could then be used in a variety of ways. The D-glucose from cellulose can be used in the production of bioethanol at the existing bioethanol plant, whilst the main sugars from the pectin; L-arabinose and D-galacturonic acid can be used as substrates for biocatalytic upgrading. Any residual material from SBP processing should be compatible with use in the anaerobic digestors. The large mass of starting material (i.e. the beet pulp) also requires that investigation into the production of these chemicals considers technologies that are scalable and their techno-economic evaluation (Cárdenas-Fernández *et al.*, 2017).

1.3 SBP composition, pretreatment and breakdown

1.3.1 Introduction to pretreatment

In recent years, many agricultural waste streams, not just SBP, have been investigated for their potential application as sustainable resources of sugars (Sidiras and Koukios, 2004; Chundawat, Venkatesh and Dale, 2007; Huang *et al.*, 2010; Chen *et al.*, 2013; Han *et al.*, 2013). The advantages of using biomass from agricultural residues are many. First, they are rich in carbohydrates such as sugars, and heteropolymers such as lignin that can be used for the production of fine chemicals such as vanillin (Silva *et al.*, 2009). Secondly, agricultural, or lignocellulosic biomass, is typically available cheaply and in large quantities. Further, these large volumes are, in many cases, already in plants and factories (e.g. corn stover in corn syrup facilities, or sugar beet pulp in sugar refineries), thus reducing logistical problems (Mosier *et al.*, 2005; Cheng, 2010).

Lignocellulosic biomass used in biorefineries is mostly composed of plant cell wall. The main cell wall components are: cellulose; lignin; and hemicellulose. Whilst cellulose is a homopolymer composed of D-glucose, the latter two are heteropolymers. Widely studied sources of biomass for biorefineries such as corn stover, softwoods, wheat and rice straw or sugarcane bagasse, have a structure comprising straight, long cellulose fibres, interwoven with branched fibers of hemicellulose. Lignin, a heteropolymer composed of phenol-like molecules, is present to add strength to the cell wall by crosslinking fibres across the structure. Hemicellulose consists of a sugar backbone with *substitutions,* or other sugars interspersed through the length of the backbone (Ademark *et al.*, 1998). These substitutions can be a location for other sugars to branch off the main. The hemicellulose backbone

composition varies depending on the plant the biomass originates from. Grasses such as corn, wheat, rice and sugarcane are composed of D-xylose unit linked by a β 1,4-glycosidic linkage; meanwhile hemicellulose from softwoods is composed of a galactoglucomannan backbone, which contains β-1,4-linked D-mannopyranose and D-glucopyranose units (Sun and Cheng, 2002).

SBP differs from other biomasses in that its structure is composed of cellulose interwoven with pectin, rather than hemicellulose. Further, the lignin content for SBP (<5%) is lower than grasses and softwood which typically have 10-20% lignin. Unlike materials such as wheat straw and corn stover, SBP contains little D-xylose (<5%, versus 20%-35% reported for wheat straw and corn stover), and its L-arabinose content is higher (20-25% in SBP versus 5-15% in grass crops) (Mosier *et al.*, 2005; Kühnel, Schols and Gruppen, 2011b; Hamley-Bennett, Lye and Leak, 2016). Pectin, the predominant heteropolymer in SBP consists of a D-galacturonic acid backbone. Interspersed within the backbone are L-rhamnose and D-galactose substitutions. Polymeric L-arabinose, or arabinan, branches off from these substitutions forming so-called 'hairy regions' (Oosterveld *et al.*, 2000; Mosier *et al.*, 2005; Kühnel *et al.*, 2010; Li *et al.*, 2018). Lignin, is present in SBP in small amounts, and is involved in the crosslinking of the hemicellulose, pectin and cellulose (Gargulak, Lebo and McNally, 2015). Figure 1.4 shows a representation of the lignocellulosic structure of SBP.

Disruption of the structure of the biomass is therefore needed to allow for further downstream steps, such as enzymatic depolymerisation (Section 1.3.3) and bioconversion (Section 1.4.4). To achieve this, a number of processes, termed "pretreatment steps" are usually required. These processes can change the lignocellulosic structure by physical, chemical or enzymatic means, or a combination of these (Mosier *et al.*, 2005; Cheng, 2010; Zheng *et al.*, 2012, 2014). To choose the best pretreatment strategy, understanding of the various available techniques, as well as properties of the target biomass are important (Mosier, Ladisch and Ladisch, 2002).

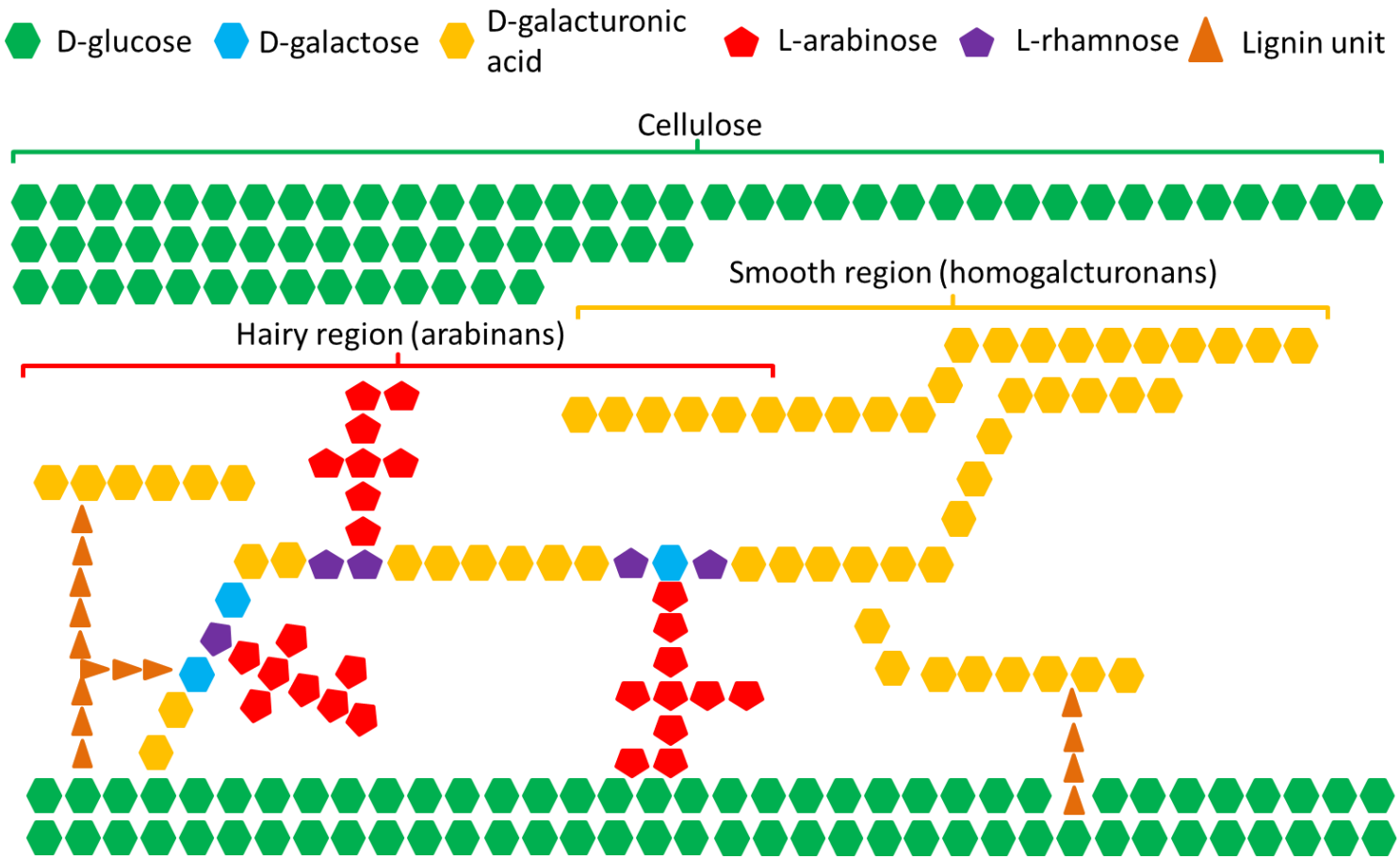

Figure 1.4. Simplified schematic representation of lignocellulosic biomass structure. Long straight cellulose fibres (green) are interwoven with pectin fibres and lignin structure. Pectin consists of hairy branched areas rich in L-arabinose and smooth regions made of repeating D-galacturonic acid units. Figure adapted from Mosier et al. (2015).

Sugar beet cossettes exit the diffuser (Figure 1.2) and are then pressed to remove as much of the sugar-water mixture as possible as described in Section 1.2.2. Despite the pressing process, the SBP has a moisture content of approximately 75-80% (Kühnel, 2011), making incineration an energetically unfavourable option and making transportation costs substantial. Further processing of SBP should therefore be carried out in close proximity to the sugar refinery.

As shown in Figure 1.5, carbohydrates make up approximately 75% w/w of the dry SBP mass and the main sugars present are D-glucose, L-arabinose and D-galacturonic acid. Furthermore, SBP has a comparatively low lignin content (~2% w/w) with respect to other lignocellulosic materials (e.g. wheat straw has 18% w/w lignin), making it an interesting biomass to study for valorisation (Kühnel, Schols and Gruppen, 2011b).

Pressed SBP cossettes are less than 2 cm in length and only a few millimetres in diameter as shown in Figure 1.5. This small size, due to the processing requirements for sugar production, is also advantageous for pretreatment steps: these small "chips" may be used directly in some applications without further size reduction, or, if size reduction is required, grinding or milling can be achieved more cheaply. Indeed, milling cellulose to 1 mm can account for up to 33% of the total electricity needs for ethanol production with some feedstocks (Hinman *et al.*, 1992).

1.3.2 Physicochemical pretreatment

A wide range of physicochemical pretreatment options are available (Mes-Hartree, Dale and Craig, 1988). Here some promising techniques that may be, or already have been, applied to the processing of SBP are discussed. Aspects to note for the pretreatment of any biomass, are cost-effectiveness, energy efficiency, and generation of further waste streams (e.g. organic solvents used). A further point of note is the final application of the sugars released during pretreatment. Often sugars are used in fermentation or biotransformation reactions. Some pretreatment conditions may cause side reactions or degradation reactions to occur, resulting in the production of inhibitory compounds which may slow cell growth rate or hinder enzymatic activity (Mosier *et al.*, 2005; Zheng *et al.*, 2014). A summary of some of SBP pretreatment studies is provided in Table 1.1 and major advantages and disadvantages of the pretreatment options explored is given in Figure 1.7.

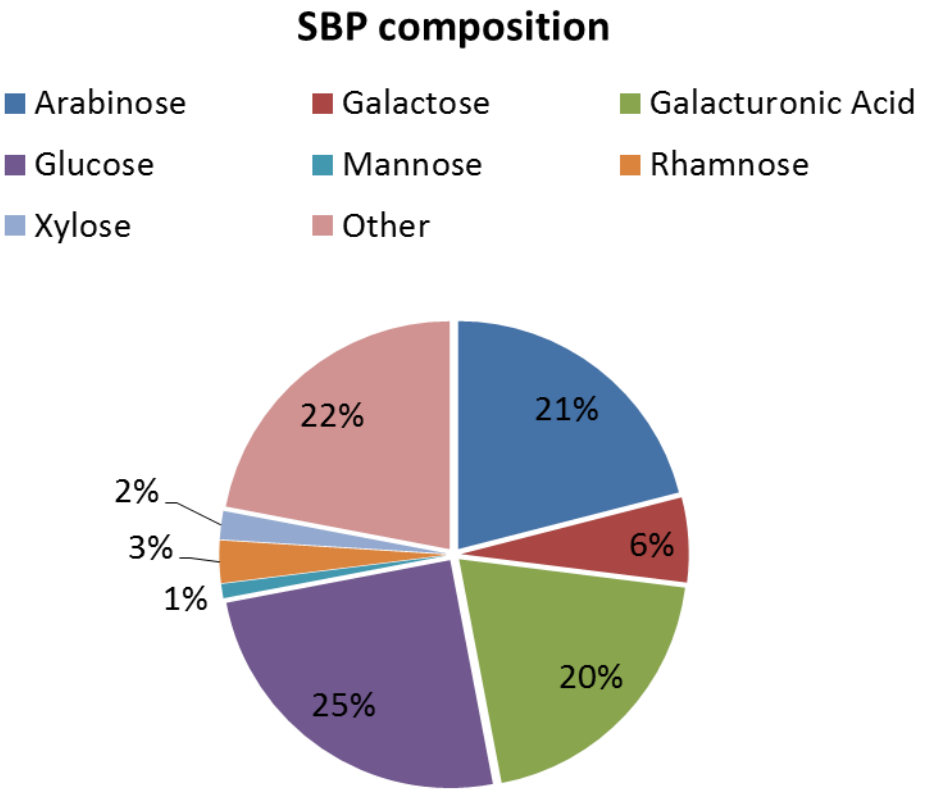

Figure 1.5. Composition of sugar beet pulp. D-glucose present is both from cellulose and residual sucrose (~3.0% w/w). Compositions obtained from Hamley-Bennet et al. (2016) on the same batch of SBP as used in this work.

Figure 1.6. Photograph of different forms of SBP. From left to right: wet SBP from diffuser; dried SBP; coarsely ground dry SBP to >0.5 mm; and milled SBP to < 0.5 mm. Scale bar is 1 cm.

Table 1.1. Comparison of selected SBP pretreatment options reported in the literature.

Pretreatment method	Details	Pretreatment goal	Outcome/yield (% w/w)	Comment	Reference
Steam Explosion	5 bar 24 min 150 °C – 180 °C	Arabinose and D-galacturonic acid release	90% L-arabinose 44% D-galacturonic acid 5% D-glucose	Mostly oligo and polymeric sugars	Hamley-Bennett et al. (2016)
Liquid Hot Water	120 °C – 200 °C 20 min	Pretreatment Methane fermentation	Complete solubilisation of L-arabinose and D-galacturonic acid at 200 °C	At higher temperatures considerable increase of acids and aldehydes in soluble fraction	Zieminski et al. (2014)
Dilute Acid Pretreatment	120-170 °C 1%w/w_{SBP} H_2SO_4 15 min	Release of all sugars	60% of total carbohydrates released	Mostly L-arabinose and D-galacturonic acid	Kuhnel et al. (2011)
Dilute Acid Pretreatment	160 °C to 190 °C 0 to 50 min	Multipurpose use of sugars	33.6% of all carbohydrates extracted 4.6 fold increase in D-glucose after enzymatic digestion	Higher temperatures led to more monosaccharide production	Kharina et al. (2016)
Ammonia Fibre Explosion	80 °C and 5 min 50%-100% ammonia:SBP ratio	Pretreatment for enzymatic hydrolysis	3.5 times more sugar released than untreated SBP	Microscopy revealed noticeably more disrupted SBP structure	Foster et al. (2001)
Enzymatic Digestion	Commercial pectinase mix 50 °C – whole SBP	Pectic sugar release	79% D-galacturonic acid 82% L-arabinose 17% Cellulose solubilisation	Sugars were in large part oligo- and polymeric Long reaction times (>24 hrs)	Leijdekkers et al. (2013)
Enzymatic Depolymerisation	Free and immobilized AraF	Depolymerisation of arabinans	92% L-arabinose recovery	Little depolymerisation of D-galacturonic acid	Cardenas Fernandez et al. (2018)

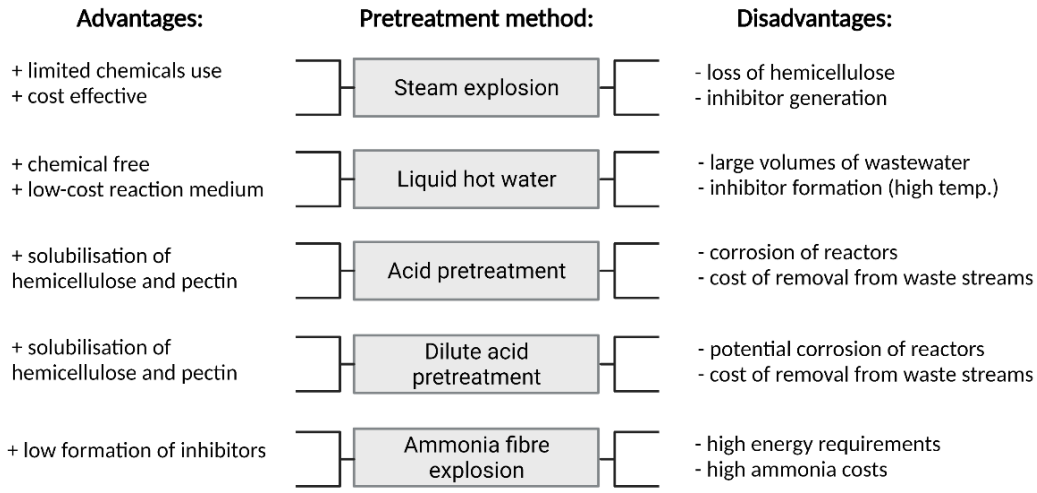

Figure 1.7. Pretreatment method and related advantages and disadvantages in the context of SBP valorisation. References found in text in Section 1.3. Figure made using biorender.com

1.3.2.1 Steam explosion

Steam explosion, also called autohydrolysis, is a process whereby biomass is placed in a vessel, and steam is then added added to the reactor to increase both temperature and pressure. After a predetermined holding period, the steam and pressure are suddenly released, causing an explosive decompression. The conditions inside the reactor lead to hemicellulose and pectin hydrolysis and lignin degradation. In turn, this separates the insoluble cellulose from hemicellulose and pectin and allows the cellulose to be more readily accessible for hydrolysis under the mildly acidic conditions created (Sun and Cheng, 2002; Mosier *et al.*, 2005; Zheng *et al.*, 2014). A further option is to add a catalyst to the system: typically, an acid or a base such as H_2SO_4 or NaOH. The catalyst is employed to increase hydrolysis and separation from cellulose as well as reducing the formation of side products, that may have inhibitory effects in later stages, especially in fermentations (Morjanoff and Gray, 1987).

At present, steam explosion is seen as one of the most cost-effective pretreatment options, with lower energy requirements than milling to increase surface area (Holtzapple, Humphrey and Taylor, 1989) and with some operations being carried out at pilot and even commercial scale (Hooper and Li, 1996; Schumacher *et al.*, 2010). Furthermore, although it was originally conceived as a batch process, equipment designs have been proposed for continuous operation. Scalable technologies able to handle large volumes are required and continuous operation can show some advantages when compared to a batch process (Fang, Deng and Zhang, 2011).

A commonly cited disadvantage of steam explosion is that when washing the treated biomass, some of the hydrolysed hemicellulose sugars are lost (Zheng *et al.*, 2014). This is only an issue if the sugars obtained are to be used in fermentative processes or subsequent catalytic upgrading. If, on the other hand, a fractionation between hemicellulose and pectin sugars, and D-glucose from cellulose is desired, steam explosion can be quite efficient: the cellulose will be found in a solid state, whilst other lignocellulosic components will be found in the aqueous phase, as a mixture of soluble polymers and monomers, ready for further processing (Hamley-Bennett, Lye and Leak, 2016).

Within the Sustainable Chemical Feedstocks group, Hamley-Bennet et al. (2016) have worked with the steam pretreatment of SBP. This has proven effective in separating cellulose, which

can then be hydrolysed for bioethanol production by yeast fermentation, from the SBP pectin. The steam pretreatment variables were also optimised to maximise the amount of oligomeric and monomeric L-arabinose released in the aqueous phase. Under the optimised conditions of 5 bar pressure and 24 minutes holding time, 90% w/w and 44% w/w of the available L-arabinose and D-galacturonic acid were solubilised in both monomeric and polymeric form. Meanwhile only 5% of the D-glucose was found in the aqueous phase. The low D-galacturonic acid yield is attributed to its degradation into other molecules (Bornik and Kroh, 2013; Hamley-Bennett, Lye and Leak, 2016). Additionally, it was found that the addition of H_2SO_4 as a catalyst yielded a higher proportion of monomeric L-arabinose, but lower overall yields (Hamley-Bennett, Lye and Leak, 2016). Moreover, the addition of acid for prolonged periods can lead to formation of inhibitory compounds such as furfural (Kühnel, Schols and Gruppen, 2011b).

1.3.2.2 Liquid Hot Water

Despite the many names it has been called (hydrothermolysis, aqueous fractionation, uncatalysed solvolysis, and aquasolv (Bouchard *et al.*, 1991; Mok and Antal, 1992; Allen *et al.*, 1996) Liquid Hot Water (LHW) pretreatment is a simple process. In essence, the biomass is 'cooked' at high temperatures and pressures, thereby solubilising hemicellulose and lignin (Bobleter, Niesner and Röhr, 1976; Mosier *et al.*, 2005; Brandon *et al.*, 2008; Zheng *et al.*, 2014). LHW pretreatment has been used at scale for the production of ethanol from corn (Weil et al. 1998) and because it does not require prior size reduction it has demonstrated interesting commercial potential (Weil *et al.*, 1997). Its simple mechanism allows for various types of operation, mainly co-current, counter-current and flow-through modes depending on the reactor design (Mosier *et al.*, 2005).

At high temperatures the pK_a of water changes leading to a decrease in solution pH. At 200 °C, the pH of water is 5.0. This acidity, alongside the higher temperatures, leads to the breakdown of some of the hemiacetal linkages in the hemicellulose, thus freeing acids which in turn further hydrolyse the biomass (Weil, Brewer, *et al.*, 1998; Mosier *et al.*, 2005). Similarly to steam explosion, prolonged holding at high temperature can lead to the degradation of sugars such as D-xylose into fermentation inhibitors such as furfural (Palmqvist and Hahn-Hägerdal, 2000).

A number of studies have investigated LHW pretreatment as a potential option for SBP pretreatment. The aim of these studies was to prepare the biomass for methane production

(Ziemiński *et al.*, 2014), for bioethanol production (Kühnel, Schols and Gruppen, 2011b) or for the release of pectin compounds (Martínez *et al.*, 2010). It was found that LHW pretreatment yielded good results with L-arabinose and D-galacturonic acid being increasingly released in the aqueous phase with higher temperature, though Zieminski et al. (2014) noticed a drop in their yields at the highest reaction temperature (200 °C). The insoluble, polymeric, forms of D-galacturonic acid and L-arabinose, galacturonate and arabinan, respectively, were found to be increasingly hydrolysed and more soluble with higher temperature treatments (Martínez *et al.*, 2010; Kühnel, Schols and Gruppen, 2011a). Additionally, it was also found that higher temperatures led to substantial decrease in the final pH of the pretreated slurry: at 120 °C the pH was 5.01 and at 200 °C the pH was 3.20. This drop was attributed to higher levels of organic acids formed during lignin, hemicellulose and pectin degradation (Ziemiński *et al.*, 2014). This finding can be important as subsequent steps, such as enzymatic digestion or bioconversion (Section 1.3.4 and Section 1.4), may require specific pH conditions. As such, slurry pH may need adjustment via the addition of alkali/acid, which could impact on overall process cost and sustainability.

1.3.2.3 Acid pretreatment

Acid pretreatment involves the utilisation of an acid to disrupt the lignocellulosic structure. Pretreatment typically requires either concentrated acid at low temperatures (30-70% by volume and ~40 °C) or lower concentrations and higher temperatures (<2% by volume with temperatures often >120 °C) (Zheng *et al.*, 2014). Dilute acid pretreatment (DAP) has primarily been studied in batch mode with low temperatures (<160 °C), but high solids loading (10-40% w/w); or in continuous mode, in a flow-through reactor, with lower solids loading and higher temperatures (5-10% w/w and temperatures >160 °C) (Cahela, Lee and Chambers, 1983; Esteghlalian *et al.*, 1997; Sun and Cheng, 2002). Although H_2SO_4 is the most commonly used acid, pretreatment can be carried out with a number of different reagents: nitric acid (Brink, 1993, 1994), hydrochloric acid (Israilides, Grant and Han, 1978; Kühnel, Schols and Gruppen, 2011a), phosophoric acid (Israilides, Grant and Han, 1978) and organic acids such as acetic and maleic acid (Zheng *et al.*, 2014) have all been used.

Commercially, mild acid treatment has been used for the production of furfural from hemicellulose, using H_2SO_4 (Mosier *et al.*, 2005). Nonetheless, as a pretreatment option, acid hydrolysis poses issues such as the cost of removing acid from waste streams, and also requires expensive reactors designed to withstand corrosion. Furthermore, this treatment

appears to be more expensive than steam explosion and requires a pH neutralisation step prior to both fermentation or enzymatic digestion (Sun and Cheng, 2002; Mosier *et al.*, 2005; Zheng *et al.*, 2014).

A number of studies have shown the effectiveness of DAP on SBP. Kűhnel et al. (2011) analysed the effect of H_2SO_4 on the release of D-glucose and pectic sugars. It was found that at high temperatures more product was lost to the formation of volatile compounds and Maillard-type reactions. The majority of the D-glucose remained in the solid form, whilst most of the arabinan was degraded into L-arabinose oligo- and monomers (Kühnel, Schols and Gruppen, 2011b). Pectin side chains such as arabinan have been shown to absorb cellulose *in vitro* and therefore their removal could greatly increase enzymatic digestibility of the cellulose (Zykwinska, Ralet and Garnier, 2005). Zheng and colleagues (2013) worked with similar temperatures as Kűhnel's group (120-160 °C) and found similar results: they achieved up to 94% of pectin hydrolysis, yet the harshest conditions did not yield the most favourable results due to byproduct formation, e.g. furfural (Zheng *et al.*, 2013). Illanes' work, on the other hand, involved mild acid hydrolysis and investigation of both HCl and H_2SO_4, but at lower temperatures (<80 °C). The group's aim was to isolate hemicellulose and pectin sugar for pentose fermentations. They found that with higher temperatures more of these pentoses were released; however, more cellulose was hydrolysed leading to a less pure pectic fraction. They also found that higher solid loading for the same condition yielded relatively more solid removal but also more cellulose release. Thus, if cellulose and hemicellulose were required to be separated, a trade-off between higher yields and lower D-glucose carryover is required (Illanes and Nufiez, 1994).

1.3.2.4 ORGANOSOLV

ORGANOSOLV is a process developed in the 1960's as an alternative to the Kraft pulping process to convert lignocellulosic material into paper (Johansson et al. 1987). This process uses an organic solvent in an aqueous solution to de-lignify cellulose. The lignocellulosic material is typically processed at relatively high temperature and pressures (100 °C-200 °C and 1-3 atm) to yield a two phase system: the majority of the cellulose is present as a pulp, whilst the lignin and the depolymerised hemicellulose monomer and oligomers are present in a solution (Johansson, Aaltonen and Ylinen, 1987; Wildschut *et al.*, 2013). The lignin is then precipitated by removal of the solvent (lignin is not soluble in water). Despite the easy separation of lignin and cellulose, the cellulose pulp is often not of sufficient quality for paper

making. Furthermore, yields from the Kraft process benefit from over 100 years of optimisation and switching pulping method is seen as difficult despite the benefits of improved separation and reduced pollutant discharge.

Recently the ORGANOSOLV process has been considered for use in biorefineries: the easy separation of the various biomass components as well as the breakdown of lignin for further use can be advantageous in exploiting agricultural waste (Johansson, Aaltonen and Ylinen, 1987; Sidiras and Koukios, 2004; Ferrer *et al.*, 2013; Wildschut *et al.*, 2013; Snelders *et al.*, 2014). After the ORGANOSOLV pretreatment, the pulp would have to be separated from the liquor via filtration. This cellulose pulp could then be washed until an appropriate pH is reached for fermentation or other applications. The acids can be extracted from the liquor via vacuum evaporation and the lignin can be removed by precipitating it via water addition followed by filtration. Further, the hemicellulose rich fraction can be concentrated by vacuum evaporation and de-acidified steam stripping (Snelders *et al.*, 2014). This can result in an easily fractionated lignocellulosic material that would allow for complete feedstock utilisation.

The low lignin content of SBP when compared to other biomass sources could mean that lower temperatures are required. This is in line with findings that suggest that good pulp (i.e. cellulose) yields are obtained at lower temperature (Sidiras and Koukios, 2004). ORGANOSOLV treatment has also been carried out with formic and acetic acid. These solvents operate at lower temperatures (90- 130 °C) (Johansson, Aaltonen and Ylinen, 1987; Snelders *et al.*, 2014); furthermore these acids could favour the hydrolysis of pectin, thus removing the need for further enzymatic pectin breakdown.

1.3.2.5 Ammonia fibre explosion

Similarly to steam explosion, Ammonia fibre explosion (AFEX) involves high temperatures and the pressurisation of biomass, followed by sudden decompression. Instead of using water and steam, AFEX employs liquid ammonia. Temperatures of approximately 90 °C and residence times of approximately 30 minutes per batch are used. Typical ammonia loading ranges are 0.5-2 $kg_{Ammonia}.kg^{-1}_{Dry\ Biomass}$ (Holtzapple *et al.*, 1991; Sun and Cheng, 2002). AFEX achieves less hemicellulose solubilisation compared to acid hydrolysis (Vlasenko *et al.*, 1997) and is not very effective for materials with high lignin contents (Sun and Cheng, 2002). However, ammonia pretreatment does not produce inhibitors, which eliminates the need for a wash stage before fermentations or enzymatic digestion and does not require small

particle size, reducing the need for energy intensive milling (Holtzapple *et al.*, 1991; Sun and Cheng, 2002).

Foster et al. (2001) studied enzymatic digestibility of SBP after AFEX treatment. Scanning electron microscopy showed noticeable changes in the structure after ammonia treatment. With higher ammonia loads a decrease in hemicellulose and pectin and an increase in lignin was observed. Digestion with cellulase and cellobiase enzymes showed that pretreatment led to increased release in sugars. However, when digestion was carried out with hemicellulases, pectinases and polygalacturonases, ammonia pretreatment showed no increase in sugar yields. This finding gives further credit to the hypothesis, demonstrated *in vitro*, that pectin binds to cellulose (Foster, Dale and Doran-Peterson, 2001; Zykwinska, Ralet and Garnier, 2005).

1.3.3 Enzymatic digestion

Different sugar polymers can be broken into their constituent monomeric sugars through enzymes. D-glucose homopolymer, starch, requires alpha and beta-amylases (Visuri and Klibanov, 1986), whilst cellulose is hydrolysed via different types of cellulases typically obtained from fungi. Exocellulase attack the outer glycosidic bonds of cellulose yielding di-, tri- or tetramer hydrolysis products, endocellulases randomly cleave internal bonds and cellobiases hydrolyses oligomers to yield D-glucose (Cheng, 2010). Heteropolymers, such as hemicellulose and pectin, often require specific enzymatic activities to hydrolyse the various types of bonds and different types of sugars (Ademark *et al.*, 1998). Furthermore, the higher level of branching in these polymers means that they are more susceptible to thermal degradation (Zheng *et al.*, 2014).

The potential for enzymatic hydrolysis of hemicellulose and pectin was shown by Lejdekkers et al. (2013) who carried out hydrolysis at the kilogram scale. Foster et al. (2001) added a mix of polygalacturonases and hemicellulases to a cellulose digestion step and obtained similar sugar yields as an AFEX pretreatment (Foster, Dale and Doran-Peterson, 2001). Not only does the hydrolysis of pectin and hemicellulose free the cellulose for further digestion but it also shows that if specific enzymes were added in series, specific hydrolysates could be removed, before hydrolysis of other sugars. Kűhnel et al. (2010) used arabinases (an endoarabinase, an exoarabinase and two arabinofuranosidases) obtained from the fungus *Chrysosporium lucknowense*. The hydrolysis process yielded oligomers of various lengths, both branched

and linear; however, the addition of arabinofuranosidase led to a decrease in the total number of branched arabinan oligomers (Kühnel *et al.*, 2010).

1.3.4 Monomerization by enzymatic hydrolysis

Due to the approximately similar D-glucose, L-arabinose and D-galacturonic acid contents in SBP (Figure 1.4), rather than obtaining complete hydrolysis of all sugars simultaneously, studies have focused on sequentially fractionating the pulp to fully utilise each individual sugar (Spagnuolo *et al.*, 1999; Martínez *et al.*, 2010; Leijdekkers *et al.*, 2013) . Spagnuolo et al. (1999) studied the effect of two arabinases: an arabinofuranosidase (AraF, E.C.3.2.1.55) and an endoarabinase (E.C.3.2.1.99) on deproteinated SBP. Their process involved an optional thermal treatment (autoclaving of the samples), followed by either DAP (Section 1.3.2.3) or an enzymatic hydrolysis. A filtration step was used to remove the cellulose fraction and the pectic, non-hydrolysed substance was then precipitated by addition of acetone which reduced the solubility of large polysaccharides. Similarly to previous work, they found that the two enzymes, combined, worked better synergistically than on their own. The most effective conditions for arabinan hydrolysis were found to be the two arabinases, combined with a thermal treatment. These conditions also gave the highest pectic substance (e.g. D-galacturonic acid) yield, suggesting that arabinan hydrolysation favours solubilisation of pectin (Spagnuolo *et al.*, 1997).

The Spagnuolo group carried out the reaction into a semi-continuous mode by adding an ultrafiltration step after enzymatic digestion to separate the oligomer fraction and retain the enzymes for further use. They demonstrated enzymatic stability even after a number of reiterations and potential applications of the system in a continuous process (Spagnuolo *et al.*, 1999). Similar work was carried out by the Sustainable Chemical Feedstocks group. Using only a thermostable AraF, a continuous membrane reactor that selectively depolymerised arabinans was set up. Larger oligomers and other sugars from steam exploded SBP were retained, whilst monomeric L-arabinose was filtered through. To increase enzyme retention, AraF was immobilized on an epoxy methacrylate resin. Furthermore, a decolourisation step was implemented as some compounds in the steam exploded SBP caused rapid fouling and deterioration in the performance of the immobilized enzyme (Hamley-Bennett, Lye and Leak, 2016; Cárdenas-Fernández *et al.*, 2018).

1.3.5 Hydrolysate separation

Despite the good fractionation shown in many of the above studies, each individual fraction is bound to have undesired sugar carry-over. If subsequent applications demand pure, or largely pure, sugar solutions then a purification step is required to separate the different soluble sugar moieties. However, monomeric sugars are typically similar in size and therefore, size-based separation techniques such as filtration and size-exclusion chromatography cannot be used.

Sugars may, however, be separated via strong cation exchange chromatography (Saari *et al.*, 2010). Commercially, the use of simulated moving bed chromatography technologies is employed. This type of chromatography allows for continuous, cost efficient separation, and is used in a variety of applications, e.g. for the separation of fructose from sucrose, in the production of high fructose corn syrup (Azevedo and Rodrigues, 2001; Aniceto and Silva, 2014).

Liquid-liquid separation of sugars is more challenging as sugars are very hydrophilic and miscible in water. However, within the Sustainable Chemical Feedstocks group, Ward et al. (2017) was able to use centrifugal partition chromatography to separate a synthetic mix of monomeric L-arabinose (41%), D-galacturonic acid (41%), L-rhamnose (5%) and D-galactose (11%) into three fractions: an early elution containing L-rhamnose; a middle elution composed of L-arabinose and D-galactose; and a late elution containing D-galacturonic acid. This work was performed using a phase system comprising of ethanol and aqueous ammonium sulfate to separate the sugars in three fractions containing 92% pure L-rhamonose, 84% pure L-arabinose (in presence of D-galactose) and 96% pure D-galacturonic acid. The possibility of producing relatively pure streams of sugars could enable a wider scope of applications from pretreated material (Ward *et al.*, 2015, 2017).

1.4 Biocatalysis

1.4.1 Overview

After the initial pretreatment and possible depolymerisation of lignocellulosic waste (Section 1.3), the released sugars can be catalytically upgraded into higher value compounds. Although some reactions, such as the production of vanillin from lignin, are purely chemical (Silva *et al.*, 2009; Gargulak, Lebo and McNally, 2015), most catalytic upgrading reactions utilising sugars in the literature involve biocatalysis. Commercially, the use of enzymes can offer some advantages over traditional chemical catalysts, making biocatalysis an interesting and growing research area (Turner, 2012). Typically, enzymes will offer fast reaction rates and high selectivity for specific substrates. Biocatalytic reactions also tend to occur at mild temperature and pH conditions. This reduces energy requirements and waste stream generation (Bommarius and Riebel-Bommarius, 2004; Alberts *et al.*, 2012). On the other hand, despite continued progress, substrate specificity and availability of enzymes can limit their application. Space-time yields tend to be low because of the low product concentration often obtained. Although progress has been made it is still difficult to carry out biocatalytic reactions in some desired conditions (for example with presence of certain solvents) (Schmid *et al.*, 2001). Additionally, development cycles are still quite long making investments in biocatalysis more uncertain (Zaks, 2001; Bommarius and Riebel-Bommarius, 2004). This section considers the application of enzymes to convert sugars derived from SBP to valuable chemical feedstocks.

1.4.2 Types of Biocatalysis

Commercial application of biocatalytic reactions can be separated into four different categories (Bommarius and Riebel-Bommarius, 2004):

1. Enzyme catalysis. Product formation is catalysed by (crude) enzymatic extracts or partially purified enzymes. Use of completely pure enzymes is rare and typically only used in production of high value, fine chemicals.
2. Biotransformation. A substrate is transformed into product with enzymes or resting cells.

3. Fermentation. Whole living cells take up one or more carbon sources (e.g. sugar, starch, methanol etc) to use as nutrients, and transform them into target products. Alcohol brewing, the oldest known biocatalytic reaction belongs to this category.
4. Precursor fermentation. Living cells use a defined substrate and transform it to a product.

To choose the most suitable reaction type for a particular application, factors such as cost of immobilization, complexity of the final product stability and cost of the catalyst, and type of substrate and cofactor have to be considered. Table 1.2 shows some commercial products of biocatalytic reactions and their production scale.

1.4.3 Fine chemical production

Products of the chemical industry can, broadly speaking, be divided into three categories: commodity chemical, fine chemicals and specialty chemicals (Pollack 2012). Commodity chemicals are those chemicals that are produced in very large quantities and at low price. Petrochemicals and plastic precursors such as ethylene and propylene are typical examples. Fine chemicals on the other hand are typically more expensive (sold at more than 10 $\$.kg^{-1}$ instead of less than $1\$.kg^{-1}$) and produced in lower volumes (less than 1000 tonnes). Active pharmaceutical ingredients (APIs), vitamins and amino acids are examples of fine chemicals. These definitions are rather arbitrary and not always true. Salicylic acid, one of the most sold fine chemicals, is sold at less than 10 $\$.kg^{-1}$ and more than 10 000 tonnes are produced each year. Specialty chemicals, on the other hand, are formulations of chemicals and may contain one or more fine chemicals in their make-up. Whilst the distinction between commodity and fine chemicals can be vague, specialty chemicals are very different in their definition. Fine chemicals are bought for what they are (e.g. their molecular structure). Specialty chemicals are bought for what they can do. In the pharma sector APIs are fine chemicals because of the benefit they can bring to patients; however, the drugs APIs are sold as (typically APIs will be mixed with other chemicals) are specialty chemicals (Pollack, 2012).

Chemicals that have recently received increasing attention are chiral molecules. Since 1992 both regulators in Europe and the United States require physiological action characterization of individual enantiomers of molecules. Moreover, the Food and Drug Administration (FDA) in the US has incentivised production of enantiomerically pure drugs over racemic mixtures by establishing a fast track application process for single enantiomer drugs (Breuer *et al.*, 2004).

1.4.4 Multi-step biocatalysis

Despite the generally "greener" perception of biocatalysis over chemical synthesis, enzymes can present some disadvantages. Biocatalytic reactions, for example, could suffer from unfavourable reaction equilibrium. Additionally, substrates and or intermediate products could be unstable, making final conversion yields lower than desired. Some techniques such as *in-situ* product removal can move reaction equilibrium (Lye and Woodley, 1999), but a technique that has become increasingly studied is that of a biocatalytic cascade: a series of enzymes that catalyse a subsequent or parallel step to, regenerate cofactors or resolve a racemic product or increase final yields. Examples of some biocatalytic cascades are shown in Table 1.3.

In previous work by the Sustainable Chemical Feedstocks group, L-gluco-heptulose was selected as a potential target for upgrading of L-arabinose from pretreated SBP (Subrizi *et al.*, 2016). Ketoheptoses are 7-carbon sugars that, while rare in nature, could have important pharmacological potential (Paulsen, Richenderfer and Winick, 1967). D-manno-heptulose was found to inhibit D-glucose metabolism and insulin secretion, and L-gluco-heptulose was found to have possible application in cancer and hypoglycaemia treatments (Board, Colquhoun and Newsholme, 1995). Further, despite the chemical synthesis of ketoheptoses having been described, low yields and poor resolutions were reported, with D-gluco-heptulose synthesis requiring 8 chemical steps, and the use of toxic reagents (Morin, 2003; Cheng *et al.*, 2009; Waschke, Thimm and Thiem, 2011).

The enzymatic production of L-gluco-heptulose used a transketolase enzyme (TK) which transferred a C-C group from a ketol-donor, hydroxypyruvate (HPA) to L-arabinose to produce L-gluco-heptulose. However, HPA degradation can severely limit the amount of L-gluco-heptulose produced (Dickens and Williamson, 1958), so a one-pot two-step reaction was proposed where HPA was first synthesised by the deamination of L-serine as catalysed by an ω-transaminase (TAm) (Bawn *et al.*, 2018). This was followed by the utilisation of HPA and L-arabinose for the production of L-gluco-heptulose and CO_2. The production of CO_2 would cause the TK reaction to become irreversible driving the reaction equilibrium forward (Hibbert *et al.*, 2007).

Table 1.2. Biocatalysis products and respective enzymes, type of biocatalysis, production scale and producing company.

Product	Enzyme(s)	Type of reaction	Scale ($t.yr^{-1}$)	Company	Reference
Ethanol	Several	Fermentation	>1 000 000	Several	(Cai and Stieger, 2014)
High-Fructose corn syrup	Glucose Isomerase	Bio-transformation	>1 000 000	Several	(Bommarius and Riebel-Bommarius, 2004)
Lactose free milk	Lactase	Bio-transformation	>100 000	Several	(Bommarius and Riebel-Bommarius, 2004)
aspartame®	Thermolysin	Enzyme Catalysis	>1 000	Tosoh/DSM	(Schmid *et al.*, 2001; Bommarius and Riebel-Bommarius, 2004)
D-*p*OH-phenyl glycine	Hydantoinase	Biotransformation (resting cell)	>1 000	Kanegafuchi	(Bommarius and Riebel-Bommarius, 2004)
L-aspartic acid	Ammonia lyase	Precursor fermentation	>1 000	DSM	(Schmid *et al.*, 2001)
6-Hydroxy nicotinic acid (insecticide)	Niacin Hydroxylase	Precursor fermentation	<100	Lonza	(Schmid *et al.*, 2001)

Table 1.3. Examples of biocatalytic cascades for differing purposes.

Reaction	Enzymes	Comment	Reference
Amine Dealkylatoin and deracemisation	Monoamine oxidase and ω-Transaminase	Racemic mixture of amines is first separated oxidising a particular amine enantiomer which is then "re-aminated" through transaminase action	O'Reilly et al. (2014)
Asymmetric reductive amination	ω-Transaminase with amino acid dehydrogenase and D-glucose dehydrogenase	Byproduct is regenerated into substrate and cofactor is regenerated with addition of D-glucose	Koszelewski et al. (2008)
Cyclohexanol to oligomeric caprolactone	Alcohol dehydrogenase followed by Baeyer Villiger Monooxygenase and CalA lipase	CalA lipase avoids strong product inhibition on Monooxygenase by catalyses polymerisation of caprolactone monomer	Schmidt et al. (2015)
4-Toluic acid from 4-Tolyl-alcohol	Esterase, Carboxylic acid reductase, Alcohol dehydrogenase + Cofactor regeneration enzymes	7-enzyme cascade designed through use of *in vitro* characterisation and *in silico* modelling	Finnigan et al. (2019)
Chiral amino alcohol synthesis	Transketolase followed by ω-Transaminase	Use of HPA as ketol donor leads to formation of CO_2 making TK reaction irreversible	Villegas-Torres et al. (2015)
L-gluco-heptulose synthesis from L-arabinose	ω-Transaminase followed by Transketolase	Thermostable enzymes used to produce heat labile HPA by Transaminase reaction followed by ketol production	Lorillière et al. (2017); Bawn et al. (2018)

The continuous operation of this reaction for the upgrading of SBP-derived L-arabinose is explored in this work. Details of the enzymes involved are described in Sections 1.4.5 and the results of the studies are presented in Chapter 5 and Chapter 6.

1.4.5 Transaminase and Transketolase as biocatalysts

Amino acid dehydrogenases, amine dehydrogenases and transaminases (TAm) are all enzyme classes capable of synthesising chiral amino alcohols from keto alcohols (Christen and Metzler, 1985; Kwon and Ko, 2001; Takagi *et al.*, 2001; Brunhuber and Blanchard, 2008). Stereoselectivity and broad specificity to substrates other than keto acids or ketones are important features; and TAms (EC 2.6.1-) show some of these advantages such as high stereoselectivity and unlike dehydrogenase enzymes are not redox reactions, which in turn leads to lower cost as cofactor recycling is not needed (Kaulmann *et al.*, 2007; Kara *et al.*, 2014). TAms, common enzymes in microorganisms, are used in nitrogen metabolism and employ coenzyme pyridoxal 5'-phopshate (PLP). The reaction (Figure 1.6) follows a ping-pong mechanism. Firstly, the amine group is transferred from the amine donor to the PLP molecule. This in turn becomes pyridoxamine 5'-phosphate (PMP). The reaction is then completed with the transfer of the amino group from PMP to the amino acceptor (Christen and Metzler, 1985; Kaulmann *et al.*, 2007). Currently, despite the wide range of substrate acceptability, commercial use of transaminases is uncommon due to low equilibrium conversion yields (Shin and Kim, 2014).

Transketolase (TK) is a homodimer and is a thiamine diphosphate dependent enzyme; it was discovered by Racker and Horecker in 1953. TK is employed in cells for carbohydrate transformation as a part of the non-oxidative branch of the pentose pathway. Its role is essentially to extend a carbon chain by the addition of a C-C group, or ketol group (Figure 1.8). TKs catalyse the cleavage of a C-C bond in a ketone and reversibly transfer the active glycolaldehyde (i.e. the cleaved C-C fragment) onto an aldose (Horecker, 2002; Kochetov and Solovjeva, 2014). This results in the lengthening of the substrate, via the addition of a C-C fragment. Additionally, TK has high tolerance for hydroxylated substances, and forms *S*-configuration keto-diol products stereoselectively, making it interesting for industrial biocatalysis (Schenk, Duggleby and Nixon, 1998; Turner, 2000; Shaeri, Wohlgemuth and Woodley, 2006; Ingram *et al.*, 2007).

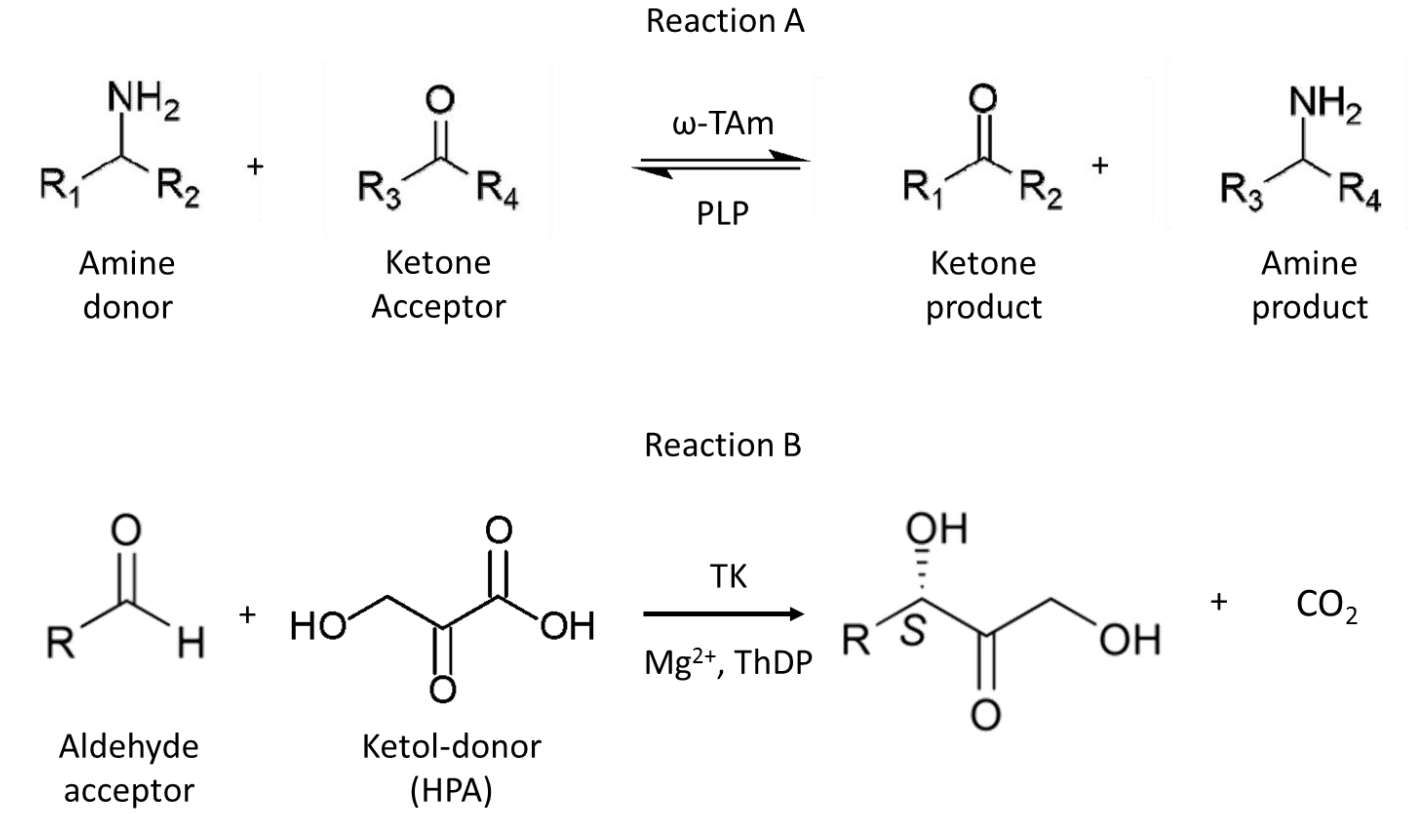

Figure 1.8. Transaminase and Transketolase reaction scheme. Reaction A shows the typical ω-TAm reaction for the replacement of a keto group with an amine group. Reaction B shows the extension of an aldehyde acceptor by a C-C bond, as catalysed by TK. Reaction B also shows how, by using HPA which is converted in CO_2, the reaction is made irreversible. Adapted from Patil et al (2018) and Subrizi et al. (2016).

Despite the ability of wild type enzymes to catalyse a range of unnatural substrates or product, some reactions may require modifications to the structure of the enzyme. To accommodate different reaction requirements many techniques have been developed for the molecular engineering of enzymes and proteins (Bommarius and Riebel, 2004). The changes made to the enzymes can originate either from rational design or from directed evolution or a combination of both. In rational design the structure of the catalyst is known, and small changes that are thought to have an effect are made and subsequently tested. Directed evolution on the other hand uses techniques such as error-prone PCR to cause random mutations in the enzyme-encoding DNA that in turn may cause changes in the molecule which may result in better catalysts. Often, however, the two techniques are used in combination. Prior knowledge of the active site of an enzyme or mechanism of action can focus directed evolution efforts to particular fragments of DNA or even individual amino acids. Saturation mutagenesis is one of such techniques, whereby all possible mutations of a specific part of an enzyme are tested (Marshall *et al.*, 2003; Bommarius and Riebel, 2004; Otten and Quax, 2005; Payongsri *et al.*, 2012). Newly formed mutants need to be tested to assess any potential hits. This is typically done through the use of high throughput screening using chromatographic or colorimetric methods (Smith *et al.*, 2006; Hailes *et al.*, 2009).

Like many other enzymes, TAms and TKs have been studied and mutated. Different mutagenesis studies have had different aims. Some aimed at widening the range of substrates that could be converted: TKs were mutated to accept non-phosphorylated substrates (Hibbert *et al.*, 2007), and linear and cyclic aliphatic aldehydes (Cázares *et al.*, 2010). Mutagenesis could also be aimed at allowing use of a specific substrate, for example using aliphatic aldehyde propionaldehyde (Hibbert *et al.*, 2008), or to reduce inhibition from substrate (to allow larger loading) as was the case for the error prone PCR mutagenesis used on transaminase enzyme to reduce inhibition from aliphatic ketones (Yun *et al.*, 2005).

Although not explored in this work, D-galacturonic acid could also be used as substrate for bioconversions. For example, by using transaminases, D-galacturonic acid can be converted into an ω-amino acid. These amino acids can then be used as monomers for the production of polyhydroxypolyamides (PHPAs), used in plastics (Morton and Kiely, 2000), or further converted into therapeutic molecules in the form of polyhydroxyazepanes as shown by the reaction scheme in Figure 1.8 (Andreana *et al.*, 2002).

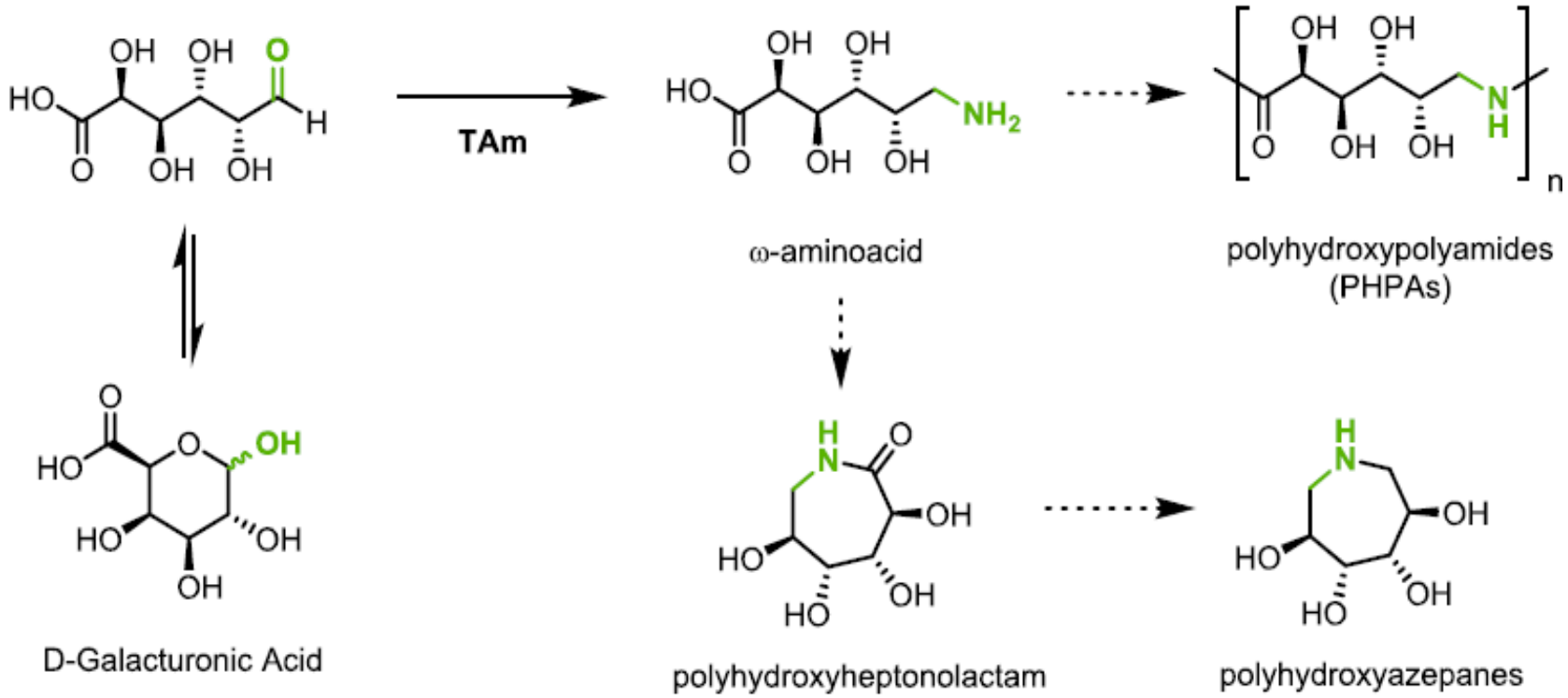

Figure 1.9. Conversion of D-galacturonic acid into an ω-amino acid, which could subsequently be converted into a polyamide plastic or into therapeutic precursors. Adapted from Subrizi et al. (2016)

1.5 Continuous reactors and flow biocatalysis

1.5.1 Continuous SBP processing

Chemical and biochemical reactions can take place in three types of reactors: batch, fed-batch and continuous (Scott Fogler, 2008). For batch operation, all the reagents are added at once, the system is closed, and the reaction is started. Once the reaction has been completed, the products are collected; the reactor is then emptied and prepared for the following reaction. Fed-batch reactors operate in a very similar way. However, the addition of reagents continues throughout the reaction. Reagent addition can occur sporadically or it could occur for prolonged periods of time throughout the reaction. The third type of reactor is when the reactor is run in a continuous mode. Addition of reagent and removal of product takes place continuously. Examples of continuous reactors are *chemostats*, where concentrations of the reagents and products in the reactor is kept constant; and *rheostats* where the fluid's viscosity is kept constant for the duration of the reaction (Scott Fogler, 2008; Doran, 2012). Batch and fed-batch reactors are typically used for smaller production scales and have typically lower capital costs. Continuous reactors, on the other hands, are used for larger production scales, offer higher productivities, lower down-time as no cleaning and preparation between batches is required as well as improved safety and control over the reaction (Roberge *et al.*, 2005; Scott Fogler, 2008).

Sugar beet is processed in large quantities and, during the "campaign" period, which lasts 4-6 months, many of the operations are run continuously. If SBP were to be used for further valorisation, continuous operation would ideally be employed to reduce the need for additional storage of SBP and facilitate integration into wider biorefinery operations. Most of the processes and reactions discussed so far could be carried out in continuous mode. Steam explosion (Section 1.3.2.1), designed originally as a batch process has actually been carried out continuously on wheat straw (Fang, Deng and Zhang, 2011). Liquid hot water (LHW) pretreatment can also be carried out continuously as biomass and water could just flow through a pressurised reactor. Mild acid hydrolysis of wheat straw has also been carried out in a continuous plug flow reactor (Jaramillo, Gómez-García and Fontalvo, 2013). Kleinert's patent application for ORGANOSOLV, a process designed and patented for the production of cellulose pulp from biomass, also included the description for a continuous processing set-up (Kleinert, 1971).

Enzymatic breakdown could be carried out continuously, especially as enzymes have specific optimal conditions and as such, could benefit from the easier control offered by flow reactor. Implementing recycling and retention of enzymes could also be important to reduce process costs. Enzyme immobilization onto supports or resting cells would likely be impractical for pretreatment (Spagnuolo *et al.*, 1999) but could be employed in the depolymerisation step as shown by Cardenas-Fernandes et al. (2018). Countercurrent chromatography and simulated moving bed chromatography are potential continuous technologies that could be used for sugar separation after pretreatment and breakdown of lignocellulosic material (Azevedo and Rodrigues, 2001; Shinomiya and Ito, 2006; Ward *et al.*, 2015).

Continuous enzymatic reactions have been investigated in research, but have also been applied in commercial settings (Table 1.4). A study on 22 fine chemicals and pharmaceuticals produced in batch by Lonza, showed that 50% could benefit from continuous operations. Although this study was conducted on chemical synthesis reactions rather than biocatalytic reactions, the usefulness of enzymes in yielding single-enantiomer solutions, an important feature in the fine-chemical and therapeutic precursor industries, means that biocatalysis too could benefit from being translated into continuous operations (Roberge *et al.*, 2005; Mak, Laurino and Seeberger, 2009).

The production of fine chemicals often requires high catalyst purity. The purification process can be costly, and as such enzyme retention is required. O'Sullivan and colleagues (2012) showed on a microfluidic reactor that a TK could be separated from the biocatalysis product via an ultrafiltration membrane (O'Sullivan *et al.*, 2012; Lawrence *et al.*, 2013). Halim et al. (2013) immobilized transketolases and transaminases via the addition of a hexahistidine tag (His-Tag), which has a high affinity to nickel. A microreactor was packed with His-Select Nickel affinity agarose beads and in this way retained the enzymes as the substrates passed through (Halim et al. 2013). More recently, Kulsharova et al. (2018) immobilized His-tagged enzymes directly onto the surface of a microfluidic chip (Kulsharova *et al.*, 2018). Despite a growing number of publications released on continuous flow biocatalysis, many groups work at a milli- microfluidic scale with reactors often operating in laminar regimes (Britton, Majumdar and Weiss, 2018).

Table 1.4. Examples of continuous biocatalysis from literature.

Product	Enzyme	Type of reactor	Reference
High-fructose corn syrup	Glucose isomerase	Fixed bed- Immobilized enzyme reactor	(Visuri and Klibanov, 1986)
Enantioselective cyanohydrins	Hydroxynitrile lyases	Microreactor (crude lysate)	(Koch *et al.*, 2008)
L-methionine	Aminoacylase	Enzyme membrane reactor	(Bommarius and Riebel-Bommarius, 2004)
L-alanine	D-amino acid oxidase	Agitated Cell Reactor	(Jones *et al.*, 2012)
Peracetic acid	Lipase B from *candida artica*	Packed bed reactor (enzyme immobilized on acrilyc resin)	(Wiles, Hammond and Watts, 2009)
L-erythrulose	TK	Microreactor (clarified lysate and filtration step to retain enzyme)	(O'Sullivan *et al.*, 2012; Lawrence *et al.*, 2013)
(2S,3R)-2-amino-1,3,4-butanetriol (ABT)	TK followed by TAm	Microreactor with two individual pH regions	(Gruber *et al.*, 2018)

1.5.2 Coflore® reactor technology

1.5.2.1 Coflore® reactor design

At the microfluidic scale, continuous flow reactors are governed by laminar flow regimes and good mixing is not often achievable. However, at large scale two designs of continuous reactor are available (Pustelnik, 1986); statically and dynamically mixed reactors. The former achieve mixing through reactor configuration; dispersion is obtained via corners, baffles and narrow channels coupled with high fluid velocities. Despite this, often suboptimal mixing, phase separation and blockage in case of solid processing occur. Dynamically mixed reactors, on the other hand, achieve effective mixing through an external input of energy into the system. An example of this is the continuous stirred tank reactor (CSTR): a vessel with an entry and an exit port, and with impellers that mix the reagents (Scott Fogler, 2008; Browne *et al.*, 2011). However, mechanical stirrers often require seals which are potential sources of contamination and leaking (Ashe and Wühr, 2012). Due to the advantages and disadvantages of each category, reactors are often custom-designed for each application (Browne *et al.*, 2011). This in turn slows down process development and makes uptake of flow technologies in multi-product facilities (as many fine-chemical processing plants are) difficult (Roberge *et al.*, 2005).

A flow reactor manufacturer, AM Technology, has recently produced the Coflore® range of continuous reactor that span from laboratory scale to production scale. Coflore® reactors employ a novel mixing technology, whereby the entire reactor block is shaken, and agitators inside the reactor shake with it causing turbulence and mixing. This type of mixing allows these reactors to handle dispersed solid phases, as well as providing good mixing conditions without mechanical seals (Browne *et al.*, 2011; Jones *et al.*, 2012).

Coflore® mixing technology is used in the Agitated Cell Reactor (ACR): a monolithic block made of 10 interconnected wells each of approximately 10 mL in volume. A plate placed behind the cells, is used for temperature control. The ACR's reactor block is placed on a shaking platform. Compressed air is supplied to the platform to provide energy for the shaking mechanism. Each cell also has a side inlet port that allows for side streams to be injected into the reactor (Gómez-Quero, Cárdenas-Lizana and Keane, 2011; Salice *et al.*, 2012).

Larger reactors are the Agitated Tube Reactor (ATR), which instead of 10 mL cells employs 100 mL tubes; and the Rotating Tube Reactor which is a 100L production scale reactor.

1.5.2.2 Coflore® applications

Scale-up studies on whole cell biocatalysis showed how in a two phase (gas-liquid) system, where uniform mixing is crucial ACR and ATR both outperformed stirred tank batch processes; and, additionally, also showed comparable results across scales (Gasparini *et al.*, 2012). The ACR has also been employed in enzymatic oxidation of D-glucose showing good ability at handling oxygen mixing (Toftgaard Pedersen *et al.*, 2017). Beyond their ability to handle gas mixing, the ACR and ATR were shown to handle solids and solid formation in flow with the production of an N-iodomorpholinium hydroiodide salt (Browne *et al.*, 2011; Filipponi, Gioiello and Baxendale, 2016). At present, no report on the ability of the ACR to handle larger solids such as milled SBP or the ability to perform an enzymatic cascade has been reported.

1.6 Critical appraisal of the literature

The need for the creation of sustainable and renewable processes is accepted by the scientific community and the wider public (Section 1.1). A range of fuels, chemicals and materials, that are currently made from non-renewable fossil fuels, are being studied as potential replacement products or alternatives derived from renewable resources (Liu *et al.*, 2005; Hamley-Bennett, Lye and Leak, 2016; Gienau, Kraume and Rosenberger, 2018). It is also clear that biological and bioprocessing techniques will feature heavily in the creation of a diverse portfolio of sustainable products. Agricultural crops such as sugarcane and corn have been used to make sustainable fuels and other products; but they also put pressure on food supply, causing prices to rise (Costa and de Morais, 2011). Agricultural waste streams are increasingly studied as a potential sustainable feedstock alternative to mainstream crops, as they would not affect food prices, but also create a further income stream for farmers (Section 1.3.1).

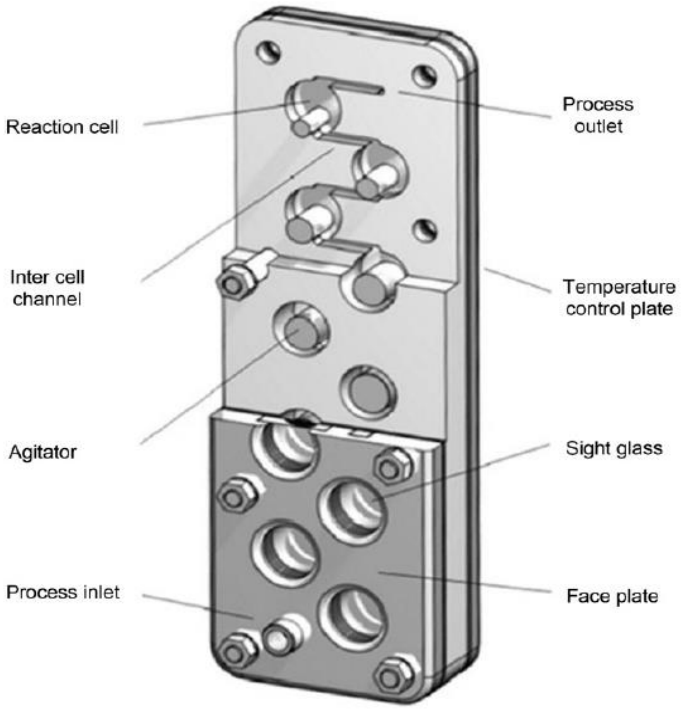

Figure 1.10. The Agitated Cell Reactor (ACR) is a continuous reactor that employs lateral shaking of the entire block to cause the agitators to move and create turbulence. Figure reproduced with permission from AM Technology UK.

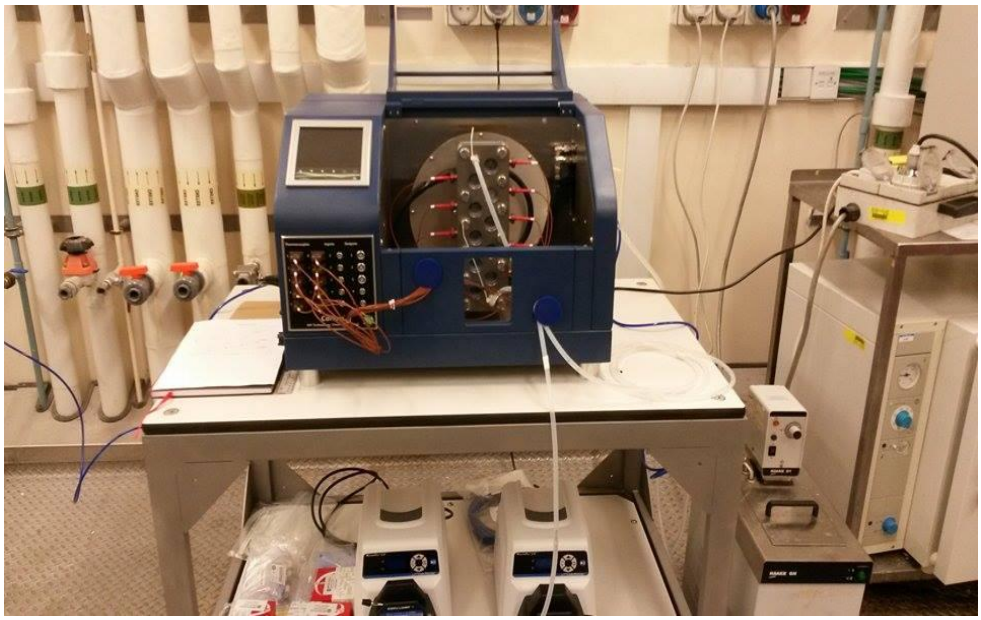

Figure 1.11. The ACR reactor block inside its shaking platform. The blue plastic tube on the left-hand-side supplies compressed air for shaking of the reactor block.

Despite this great potential, an important obstacle to using agricultural waste is the lignocellulosic structure of the biomass. The recalcitrant structure of biomass makes it difficult to obtain sugars from fibres such as cellulose and pectin (Mosier *et al.*, 2005; Zheng *et al.*, 2013). Pretreatment reactions, which use a combination of mechanical, physical, chemical and enzymatic steps, aim at disrupting the structure and exposing target molecules for conversion into value added products. Amongst various agricultural wastes, SBP stands out as it is already found in a concentrated form at the outlet of sugar diffusers, and therefore, does not require any collection from fields or additional logistics (Section 1.3.1). Additionally, SBP has a low lignin content, thus requiring milder pretreatment conditions (Figure 1.5). Harsher pretreatment conditions of SBP (higher temperatures and stronger chemical environments) produce monomeric sugars but also large amounts of byproducts that could act as inhibitors to fermentative and enzymatic reactions (Hamley-Bennett, Lye and Leak, 2016). Milder conditions, on the other hand, would release sugars in oligomeric and polymeric form, allowing further, more selective, depolymerisation downstream (Spagnuolo *et al.*, 1999; Cárdenas-Fernández *et al.*, 2018). The challenge here lies in finding appropriate pretreatment conditions that maximise the release of the target molecules for the intended products.

Although, most literature efforts have focused on pretreating wastes to release sugars for fermentations; increasingly, studies have worked on approaches to convert sugars into value added products through enzymatic reactions (Kühnel, Schols and Gruppen, 2011b; Leijdekkers *et al.*, 2013; Kharina *et al.*, 2016). Biocatalysis is a growing field, owing to the enantio-, regio- and chemical-selectivity that enzymes can have, removing undesired side-reactions and requiring safer and cheaper reaction conditions than chemical synthesis routes. Furthermore, enzyme engineering can lead to enzyme mutants with more or less affinity to certain molecules, thus increasing the substrate and reaction scope.

With an ever-increasing library of enzymes, biocatalytic cascades are also becoming of increasing interest (Köhler *et al.*, 2013). One-pot reactions could remove problems such as intermediate product inhibition by pushing reaction equilibria towards the final product. Transaminase and transketolase are industrially relevant enzymes (Section 1.4) which can be used to make a range of chiral compounds. A variety of previous studies have shown that one-pot reactions using these two enzymes are possible.

Despite the promising advances in the fields of lignocellulosic biomass pretreatment and bioconversion, for these technologies to become commercial realities, they need to be

scalable and financially viable. A way to achieve this is through continuous processing however, most pretreatment processes investigated in the literature are inherently batchwise operations (Mosier *et al.*, 2005). Continuous pretreatment has been studied on only a few occasions, although not using SBP (Choi and Oh, 2012; Da Silva *et al.*, 2013; Han *et al.*, 2013). Pretreatment under continuous flow conditions can offer safer operation (e.g. only a small amount of volume would be very hot at any one time), but solid handling remains a challenge. Continuous biocatalysis, on the other hand, has been studied more extensively, although often at the microreactor scale. Flow bioconversion does offer advantages over batch processing, such as lower downtimes, improved control and kinetics.

The Coflore® range of reactors offers a range of sizes with good scalability from benchtop to production scale (Section 1.5.2). In a range of publications, the small scale reactor, the ACR, has been shown to work with a range of fluids and even solid-containing slurries. However, no work has been reported on biomass pretreatment in Coflore® reactors, or the utilisation of this technology for biocatalytic cascades. A further consideration when considering biocatalytic cascades, is the production and utilisation of the catalyst. This involves developing efficient fermentation, recovery, and purification techniques to reduce the cost of the enzymes. Enzyme immobilization or retention could provide further cost efficiencies by reducing the frequency with which new enzymes are required (Gräslund *et al.*, 2008).

1.7 Aim and objectives

Based on the considerations in Section 1.6, the **aim** of this thesis is to explore continuous bioprocess options for the pretreatment of SBP and the subsequent conversion of the released monosaccharides into value added products via biocatalytic approaches. The ACR will be used as an example of a continuous lab-scale reactor, able to handle suspended solids, to translate batch reactions into flow studies (Section 1.5). Dilute acid pretreatment (Section 1.3.2.3) will be evaluated for the initial hydrolysis of SBP as opposed to more expensive and energy intensive thermal methods (Section 1.3.2). The one-pot, two-step TAm-TK bioconversion for the production of L-gluco-heptulose (Section 1.4.5) will be used as a model reaction that could fit in a wider biorefinery context. Production and purification of thermostable versions of the TAm and TK enzymes will be investigated given the conditions under which the SBP process stream is generated in a sugar beet biorefinery (Section 1.2). The key project **objectives** are outlined below.

- The first objective will be to characterise the hydrodynamics of the ACR for the processing of both single-phase liquid and multi-phase, solid-liquid process streams. This will initially involve a rheological study of the SBP slurry to characterise the viscosity of the solid-liquid system. Next a Residence Time Distribution study will be undertaken using model liquids. A range of agitation conditions, flowrates, fluid viscosity and agitator types will be investigated to help understand how these impact on ACR performance. This will lead into characterisation work using the real SBP slurry. Particle size distribution will be evaluated over time to monitor how differently sized particles flow through the reactor. This work is described in Chapter 3.
- The second objective will be to investigate continuous SBP pretreatment options. Most of the work will revolve around characterising mild acid pretreatment of SBP (Section 1.3.2.3). A batch system will be used to gain initial insights into the reaction kinetics. This will be followed by a Design of Experiments study to understand how pretreatment variables affect release of SBP-derived monosaccharides: L-arabinose, D-galacturonic acid and D-glucose. Optimised mild-acid hydrolysis conditions will then be studied in the ACR, where the effects of flowrate, SBP loading, acid concentration and temperature on sugar release will be further investigated. Considerations of throughput and reactor productivity will be made and compared to other pretreatment methods from literature. Enzymatic treatment routes will also be briefly investigated as a stand-alone pretreatment of SBP or as the hydrolysis step to obtain monomeric sugars from pretreated SBP. This work is described in Chapter 4.
- The third objective will investigate biocatalyst production and scale-up in order to produce the quantity of enzymes needed for ACR studies. Fermentations in a stirred tank reactor will be investigated as a replacement for shake flask production. Finally, the disruption of the *Escherichia coli (E. coli)* cells and subsequent enzyme purification techniques will be studied. This work is described in Chapter 5.
- The final objective will be to evaluate a possible multi-enzyme bioconversion of L-arabinose using thermostable TAm and TK enzymes. First, the single enzyme reactions will be investigated in small scale (~1mL) batch reactions. The ability of TAm and TK reactions to produce HPA and L-gluco-heptulose, respectively, will be studied under a range of pH, temperatures and substrate concentrations. This will lead into a characterisation of the batch one-pot two-step reaction using different

substrate concentrations and at different scales. Immobilization of the enzymes will then be explored using different enzyme immobilization strategies in batch mode. The enzymes will then be used with the real hydrolysed and enzymatically depolymerised SBP for the production of L-gluco-heptulose. This will be done with free enzymes at a range of volumes and will be translated into continuous mode using the ACR. This work is described in Chapter 6.

Chapter 2 will describe the materials and methods used throughout this Thesis. Chapter 7 will provide overall conclusions of this study and summarise priorities for future work. Chapter 8 will discuss possible commercial and industrial applications of this work.

2

Materials and Methods

2.1 Description, setup and operation of the Agitated Cell Reactor

2.1.1 ACR description

The ACR is a continuous flow reactor designed and produced by AM Technology (Runcorn, UK) as described in Section 1.5.2. The core of the ACR is the reactor block as shown in Figure 2.1(a). The block is made of Hastelloy metal and consists of 10 interconnected reaction cells, totalling a volume of approximately 120 mL. The cells are separated by small rectangular channels 4 mm wide and 4 mm high and each cell contains an agitator that provides mixing to the system.

The reactor block is mounted vertically on a platform within the reactor (Figure 2.1(b)), powered by compressed air, which shakes the reactor left and right, with a variable frequency between 0 and 9 Hz. As the block shakes, the agitators inside each cell (Figure 2.1 (c and d)) also move, promoting turbulence and mixing within the fluid. Aside from a main inlet and outlet for the reactor, each cell has additional entry points (Figure 2.1(a)). Side entry ports provide access for either temperature probes or additional inlets or outlets. The sight glass covering each reaction cell can be removed and replaced by an additional entry/exit port if required.

Temperature control inside the ACR is achieved by flowing heating or cooling fluid through a heat exchange block placed behind the cells. The heat exchange block's configuration mirrors the structure of the reaction block, having 10 interconnected wells. In the heat exchange block, small copper cylinders act as agitators to promote heat exchange within the reaction block.

To operate the ACR a Masterflex LS peristaltic pump (Cole-Parmer, Vernon Hills, USA), was employed to pump the main process fluid through the ACR. Side-streams were pumped through the side inlet ports using a SP120PZ syringe pump (World Precision Instruments, Hitchin, UK), a 50 mL Luer Lock syringe (BD, East Rutherford, USA) and a 1/8 OD x 1.60 mm ID PTFE tubing (VWR, Radnor, USA)

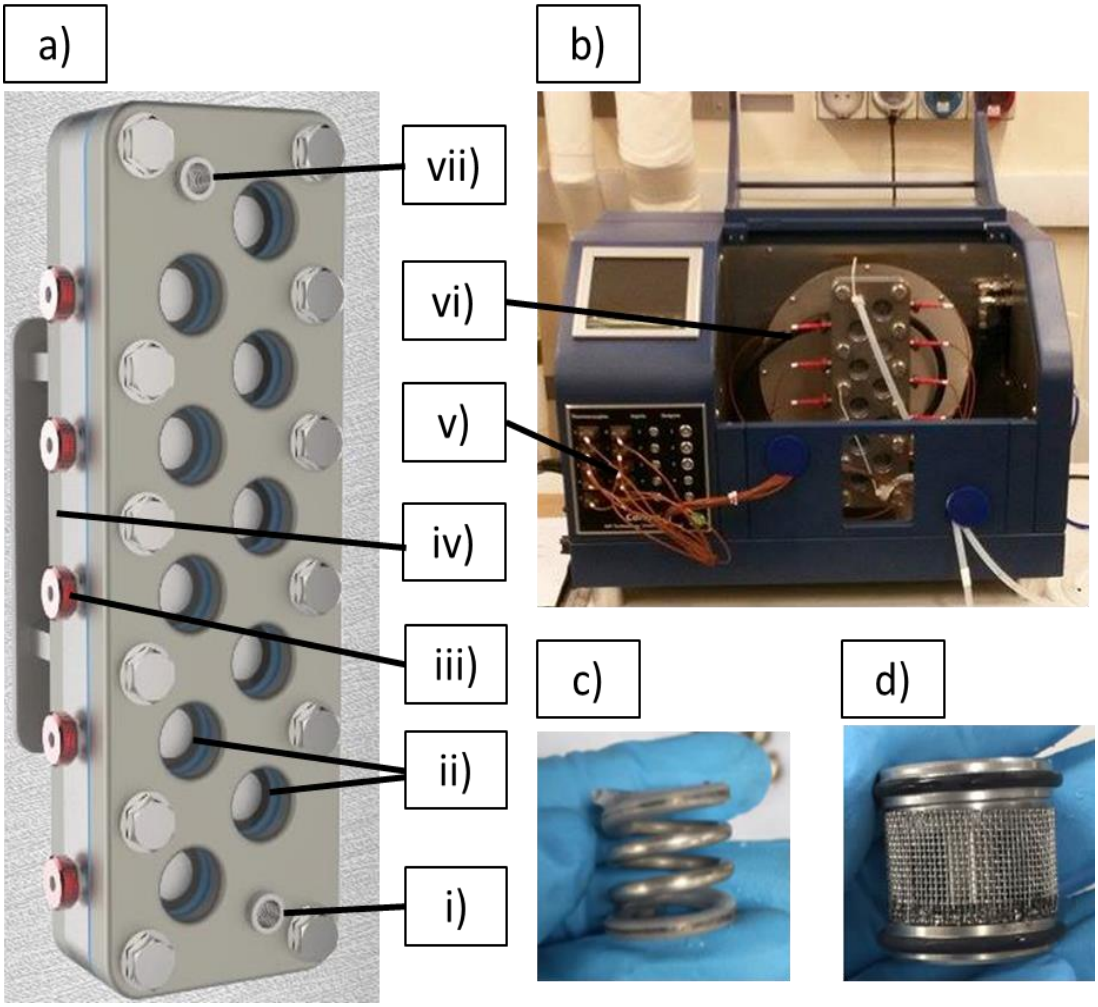

Figure 2.1. Agitated Cell Reactor setup and main components. The process fluid enters the base of the ACR reactor block (a) through an inlet port (i), flows sequentially through each reaction cell that is sealed with a sight glass (ii), and exits via the outlet port at the top (vii). Additional streams can be added via side entry ports (iii) or via the removal of sight glasses inside cells. The reactor block sits in the shaking platform (b); where heating fluid can be delivered (vi) and flown through the heat exchange unit (iv) to maintain the reactor temperature. Inside each reaction cell is an agitator, which can take various shapes, such as a high shear agitator (c) or a catalyst basket agitator (d).

2.1.2 ACR residence time distribution study

The main method used to characterise the performance of the ACR under various fluid flow regimes was to evaluate the equivalent number of tanks, N, through a Residence Time Distribution (RTD) study. This number represents how many ideally mixed continuous stirred tank reactors (CSTR) in series would be required to mimic the flow regime of the ACR (Levenspiel, 1999). A mathematical derivation to explain the underlying principles is shown in Section 3.3.2.1.

Experimentally, N was determined by using a tracer that was injected at the inlet of the reactor and its concentration was measured at the outlet over time. Allura red (Sigma Aldrich, St Louis, USA) a soluble tracer dye, was used to create the step change in tracer concentration required for the determination of N. A 4 mM solution of Allura red in deionised water was prepared and placed in a Luer-lock syringe and connected to PEEK tubing that would lead from the syringe pump to the side entry port in the first cell as described in Section 2.1.1. The process fluid in the ACR was either deionised water or aqueous glycerol solutions of varying viscosity that were pumped via the main inlet. The volumetric ratio between the process fluid and the secondary fluid entering from the side port (tracer solution) was kept constant at 100:1 at different flowrates. At the outlet of the ACR, samples were collected over time and absorbance was measured at 540 nm. Sampling was halted after steady state was reached. The absorbance readings were then converted into a normalised response by applying Equation 2.1:

$$\boldsymbol{Normalised\ response_i} = \frac{\boldsymbol{Absorbance_{sample,i} - Absorbance_{background}}}{\boldsymbol{Absorbance_{steate\ state} - Absorbance_{background}}} \quad \text{[Equation 2.1]}$$

RTD experiments were performed at various shaking frequencies, flowrates, process fluid viscosities and agitator types and were tested in triplicate, unless stated otherwise. ACR reactor block shaking frequencies were varied between 0, 2, 4, 5, and 6 Hz via the control panel of the ACR. Unless stated otherwise RTD experiments were carried out with a 15.2 min residence time which was obtained at using the peristaltic pump set at a speed of 10 rpm using a Masterflex LS/25 silicone tubing and a syringe pump speed of 5.0 $mL.hr^{-1}$. When the process fluid flowrate was increased, the syringe flowrate was increased by the proportional amount. A pump calibration graph for the fluids used in the RTD study is given in Appendix

9.1. Processing fluid of varying viscosities were obtained by using different concentrations of glycerol and water 20% v/v, 50% v/v and 80% v/v of glycerol were used to match SBP slurry viscosities. Effect of the type of agitators was tested by replacing the high shear agitators with catalyst baskets.

2.1.3 Effect of PSD on ACR operation

To investigate if particles of different sizes travelled through the ACR with different residence times, the ACR feed stream was switched from deionised water to a 2% w/v SBP slurry. The residence time was set at 15.2 minutes and the ACR was shaken either at 5 or 6 Hz. 44 minutes after the switch from water to SBP slurry for 5 Hz and 40 minutes for 6 Hz, the feed was switched again from SBP slurry to water. On one occasion rather than switching the feed line back to water, SBP slurry was pumped for 90 minutes to monitor steady state particle size distribution (PSD). The PSD of the outlet samples was analysed using diffractive light scattering.

The Mastersizer 3000 (Malvern Panalytical, Malvern, UK) determines particle size based on diffractive light. Samples are suspended in a dispersion fluid (in this work, deionised water) inside a glass chamber. A light is shone through the sample, which diffracts the light according to its size. An array of detectors measures the extent of the diffraction and derives a PSD of the sample from it (Pareek *et al.*, 2001). A diffractive index of 1.53 and an obscuration rate range of 10%-20% were employed. The dimension values corresponding to the 10^{th} percentile, 50^{th} percentile (i.e. median) and 90^{th} percentile were reported as D10, D50 and D90 respectively.

2.1.4 Rheological measurements

Rheological measurements of liquid and solid-liquid dispersions were carried out using a Kinexus rheometer (Malvern Panalytical, Malvern, UK). The rotational viscometer consisted of a temperature controlled fixed bottom plate, set to 25 °C, and a rotating upper plate (D50 mm) able to measure torque at different shear rates. These torque readings are converted into kinematic viscosity measurements. Viscosity of SBP dispersions (loadings of 1% w/v, 2% w/v, 4% w/v, 8% and 10%) and glycerol and water mixtures (0% v/v, 20% v/v, 50% v/v and 80% v/v glycerol) was measured by placing 1 mL of well mixed sample onto the lower plate. The upper plate was then lowered onto the fixed plate with a gap of 1 mm. 10 measurements were taken in triplicate over the shear rate range of between 100 s^{-1} and 1000 s^{-1}.

2.2 Pretreatment of sugar beet pulp (SBP)

2.2.1 SBP preparation and characteristics

Wet SBP provided by AB Sugar (Wissington, UK) from the 2015/2016 season was kept in airtight plastic bags and stored until needed at -20 °C. The SBP had a 28.0% w/w dry matter content. Analysis of the same batch of SBP by Hamley-Bennett et al. (2016), revealed the following sugar composition as a fraction of the total dry SBP solids (% w/w): L-arabinose 21%, D-galactose 6%, D-galacturonic acid 20%, D-glucose 25%, D-mannose 1%, L-rhamnose 3% and D-xylose 2% (Figure 1.5).

After thawing at room temperature, the SBP was placed on trays in an oven at 50 °C for 48 hours to dry. Dry SBP was then milled in 10 g batches in a vibrating ball mill (Fritsch, Idar-Oberstein, Germany) for 10 minutes on the highest setting. To ensure consistent size the SBP was then passed through a series of sieves. Unless stated otherwise the final sieve size was 212 μm, meaning only the SBP particles smaller than the nominal 212 μm mesh were used.

2.2.2 Batch pretreatment of SBP

2.2.2.1 Preliminary batch hydrolysis experiments

The first series of dilute acid pretreatment (DAP) reactions was aimed at gaining initial insights into SBP breakdown under acidic conditions (Chamy *et al.*, 1994). Two different methods of acid addition were employed: 5 mL addition of 0.1 M HCl or H_2SO_4 (Sigma Aldrich, St Louis, USA), or gradual addition of 2M HCl or H_2SO_4 until a pH of 1.8 was measured. The effect of temperature (80 °C versus 20 °C), type of acid (HCl versus H_2SO_4), solid loading (2.5% w/v and 5% w/v) and particle size (fine grind versus coarse grind) was analysed in 7 experiments. Particle size was investigated by comparing a breakdown of SBP particles that passed through a 500 μm sieve (fine grind) against particles that were larger than 500 μm (coarse grind). The milling and sieving setup, along with the resulting milled SBP fractions, are shown in Figure 2.2.

Figure 2.2. Ball mill and sieve set up and SBP fractions. Ball mill (a) and sieve (b) setup used for milling and sieving dry SBP. Images below show samples of the dried and sieved SBP: (c) dried *cossettes*; (d) milled SBP larger than 1 mm; (e) milled SBP larger than 500 µm and smaller than 1 mm; (f) milled SBP larger than 212 µm and smaller than 500 µm; and (g) milled SBP smaller than 212 µm.

50 mL of SBP slurries were prepared in 250 mL Duran bottles and their pH was measured at the start and end of the reactions. To maintain temperature at 80 °C, bottles were placed in a water bath. Reactions lasted 2 hours, with one vigorous shaking by hand being carried out after 1 hour. After the reaction, the slurry pH was neutralised to pH 7 by potassium hydroxide addition. The slurry was then placed in Falcon tubes and centrifuged at 15,000g for 30 minutes at 4 °C. The samples were then decanted and the supernatant was stored at -20 °C. Samples were processed as described in described in Section 2.3.3. prior to analysis by High Performance Anion Exchange Chromatography with Pulsed Amperometric Detection (HPAEC-PAD) as described in Section 2.5. A summary of the various conditions studied is shown in Table 2.1.

Table 2.1. Static batch reaction conditions for SBP pretreatment studies. Acid addition method refers to method used to add acid to the system: 5 mL refers to the addition of 5 mL of 0.1 M acid, whilst gradual refers to the addition of 2 M acid until a pH of 1.8 is reached.

Experiment number	Solid loading (% w/v)	Particle size	Temperature(°C)	Acid addition method	Acid type
1	5	Fine	20	5 mL	HCl
2	5	Fine	80	None	None
3	5	Fine	80	5 mL	HCl
4	5	Coarse	80	5 mL	HCl
5	2.5	Fine	80	Gradual	HCl
6	2.5	Fine	80	Gradual	H_2SO_4
7	5	Fine	80	Gradual	H_2SO_4

2.2.2.2 Effect of particle size on sugar release

The sieving of ground SBP results in 4 different size fractions as shown in Figure 2.2: particles smaller than 212 µm, particles that are between 212 µm and 500 µm, particles that are between 500 µm and 1000 µm and particles that are larger than 1000 µm. These SBP particles were pretreated alongside, dried whole SBP cossettes. DAP was carried out at 60 °C, in stirred condition in a jacketed Duran bottle with 200 mL working volume, an H_2SO_4 concentration of 50 mM at 60 °C. Samples obtained were stored at -20 °C until analysis as described in Section 2.3.3 and Section 2.5.

2.2.2.3 Dilute Acid Pretreatment DoE investigation (Central Composite Design)

To provide further insight into the main factors and interactions involved in the release of sugars during mild acid hydrolysis a Design of Experiments (DoE) approach was taken. In a stirred 250 mL Duran bottle, a 200 mL working volume was used. The glass bottle was insulated and the cap had a sampling hole and a temperature probe added for easy access. It was found that with careful monitoring the temperature could be controlled to within +/- 1.0 °C. A 4-factor, Centre-Faced Central Composite Design (cf-CCD) design was chosen (Huang *et al.*, 2010). The factors investigated were H_2SO_4 concentration (0-100 mM), SBP solids loading (2% w/v – 6% w/v), temperature (60 °C to 80 °C), and time (1 minute to 60 minutes). The cf-CCD design also required 3 repeat experiments of the centre point for a total of 17 experiments. Samples were taken and stored at -20 °C for processing and subsequent analysis by HPAEC-PAD as described in Section 2.3.3 and Section 2.5, respectively. The statistical analysis of results was carried out in the DoE software DesignExpert 9.0 (StatEase, Minneapolis, US).

2.2.3 Continuous hydrolysis: ACR Set up and operation

Continuous pretreatment in the ACR was investigated with runs taking place at different flowrates, temperatures, acid concentrations and solids loading. To develop a first awareness of the reactor operation, initially water and SBP only mixtures were studied. An inoculation bottle, with an outlet port at the base, was used to keep the SBP and water mixture in suspension. The stirred suspension was kept at room temperature to feed the ACR as described in Section 2.1.1. Runs were carried out at various temperatures (60 °C – 80 °C), solids loading (1% - 5 % w/v), acid concentrations (0 – 100 mM) and residence times through the reactor (3.8 minutes – 19.0 minutes). The shaking frequency of the reactor block was kept at 6 Hz throughout the experiments. Typically, the equivalent of approximately 4 residence times after SBP addition to the feed bottle was allowed for the system to reach steady state. Samples were collected at the exit port and frozen for analysis as described in Section 2.3.3 and Section 2.5.

2.3 Enzymatic hydrolysis

2.3.1 Commercial enzyme pretreatment

A commercial enzyme mix, Viscozyme®L (Sigma Aldrich, St Louis, USA) was used to pretreat whole dried SBP, that had not undergone any physicochemical pretreatment. Temperature and enzyme loading were kept the same as in the original publication by Leijdekkers et al. (2013). Dried whole SBP was placed in a 250 mL flask with 50 mL working volume, and placed in a shaking incubator at 250 rpm, 2.5 cm throw at 45 °C. 10.66 mL of Viscozyme®L mix per kg of dry SBP was used. A concentration of 7.5% w/v SBP, as in the publication by Leijdekkers et al. (2015), was compared to a lower concentration of 2.5% w/v. Reactions were carried out over a 48 hour period. Samples were taken throughout the reaction and spun down at 21,130g, for 20 minutes. The supernatant was stored at -20 °C until analysis as described in Section 2.3.3 and Section 2.5.

2.3.2 Arabinofuranosidase production and hydrolysis

A novel Arabinofuranosidase (AraF) was expressed from a pET28A plasmid in an *E. coli* BL21(DE3) strain (Cárdenas-Fernández *et al.*, 2017). A scraping of cells from a glycerol stock stored at -80 °C was used to inoculate a 250 mL shake flask, with a 50 mL working volume, using Terrific Broth (TB) as a growth medium (Fisher Scientific, Pittsburgh, USA). Flasks were incubated at 37 °C, in a shaking incubator set at 250 rpm and 2.5 cm throw. After 6 hours 0.1 mM Isopropyl β-D-1-thiogalactopyranoside (IPTG) was added to induce enzyme production. After 24 hours, the cells were harvested in a 50 mL Falcon tube (30 min, 15,000x g) and stored at -20 °C until needed. Cell pellets were resuspended in 0.1 mM TRIS-HCL to a final concentration of 0.5 mg mL^{-1} and disrupted using a Soniprep sonicator (MSE, Sanyo, Japan) with 3 cycles of 45s ON/60s OFF at 10 µm amplitude. The sonicated material was then spun down again (30 min, 15,000x g) and the material was concentrated 2-fold using Vivaspin 10 kDa centrifugal concentrator (Sigma Aldrich, St Louis, USA).

AraF activity was measured by analysing the cleavage of paranitrophenyl alpha l-arabinofuranoside (pnp-l-Ara) into p-nitrophenol (pnp) and l-arabinofuranoside (l-ara) as described by Cárdenas-Fernández et al. (2018). 160 µL of 5 mM pnp-l-Ara and 10 µL of AraF solution were mixed in a centrifuge tube with 230 µL of 0.1 M TRIS-HCL to which 400 µL of Sodium Borate 0.2 M pH 9.8 were added. The reagents were allowed to react for 5 minutes at 37 °C in an Eppendorf Thermomixer (Eppendorf, Hamburg, Germany). P-nitrophenol

absorbance was then measured at 405 nm. Alongside the sample to be tested a blank accounting for the absorbance of the pnp-l-ara and a blank accounting for the absorbance of the enzyme mix were also prepared. Their combined absorbance was subtracted from the sample absorbance. Using an extinction coefficient of 18.5 mM^{-1} cm^{-1} for pnp, the AraF activity was quantified by defining 1 unit as the amount of enzyme required to convert 1 µmol of pnp-l-ara to pnp per min.

Acid pretreated SBP (2% w/v SBP concentration, 75 mM H_2SO_4 and 80 °C, and 15.2 min residence time was used) from the ACR was collected and spun down (30 min, 15,000xg), and frozen until needed. 0.8 mL of acid hydrolysed SBP was mixed with 0.2 mL of AraF clarified cell lysate diluted as to obtain solutions of known activity (5, 10, 20 and 50 U mL^{-1}). Reactions in 1.5 mL centrifuge tubes were carried out in shaking Thermomixers at 60 °C, over a period of 60 minutes. Samples were quenched with 0.5% v/v TFA and stored at -20 °C. As the reaction aimed to measure the amount of monomeric L-arabinose produced by the enzyme, the sample processing steps described in Section 2.3.3 were omitted prior to HPAEC-PAD analysis as described in Section 2.5.

For the second set of hydrolysis reactions, it was not possible to carry out the activity assay, due to a lack of substrate, so 1 in 400 dilution of the clarified cell lysate was used on acid pretreated SBP (1% w/v SBP concentration, 75 mM H_2SO_4 and 80 °C, and 15.2 min residence time was used). Pretreated and clarified SBP was mixed with the cell lysate in 250 mL flasks. To investigate possible mass transfer limitations, one flask was kept at 50 °C and 250 rpm, 2.5 cm throw, whilst the other flask was kept in a different incubator with no shaking. The remaining pretreated SBP was pumped in the ACR with a residence time of 30 minutes. The clarified cell lysate was pumped from the first entry port so that this flowrate would account for 0.25% of the total flowrate, equating to 1:400 dilution.

2.3.3 Sugar analysis and quantification

Samples from SBP pretreatment and enzymatic reactions were separated from the solid, cellulose-rich fraction via centrifugation (15,000x g, 20 minutes in 15 mL Falcon tubes) and were stored at -20 °C until needed. To assess the extent of SBP solubilisation, the soluble polymeric and oligmeric sugars in the liquid fraction were hydrolysed into monosaccharides to enable HPAEC-PAD analysis (Section 2.5). For this, the method utilised by Hamley-Bennett et al. (2016) was followed. A workflow for this procedure is presented in Figure 4.2. 35 µL of 72% v/v H_2SO_4 (equivalent to 3% v/v) was added to 1 mL of solid-free sample before being

placed in an autoclave at 121 °C for 1 hour. After this the sample was spun down in an Eppendorf centrifuge tube at 21,130xg, for 20 minutes. The liquid fraction was then diluted further before being placed in vials for HPAEC-PAD analysis. The yield for each sugar was defined as the proportion of that sugar that was solubilised, both in monomeric and oligomeric form, from the starting amount present in SBP. This was calculated as shown in Equation 4.1.

2.4 Biocatalytic Transformations

2.4.1 Enzyme production, purification and analysis

2.4.1.1 Scaling up enzyme production (Shake Flasks)

The enzymes used in this study were isolated, tested and cloned by Bawn et al. (2018). transaminase (TAm) and transketolase (TK), isolated from *Deinococcus geothermalis* DSM11300, were cloned into separate BL21 (DE3) *E.coli* cells using a pET29+ plasmid (Invitrogen, Carlsbad, USA) with a IPTG inducible promoter, a kanamycin resistance gene and a His6 tag to facilitate purification (Hannig and Makrides, 1998). To scale up the *E. coli*-BL21 (DE3)-TAm and *E. coli*-BL21 (DE3)-TK strain culture and the production of the respective enzymes, the original enzyme production and expression strategy was tested in 250 mL baffled plastic shake flasks (20% v/v fill volume) using standard aseptic techniques. The influence of Luria Bertani broth (LB) and Terrific Broth (TB) (Fisher Scientific, Hampton, USA) were compared. Then, the induction strategy was compared by either inducing during the mid-exponential phase or during the late exponential phase. For this, 10 mL of LB were inoculated with a scraping of either TAm or TK expressing *E. coli* glycerol stocks and 50 µg.mL^{-1} of kanamycin was added from a 1000-fold concentrated stock solution. The inocula were left in a shaking incubator overnight at 37 °C and in the morning, each flask was inoculated with the overnight culture to a starting OD of 0.1. The flasks were kept shaking at 250 rpm and at 37 °C. Induction was carried out with 1mM IPTG using a 1000-fold concentrated stock solution. The induction occurred either 4 or 7 hours after inoculation. The incubator temperature was lowered to 25 °C, 7 hours after inoculation; and left overnight. In the morning the cultures were harvested by centrifugation (30 min, 15,000g in a 50 mL Falcon tube). Optical Density ($OD_{600\ nm}$) measurements were taken throughout the course of the fermentation and SDS-PAGE analysis was conducted as described in Section 2.4.1.8 on end-of-run samples.

2.4.1.2 Enzyme production in STR

To produce the enzymes at larger scale a jacketed, stainless steel STR bioreactor with a 15 L working volume (Sartorius, Goettingen, Germany) was used. TB media was prepared as described in Section 2.4.1.1 and sterilised in place after the addition of glycerol. pH was maintained via 12.5% v/v Ammonia or 8.5% v/v Orthophosphoric acid (Fisher Scientific, Hampton, USA) at pH 6.00, whilst dissolved oxygen (DO) was maintained at 30%. After STR fermentation following the same timings and conditions as set out in in Section 2.4.1.1, cells were harvest by centrifugation and stored in 50 mL falcon tube at -20 °C. Each falcon tube contained cells from the equivalent of 200 mL of cell culture.

2.4.1.3 Enzyme Release (Sonication)

Cell pellets containing the equivalent of 200 mL of cell culture were resuspended in 15 mL of either N1 buffer (Section 2.4.1.4) or 50 mM HEPES pH 8 buffer (Sigma Aldrich, St Louis, USA) depending on the requirements. Cells were then sonicated in a Soniprep sonicator (MSE, Sanyo, Japan) with 3 cycles of 45s ON/60s OFF with an amplitude of 10 µm. The lysed cells were then placed in 2 mL centrifugation tubes and spun for 20 minutes 4 °C at 21,130g. The supernatant was then removed for further purification or for direct use (clarified cell lysate).

2.4.1.4 Immobilized Metal Affinity Chromatogaphy Purification

TAm and TK enzymes were isolated and purified using Immobilized Metal Affinity Chromatography (IMAC), employing the interaction between the His6 tag attached to the enzymes and nickel-chelated beads (Schmitt, Hess and Stunnenberg, 1993). Three buffers were prepared with varying concentration of imidazole. N1 (10 mM Imidazole, 50 mM NaH_2PO_4, and 300 mM NaCl at pH 8.0), N2 (20 mM Imidazole, 50 mM NaH_2PO_4, and 300 mM NaCl at pH 8.0), and N3 (250 mM Imidazole, 50 mM NaH_2PO_4, and 300 mM NaCl at pH 8.0). A prepacked 5mL Nickel-Nitrilotraicetic Acid (Ni-NTA) Superflow cartridge (Qiagen, Hilden, Germany) was loaded using Luer-lock syringes, fed via a syringe pump. The stages of the setup are summarised in Table 2.2. Before storage at 4 °C, 50% w/v ammonium sulphate was added to the eluate fraction to precipitate the enzymes. To utilise the purified enzymes they were first spun at 21,130g for 20 minutes at 4 °C, separated from the solution containing ammonium sulphate, and then resuspended to the desired concentration in the required buffer.

Table 2.2. Steps, buffers, volumes and flowrates used to separate and purify TAm and TK enzymes using IMAC. Enzymes produced as described in Section 2.4.1.2.

Step	Buffer	Volume (mL)	Flowrate (mL min^{-1})
Flush and Equilibration	N1	50	5
Loading	Clarified Cell lysate in N1	5	2
Wash 1	N1	50	5
Wash 2	N2	30	5
Elute	N3	30	2
Clean	0.5 M NaOH	30	1
Storage	20% v/v Ethanol	20	1

2.4.1.5 Enzyme release (Homogenisation)

High pressure homogenisation was investigated as a scalable alternative to sonication (Bláha *et al.*, 2018) using a Lab40 high pressure homogeniser (APV Gaulin, Mills, USA). Falcon tubes containing frozen cell paste equivalent to 200 mL of cell culture, or approximately 4.0 grams, were resuspended in 40 mL of 50 mM HEPES pH 8. The homogeniser was operated at 800 bar with 3 passes. To avoid overheating the machine and the samples, glycol at 6 °C was circulated through a cooling coil around the system for 30 minutes prior to the start, and throughout the duration of the experiments. To study the effect of passes on enzyme release, 300 µL of homogenate were taken after each pass, clarified by centrifugation at 21,130xg for 10 min and used in bioconversion reactions as described in Sections 2.4.2.2 and Section 2.4.2.3.

2.4.1.6 Heat precipitation of clarified cell lysate

An alternative to IMAC purification, was the exploitation of the heat resistant characteristics of the themostable TAm and TK enzymes to enable selective precipitation (Patchett *et al.*, 1989). To investigate the partial purification of the clarified cell lysate via heat precipitation 1 mL samples in centrifuges were held over a range of times (5, 10, 15 and 20 minutes) and temperatures (50 °C and 55 °C). The heat precipitated samples were then spun down at 21,130g for 20 minutes at 4 °C. The liquid fraction was decanted and either used immediately for enzymatic reactions and small amounts (~100 µL) were stored at -20°C for subsequent SDS-PAGE analysis as described in Section 2.4.1.8.

2.4.1.7 Bradford Total protein assay

The total protein content of solutions was determined using the Bradford assay (Bradford, 1976). Briefly, 1 mL of Bradford assay reagent (Bio-Rad, Hercules, USA) was allowed to react with 30 µL of sample solution at room temperature for 10 minutes before measuring the absorbance at 595 nm. Serial dilutions of a Bovine Serum Albumin (BSA) (Sigma Aldrich, St Louis, USA) standard at 1 g L^{-1} until 0.03125 g L^{-1} (1 in 32 dilution) were used as a standard curve as shown in Appendix 9.2.

2.4.1.8 Sodium dodecyl sulphate polyacrylamide gel electrophoresis (SDS-PAGE)

To analyse expression and the approximate concentration of the TAm and/or TK enzymes SDS PAGE was also employed. 3 µL of protein solutions were mixed with 72 µL of water and 25 µL of 4X NuPAGE LDS sample buffer (Novex, Waltham, USA), and incubated at 72 °C for 10 minutes. The samples were subsequently loaded onto NuPAGE® Bis-Tris Mini Gels, alongside 4 µL of PageRuler prestained protein ladder (Novex, Waltham, USA) and run using 20X MOPS buffer (ThermoFisher Scientific, Waltham, USA) (50 mM MOPS, 50 mM Tris Base, 0.1% SDS, 1 mM EDTA, pH 7.7) at 200 volts for 50 minutes. Gels were stained with InstantBlue™ (Sigma Aldrich, St Louis, USA) for 1 hour and de-stained with deionised water overnight on a shaking platform, to be imaged the next day on an Amersham imager 680 (GE Life Sciences, Chicago, USA). TAm and TK were recognized visually by comparison to the prestained protein ladder due to their known sizes, 45.2 kDa and 71.5 kDa, respectively.

2.4.2 Free enzyme reactions

2.4.2.1 Buffers, substrates and standard reaction conditions

Typical bioconversion reactions using either TAm, TK or a combination of both enzymes were carried out in HEPES 50 mM pH 8. However, substrates and cofactors, for both TAm and TK reactions, were prepared in de-ionised ultrapure water (18 MΩ). A more concentrated HEPES buffer (200 mM pH 8) was prepared and used to ensure the final HEPES concentration remained at 50 mM. pH corrections for HEPES buffers was carried out at 50 °C, as a pH drop was noticed with increase in temperature. 1 M solutions of L-serine, L-arabinose, lithium hydroxypyruvate (Li-HPA) and α-ketoglutaric acid were prepared and stored in aliquots at -20 °C until required. A TAm cofactor pyridoxal-5'-phosphate solution (PLP) at 10 mM pH 7 was also prepared. A TK cofactors solution containing 48 mM thiamine pyrophosphate (ThDP) and 153 mM magnesium chloride ($MgCl_2$) was also prepared to pH 7. The two cofactor solutions had a concentration factor of 50-fold and 30-fold respectively.

Standards for HPAEC-PAD analysis were prepared from analytical grade powders (Sigma Aldrich, St Louis, USA) with the exception of L-gluco-heptulose, which was synthesised and characterised at preparative scale for a previous study (Subrizi *et al.*, 2016).

Unless stated otherwise all batch enzymatic reactions had a total working volume of 1200 µL in 2.0 mL centrifuge tubes, with an individual free enzyme loading of 10% v/v, meaning that if the two enzymes were used together in a one-pot two-step reaction, each enzyme would

make up 10% v/v, for a total of 20% v/v. The reactions were carried out in 50 mM HEPES pH 8.0 at 50 °C in an Eppendorf Thermomixer shaken at 1000 rpm. Under standard reaction conditions L-serine and α-ketoglutaric acid concentration were kept at 10 mM each and L-arabinose and HPA concentrations were kept at 33 mM. For the one-pot two-step reaction the concentrations were kept the same, but no Li-HPA was added.

Enzyme activities were calculated by measuring the slope of the product concentration over the first two hours of the reactions (samples taken every 15 minutes). After the first two hours samples were taken after: 4, 6, 19 and 24 hours. Concentrations of substrates and products were measured by HPAEC-PAD as described in Section 2.5. Sample calibration curves are shown in Appendix 9.3.

2.4.2.2 Transaminase bioconversion

TAm catalyses the production of HPA from L-serine and α-ketoglutaric acid with the aid of the PLP cofactor (Figure 1.6). Unless stated otherwise reactions were carried out at 10% v/v enzyme loading, using HEPES 50 mM pH as a reaction buffer. TAm was always prepared fresh before the start of the experiment as described in Section 2.4.1.3. The clarified cell lysate would be added to 2 mL centrifugation tubes with buffers and cofactor 30 minutes prior to the addition of substrates to initiate the reaction. 25 µL samples were taken over the course of the reaction and quenched with an equal volume of 0.5% v/v trifluoroacetic acid (TFA) (Sigma Aldrich, St Louis, USA). Different reaction conditions were tested to characterise the enzyme activity. Buffer pH was changed from 6.5 to 8.5 at 0.5 intervals. Different substrate concentrations were tested (5, 10, 20, 50 and 100 mM of L-serine and α-ketoglutaric acid, whilst keeping the other substrate at 10 mM); and different enzymatic loadings were investigated (5% v/v, 10% v/v, 26.6% v/v and 40% v/v) using homogenate cell lysate rather than sonicated cell lysate.

2.4.2.3 Transketolase bioconversion

The TK catalysed reaction, using $MgCl_2$ and ThDP as cofactors, converted L-arabinose and HPA into L-gluco-heptulose (Figure 1.6). The TK catalysed reaction was investigated for effects of pH (6.5 to 8.5); different substrate conditions (5, 10, 20, 33, 50, 100 mM of L-arabinose and HPA); different enzymatic loadings (5% v/v, 10% v/v, 26.6% v/v and 40% v/v using homogenate cell lysate rather than sonicated cell lysate); and temperature (37 °C, 50 °C, 60 °C and 70 °C).

2.4.2.4 One-pot, two-step enzymatic batch synthesis of L-gluco-heptulose at varying scales

The one-pot, two-step enzymatic reaction was carried out at various scales. 10% v/v enzyme loading was used for both TAm and TK and all reactions were carried out at 50 °C. Both enzymes were allowed to incubate together with their cofactors prior to the addition of the substrates. Different substrate amounts were tested at small scale as shown in Table 2.3. The reaction was then carried out at a 10 mL scale, in a Falcon tube, and at a 50 mL scale in a 250 mL flask. Samples were taken at 15 minute intervals over the first two hours and then after 4, 6, 19 and 24 hours. Samples were quenched with an equal volume of 0.5 v/v TFA, stored at -20 °C until analysis by HPAEC-PAD as described in Section 2.5.

2.4.2.5 One-pot two-step synthesis L-gluco-heptulose using SBP-derived L-arabinose

An L-arabinose-rich pretreated slurry was obtained from a previous project employing steam explosion of SBP followed by a selective enzymatic depolymerisation by AraF (Cárdenas-Fernández *et al.*, 2018). This slurry contained approximately 21.5 mM of L-arabinose and other monomeric sugars. The viability of the slurry as a potential sustainable source of L-arabinose for the production of L-gluco-heptulose was investigated by comparing performance of the slurry versus a control using the reagent-grade L-arabinose. This comparison was done by matching substrate concentrations (control: 14 mM of L-serine, α-ketoglutaric acid and L-arabinose; and slurry: 14 mM of L-serine and α-ketoglutaric acid, and 65% v/v of total volume of slurry to obtain 14 mM of L-arabinose). The slurry was tested in small scale (1.2 mL), in 50 mL flasks and in the ACR as described in Section 2.4.2.6.

2.4.2.6 One-pot two-step continuous synthesis of L-gluco-heptulose in ACR

The ACR was set up as described in Section 2.1.1 with a total flowrate was 65 $mL.hr^{-1}$, equating to a 2 hour residence time and an agitation frequency of 6 HZ was employed. To allow the enzymes and cofactors to incubate for 30 minutes prior to coming into contact with the substrates, two inlet feeds were created. The main process feed contained the substrates, whilst the side-stream feed contained the TAm and TK enzymes. This enzyme feed was pumped at a flowrate equivalent to 30% of the total flowrate in the ACR, and the feed comprised the two clarified enzyme enzyme lysates (10% of total flowrate, each), prepared as described in 2.4.1.3, and cofactors and HEPES buffer pH 8. The enzyme feed was pumped via a syringe pump through a length of PEEK tubing with 30 minute residence time.

Table 2.3. Substrate concentrations for the one-pot two-step enzymatic synthesis of L-gluco-heptulose. Experiments performed as described in Section 2.4.2.4

Experiment number	L-arabinose concentration (mM)	L-serine concentration (mM)	α-ketoglutaric acid concentration (mM)
1	33	10	10
2	33	20	20
3	33	33	33
4	50	50	50
5	100	100	100
6	200	200	200

The process fluid consisted of L-Serine, L-Arabinose, and α-ketoglutaric acid, and made up the remaining 70% of the total flowrate. The two fluids met and mixed in the first reaction cell and samples were taken at the outlet.

ACR runs carried out to investigate the production of L-gluco-heptulose used: 10% v/v TAm and TK; 2 hour residence time (65 mL hr^{-1}); HEPES 50 mM pH 8; 50 °C operating temperature and a 6 Hz agitation rate. Samples were taken every 30 minutes and quenched with an equal volume of 0.5% v/v TFA. The first run used 33 mM L-arabinose, 10 mM L-serine and 10 mM α-ketoglutaric acid as the substrates. The second run investigated the effects increasing the substrate concentrations from 33 mM L-arabinose, 10 mM L-serine and 10 mM α-ketoglutaric acid to 100 mM L-arabinose, 100 mM L-serine and 100 mM α-ketoglutaric acid. The third run compared L-gluco-heptulose synthesis using the SBP derived L-arabinose feed (containing also 14 mM each of L-serine and α-ketoglutaric acid) and the same reaction with lab-procured substrates (14 mM each of L-serine, L-arabinose and α-ketoglutaric acid).

2.4.3 Enzyme immobilization and immobilized enzyme bioconversion

2.4.3.1 IMAC resin Immobilization

To immobilize the enzymes a first attempt was made using Ni-NTA resin (Qiagen, Hilden, Germany). A 10:1 solution of sonicated, clarified cell lysate in N1 buffer (Section 2.4.1.4) was mixed with Ni-NTA resin in a Falcon tube. The tubes were gently mixed at room temperature for 90 minutes and samples were taken over the course of the procedure. Thereafter, the Falcon tubes were gently spun down at 4 °C 1,000g for 5 minutes. The clarified cell lysate was then discarded and N2 buffer (see Section 2.4.1.4) was added as a wash step. The tube was gently mixed for ten minutes and then spun down again at 4 °C 1,000g for 5 minutes. The N2 buffer was also discarded and the resin was stored as a pellet at 4 °C until it was used in reactions as described in Section 2.4.3.3.

2.4.3.2 Epoxy resin immobilization

The epoxy resins, ECR8204F and ECR8204M by Purolite (King of Prussia, USA) were tested as a potential more economical alternative to IMAC immobilization. Both resins were sized in the Masterizer 3000 (Section 2.1.3, refractive index of 1.53) by laser diffraction. Following this, immobilization studies were carried out using the ECR8204M resin (ECR from hereon). Both TAm and TK clarified cell lysates were diluted in a sodium bicarbonate buffer (1M pH 10) and placed in Falcon tubes in a ratio of 10:1 with the epoxy carriers. The resin beads were

gently mixed in the sodium bicarbonate buffer overnight at room temperature and recovered through vacuum filtration. The beads were then incubated for 20 minutes with a desorption buffer (0.5 M NaCl in 10 mM Tris-HCl pH 7). The recovered beads were then briefly mixed with a washing buffer (10 mM Tris-HCl pH 7) for 1 minute before being recovered again by vacuum filtration and stored at 4 °C in sealed containers.

Different amounts of enzyme per gram of resin were tested (10 mg_{enzyme} g_{resin}^{-1}, 50 mg_{enzyme} g_{resin}^{-1}, and 100 mg_{enzyme} g_{resin}^{-1}) as well as co immobilizing TAm and TK enzymes with a concentration of 50 mg_{enzyme} g_{resin}^{-1} each. Eventually, TAm immobilization was also attempted with a modified immobilization buffer containing TAm cofactor (0.2 mM PLP, 1 M $NaHCO_3$ pH 10). All enzymatic reactions with immobilized enzymes contained 5% w/v enzyme loading of each enzyme (i.e. 5% w/v of TAm and 5% w/v of TK for the one-pot two-step reaction).

2.4.3.3 Immobilized enzyme bioconversion

Ni-NTA and epoxy immobilized TAm and TK enzymes were used in both single enzyme bioconversions and one-pot two-step bioconversions. For the stand-alone bioconversions, 5% w/v of either immobilized TAm or TK were taken by carefully weighing 60 mg of resin for 1200 µL reactions. For the one-pot two-step reaction 60 mg each of immobilized TAm and TK were used. 10 mM of α-ketoglutaric acid and L-serine were used as substrate for TAm catalysed production of HPA. 33 mM of L-arabinose and Li-HPA were used for the TK catalysed production of L-gluco-heptulose. For the one-pot two-step production of L-gluco-heptulose, 10 mM α-ketoglutaric acid, L-serine and 33 mM L-arabinose were added. Addition of Li-HPA was omitted except for one instance using epoxy immobilized TAm and TK. Prior to the start of the reaction, by addition of the substrates, the enzymes were incubated for 30 minutes in 50 mM HEPES pH 8 buffer containing the enzyme cofactors (0.2 mM PLP and 1.6mM ThDP and 5.1 mM $MgCl_2$ for TAm and TK, respectively). The reactions were carried out in 2 mL centrifugation tubes used as reaction vessel. As in the free enzyme reactions, the tubes were agitated at 1000 rpm in a Thermomixer and kept at 50 °C. 25 µL of reaction mix was taken for sampling and mixed with 25 µL with 0.5% v/v TFA to quench the reaction. Samples were taken every 15 minutes for the first 2 hours and then after 4 and 6 hours and again after 19 and 24 hours.

2.5 High Performance Anion Exchange Chromatography – Pulsed Amperometric Detection (HPAEC-PAD)

Formation of products of both pretreatment reactions and enzymatic bioconversions (Section 2.2, Section 2.3 and Section 2.4) was monitored via High Performance Anion Exchange Chromatography with Pulsed Amperometric Detection (HPAEC-PAD). A PA-10 column (Thermo Scientific) was set up in a Dionex 5000 Ion Chromatography System. Isocratic elutions were carried out at 0.250 mL min^{-1}. For analysis of neutral sugars from pretreatment reactions, such as L-arabinose, D-galactose, D-glucose and L-rhamnose a 7.5 mM KOH elution was used. D-galacturonic acid, on the other hand, was analysed separately by using a 50 mM Sodium acetate elution. To calculate pretreatment yield these samples were also processed as described in Section 2.3.3. Finally, L-gluco-heptulose and HPA were eluted at 30 mM KOH. Analysis was carried out using the provided Chromeleon 7.0 software with external standards. Calibration curves and standard chromatograms are provided in Appendix 9.3.

3

Characterisation of Sugar Beet Pulp slurry rheology, particle size distribution, and Agitated Cell Reactor performance

3.1 Introduction

Prior to investigating sugar beet pulp pretreatment and monosaccharide bioconversions into platform chemicals within a continuous flow reactor, it is necessary to understand and characterise the systems that will be employed. Since the intended conversions involve both homogenous and heterogeneous reactions (Section 1.5), it is essential to understand how the ACR would handle single-phase liquids or a solid-liquid dispersion.

Understanding the rheology of process fluids can help predict behaviour inside the reactor and therefore, is paramount for system characterisation. An especially important rheological parameter is the viscosity of SBP dispersions. Viscosity is the ratio between shear stress and shear rate exerted on the fluid (Metzner and Otto, 1957). A Newtonian fluid has the same viscosity at different shear rates, whilst non-Newtonian fluids can have differing relationships between viscosity and shear rate. As an example, a shear thickening fluid will have a greater viscosity at larger shear rates, whilst shear thinning fluids have lower viscosity at higher shear rates. Many bioprocessing fluids tend to exhibit shear-thinning behaviour, which can impact on how reactors and reactions are operated (Metzner and Otto, 1957; Kindstedt, 1993).

Another aspect of SBP dispersions is the particle size. In a biorefinery context, particle size reduction plays an important part in increasing the efficiency of pretreatment operations by increasing the surface area available for "attack" by chemical or enzymatic treatments (Holtzapple, Humphrey and Taylor, 1989). A number of size reduction technologies, such as knife mills, ball mills and hammer mills are available at various scales with differing power consumption. (Licari *et al.*, 2016; Wendt *et al.*, 2018). Characterising the particle size distribution of the SBP used in the ACR would provide further insight into the properties of the solid-liquid dispersion.

As mentioned in Section 1.5.1, the ACR is a continuous reactor consisting of 10 interconnected cells, which could be visualised as 10 separate stirred tanks that are placed in series. This design also allows for an easy characterisation of the ACR performance. The tanks-in-series approach is a widely used method to determine the probabilistic distribution of the exit time of a fluid from the reactor, also known as the residence time distribution (RTD). The underlying theory is that a continuously stirred tank reactor (CSTR) has a lower volumetric efficiency than a plug flow reactor (PFR); meaning that a larger CSTR volume will be required to achieve the same level of conversion (Britton, Majumdar and Weiss, 2018).

By using experimental data it is possible, using mathematical models, to characterise a reactor in terms of how many interconnected theoretical CSTRs it is equivalent to (Scott Fogler, 2008; Gao, Muzzio and Ierapetritou, 2012). The number of interconnected CSTRs is also known as the equivalent number of tanks, N; and generally the higher the N, the better the volumetric efficiency of the reactor, and the more efficient the reactor. In the case of the ACR, different operating conditions such as flowrate, system viscosity and agitation rate could have an effect on N. As such, the effect of these parameters should be characterised in any novel bioreactor design (Levenspiel, 1999).

Finally, using a model system to characterise the reactor can provide interesting insights, but effort should be made to ensure that the model system behaves as close as possible to the real conditions. This is especially challenging in the case of the SBP pretreatment reactions, where solids are also passed through the reactor. Differently sized solids could travel through the reactor at different speeds. As such, a characterisation method that accounts for size should be implemented. Reactor characterisation studies present in the literature propose a number of possible solutions such as assuming that solids of different sizes travel at the same speed, using detectable radioactive or fluorescent tracers or even using laser diffraction (Pareek *et al.*, 2001; Harris, Davidson and Thorpe, 2003; Bhusarapu, Al-Dahhan and Dudukovic, 2004; Sievers *et al.*, 2016). Whilst no reports were found in the literature showing the implementation of laser diffraction to determine particle travel time based on size, this technique could be applied to characterize the ACR.

3.2 Aim and Objectives

The aim of this chapter is to establish a window of optimal operating conditions for the ACR in terms of flow rates and solids loading. Mixing and mass transfer effects may play important roles in the reactions studied so ensuring that the ACR can operate at the conditions required is essential. One of the main challenges is for the ACR to handle solids. Previous reports have shown the ability of the ACR to cope with the formation of an N-iodomorpholinium salt product up to 0.091 M or 30.9 $g.L^{-1}$ during processing, however, SBP solids used are much larger and may pose more challenges during processing (Browne *et al.*, 2011).

This chapter uses the derivation of the RTD and the equivalent number of tanks to measure and compare ACR performance with different mixing and flow conditions and feed properties. It combines this with viscosity measurements to determine the rheological behaviour of SBP slurries and with diffractive light scattering measurements to analyse if particle size affects residence time distribution. The key objectives are outlined below:

- Determine the basic rheological characteristics of SBP slurries.
- Ascertain the particle size distribution (PSD) of the milled SBP.
- Understand, compare and evaluate the performance of the ACR for a range of differing mixing and flow conditions.
- Understand the effect of solids presence on the ACR performance and specifically how particle size distribution influences solids residence time.

3.3 Results

3.3.1 Feed material characterisation

3.3.1.1 Rheological behaviour

Initial work focused on assessing the rheological properties of SBP slurry. This would reveal the range of viscosities that the ACR reactor would have to work over. Additionally, no information of shear rates inside the ACR is currently available and estimation of shear through computational fluid dynamics models was beyond the scope of this thesis. Thus obtaining information as to the rheological behaviour of the SBP slurry viscosity with increasing shear would enable the characterisation of the ACR performance using Newtonian fluids of known viscosity.

Figure 3.1 shows the measured viscosity as a function of shear rate for various SBP slurry concentrations using SBP that was sieved through a 212 µm mesh sieve. A shear thinning effect was observed for all SBP concentrations. Shear thinning properties are not uncommon in biorefinery contexts. Anaerobic digestate and pretreated softwood slurries, for example, have been shown to exhibit the same behaviour (Palmqvist *et al.*, 2016; Gienau, Kraume and Rosenberger, 2018). SBP slurry viscosities were found to be close to water at low solids concentration (0.0011 Pa.s compared to 0.001 Pa.s for water at 25 °C), whilst they were much larger at higher SBP concentrations. For example, at 10% w/v SBP slurry viscosity was between 25 and 33 times larger than water viscosities at the same conditions. It was also noticed that the measurements became less precise, both absolutely and relatively, at higher SBP concentrations. The standard error of the mean (SEM) as a percentage of the viscosity was found to be less than 5% for the 1% w/v SBP slurry and between 13.9% and 17.4% for the 10% w/v SBP slurry.

This increased imprecision could be due to an effect called wall depletion or “slip” (Barnes, 1995). Briefly, in two-phase fluids the dispersed phase (in this case SBP) is displaced creating a thin “depleted” boundary layer near the walls of the rheometer. This depleted boundary layer consisting of the liquid phase (water, in this case) flows more easily than the rest of the solution giving rise to an effect dubbed “slip”. This slip effect appears to be larger with solutions containing more of the dispersed phase.

To reduce this effect vanes could be employed in the rheometer; and sometimes rheometer walls are roughened to increase adherence and reduce slippage (Barnes, 1995). Palmqvist et al. used a special 4-bladed vane attachment with a splined cup on the Kinexus rheometer (Malvern Panalytical, Malvern UK) to reduce slip in the studying of steam pretreated softwoods.

Figure 3.2 shows in more detail the effect of SBP concentration on the measured viscosity. Whilst at low SBP concentrations the viscosity can be seen to remain close to the viscosity of water; as the concentration increases, so does the viscosity. A higher viscosity could also be seen at lower shear rates, again indicating the shear thinning behaviour of the SBP slurry. Polynomial fits of second order were used on the data sets to provide quadratic equations for each shear level. These are shown below (with 'SBP' representing the SBP slurry concentration):

$\boldsymbol{At\ 100\ s^{-1}}$:

$$\textbf{viscosity}\ (\boldsymbol{Pa.s}) = \mathbf{3.692\ x\ 10^{-4}\ x}\ \boldsymbol{SBP^2} - \mathbf{9.442\ x\ 10^{-4}\ x}\ \boldsymbol{SBP} + \mathbf{0.00175}$$

[Equation 3.1]

$\boldsymbol{At\ 500\ s^{-1}}$:

$$\textbf{viscosity}\ (\boldsymbol{Pa.s}) = \mathbf{2.931\ x\ 10^{-4}\ x}\ \boldsymbol{SBP^2} - \mathbf{7.124\ x\ 10^{-4}\ x}\ \boldsymbol{SBP} + \mathbf{0.0016}$$

[Equation 3.2]

$\boldsymbol{At\ 1000\ s^{-1}}$:

$$\textbf{viscosity}\ (\boldsymbol{Pa.s}) = \mathbf{2.752\ x\ 10^{-4}\ x}\ \boldsymbol{SBP^2} - \mathbf{6.122\ x\ 10^{-4}\ x}\ \boldsymbol{SBP} + \mathbf{0.00165}$$

[Equation 3.3]

R^2 values were 0.9894, 0.9921 and 0.9970 respectively. A quadratic behaviour of viscosity in relation to solids concentration is not uncommon, and was found for example in anaerobic sludge (Gienau, Kraume and Rosenberger, 2018).

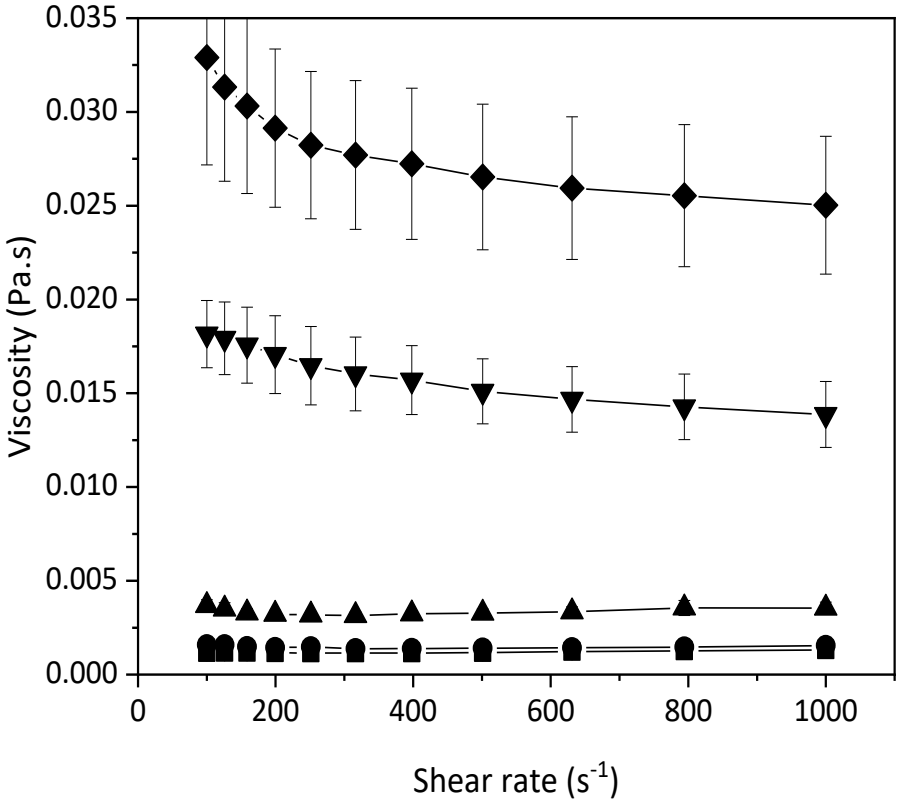

Figure 3.1. Slurry viscosities over a range of shear rates (100 s^{-1} to 1000 s^{-1}) for differing SBP concentrations. SBP concentrations evaluated were: 1% w/v (■); 2% w/v (●); 4% w/v (▲); 8% w/v (▼) and 10% w/v (◆). Error bars denote standard error of the mean, SEM (n=2). Viscosity was determined as described in 2.1.4. Solid lines indicate data trend.

Using a SBP dispersion to evaluate the number of tanks, N, would be challenging as the shear forces exerted within the ACR have not been quantified and the viscosity of the dispersion would be affected by the shear in each section of the reactor. Instead, a Newtonian fluid (i.e. a fluid whose viscosity is not affected by shear rate) could be employed to determine the ACR performance. For example, water and glycerol could be used together in solutions of differing concentrations so that a range of viscosities can be obtained (from 0.001 Pas for pure water to 1.412 Pas for pure glycerol at 25 °C (Ferreira *et al.*, 2017)). An additional remark is that both the rheological work presented in this Section and the determination of the equivalent number of tanks, N, presented in Section 3.3.2 was carried out at room temperature instead of the higher temperatures used in the pretreatment and enzymatic reactions studied in subsequent chapters. This was done to reduce hazards in the laboratory. Additionally, fluids become less viscous at higher temperatures meaning that, if higher viscosity were to hamper ACR performance, it would do so more at lower temperatures.

3.3.1.2 Ground sugar beet pulp particle size distribution

On the recommendation of the ACR manufacturer, to avoid blockages within the reactor, a rule of thumb regarding maximum particle size in the reactor was applied. The rule states that the particles should be smaller than 10% of the smallest dimension in the reactor. In the ACR, the interconnecting channels between the cells are rectangular in cross section, 4 mm wide, and 4 mm high, as such a maximum particle size of 400 µm was employed. Following grinding of the dry SBP in a ball mill as described in Section 2.2.1 the powder was passed through a series of screens, with mesh sizes of 1000, 500 and 212 µm to obtain differently sized fractions. The PSD of the fractions collected after each sieve was measured and is shown in Figure 3.3. The sieving produced intermediate fractions with narrow distributions; on the other hand, the smallest fraction (i.e. particles in sizes between Particles >0 µm and <212 µm) had a less symmetrical PSD as can be seen from the tail of the solid line. This is likely due to the lack of a smaller mesh size that could remove the finest particles. For the powder that passed through the 212 µm sieve, the smallest decile (d10) size was 15 µm, the highest decile (d90) was 446 µm and the median (d50) was 128 µm.

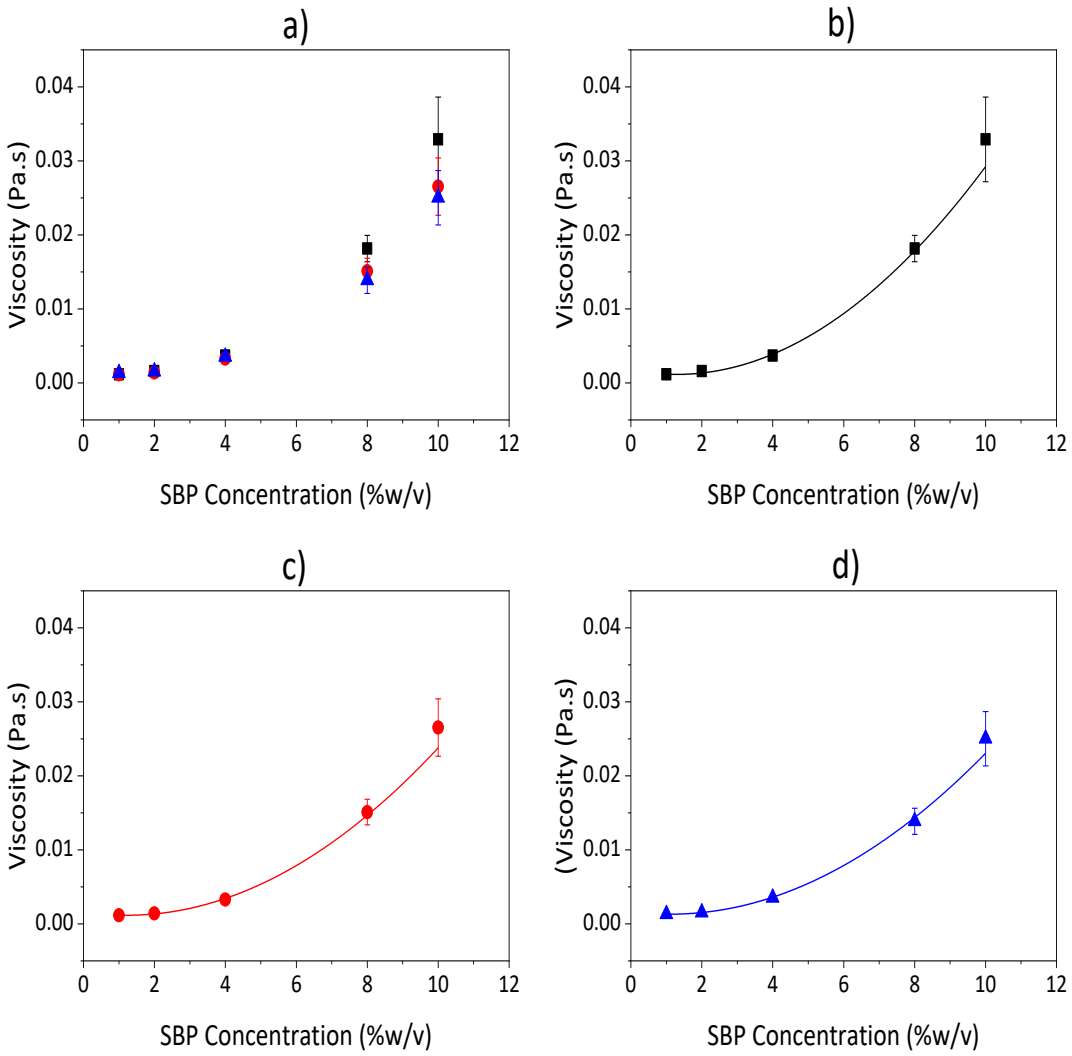

Figure 3.2. Experimental and modelled variation of slurry viscosity versus SBP concentration. Viscosity data from Figure 3.1 as a function of shear rate: (a) 100 s^{-1} (■); 500 s^{-1} (●) and 1000 s^{-1} (▲). Figures (b), (c) and (d) show the viscosities at the individual shear rates (100 s^{-1}, 500 s^{-1} and 1000 s^{-1}, respectively) together with the fitted quadratic models (Equations 3.1 – 3.3). Error bars denote SEM (n=2). Viscosity was determined at 25 °C as described in Section 2.1.4.

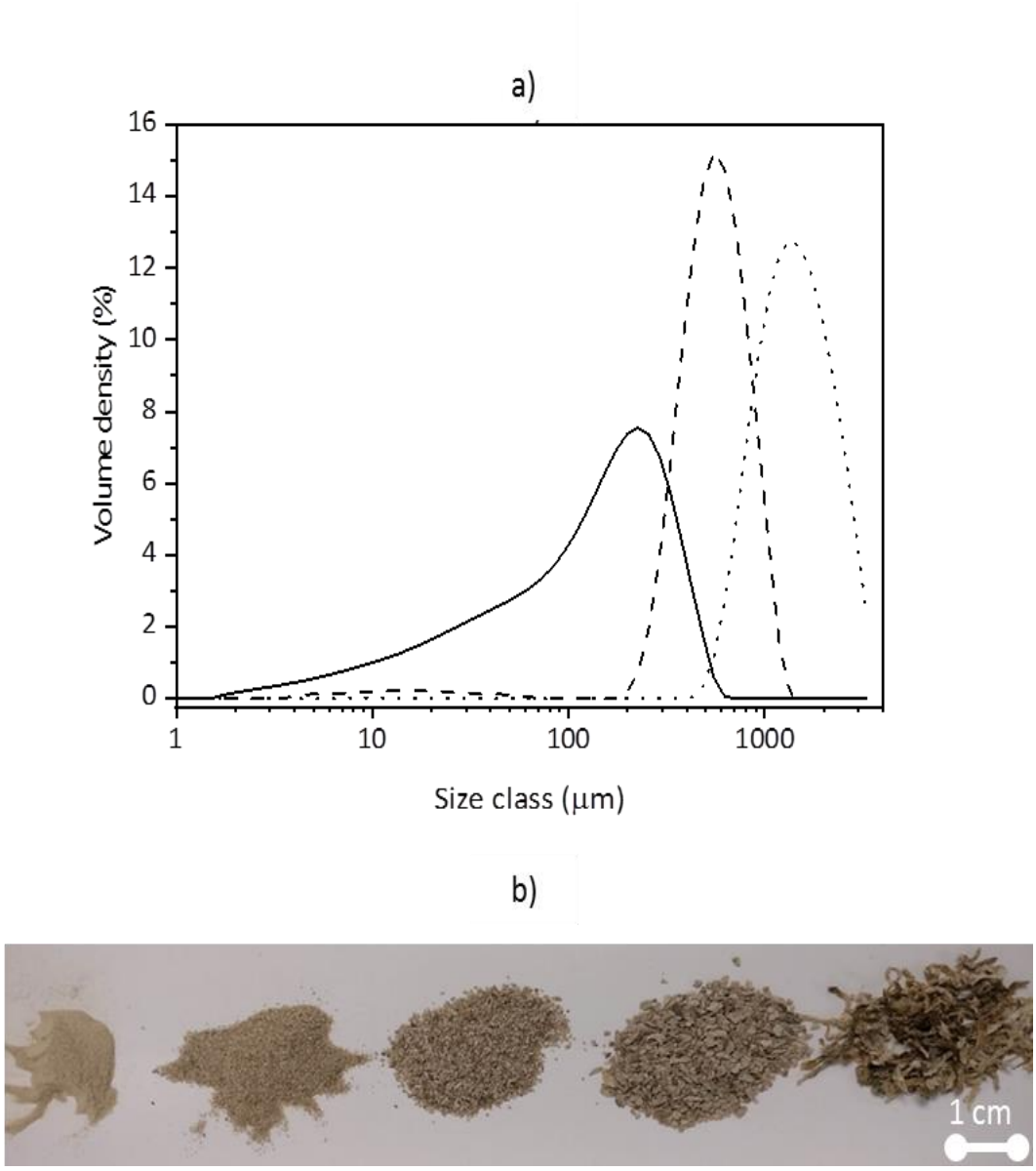

Figure 3.3 Particle size distribution and appearance of milled SBP. The PSD of three fractions (x<212 µm; 212 µm < x <500 µm; and 500 µm < x < 1000 µm) of the milled SBP was measured by laser diffraction and their corresponding PSDs are shown in (a) (solid line, dashed line and dotted line, respectively). (b) shows the appearance of the various milled fractions along with the whole SBP. Milling and sieving, and laser diffraction carried out as described in Section 2.2.1.

The wide range of particle sizes of the milled SBP employed in the ACR highlights the need to consider how differently sized particles will behave in the reactor. This is discussed further in Section 3.3.3. Furthermore, the effect that differently sized particles will have on pretreatment operations is investigated in Section 4.3.1.

3.3.2 ACR Characterisation with single-phase fluid

3.3.2.1 Theoretical determination of number of theoretical tanks

As explained in Section 2.1.2, the main method used to characterise the ACR performance under various mixing regimes was to evaluate the equivalent number of tanks, N. This number represents how many CSTRs would be required to mimic the flow regime of the ACR. A higher N indicates that the reactor is equivalent to more CSTRs in series and therefore has a mixing regime closer to plug flow (when $N \rightarrow \infty$) (Tufvesson *et al.*, 2010). This method has been applied to a wide range of flow reactors, and is an important tool to understand transport phenomena inside the reactor (Gao, Muzzio and Ierapetritou, 2012). Experimentally, N can be determined by using a tracer that is injected at the inlet of the reactor and its concentration is measured at the outlet over time. A tracer is a material that would mix well with the fluid inside the reactor and not affect the flow properties. Two practical methods can be used for the determination of the N number of a reactor: a pulse injection; or a step change. In the former, a small amount of tracer is injected over a very small period of time and the tracer concentration is then measured at the outlet. Although pulse injections allow for a simpler calculation of N, they are harder to set up experimentally (Scott Fogler, 2008).

The N value in this study was determined by analysing the effects of a step change to the ACR system. To understand the derivation better, however, it is easier to first consider a tracer pulse injection setup. As a pulse injected at the reactor entrance, travels through the reactor, the tracer becomes increasingly dispersed along the length of the reactor through effects such as diffusion and backmixing (Wei and Zhu, 1996; Scott Fogler, 2008). This is exemplified in Figure 3.4. This spreading process is represented by the dispersion coefficient D ($m^2.s^{-1}$). A lower dispersion coefficient indicates less spreading, and when D = 0, there is no spreading, meaning that the reactor is operating in plug flow.

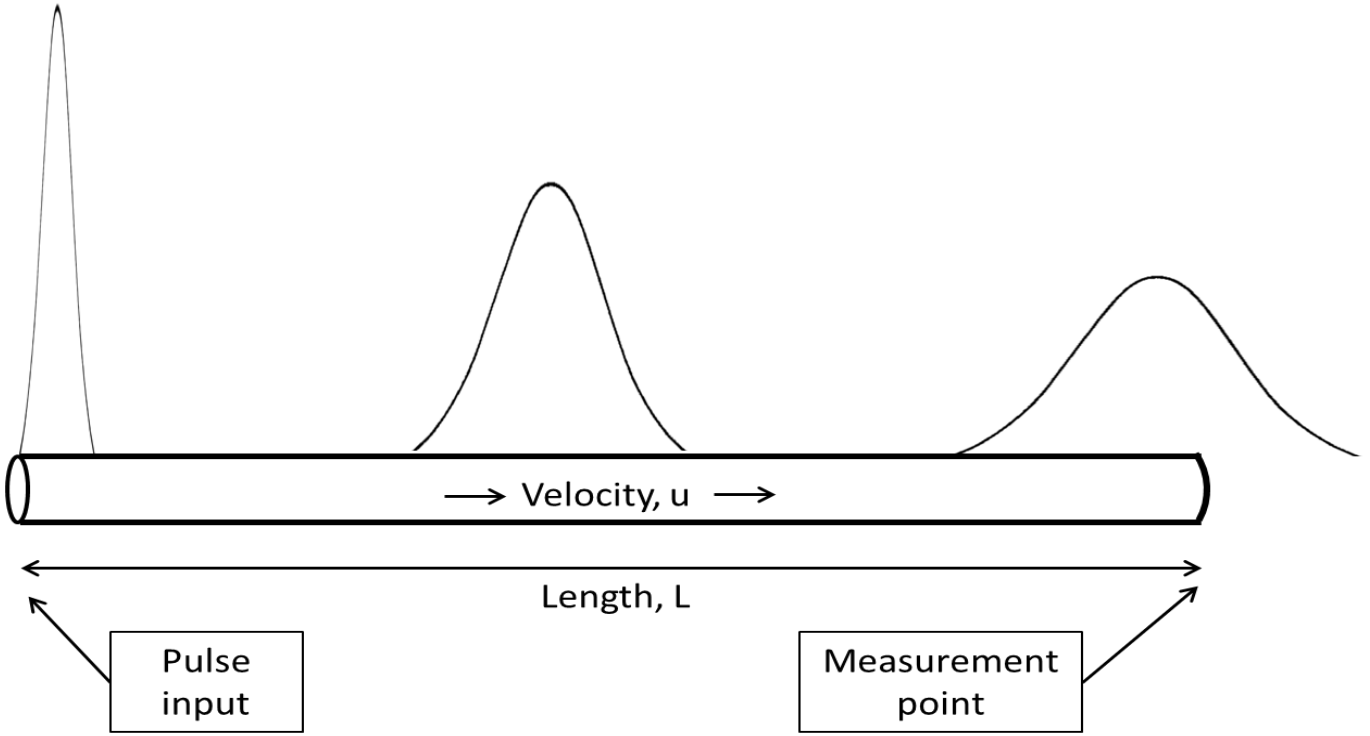

Figure 3.4. Schematic diagram of tracer behaviour along a flow reactor. A reactor, shown here as a pipe, has a pulse input of tracer dye injected at the entrance (left). As the tracer moves through the reactor it becomes progressively more dispersed.

To characterise the whole reactor the dimensionless number D/uL is used, where D is the dispersion coefficient, u is the fluid velocity, and L is the characteristic length of the reactor. To evaluate D/uL the tracer curve needs to be recorded. This is done by evaluating $\overline{t}$ and σ^2. $\overline{t}$ represents the mean passage of time, whilst σ^2 is the variance which measures the spread of the curve. Equations 3.4 and 3.5 show how $\overline{t}$ and σ^2 are calculated both in a continuous (integrals) or discrete (summation) form:

$$\boldsymbol{Let\ \bar{t} = \frac{\int_0^\infty tCdt}{\int_0^\infty Cdt} = \frac{\sum t_i C_i \Delta t_i}{\sum C_i \Delta t_i}} \qquad \text{[Equation 3.4]}$$

$$\boldsymbol{Let\ \sigma^2 = \frac{\int_0^\infty (t-\bar{t})^2 Cdt}{\int_0^\infty Cdt} = \frac{\int_0^\infty t^2 Cdt}{\int_0^\infty Cdt} - \bar{t}^2 = \frac{\sum t_i{}^2 C_i \Delta t_i}{\sum C_i \Delta t_i} - \bar{t}^2} \qquad \text{[Equation 3.5]}$$

where *C* and *t* are the measured concentration at the exit of the reactor and the time at which the measurement took place. It is then possible to combine $\overline{t}$ and σ^2, in one variable that can be related to D; the fluid velocity in the reactor, u and the characteristic reactor length, L.

$$\sigma_\theta^2 = \frac{\sigma^2}{\bar{t}^2} \qquad \text{[Equation 3.6]}$$

$$\boldsymbol{\sigma_\theta^2 = \frac{2D}{uL} - 2\left(\frac{D}{uL}\right)^2\left(1 - e^{-\frac{uL}{D}}\right)} \qquad \text{[Equation 3.7]}$$

From the D/uL value the equivalent number of tanks N can be obtained.

$$\boldsymbol{N = \frac{1}{2}\frac{uL}{D}} \qquad \text{[Equation 3.8]}$$

For a step-change setup, on the other hand, it helps to first imagine an ideal plug flow reactor in which the conditions at the entrance of the reactor are instantly changed (e.g. a different fluid is fed to the reactor). In a perfect plug flow reactor one would expect the same instantaneous step change to be seen exactly one residence time after at the exit of the reactor. On the other hand, a step change in a CSTR will produce a curved response as the reactor is gradually filled to the new feed. Indeed, the response to the step change, often termed F-curve, or F(t), can be modelled with the following equation:

$$\boldsymbol{Response\ = F(t) = 1 - e^{-\frac{n}{t}}\left(\sum \frac{Nt^{N-1}}{(N-1)!}\right)} \qquad \text{[Equation 3.9]}$$

with N representing the number of tanks in series. For example:

$$\textbf{For N} = \mathbf{5}$$

$$\boldsymbol{F(t) = 1 - e^{-\frac{5}{t}}\left(1 + 5t + \frac{5t^2}{2} + \frac{5t^3}{3!} + \frac{5t^4}{4!}\right)}$$

The effect of a step change was modelled using Equation 3.9 on setups with differing number of tanks and is shown in Figure 3.5. It is possible to see that the curve becomes sharper and straighter as the number of tanks increases.

To normalise the response and allow easier calculations, the measurements such as concentration of tracer or time are typically turned into dimensionless, normalised values as shown in Equation 3.10 and 3.11. In this work, where the tracer used was Allura red, a miscible food dye, the absorbance at 504 nm (Abs_{504}) was used to determine concentration as described in Section 2.1.2.

$$\boldsymbol{Normalised\ response_i = \frac{Absorbance_{sample,i} - Absorbance_{background}}{Absorbance_{steate\ state} - Absorbance_{background}}} \quad \text{[Equation 3.10]}$$

$$\boldsymbol{Dimensionless\ time = \frac{time\ after\ step\ change\ occurred}{hydraulic\ residence\ time} = \frac{t}{\tau}} \quad \text{[Equation 3.11]}$$

$$\boldsymbol{Hydraulic\ residence\ time = \tau = \frac{Total\ reactor\ volume}{Flowrate}} \quad \text{[Equation 3.12]}$$

To calculate the equivalent number of tanks, N, from a step change, the first step is to convert the response data into something analogous to a pulse injection. This can be achieved by differentiating the F(t) curve into the so called E(t) curve, as indicated by Equation 3.13.

$$\boldsymbol{E(t) = \frac{dF}{dt}} \quad \text{[Equation 3.13]}$$

Figure 3.6 shows how the E(t) curve for reactor with N = 15 is narrower and taller than the curve for the reactor with a lower equivalent number of tanks. If a pulse injection were to be applied to the same reactors, the same behaviour would be observed: the curve would be narrower and taller for the reactor that is closer to ideal plug flow. So, it is possible to convert the equations for $\bar{t}$ and σ^2 in terms of the E(t) curve rather than a curve obtained from a pulse injection.

$$\bar{t} = \frac{\int_0^\infty tCdt}{\int_0^\infty Cdt} = \frac{\sum t_i C_i \Delta t_i}{\sum C_i \Delta t_i} \quad \text{[Equation 3.4]}$$

$$\bar{t} = \frac{\sum t_i E(t_i)}{\sum E(t_i)} \quad \text{[Equation 3.14]}$$

And:

$$\boldsymbol{\sigma^2 = \frac{\int_0^\infty (t-\bar{t})^2 C dt}{\int_0^\infty C dt} = \frac{\int_0^\infty t^2 C dt}{\int_0^\infty C dt} - \bar{t}^2 = \frac{\sum t_i^2 C_i \Delta t_i}{\sum C_i \Delta t_i} - \bar{t}^2}$$ [Equation 3.4]

$$\boldsymbol{\sigma^2 = \frac{\sum t_i^2 E(t_i)}{\sum E(t_i)} - \bar{t}^2}$$ [Equation 3.15]

At this point, $\boldsymbol{\sigma^2}$ and $\bar{\mathbf{t}}$ are known for the step change. Using Equation 3.6, $\boldsymbol{\sigma_\theta^2}$ can be calculated. By using the GoalSeek function in Microsoft Excel, D/uL can be estimated from Equation 3.7. Then, D/uL can in turn be applied to Equation 3.8 to obtain N.

$$\boldsymbol{\sigma_\theta^2 = \frac{\sigma^2}{\bar{t}^2}}$$ [Equation 3.6]

$$\boldsymbol{\sigma_\theta^2 = \frac{2D}{uL} - 2\left(\frac{D}{uL}\right)^2 \left(1 - e^{-\frac{uL}{D}}\right)}$$ [Equation 3.7]

$$\boldsymbol{N = \frac{1}{2}\frac{uL}{D}}$$ [Equation 3.8]

3.3.2.2 Experimental determination of number of theoretical tanks

To calculate N experimentally, the ACR was set up to allow the main process fluid to be pumped through the main inlet via a peristaltic pump as shown in Figure 3.6. The secondary process fluid, which in this instance was the tracer, was fed through additional tubing and pumped via a syringe pump, in the first reaction cell through the side entry port. A 0.75 m long piece of Masterflex LS/25 flexible silicone tubing (Cole-Parmer, Vernon Hills, USA) was connected to the outlet. This tubing was either directed to a waste collection bucket or, when sampling was required, it was placed in a vial prior to absorbance measurements being made. It is important to note that the outlet tubing contributed to the reactor volume and was included in the calculations.

The calculations outlined in Section 3.3.2.1 were applied to the experimental data; and a sample derivation of N is shown in full below. In this instance, the ACR agitation rate was set to 6 Hz, the peristaltic pump was set to 10 rpm, giving a hydraulic residence time of 15.2 minutes across the reactor. At time 0, the tracer was pumped through the syringe pump at 5 $mL.hr^{-1}$ (approximately 1% v/v of the total flowrate in the reactor). The normalised response obtained is shown alongside the E(t) curve in Figure 3.8.

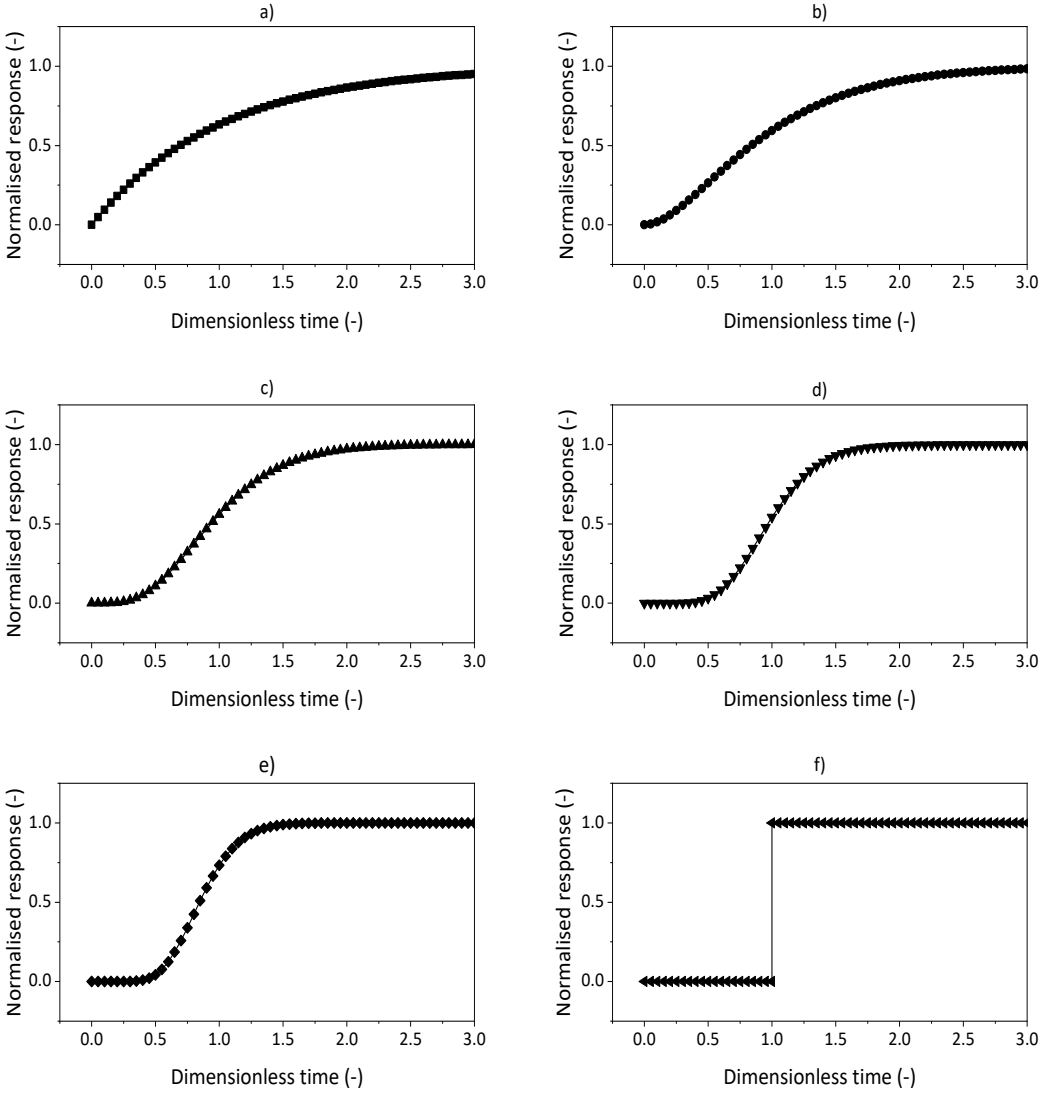

Figure 3.5. Normalised response, F(t), as a function of dimensionless time for different equivalent number of tanks. The normalised response and dimensionless time was calculated as described in Equation 3.9. Varying number of tanks were used: N=1, panel (a), (■); N=2, panel (b), (●); N=5, panel (c), (▲); N=10, panel (d), (▼); N=15, panel (e), (◆); and N=∞, or plug flow reactor, panel (f), (◀).

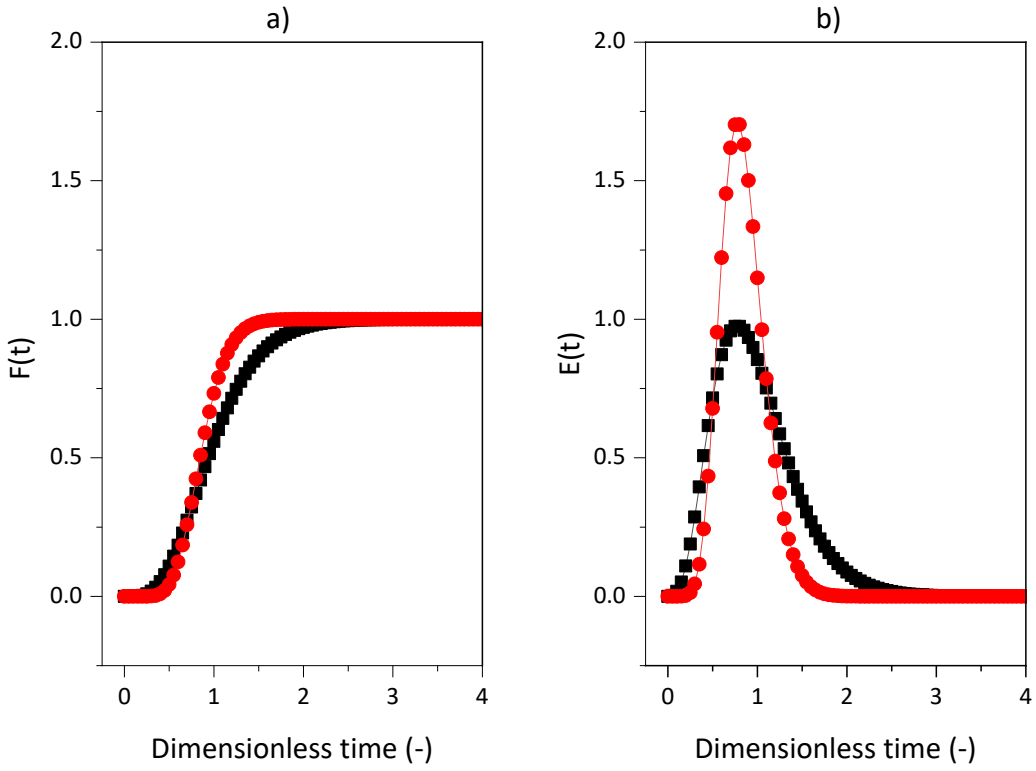

Figure 3.6. Modelled normalised response, F(t) and derived response E(t) over dimensionless time. (a) F(t) curves for a 5 tanks-in-series system (■) and a 15 tanks series system (●). (b) The derivative of F(t) with respect to dimensionless time, E(t), for the same two systems. F(t) or normalised response, and E(t) were calculated from Equations 3.9 and 3.13, respectively.

The experimental curves obtained here, are very similar to the theoretical curves shown in Figure 3.5 and Figure 3.6. It is worth noting that small variations during the measurements of a step change are amplified when they are differentiated; meaning that a small error in the reading can lead to a larger error in the subsequent analysis, which is why pulse injections, if possible, are favoured. To analyse the data it is possible to modify Equation 3.16 for discrete data as shown below

$$\boldsymbol{E(t_i) = \frac{Abs_i - Abs_{i-1}}{t_i - t_{i-1}}} \qquad \text{[Equation 3.16]}$$

Once the E(t_i) value is calculated for each time point it is possible to calculate $\bar{t}$ and σ^2 from Equation 3.14 and 3.15. The values calculated below are shown for the graph in Figure Figure 3.8.

$$\boldsymbol{\bar{t} = \frac{\sum t_i E(t_i)}{\sum E(t_i)} = \frac{15.70}{14.09} = 1.114}$$

$$\boldsymbol{\sigma^2 = \frac{\sum t_i^2 E(t_i)}{\sum E(t_i)} - \bar{t}^2 = \frac{18.75}{14.09} - (1.114)^2 = 0.0891}$$

$$\boldsymbol{\sigma_\theta^2 = \frac{\sigma^2}{\bar{t}^2} = \frac{0.0891}{1.114^2} = 0.0718}$$

By using the GoalSeek function on Excel it is then possible to find $\frac{D}{uL}$ by applying Equation 3.7. Once a value for $\frac{D}{uL}$ has been found, equation 3.8 can be applied to find N.

$$\boldsymbol{\sigma_\theta^2 = \frac{2D}{uL} - 2\left(\frac{D}{uL}\right)^2 \left(1 - e^{-\frac{uL}{D}}\right) = 0.0718} \qquad \text{[Equation 3.7]}$$

$$\boldsymbol{N = \frac{1}{2}uLD} \qquad \text{[Equation 3.8]}$$

In this instance, $\frac{D}{uL}$ was found to be 0.0373, and the equivalent number of tanks, N, was determined to be 13.4.

This calculation of N was performed for all conditions explored in this chapter.

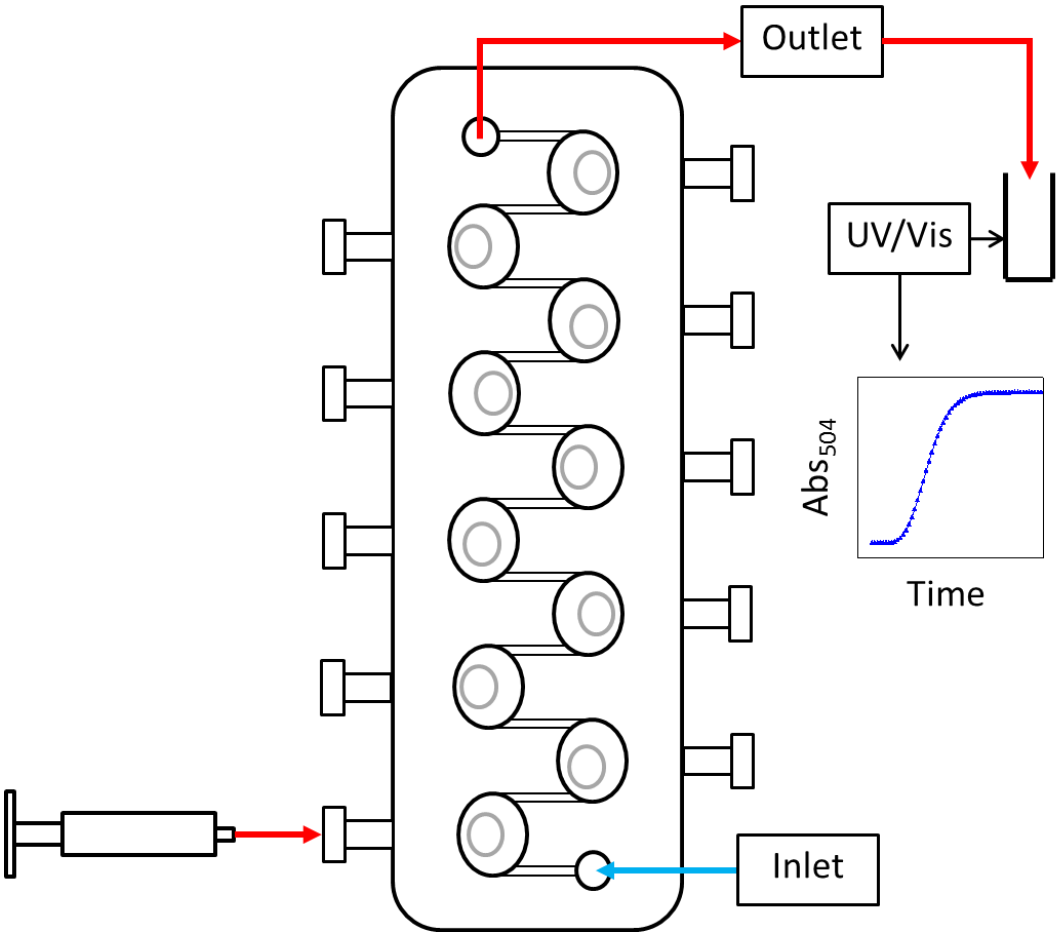

Figure 3.7. ACR reactor set-up for experimental quantification of equivalent number of tanks, N. Fluid was pumped in the reactor from the bottom inlet and tracer dye was pumped via a syringe pump in the first reaction cell. 1 mL samples were collected at the outlet before Abs_{540nm} was recorded. Experiments performed as described in Section 2.1.2.

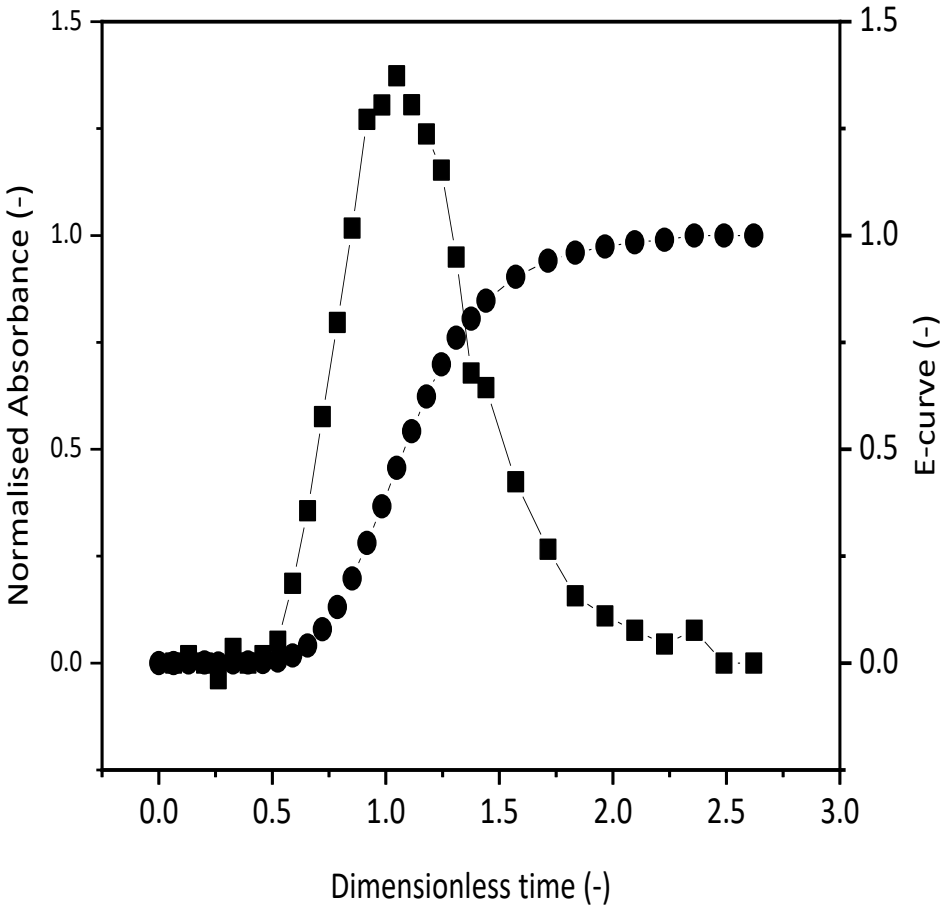

Figure 3.8. Normalised absorbance and its derivative for ACR performance with a single-phase fluid at an agitation rate of 6 Hz. Normalised absorbance (■) and its derivative, "E-curve", (●) are plotted against dimensionless time. ACR was operated with water, agitation frequency was set to 6 Hz, and with a hydraulic residence time of 15.2 min. ACR was set up as described in Section 2.1.1. Absorbance values were obtained as detailed in Section 2.1.2.

3.3.2.3 Variation of N with agitation frequency

The first set of experiments aimed to look at the effect of agitation frequency on N. The ACR's proprietary technology relies on the Coflore® mixing strategy which is linked to mechanical agitation of the whole reactor block (Section 1.5.2). It was therefore important to determine the effect of agitation on the reactor performance. The agitation frequency was studied with a hydraulic residence time of 15.2 min; tracer was injected via the side entry port at 5 $mL.hr^{-1}$. The agitation frequency is measured as the number of times that the reactor block completes a horizontal oscillation per second (in Hertz) and can be between 0 and 9. Agitation frequencies of 0, 2, 4, 5 and 6 Hz were tested as shown in Figure 3.9. A higher agitation rate of 7 Hz was attempted, but the shaking of the entire set-up was deemed excessive and could have damaged the reactor.

As mentioned in Section 3.3.2.1, small variations in the measurements can result in large discrepancies in the evaluation of N. This large variability is an unfortunate side effect of this technique and as such, the standard error of the mean (SEM) is included in subsequent results. It does appear that larger agitation frequencies lead to a better performance of the reactor. Indeed, the manufacturer's recommended agitation rate is 6 Hz, which appears here to provide the highest number of tanks and therefore the highest volumetric efficiency (Levenspiel, 1999). However, even with no agitation N is determined to be approximately 7.8. This could be because the changing shape of the reactor (cylindrical cells followed by straight narrow channels and exiting through a wider exit tube) could improve the fluid mixing performance.

The mathematical derivation outlined in Section 3.3.2.1 has the added complication of producing N values that are not integers. As an example, for an agitation frequency of 0 Hz the N value is 7.8. The way to interpret this is to consider the ACR as being composed of seven equally sized reactors, followed by an eighth reactor with a volume corresponding to the non-integer part of the N value (e.g. in this case an eighth reactor with 80% of the volume of the others)(Stokes and Nauman, 1970; Phan and Harvey, 2010; Gao, Muzzio and Ierapetritou, 2012).

3.3.2.4 Variation of N with ACR flow rate and configuration

For the ACR to be a flexible reactor it should be able to perform well in a range of different conditions such as flowrate and residence time requirements. This was studied by changing

the peristaltic pump speed and ensuring the tracer was injected proportionally at the same rate (100:1). The different residence times (from 1.9 to 15.2 min) investigated and the corresponding equivalent number of tanks are shown in Table 3.1**.**

Differing residence times do not appear to affect the equivalent number of tanks which, with the exception of the 7.6 min residence times, is between 13.1 and 14.1. This finding indicates that the ACR performance would likely not be affected by liquid flowrates. A useful tool to assess the flow regime is the dimensionless number, Reynolds number, which is a ratio between the inertial forces and the viscous forces. A higher Reynolds number indicates a more turbulent (and thus better mixed) flow regime (Levenspiel, 1999).

At lower residence times the fluid would spend less time in each reaction cell and undergo less mixing provided by the agitators. However, a lower residence time would also result in a higher Reynolds number (as the inertial forces acting on the fluid are larger, making the fluid flow faster) and thus a relatively more turbulent flow in the reactor, thereby countering the reduced time spent in a mixed environment. At low flowrates the dispersion of the tracer would be greater; however, each reactor would have more time to mix the tracer and the main process fluid. Despite this, the manufacturer recommends using residence times in the ACR of 2 hours or less as diffusivity effects may become too strong at very low flowrates.

The choice of agitator could also influence ACR performance. The ACR was operated with high shear agitators (Figure 3.10 (a)); however, although not investigated in this work, the catalyst basket agitator, Figure 3.10 (b), could be employed for the retention of immobilized enzymes. For this potential use, the ACR's performance with a catalyst basket agitator was compared to the high shear agitator. To do this, the reactor block was dismantled and the high shear agitators were replaced with catalyst baskets in each reaction cell. The experimental conditions were: 15.2 min residence time; 6 Hz agitation rate; water as main process fluid; and tracer flowrate was kept at 1% v/v of the main process fluid flowrate. It is important to note that the catalyst baskets were empty for this study. As shown in Table 3.2 the performance between the two is very similar, indicating at these conditions the choice of agitator does not affect mixing. A limitation of this finding is that it does not say how the new catalyst basket would perform when full of catalyst or in less favourable conditions such as high viscosity. However, this initial finding suggests that the ACR would still perform well with the different agitator designs.

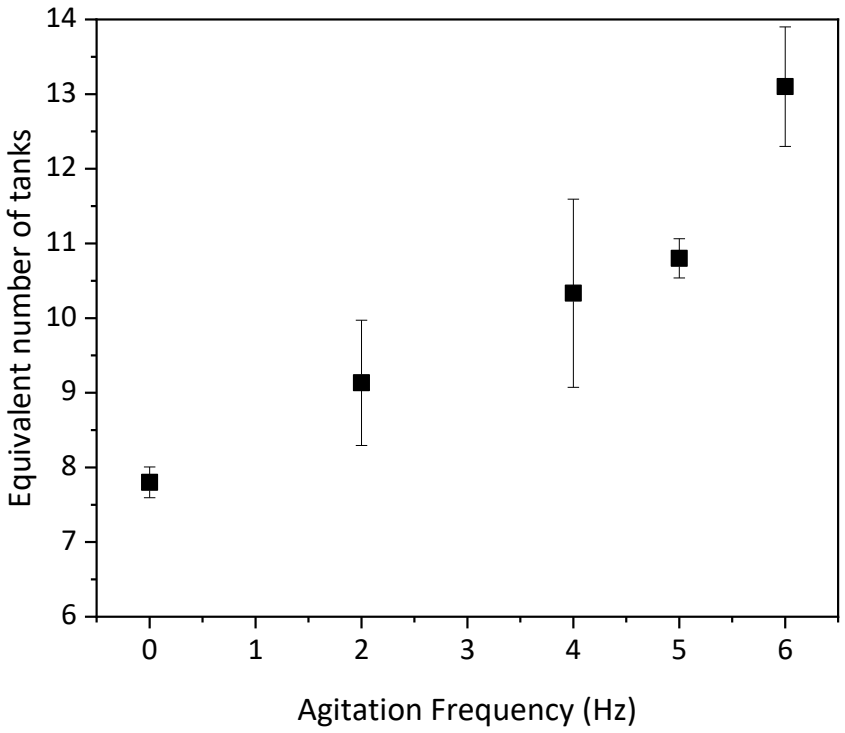

Figure 3.9 Equivalent number of tanks in the ACR as a function of agitation frequency for a single-phase fluid. Error bars indicate SEM (n=3). N, equivalent number of tanks was calculated as explained in Section 3.3.2.1. Absorbance values were obtained for different reactor block agitation rates, using a 15.2 min residence time, as outlined in Section 2.1.2.

Table 3.1. Variation of calculated equivalent number of tanks for different residence times. Residence time in the ACR was varied by changing the main pump speed as described in Section 2.1.2. Equivalent number of tanks was calculated as described in Section 3.3.2.1. The SEM was calculated based on the number of repeats for each condition (n).

Pump speed (rpm)	Flowrate ($mL.min^{-1}$)	Residence time (min)	Equivalent number of tanks	SEM	n
10	**8.8**	**15.2**	13.1	0.80	5
20	**17.6**	**7.6**	10.0	1.38	4
40	**35.3**	**3.8**	13.1	1.22	5
60	**70.5**	**2.5**	14.1	2.52	5
80	**141.0**	**1.9**	13.9	1.94	5

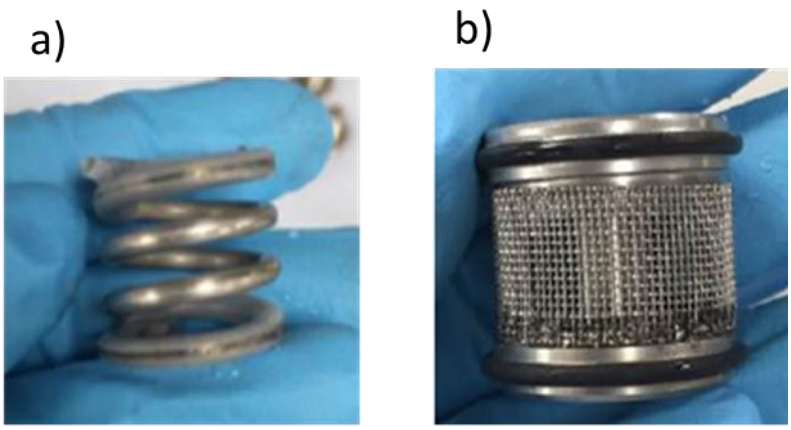

Figure 3.10. Photographs of different ACR agitator designs. Different agitators are available for use in the ACR. Shown in (a) is the high shear agitator, whilst in (b) is the catalyst basked agitator. The catalyst basket agitator has a removable screw-in lid that allows a catalyst to be placed inside. The catalyst is retained by a mesh of approximately 400 µm.

Table 3.2 ACR performance for high shear agitators and catalyst baskets. Equivalent number of tanks N, calculated for the two agitator types, along with SEM and number of repeats, n as described in Section 2.1.2.

Agitator type	Equivalent number of tanks	SEM	N
High shear	13.1	0.80	5
Catalyst basket	13.7	0.54	3

3.3.2.5 Effect of viscosity on reactor performance

As the ACR is intended to be used to process a SBP dispersion it was hoped to characterise the fluid residence time distribution with the real SBP slurry rather than using water as the process fluid. An attempt was made using the tracer in conjunction with the SBP slurry, but it became impossible to measure the tracer absorbance accurately due to the obstruction caused by the SBP particles. Despite this, it is important to consider how the slurry composition might affect the reactor. One way would be through a change in viscosity. As seen in Section 3.3.1.1, increases in the dispersed SBP concentration are directly correlated to an increase in viscosity. Additionally, the SBP slurry was shear thinning. As the shear forces inside the reactor were not quantified it would have been difficult to predict the viscosity of the SBP dispersion.

To accurately characterise the flow properties and reactor performance, Newtonian fluids of viscosity higher than water were used instead. Water:glycerol solutions were chosen as they would allow the measurements of tracer absorbance, and can be mixed to provide a solution of known viscosity. As shown in Table 3.3 by changing the glycerol concentration different viscosities are achievable. Indeed, by using 0, 20, 50 and 80% glycerol concentration solutions, the range of viscosities can match the range of viscosities measured for SBP dispersions (Figure 3.1).

These water:glycerol solutions were used as the process fluid, using 6 Hz agitation and a 15.2 minute residence time, and compared to the same conditions using pure water. Since viscosity negatively impacts the Reynolds number and, thus, mixing, it was hypothesised that it may have had a negative effect on ACR performance. Despite this, it is seen in Table 3.4 that N is between 9.7 and 13.7 for the various viscosity conditions indicating the performance appears stable over the range of viscosities investigated.

For the Coflore® mixing technology to operate effectively, the agitator density needs to be different than the main fluid. The high-shear agitators used here are made of steel and therefore are much denser than either glycerol or water (1260 and 1000 $kg.m^{-3}$, respectively), meaning the mixing is likely not affected. It is also possible that if the viscosity were to increase further it could negatively impact the Reynolds number and therefore mixing and performance.

Although the tanks-in-series model has been widely used, only one publication is available investigating the ACR. Pedersen et al. (2017) studied an enzymatic reaction that employed both a liquid and a gaseous phase. RTD evaluation was carried out, as in this study, using a step change method. Oxygen concentration was measured throughout the reactor by placing Oxygen Sensor Spots (Pyroscience Gmbh, Aachen, Germany) on the sight glass with optical fibres for monitoring on the outside of the reactor so as to not interfere with the hydrodynamics. Knowing oxygen concentration allowed for a study on the reaction kinetics within the reactor. The agitation rate was kept at 9 Hz, considerably higher than what was used in this study. Over the range of residence times that they investigated it appeared that N increased with flowrate. Although this effect was not noticeable in this study, it is important to note that their largest flowrate (13 $mL.min^{-1}$) was similar to the lowest residence time studied here (8.8 $mL.min^{-1}$) and the N values obtained were quite comparable at 11.0 and 13.1, respectively (at different agitation rates). This suggests there may well be a point at which the flowrate affects the hydrodynamic performance of the reactor (Toftgaard Pedersen *et al.*, 2017).

Previous AMTechnology work carried out an RTD study on the larger Agitated Tube Reactor (ATR). The step change was achieved by switching process fluid from a low salt to a high salt concentration buffer and measuring conductivity at the outlet. The study showed that the ATR appears much closer to a PFR with a range of N values from approximately 200 to approximately 1000, for a 55 and 10 minute residence time, respectively. This indicates that plug flow characteristics that could make the ACR a compelling lab scale flow reactor, could be maintained or even improved at larger scale (Sutherland, 2015).

A further point for discussion is the use of Reynolds number (Re) in assessing the flow regime. The inertial forces in the ACR would be given by the forces pumping the fluid through the reactor and the forces involved in the Coflore® mixing technology. Unfortunately, no mathematical formulation for quantification of Re in the ACR is currently available. Despite this, an understanding of which forces are exerted inside the ACR can contextualise the results seen so far. For example, as the agitation frequency increases, a higher amount of energy is being input into the system, increasing the inertial forces and thus increasing Re and the number of tanks, N. On the other hand, increasing the flowrate at a high agitation frequency, appears to have little to no effect on N.

Table 3.3. SBP slurry and glycerol-water mixture viscosities Viscosity measurements were obtained at 25 °C as detailed in Section 2.1.4. Viscosity of 10% w/v SBP slurry is presented as a range due to the large change in viscosity over the range of shear rates used. The literature value (*) for the 100%, pure glycerol viscosity is reported (Ferreira *et al.*, 2017).

SBP Slurry Concentration (% w/v)	Viscosity (Pa.s)	Glycerol solution concentration (% v/v)	Viscosity (Pa.s)
1	0.0011	**0**	0.0010
2	0.0015	**20**	0.0015
4	0.0034	**50**	0.0060
8	0.0160	**80**	0.0449
10	0.0222 - 0.0339	**100**	1.412*

Table 3.4. Equivalent number of tanks in the ACR for different process fluid viscosities. SEM was calculated for each viscosity (n = 3, with the exception of water, n=5). Different viscosities were obtained by changing the ratio of glycerol to water in the solution as indicated in Table 3.2. Equivalent number of tanks was calculated using the method outlined in Section 2.1.2.

Solution	Equivalent number of tanks	SEM
Water	13.1	0.80
20% glycerol	10.9	0.96
50% glycerol	9.7	0.35
80% glycerol	13.7	1.13

This suggests that the Re is sufficiently large to not have an effect on the flow regime. Alternatively, the additional kinetic energy of a faster moving liquid, is negligible compared to the mixing energy exerted onto the system. This could be explained by observing the equation for the oscillatory Reynolds number shown in Equation 3.20:

$$\boldsymbol{Re_{osc}} = \frac{\boldsymbol{2\pi f x_{osc} \rho D}}{\boldsymbol{\mu}} \qquad \text{[Equation 3.17]}$$

where f (Hz) is the oscillation frequency, x_{osc}(m) is the oscillation amplitude, ρ (kg.m^{-3}) is the fluid density and μ (m^2.s^{-1}) is the fluid viscosity.

The Reynolds number formula in Equation 3.17 has previously been used to characterise a novel class of continuous tubular reactors called Oscillating Baffled Reactors, which have a similar mixing strategy as the ACR. The Re_{osc} has no fluid velocity component suggesting that the forces of the flowing fluid, at least in these reactors, are negligible (Levenspiel, 1999; Phan, Harvey and Lavender, 2011).

Another aspect that could be further investigated is the extent of micromixing. Although this is typically done for sub-millilitre scale reactors, mixing characterisation could be of importance especially for transport-limited reactions. Experiments to study micromixing often rely on a 2-reaction system: one instantaneous; and a second, slower reaction. If the reactions rely on the same reagents, poor mixing would lead to pockets of isolated reagents that would allow enough time for the slower reaction to take place (Guichardon and Falk, 2000).

Reaction 1: A + B → C [Instantaneous]

Reaction 2: A + D → E [Slower than reaction 1]

Two examples of this are the Villermaux-Dushman reaction and the Bourne reaction. The former employs an iodide-iodate compounds, whilst the latter uses azodyes. Both can be used to quantify micromixing by determining which product is made spectrophotometrically (Bourne et al. 1981; Guichardon & Falk 2000).

3.3.3 ACR performance with solid-liquid dispersions

Work on ACR characterisation using a single liquid phase showed that viscosity, flowrate and type of agitator had little to no effect on ACR residence time distribution over the range of conditions studied (Section 3.3.2). Conversely, work on agitation frequency indicated that a more vigorously shaken reactor performed better in terms of N.

Although the viscosity studies aimed to mimic how the SBP slurry would affect the ACR, it did not account for the effect of differently sized solids (Section 3.3.1.2) in the system. Preliminary work, not shown here, indicated that at residence times lower than 15.2 min, solids would settle in the ancillary piping systems leading to blockages and challenges in reactor operation.

Furthermore, it was hypothesised that small particles would travel through the reactor more quickly than larger particles. To test this hypothesis the reactor setup was slightly altered by installing a switch valve at the inlet that would allow for the seamless switch between a feed containing water and one containing SBP slurry. By doing this, a step change could be put in place. Furthermore, samples were taken at the outlet for particle size analysis as described in Section 2.1.3. A schematic diagram of the setup is shown in Figure 3.11

Preliminary work also showed that using an agitation frequency of 5 or 6 Hz would provide sufficient mixing to prevent the SBP particles from settling inside the reactor. These two agitation frequencies were used with a 2% w/v slurry concentration and a 15.2 min hydraulic residence time. Before measurements commenced, the reactor was flushed with water; at time 0, the feed was switched to SBP slurry. After 44 minutes for 5 Hz agitation and 40 minutes for 6 Hz the feed was reversed back to water. PSD was measured on samples exiting the reactor and a particle size distribution curve was obtained for each time point. Three measurements are reported here: D10; D50; and D90. D10 represents the first decile in size (smallest 10%), D50 represents the median size and D90 represents the ninth decile (largest 90%) in size. These values are reported in Figure 3.12 and Figure 3.13.

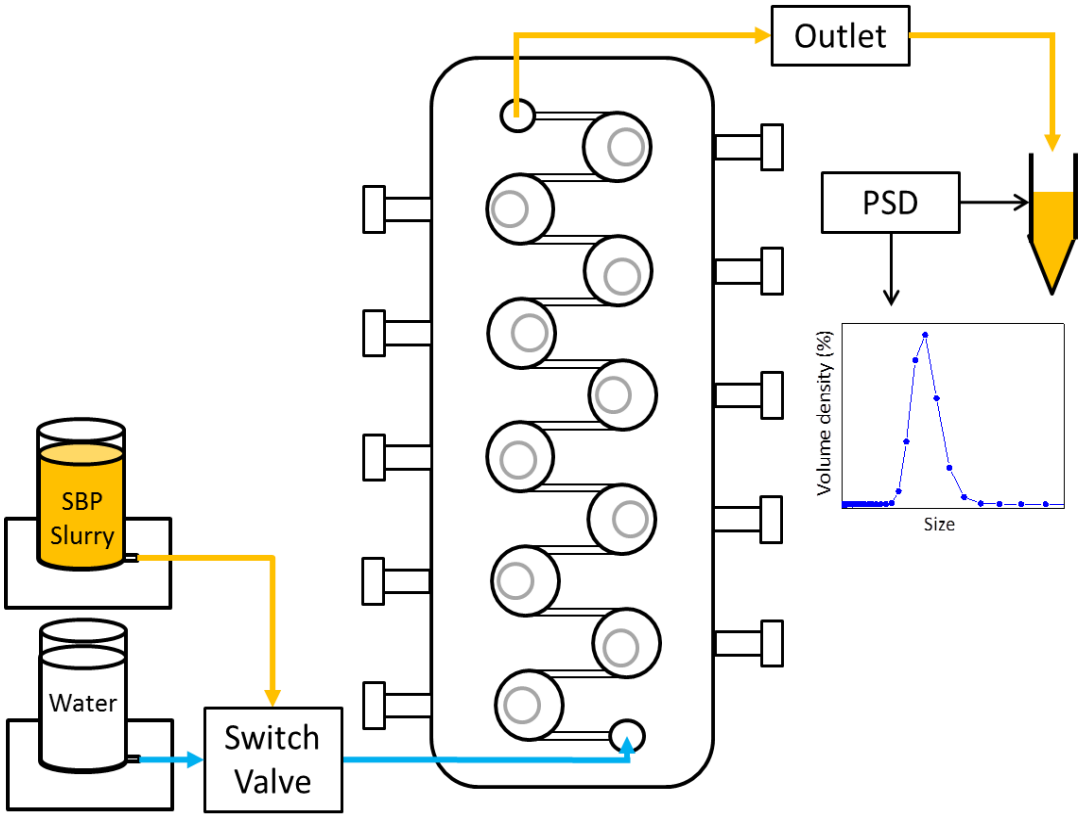

Figure 3.11. ACR and ancillary equipment configuration for determining effect of particle size on residence time. A water and an SBP slurry bottle were connected to a three-way valve to seamlessly transition between feeds. At the outlet 10 mL samples were collected for particle size distribution analysis.

In both Figure 3.12 and Figure 3.13, the experiment unfolded in three phases. In the first phase (pink shaded area), the switch from feeding water to feeding the SBP dispersion, leads to the SBP particles starting to fill the reactor. After approximately 12 minutes the solid concentration had increased sufficiently to allow for detection. In the first phase of the experiment it is possible to see an increase in D10, D50 and D90 particles. This indicates that smaller particles travel through the ACR first, and as the larger particles start to exit, the D10, D50 and D90 increase until the second phase begins (green shaded area) where steady state is reached. In this instance D10, D50 and D90 at the exit remain stable over a period of time. Finally, the feed was switched back to water (light blue shaded area). As the water flushes the reactor, the smaller particles exit more quickly than the larger ones. This is indicated by an increase in D10, D50 and D90. Interestingly, it is possible to see how the D10 increase at the end of the process appears more considerable than the increase in D50 and D90.

It was not possible to carry out an RTD derivation as shown in Section 3.3.2.1, for this solid-liquid dispersion. However, it is possible to make observations on performance by looking at the times at which particles exited the reactor. In Figure 3.12 with an agitation frequency of 5 Hz, it is possible to see that approximately 17 minutes after the switch from water to dispersion, D10, D50 and D90 values begin to increase. This is especially noticeable for D50 and D90. Similarly, approximately 16-17 minutes after the switch back to water (i.e. at minutes 60-62) the size increases again. For an agitation frequency of 6 Hz, in Figure 3.12 it is possible to see that the increase in size occurs earlier; after 12 minutes (as samples started to be taken and again after) at minute 52, or 12 minutes after the switch back to water.

This finding indicates that the higher agitation reduces the difference in speed between small and large particles. Although the single-phase performance at 5 and 6 Hz showed only a slight difference in N number (Figure 3.9), 11.0 versus 13.1, with respective SEMs of 0.3 and 0.8); the increase in agitation frequency did have a noticeable effect in the performance with solid particles. Suggesting, that characterisation of liquid-solid systems using liquid-only model systems is not sufficient.

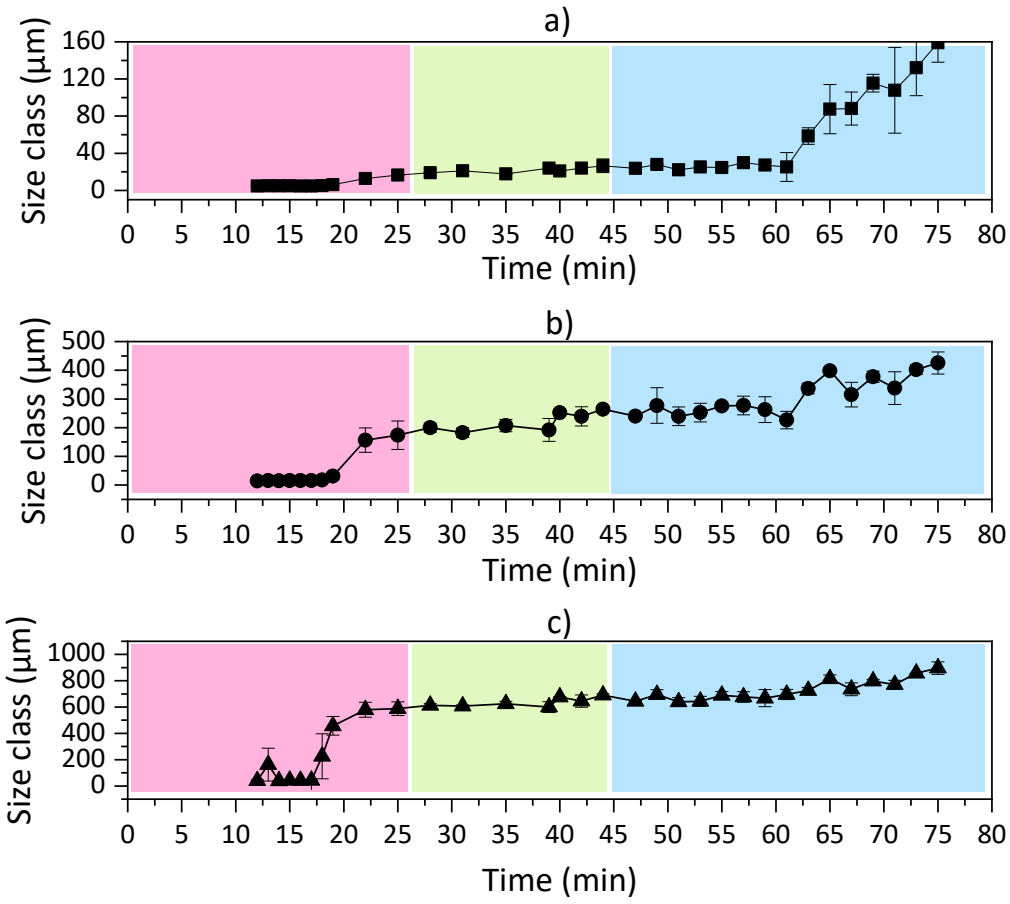

Figure 3.12. Exit particle size distribution (PSD) at various times after addition of solids in the ACR feed at 5 Hz agitation rate. D10 (panel (a), ■); D50 (panel (b), ●); and D90 (panel (c), ▲) values were obtained for each time. Time 0 represents the switch from feeding water to feeding SBP slurry. The switch from SBP slurry back to water occurred after 44 minutes. Error bars represent SEM (n=3). Particle size distribution was evaluated by laser diffraction as described in Section 2.1.3.

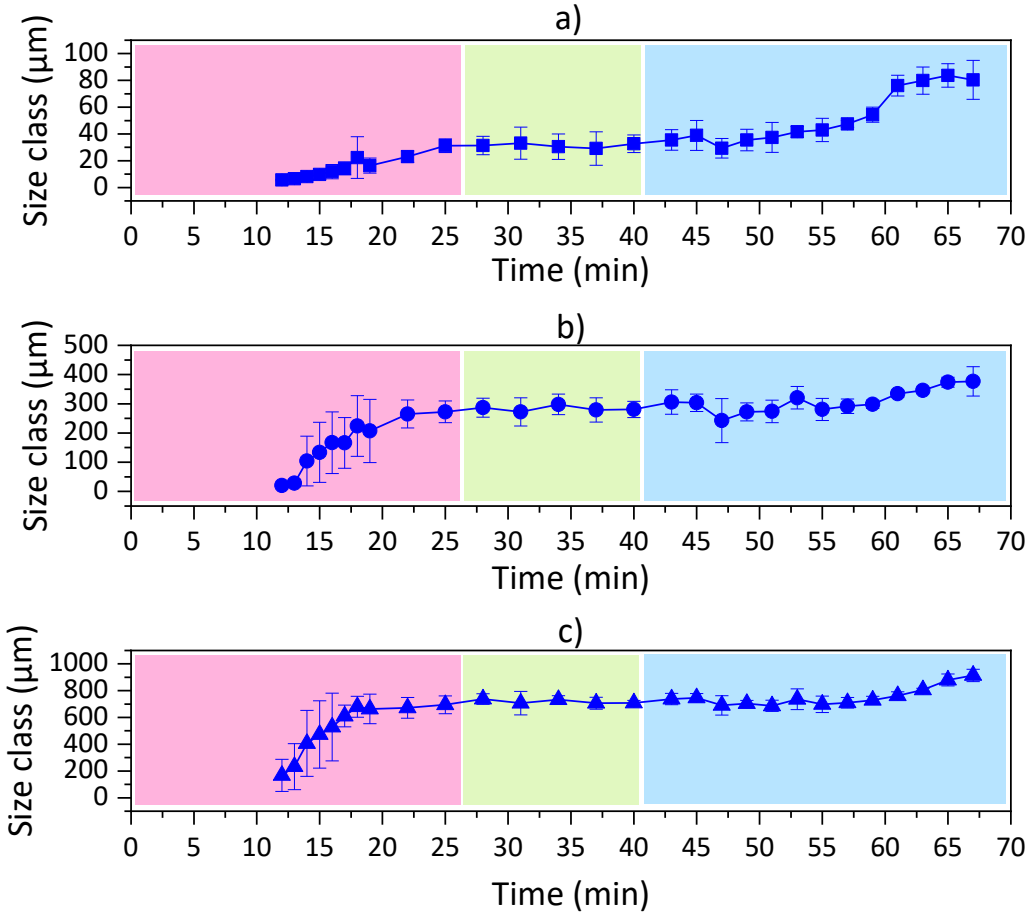

Figure 3.13. Exit PSD at various times after addition of solids in ACR feed at 6 Hz agitation rate. D10 (panel (a), ■); D50 (panel (b), ●); and D90 (panel (c), ▲) values were obtained for each time point. Time 0 represents the switch from feeding water to feeding SBP slurry. The switch from SBP slurry back to water occurred after 40 minutes. Error bars represent SEM (n=3). Particle size distribution was evaluated by laser diffraction as described in Section 2.1.3.

Shortly after the switch, samples at the outlet had very few SBP particles in them, over time the SBP content increased and then decreased gradually again after the switch back to water was made. This initial low concentration created the challenge of very inaccurate readings as the samples did not provide a sufficient obscuration rate for the laser diffraction measurements. The dry solids of each time point (known volumes of samples dried at 60 °C for 48 hours) were measured for a run at 6 Hz. In Figure 3.14 it is possible to see the change in solids concentration (i.e. dried SBP) and how it compares to D10, D50 and D90 expressed on a $\log_{10}$ size axis. Although the solids concentration is relatively inaccurate (it is quite difficult to handle small dispersion volumes of the slurry accurately); it is possible to see that as the particle size increases so does the solids concentration after the initial switch. Similarly, the solids concentration decreases to almost 0, as the rest of the slurry is flushed out after the switch back to water.

To further understand how different sized particles travel through the reactor it is also useful to look at PSD curves rather than just D10, D50 and D90 values. PSD curves for 3 time points were selected for both conditions: 15, 47 and 73 minutes for 5 Hz and 15, 40 and 65 minutes for 6 Hz. These points indicate the three phases in Figure 3.12 and Figure 3.13 used to understand the experiments: start (solid line), steady state (dashed line), and switch to water (dotted line). These are shown in Figure 3.15, where it is possible to see how curves change over time. Between the first and second time point the entire curve shifts to the right, whilst from the second to the third point, as the reactor is being flushed out, it appears that the right-hand side of the curve does not change, whilst the left-hand "tail" at the lower size ranges becomes noticeably smaller.

This further supports the hypothesis that small particles are flushed out earlier, as it means that when the reactor is being flushed out in the third phase, fewer smaller particles are present. It is also possible to see how this effect is less noticeable at 6 Hz further corroborating the notion of the improved ability to handle solid dispersions at this agitation frequency. The PSD curve obtained for milled SBP passed through a 212 µm sieve is also included in both graphs (dotted and dashed line). It is possible to see that the curve's shape is similar to the steady state curve, though shifted to the left. This shift was likely due to particle swelling that occurred during the process.

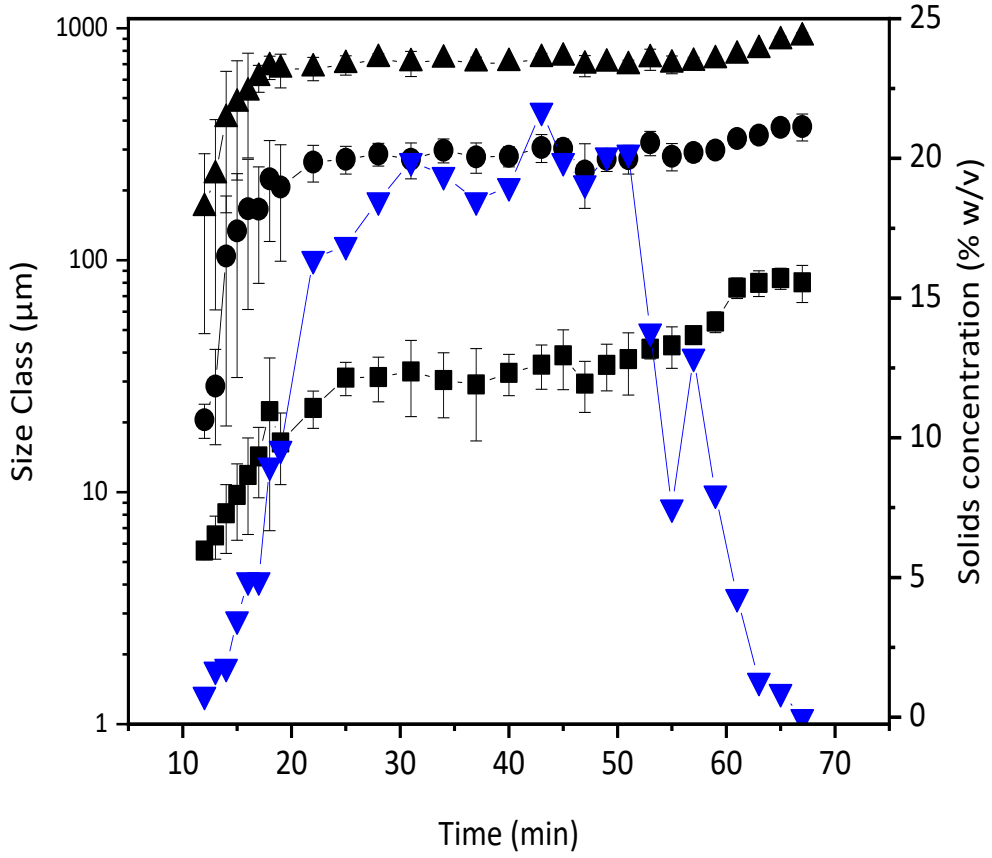

Figure 3.14. Particle size distribution and solids concentration (dry weight) at various times after addition of solids in ACR feed at 6 Hz agitation rate. D10 (■); D50 (●); and D90 (▲) shown on primary axis. Solids concentration (▼) shown on secondary y-axis. Time 0 represents the switch from feeding water to feeding SBP slurry. The switch from SBP slurry back to water occurred after 40 minutes. Error bars for the particle size distribution represent SEM (n=3). PSD values were obtained as outlined in Section 2.1.3.

A further question was whether steady state could be achieved and maintained, so a similar experiment was carried out except without a switch back to water. Figure 3.16 shows that indeed a steady state is possible and after the initial increase in particle size the particle size remains approximately the same throughout the time which covers 4 residence times, showing that steady state could be achieved.

The ACR has been successfully used in a number of reactions, including the production of *N*-iodomorpholinium hydroiodide, from morpholine and iodine. This reaction quickly produces a solid-liquid suspension, but despite the ACR's ability to handle the formation of a solid, which could quickly cause blockages and fouling, the reactor performance was never characterised with solids streams present (Browne *et al.*, 2011; Deadman *et al.*, 2015). Moreover, even literature characterising reactors for lignocellulosic pretreatment is scarce. Sievers et al. (2016) investigated a screw reactor used for the acid hydrolysis of corn stover. Using sodium chloride and a titanium dioxide powder with a size similar to the corn stover as tracers, they found that the corresponding RTDs were relatively similar. So, they replaced the offline analysis of titanium oxide with the online measurement of salt concentration for further characterisation of a number of reactor parameter (e.g. screw rotation, fill volume, and flowrate). The key limitations of this work are the equivalence between a powder and a salt, the assumption that all particles travel at the same speed, and that corn stover particles would travel at the same speed as titanium dioxide (Sievers *et al.*, 2016; Sievers and Stickel, 2018). Quiroga and colleagues combined a kinetic model of cellulose hydrolysis and an RTD model of 3 CSTRs in series to calculate how 10 CSTRs in series would perform with addition of the reagent at the inlet and in subsequent reactors. Although this was not done in the ACR, the reactor blocks design could allow for similar work, using the different entry ports for feeding different reagents or changing the conditions in parts of the reactor (González Quiroga, Costa and MacIel Filho, 2010).

A particularly challenging aspect of solids handling in continuous reactors is tracer selection. Whilst soluble tracers with assumed rheological equivalence are used often, radioactive or phosphorescent particles have also been employed. A disadvantage of the latter is the time and effort required to ensure that the selected particles have the same properties as those being studied (Harris, Davidson and Thorpe, 2003; Bhusarapu, Al-Dahhan and Dudukovic, 2004; Gao, Muzzio and Ierapetritou, 2012). One study by Pareek et al. (2001) actually used laser diffraction to determine titania

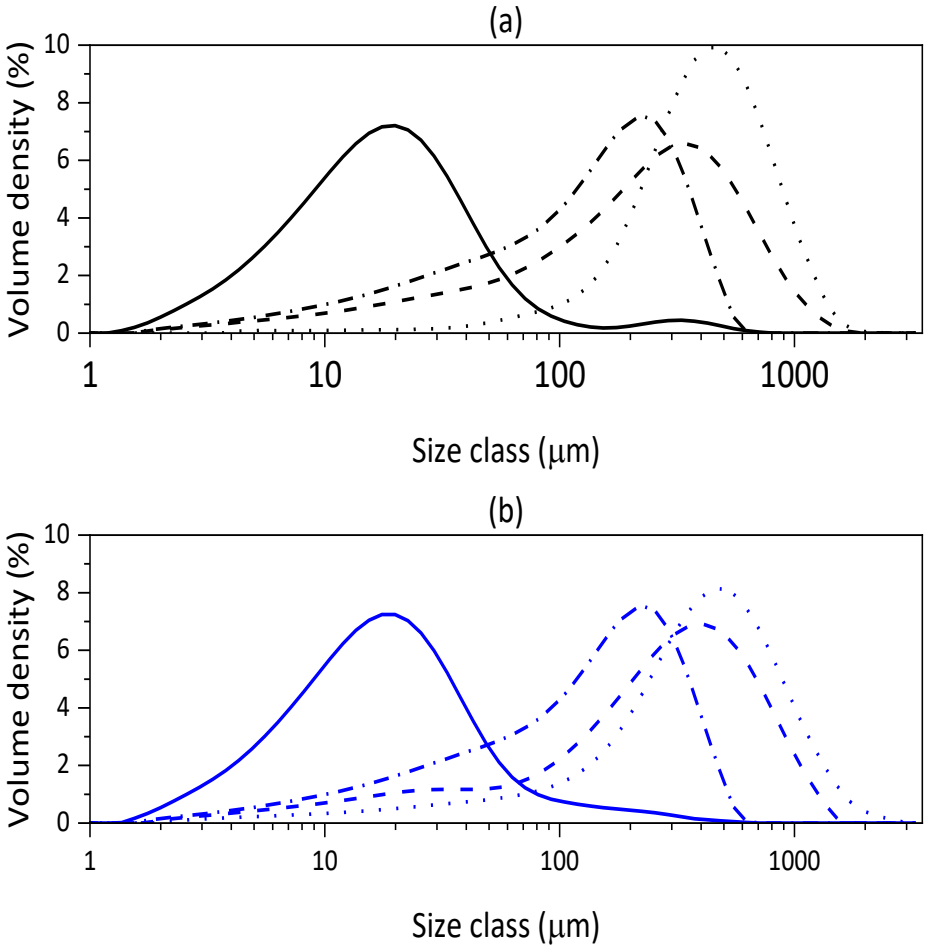

Figure 3.15. PSD curves obtained from exit samples at various times after the addition of solids in ACR feed. PSD curves are shown for three timepoints. Panel (a) shows PSD curves at 5 Hz agitation rate for samples taken after 15 (—), 47 (– –), and 73 (·····) minutes compared with milled SBP used in the feed (–·–). Panel (b) shows PSD curves at 6 Hz agitation rate for samples taken after 15 minutes (—), 40 minutes (– –) and 65 (·····) minutes compared with milled SBP used in the feed (–·–). Experiments performed as described in Section 2.1.3.

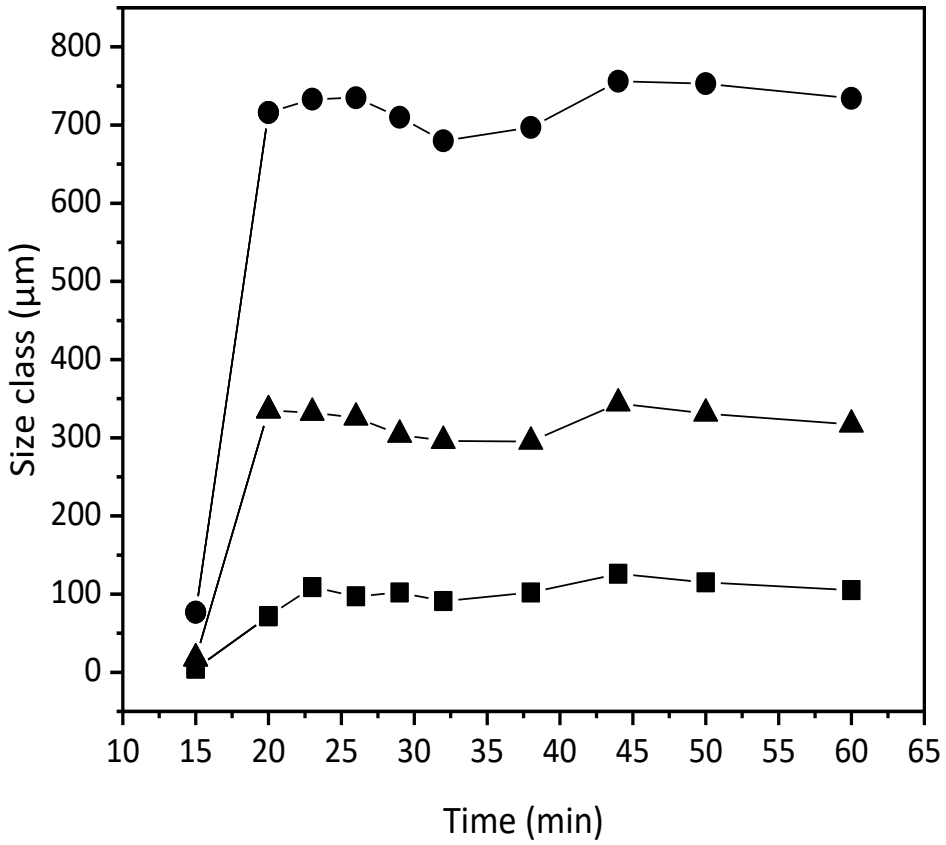

Figure 3.16. Particle sizes at various times after addition of solids in ACR feed at 6 Hz agitation rate. D10 (■); D50 (●); and D90 (▲) measurements were obtained by laser diffraction (Section 2.1.3) over time to control variation at steady state. Time 0 represents the start of the experiment, when the feed was switched from water to SBP slurry.

powder contents at the outlet of a three phase annular bubble column reactor, but no investigation in the RTDs of different particle sizes was carried out (Pareek *et al.*, 2001).

The laser diffraction work shows that, despite having different particle travel times, the ACR can still achieve steady state. Coupled with the work shown in previous section it displays a flexible range of operations over which a number of two-phase reactions that could carried out in continuous flow mode.

3.4 Summary

In this chapter, characterisation work was carried out to better understand the performance and limitations of the novel ACR. The SBP pretreatment reaction was purported to be the most challenging reaction investigated in this thesis, as it would involve a multiphase system with complex rheology (Section 3.2). Therefore, the rheology of the solid dispersion was the first aspect to be investigated. The key findings were that SBP slurries exhibit shear thinning behaviour (Figure 3.1), which is exacerbated at higher solids concentrations. It was also found that the slurry viscosity increased with the square of the SBP concentration (Equation 3.1, Equation 3.2 and Equation 3.3) which could lead to processing challenges at high SBP loadings. The PSD of the milled SBP feedstock was also studied, revealing that the fraction used in ACR trials (nominally smaller than 212 µm) had a median size of 128 µm, a D10 of 15 µm and a D90 of 446 µm. Indicating that it would not cause challenges when being processed through the ACR.

Following this, an RTD study was carried out on the ACR using water and water-glycerol solutions and a liquid tracer (Section 3.3.2). The analysis showed that the equivalent number of tanks, N, a measure of the closeness to plug flow, was affected by agitation frequency with the ACR equating to 13.1 tanks-in-series when operating at 6 Hz with a hydraulic residence time 15.2 min; an increase from an N value of 7.8 with no agitation (Figure 3.9). An increase in viscosity, altered by modulating glycerol concentration, did not affect the N value over the range of 0.001 Pa.s to 0.045 Pa.s (Table 3.3). Agitator type and flowrate through the ACR did not appear to affect N, either (Table 3.2). These findings indicated that the ACR would perform similarly over a large range of conditions. Despite this, previously published work on the ACR, at lower flowrates did show a correlation between flowrate and N, suggesting that the range of flowrates studied here was possibly sufficiently high to not affect N.

Finally, the operation of the ACR had to be characterised for use with a liquid-solid dispersion (Section 3.3.3). Indeed, preliminary work established a residence time of 15.2 min as the longest residence time in the ACR before SBP solids would cause blockages. Using laser diffraction, it was possible to show, at this residence time, that an agitation frequency of 6 Hz was more favourable than 5 Hz for SBP dispersions (Figure 3.15). It was also found that smaller particles travelled more quickly than larger particles through the ACR; however, the reactor reached steady state meaning that the ACR could be used for the SBP pretreatment reactions (Figure 3.16).

Further work in the reactor characterisation area could focus on qualifying the micromixing environment through the Villermaux-Dushman or the Bourne reaction as mentioned in Section 3.3.2.5; and quantifying ACR performance with solid dispersions via the RTD calculations used on liquid systems in Section 3.3.2.1. In the next chapter the SBP dispersion which was characterized along with its behaviour in the ACR will be pretreated in both batch and continuous mode.

4

Continuous Sugar Beet Pulp pretreatment options for the solubilisation of saccharides

4.1 Introduction

First generation biofuels are fuels produced from crops such as sugarcane and corn. The fact that these crops are also important from a nutritional standpoint has raised interest in the development of second generation biofuels from lignocellulosic waste from forestry and agricultural operations (Sims *et al.*, 2010). However, to effectively utilise lignocellulosic material pretreatment steps are necessary. These steps seek to modify the lignocellulosic structure to allow microbes and enzymes easier access to fibres and sugars. Whilst D-glucose from cellulose has typically been the target molecule for fermentation, many other hexose and pentose sugars are available for further fermentation or bioconversions (Chamy *et al.*, 1994).

A range of lignocellulose pretreatment techniques are available, these can be physical, chemical or enzymatic, or a combination thereof. With the exception of enzymatic pretreatment, most involve changing the pH and/or the temperature to disrupt the lignocellulosic structure. Liquid hot water (LHW) is a type of pretreatment that exploits the more acidic pK of water at high temperature (120 °C – 200 °C) to release sugars (Mok and Antal, 1992; Allen *et al.*, 1996; Kim *et al.*, 2014). Steam explosion reaches similar temperatures, but following incubation at high temperatures and pressures (up to 260 °C and 48 bar (Sun and Cheng, 2002)), a sudden decompression step is carried out. This causes the violent disruption of lignocellulosic material (Morjanoff and Gray, 1987; Zhang and Chen, 2012). Acid pretreatment can be carried out using either concentrated or dilute acid. Concentrated acid (30-70% v/v of total volume) hydrolysis can be carried out at lower temperatures (~40 °C), whilst dilute acid pretreatment (DAP) uses lower concentrations (<2% v/v) at higher temperatures (often >120 °C) (Zheng *et al.*, 2014). Alkaline pretreatment uses bases such as NaOH or ammonia to remove the crosslinks between lignin and carbohydrates. This increases the porosity of the material and the effectiveness of this method is related to the lignin content of the feedstock (Zheng *et al.*, 2014). A further pretreatment option is the use of enzymes. Homopolymers such as starch and cellulose (made solely of D-glucose molecules) require only a few enzymes to facilitate complete hydrolysis, whilst heteropolymers such as pectin often require different enzymes to hydrolyse various types of glycosidic bonds (Ademark *et al.*, 1998; Kühnel *et al.*, 2010). The use of enzymes usually requires some form of thermo-chemical pretreatment beforehand to make the polymers available for enzymatic hydrolysis (Li *et al.*, 2018).

Sugar beet pulp (SBP) is the waste stream from beet sugar production as described in Section 1.2.3. It is composed of 70-75% w/w carbohydrates, and its low lignin content means it requires milder pretreatment conditions than other lignocellulosic feedstocks (Chamy *et al.*, 1994). Batchwise approaches to SBP pretreatment have been demonstrated using DAP (Zheng *et al.*, 2013), ammonia (Foster, Dale and Doran-Peterson, 2001), steam explosion (Hamley-Bennett, Lye and Leak, 2016), liquid hot water (Ziemiński, Romanowska and Kowalska, 2012) and enzymes (Moloney *et al.*, 1983; Leijdekkers *et al.*, 2013). Different pretreatment reactions have been carried out in subsequent steps such as the work by Kühnel et al. (2011) which firstly used DAP followed by enzymatic hydrolysis to obtain monomeric sugars.

Continuous approaches to lignocellulosic feedstock pretreatment are far less common. To date there are no reports of continuous pretreatment of SBP. A continuous acid-catalysed steam explosion reactor was used to pretreat rice straw (Chen *et al.*, 2013). A twin screw reactor was used to pretreat sugarcane bagasse, rape and barley straw (Choi and Oh, 2012; Da Silva *et al.*, 2013; Han *et al.*, 2013). The main challenge of continuous pretreatment lies in the solid handling, which is why most publications employ variations of a screw conveyor, which enables slurries to be moved through a reactor. However, as shown in Section 3.3.3, the ACR is able to process SBP slurries at a concentration of 2% w/v making continuous pretreatment of SBP a potentially viable option.

An advantage of attempting continuous pretreatment of SBP in the ACR is that continuous processing could fit in well with the other operations carried out in sugar refineries, which tend to be operated in continuous mode. Since the operation of the ACR in the laboratory was limited to temperature ranges below 80 °C, this excluded LHW as a pretreatment option. As such dilute acid pretreatment, carried out at temperatures <100 °C was chosen as a primary lignocellulosic fractionation option. Based on previous literature findings (Hamley-Bennett, Lye and Leak, 2016), mild pretreatment conditions should be able to separate solid cellulose from soluble pectin, without fully hydrolysing the latter into monomers. The fractionated polymers could then be depolymerised using selective enzymes such as arabinases and polygalacturonases (for pectin) and endo- and exo- cellulases (for cellulose). One such enzyme, arabinofuranosidase (AraF), is of particular interest as it was found it could effectively depolymerise arabinans from steam exploded SBP (Cárdenas-Fernández *et al.*, 2018).

4.2 Aims and objectives

The aim of this chapter is to investigate novel process options for continuous SBP pretreatment to release soluble monosaccharides suitable for subsequent bioconversion. The low lignin content of SBP makes it a favourable candidate for utilisation in a biorefinery context (Section 1.3). This chapter will investigate the possibility of using DAP to separate hemicellulose from insoluble cellulose via DAP. The fractionated materials could then be used for separate production processes. Although the ultimate goal is to have a series of pretreatment steps carried out continuously, reactions should first be studied in batch before being moved to a continuous system. The specific objectives of this chapter are outlined below.

- To carry out DAP in batch to understand, through response surface methodology, the main factors affecting sugar release.
- To investigate the feasibility of DAP in continuous mode, by utilising the ACR as a pretreatment reactor.
- To compare the results of DAP in continuous mode to data from other pretreatment techniques available in the literature.
- To investigate the possibility of enzymatic pretreatment, using commercial enzymatic mixes, as an alternative to DAP.
- To understand the possibility of using a specific enzyme, AraF as a depolymerisation step following DAP.

4.3 Results

4.3.1 Batch Pretreatment

4.3.1.1 Selection of pretreatment strategy

Given the temperature constraints of the ACR setup, DAP was selected as the most suitable initial pretreatment step. Figure 4.1 shows the proposed pretreatment scheme. DAP would produce a cellulose rich solid fraction and a pectin rich liquid fraction by separating the highly branched arabinans and homogalacturonans from the more rigid cellulose fibres. These fractions could then be separately treated with hydrolytic enzymes which could then yield monomeric sugars for various uses. As the production of monomeric D-glucose has already been widely studied in the literature, and it is known that SBP-derived D-glucose can be used for fermentation by yeast to bioethanol, this work focusses on the less investigated pectin processing. Moreover, many studies have explored pretreatment techniques that solubilise all of the carbohydrates simultaneously, but some advantages can arise from having fractionated material (Kühnel, Schols and Gruppen, 2011b; Leijdekkers *et al.*, 2013).

A pretreatment reaction that results in fractionated streams comprising different sugars would reduce downstream purification costs. Further, as proposed in Figure 4.1 a set of conditions that would result in the solubilisation of sugars without the complete monomerisation of these sugars could also be advantageous. Solutions containing oligosaccharides and soluble polysaccharides made from different monosaccharide building blocks (e.g. a soluble mixture of arabinans and polygalacturonans) could be treated with specific enzymes to fractionate the solutions. For example, an arabinan specific enzyme could convert oligo- and polymeric L-arabinose into monomeric L-arabinose. Which can then be separated more effectively from larger, polygalacturonans.

It is also worth noting that a pretreatment strategy that releases polymeric sugars could allow the use of these polymers in applications other than fermentations and bioconversions. Cellulose could be used for biobased fibres or nanocomposites production (Siró and Plackett, 2010); and, whilst pectin from SBP is a less suitable gelling agent than pectin from other sources (e.g. citrus peel), it could be used as a thickener or an emulsifier (Mesbahi, Jamalian and Farahnaky, 2005). For these reasons, a milder pretreatment strategy, rather than a reaction resulting in complete hydrolysis of the SBP biomass was chosen.

The aim of the DAP reaction was to separate the main pectic sugars, L-arabinose and D-galacturonic acid, from the solid, cellulose rich fraction. To quantify the outcomes of various DAP conditions the solubilised sugars in the liquid fraction had to be measured. To do so, an analytical hydrolysis step was required to convert oligosaccharides into quantifiable monosaccharides. This procedure, described in Section 2.3.3 and outlined in Figure 4.2 , is carried out on the liquid fraction of the pretreated material. A solution of the clarified pretreatment sample was acidified (3% v/v final H_2SO_4 concentration). The sample was then treated for 1 hour at 121 °C, to depolymerise all solubilised sugars irrespective of their degree of polymerisation. The sugars obtained from this reaction were then analysed using High Performance Anion Exchange Chromatography with Pulsed Amperometric Detection (HPAEC-PAD). The pretreatment yield was defined, as outlined in Section 2.3.3, as the proportion of that sugar that was solubilised, both in monomeric and oligomeric form, from the starting amount present in SBP. This is calculated using Equation 4.1.

$$Yield_{Sugar}(\%) = \frac{100 \text{ x } Sugar\ concentration_{HPAEC-PAD}(g.L^{-1})}{SBP\ concentration(g.L^{-1}) \text{ x } Sugar\ content\ in\ SBP} \qquad \text{[Equation 4.1]}$$

Where *Sugar concentration* is the concentration of monomeric and oligomeric sugar obtained from HPAEC-PAD analysis after oligosaccharides had been hydrolysed into monosaccharides. *SBP concentration* is the starting concentration of SBP in the reaction and *Sugar content in SBP* is the initial content of that sugar as given by the SBP composition shown in Figure 1.5 (Hamley-Bennett, Lye and Leak, 2016; Kharina *et al.*, 2016).

4.3.1.2 Preliminary batch DAP screening

A preliminary set of DAP reactions was carried out to obtain an understanding of the important factors affecting release of sugars. These initial static batch experiments were carried out in 250 mL glass Duran bottles (100 mL working volume) as outlined in Section 2.2.2.1. A range of experimental conditions summarised again in Table 4.1, yielded the results shown in Figure 4.3. Only data for D-glucose, D-galacturonic acid and L-arabinose are shown here, as these are the most abundant and most relevant sugars that can be obtained from SBP.

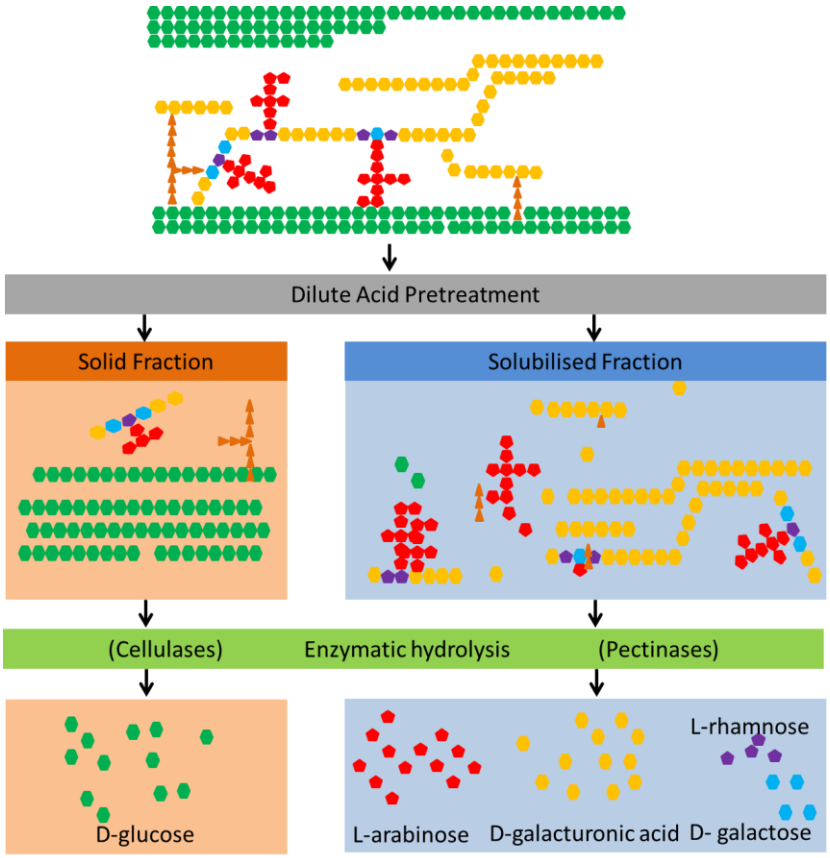

Figure 4.1. Proposed SBP pretreatment scheme. The SBP structure consists of cellulose fibres interwoven with branched pectin and a small amount of lignin. The chemical pretreatment by dilute acid results in a solid fraction mainly consisting of cellulose, and a liquid fraction consisting predominantly poly-, oligo, and monomeric pectic sugars such as L-arabinose and D-galacturonic acid. Additional chemical or enzymatic pretreatment steps could then break down the fibres and polymers into monomeric sugars.

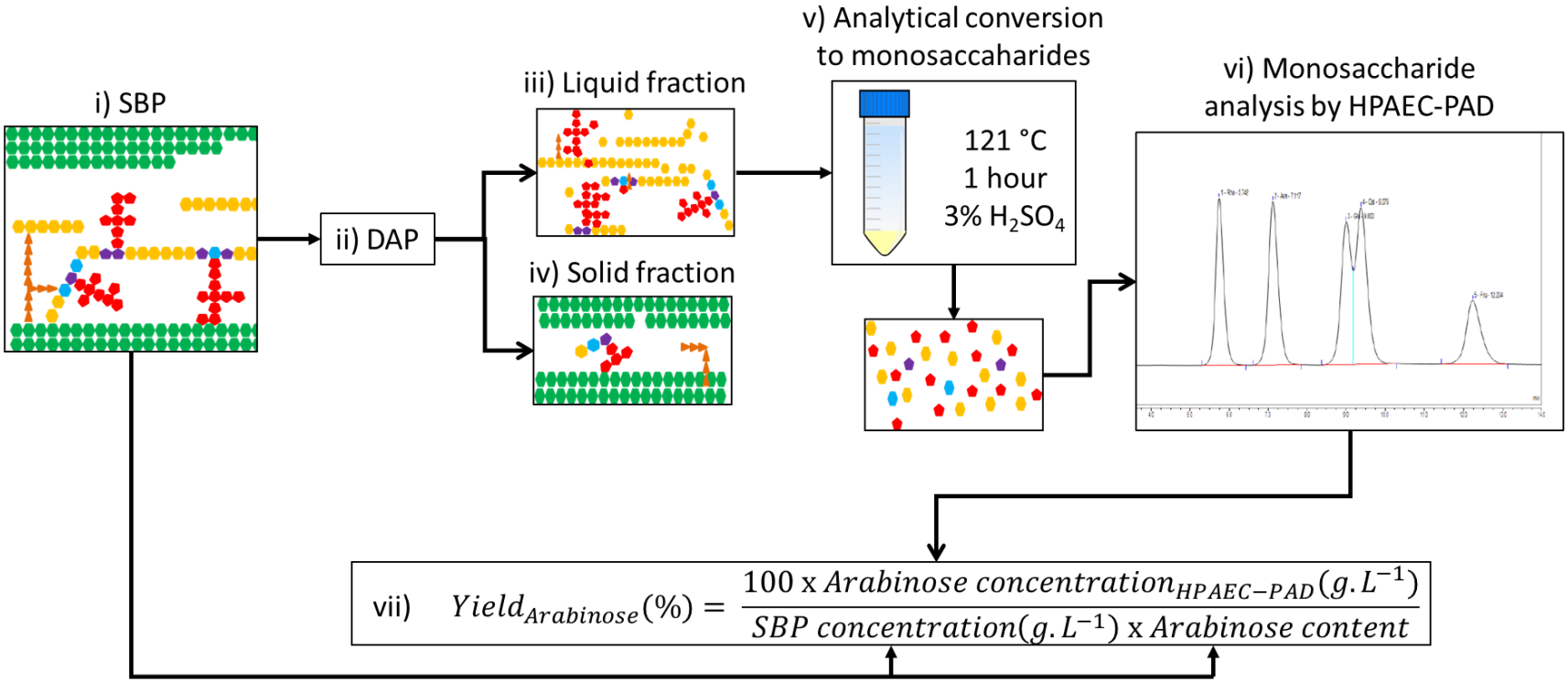

Figure 4.2 Workflow for pretreatment yield determination. i) SBP of known composition (Figure 1.5) is exposed to specific pretreatment conditions (ii) resulting in a pectin-rich liquid fraction (iii), and a cellulose rich solid fraction (iv). A sample of the pectin fraction is then reacted in 3% v/v sulfuric acid for 1 hour at 121 °C (v), causing hydrolysis of the oligosaccharides into monosaccharides, which can then be analysed by HPAEC-PAD (vi). Once the concentration of a particular sugar (e.g. L-arabinose) is known, the yield, which is the proportion of the sugar in the SBP that has been solubilised, both in oligomeric and monomeric form, is calculated (vii).

By considering experiments 1, 2 and 3, it is possible to see that incubating SBP in water at room temperature leads to no detectable solubilisation of any sugar. Experiment 2 shows that even at higher temperatures (80 °C), and no acid addition in static conditions yields very few sugars. SBP mixed in distilled water was found to be slightly acidic at approximately 4.3 as shown in experiment 2. However, acidification to approximately pH 2.0 by acid addition, in experiment 3, solubilised approximately 10% w/w of L-arabinose and D-galacturonic acid and some 5% w/w of available D-glucose.

The SBP used in experiments 1-3 had been dried, ground and passed through a 500 µm sieve. In experiment 4, however, a coarse mix composed of SBP that did not go through the 500 µm mesh was used and lower yields were obtained. The reaction pH was also slightly higher. The lower yield is probably due to a smaller surface area to volume ratio exposing less of the solid biomass. Similarly, the functional groups in SBP that cause the slightly acidic reactions conditions are also exposed less, possibly leading to the slightly higher pH.

Experiments 5, 6 and 7 had a lower pH of 1.8 obtained by the gradual addition of a concentrated acid. Lowering the pH has a very noticeable effect of increasing yields of L-arabinose and D-galacturonic acid, whilst keeping D-glucose yields relatively constant at approximately 5% w/w. It is also possible to see that HCl resulted in slightly more soluble L-arabinose compared to H_2SO_4. Additionally, experiments 6 and 7 demonstrate the limitation of a static system: a higher SBP loading leads to slightly lower D-galacturonic acid yields due to poorer mass transfer. These initial screening results revealed that, particle size, pH, and temperature had an impact on sugar release. Further, although HCl gave slightly better L-arabinose yields; H_2SO_4 was selected for further work as reports indicate it to be the most widely used DAP acid which degrades less cellulose than HCl, potentially leading to a better fractionation (Chamy *et al.*, 1994; Kamzon, Abderafi and Bounahmidi, 2016).

4.3.1.3 Effect of particle size on DAP effectiveness

Having established some important physico-chemical factors for SBP pretreatment a further batch experiment was set up to investigate the sugar solubilisation by DAP. In this instance, 250 mL mixed reactions, set up as described in Section 2.2.2.2 were used. The reaction time was lowered to 15 minutes as this was more representative of residence times that could be obtained in the ACR (Section 3.3.3). This experiment sought to investigate further the effect of particle size on sugar release. As a rule of thumb, flow reactors should only handle solids that are at most $1/10^{th}$ of the size of the smallest internal dimension. In the case of the ACR,

the interconnecting channels are 4 mm x 4 mm, thus requiring particles 400 µm or smaller. For this, SBP powder was milled and sieved through a series of filters: 1000 µm, 500 µm and 212 µm. The powders retained in each filter were also kept and were used to investigate how different PSDs affect DAP. Figure 3.3 (a) and (b) show the appearance and PSD of SBP and how sieving changes particle size. Figure 4.4, on the other hand, corroborates what was found in the initial screening experiments, namely that larger particles lead to lower release of sugars. This was true for all five sugars analysed.

Lower yields compared to Figure 4.3 were achieved due to the shorter reaction time or the reduced temperature (60 °C instead of 80 °C). Interestingly, whole, dried SBP was found to release larger amounts of sugars than the largest milled particles. As such, it appeared that the milling process reduced the amount of sugars that could be solubilised. This might be because the size reduction, which is carried out with a ball mill, causes some compression of the SBP, making it less porous not allowing as much water to penetrate. Further, the SBP cossettes, have a very different geometry (long and thin) and rougher texture potentially making it a more conducive shape for sugar extraction.

Other works have looked at the effect of particle size on sugar release of lignocellulosic material, Pedersen and Mayer (2010) investigated enzymatic digestion of wheat straw and found that particle size had an effect on total yield. Chundawat et al. (2007) investigated ammonia steam explosion on corn fibre to find that particle size had an effect on final enzymatic digestibility (Chundawat, Venkatesh and Dale, 2007; Pedersen and Meyer, 2010). Additionally, mass transfer which is related to sugar release, was found to be affected by agitation (Palmqvist *et al.*, 2016). Since the particles to be used in the ACR had to be sieved through a 212 µm mesh, this finding did not pose an immediate challenge to further study. However, milling can be an energy intensive step and thus undesirable in a biorefinery operation. Despite this, the fact that whole SBP performed better than coarsely ground SBP, could mean that at large scale, with reactors such as the ATR and RTR, whole SBP could be used without the need for milling.

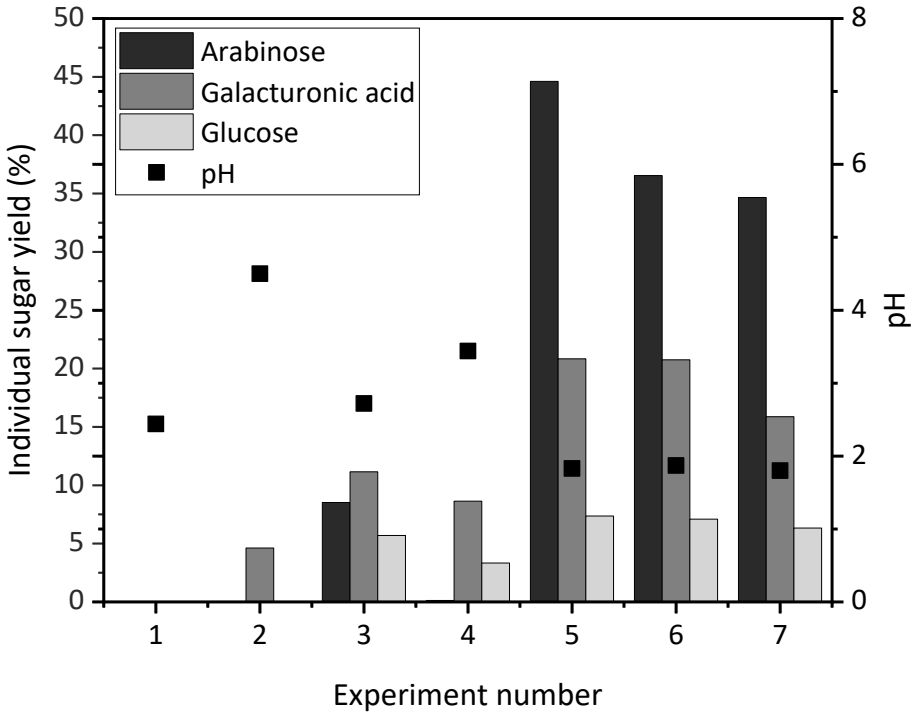

Figure 4.3. Preliminary static batch hydrolysis of SBP. Experimental conditions as outlined in Table 4.1: L-arabinose (Black), D-galacturonic acid (Dark grey) and D-glucose (Light grey) individual yields, shown as the amount of soubilised from the total available sugar (% w/w) are given for the different experimental conditions. Initial pH measurements are also reported. Experiments were carried out as described in Section 2.2.2.1 and analysed as outlined in Section 2.3.3

Table 4.1. Experimental conditions for preliminary static batch hydrolysis of SBP. Factors varied included solid loading, particle coarsensess, temperature, acid addition method and acid type.

Experiment number	Solid loading (% w/v)	Particle size	Temperature(°C)	Acid addition method	Acid type
1	5	Fine	20	5 mL	HCl
2	5	Fine	80	None	None
3	5	Fine	80	5 mL	HCl
4	5	Coarse	80	5 mL	HCl
5	2.5	Fine	80	Gradual	HCl
6	2.5	Fine	80	Gradual	H_2SO_4
7	5	Fine	80	Gradual	H_2SO_4

4.3.2 Design of Experiment investigation of batch pretreatment

4.3.2.1 Experimental design setup

Having established an initial understanding of the effects of various factors on SBP pretreatment, a more in-depth investigation of these factors was required prior to moving onto continuous operation. A good way of establishing complex interactions between several factors is to use a Design of Experiments (DoE) approach. DoE techniques rely on statistical methods to model interactions between many factors. DoE is often shown as an alternative to the "One Factor at A Time" approach, where each factor is investigated independently (Cox and Reid, 2000).

Different types of experimental design can be used. Here, the effects of time, acid concentration, temperature and SBP loading were investigated by using a centre-faced Central Composite Design (cf-CCD). This model gives a second order model and does not require a three-level factorial experimental setup. A full factorial design means that each factor would be tested in combination with every other factor at every level. As such, a 3-level factorial with 4 factors would require $3^4 = 81$ experiments. Conversely, cf-CCD requires a 2-level factorial design, followed by replicates of experiments performed at the centre point of the design space. Finally, axial points with the same conditions as the centre points except for one factor are tested.

The factor range summarised in Table 4.2 was established based on what was practically achievable in the ACR. Temperatures above 80 °C were difficult to obtain; meanwhile, in sugar refineries the SBP exits the previous diffuser step at 60 °C (Section 1.2.1), so temperatures below 60 °C were deemed too low. The H_2SO_4 range studied went from 0 to 100 mM and the SBP loading was set at a range between 2 - 6% w/v as it was thought that the ACR would not handle SBP loadings larger than 6% w/v well. Each experiment had a preset acid concentration, temperature and SBP loading. However, when a reaction was set up samples were taken at different times to study time as a factor, as well. Samples were taken after 1 minute, 15, 30.5 and 60 minutes. The experiments that were carried out and their corresponding conditions and responses are shown in Table 4.3.

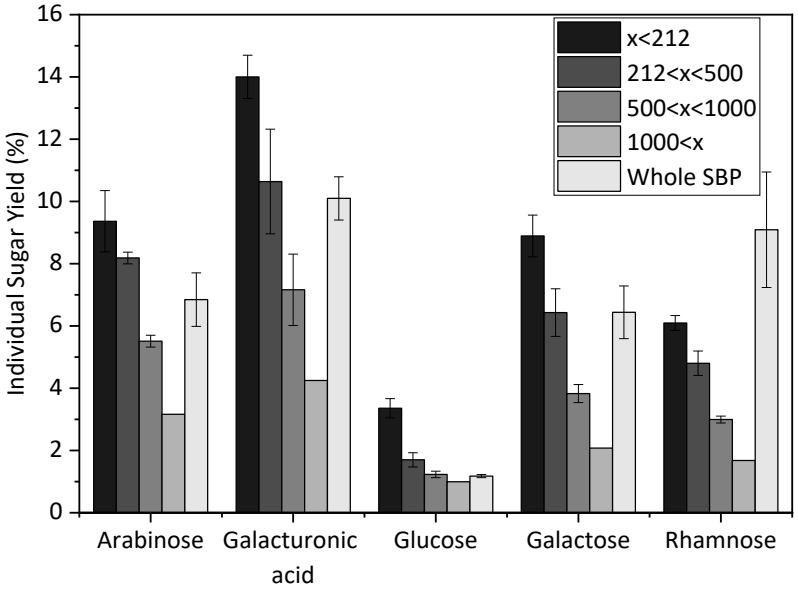

Figure 4.4. Effect of SBP particle size distributon (PSD) on sugar solubilisation, in a stirred batch system. Individual sugar yields for ground SBP that had been passed through different sized mesh. The different SBP fraction and the corresponding particle size distributions can be viewed in Section 3.3.1.2. 2% w/v SBP was used with 50 mM H_2SO_4 in a stirred batch reactor. Experiment was carried out as described in Section 2.2.2.2 and analysed as described in Section 2.3.3 Error bars represent one standard error of the mean (SEM) (n=3).

Table 4.2. Centre-Faced Central Composite Design (cf-CCD) investigation of factors affecting SBP pretreatment. The 4 factors explored in this study and their levels (low, mid-point and high) are outlined.

Factor	Low (-1)	Mid (0)	High (+1)
H_2SO_4 concentration (mM)	0	50	100
SBP (% w/v)	2	4	6
Temperature (°C)	60	70	80
Reaction Time (min)	1	30.5	60

4.3.2.2 4-factor DoE ANOVA results and model analysis

In DoE terminology, the outcome of the experiments, or what is measured, is called a 'response'. A powerful aspect of DoE analysis is that more than one response can be measured, and models for each response can be created. The aim of the study was to investigate the effectiveness of specific DAP conditions on sugar solubilisation. This could be investigated by monitoring sugar concentration. However, one of the factors studied was SBP concentration; thus, two equally effective sets of conditions could have given different results if the initial SBP concentration was different. So, the concentrations obtained from analysis were converted into the L-arabinose, D-galacturonic acid and D-glucose yields which were used as the responses in this study. The yields were calculated based on the total mono- and polymeric sugar solubilised as explained in Section 2.3.3.

The data was analysed through the DesignExpert9 software. As cf-CCD designs allow for the creation of quadratic models, the terms that were investigated for possible significance were: the individual factors (A = H_2SO_4 concentration (mM), B = SBP concentration (% w/v), C = Temperature (°C) and D = Time (min)), their combination (A*B, B*C, C*D, etc) and their quadratic values (A^2, B^2, etc). Analyses of variance (ANOVA) for each model terms were carried out on the models for the three yield responses. The significant model terms for each model are highlighted in green in Table 4.4.

H_2SO_4 concentration (A) and reaction time (D) were found to be significant for each term. This was in line with what was found in the preliminary work. SBP concentration (B) was only found to be relevant for D-galacturonic acid yield and temperature appeared to have no effect on any response. However, combinations of SBP concentration and temperature (B*C) was found to be a significant model term for D-glucose and D-galacturonic acid yields. Additionally, significant model terms for D-glucose yield were also A*B, while significant model terms for D-galacturonic acid yield were B*D and D^2.

To obtain equations describing the effect of the various factors, transformations had to be performed on L-arabinose yield (log transformation) and D-galacturonic acid yield (inverse square root). This resulted in the coded terms equations equation 4.2, 4.3 and 4 .4.

Table 4.3. List of experiments for cf-CCD study. Randomized experimental conditions used for cf-CCD study. For each experiment 4 time points were taken: 1.0, 15.0, 30.0 and 60.0 min. 1, 30 and 60 minutes were used in a 4-factor study discussed in Section 4.3.2.2 whilst the 15 minute timepoint was used for a 3-factor study presented in Section 4.3.2.3. Sugar concentrations were determined by processing samples as described in Section 2.3.3 and analysing resulting monosaccharides by HPAEC-PAD as described in and Section 2.5.

Experiment no	Acid Concentration (mM)	Temperature (°C)	SBP Concentration (% w_{drySBP}/v)	Time (min)	L-arabinose concentration ($g.L^{-1}$)	D-glucose concentration ($g.L^{-1}$)	D-Galacturonic acid concentration ($g.L^{-1}$)	L-arabinose yield (% w/w)	D-glucose yield (% w/w)	D-Galacturonic acid yield (% w/w)
1	0	80	2	1.0	0.28	0.23	0.14	6.6	4.5	3.5
				15.0	0.33	0.25	0.21	7.9	5.0	5.2
				30.5	0.31	0.25	0.24	7.4	5.0	6.0
				60.0	0.32	0.25	0.25	7.7	5.0	6.3
2	100	80	2	1.0	1.00	0.21	0.20	23.9	4.2	5.0
				15.0	2.79	0.26	0.46	66.5	5.3	11.4
				30.5	3.06	0.27	0.52	73.0	5.4	13.0
				60.0	3.54	0.32	0.63	84.4	6.3	15.7
3	100	60	2	1.0	0.52	0.20	0.35	12.4	4.0	8.7
				15.0	1.01	0.21	0.30	24.1	4.2	7.5
				30.5	1.53	0.24	0.45	36.4	4.8	11.1
				60.0	1.97	0.24	0.54	46.9	4.8	13.6

Experiment no	Acid Concentration (mM)	Temperature (°C)	SBP Concentration (% w_{drySBP}/v)	Time (min)	L-arabinose concentration ($g.L^{-1}$)	D-glucose concentration ($g.L^{-1}$)	D-Galacturonic acid concentration ($g.L^{-1}$)	L-arabinose yield (% w/w)	D-glucose yield (% w/w)	D-Galacturonic acid yield (% w/w)
4	0	60	2	1.0	0.22	0.21	0.22	5.3	4.2	5.5
				15.0	0.24	0.23	0.29	5.8	4.7	7.3
				30.5	0.25	0.24	0.30	5.9	4.8	7.4
				60.0	0.26	0.24	0.30	6.1	4.9	7.5
5	50	70	2	1.0	0.55	0.25	0.46	13.0	5.0	11.4
				15.0	1.35	0.25	0.36	32.1	5.0	8.9
				30.5	1.74	0.26	0.45	41.5	5.3	11.3
				60.0	2.20	0.28	0.62	52.4	5.5	15.4
6	50	70	4	1.0	0.98	0.48	0.59	11.7	4.8	7.4
				15.0	1.74	0.46	1.08	20.7	4.6	13.5
				30.5	3.03	0.52	1.06	36.0	5.2	13.3
				60.0	4.20	0.57	1.64	50.1	5.7	20.5
7	50	70	4	1.0	0.70	0.32	1.21	8.4	3.2	15.1
				15.0	1.83	0.42	2.25	21.8	4.2	28.2
				30.5	3.92	0.62	2.89	46.6	6.2	36.1
				60.0	3.67	0.48	1.83	43.7	4.8	22.9

Experiment no	Acid Concentration (mM)	Temperature (°C)	SBP Concentration (% w_{drySBP}/v)	Time (min)	L-arabinose concentration ($g.L^{-1}$)	D-glucose concentration ($g.L^{-1}$)	D-Galacturonic acid concentration ($g.L^{-1}$)	L-arabinose yield (% w/w)	D-glucose yield (% w/w)	D-Galacturonic acid yield (% w/w)
8	50	70	4	1.0	0.79	0.41	1.41	9.4	4.1	17.7
				15.0	2.74	0.46	2.33	32.6	4.6	29.1
				30.5	3.77	0.47	2.49	44.9	4.7	31.1
				60.0	4.90	0.51	2.75	58.3	5.1	34.4
9	0	60	6	1.0	0.77	0.63	1.17	6.1	4.2	9.8
				15.0	0.81	0.66	1.67	6.4	4.4	13.9
				30.5	0.88	0.72	1.77	7.0	4.8	14.8
				60.0	0.77	0.62	1.67	6.1	4.1	13.9
10	0	80	6	1.0	0.74	0.67	1.23	5.9	4.5	10.3
				15.0	3.53	1.04	3.57	28.0	6.9	29.7
				30.5	0.91	0.76	2.32	7.2	5.1	19.3
				60.0	0.87	0.68	1.88	6.9	4.5	15.7
11	100	60	6	1.0	1.74	0.96	1.81	13.8	6.4	15.1
				15.0	3.75	1.13	1.73	29.8	7.6	14.4
				30.5	5.02	1.03	1.61	39.8	6.9	13.4
				60.0	6.75	1.08	1.68	53.6	7.2	14.0

Experiment no	Acid Concentration (mM)	Temperature (°C)	SBP Concentration (% w_{drySBP}/v)	Time (min)	L-arabinose concentration ($g.L^{-1}$)	D-glucose concentration ($g.L^{-1}$)	D-Galacturonic acid concentration ($g.L^{-1}$)	L-arabinose yield (% w/w)	D-glucose yield (% w/w)	D-Galacturonic acid yield (% w/w)
12	100	80	6	1.0	1.62	0.74	2.81	12.9	4.9	23.4
				15.0	3.42	0.79	3.54	27.1	5.3	29.5
				30.5	4.65	0.86	4.19	36.9	5.8	35.0
				60.0	6.28	0.88	3.71	49.9	5.9	31.0
13	50	70	6	1.0	1.25	0.68	1.95	9.9	4.5	16.2
				15.0	2.51	0.70	2.95	19.9	4.7	24.6
				30.5	4.20	0.80	3.39	33.3	5.3	28.2
				60.0	6.45	0.88	4.34	51.2	5.8	36.2
14	0	70	4	1.0	0.36	0.41	0.73	4.3	4.1	9.1
				15.0	0.41	0.46	0.81	4.9	4.6	10.2
				30.5	0.43	0.46	0.83	5.1	4.6	10.4
				60.0	0.46	0.48	0.86	5.5	4.8	10.8
15	100	70	4	1.0	1.62	0.53	1.44	19.3	5.3	18.1
				15.0	3.77	0.48	2.14	44.9	4.8	26.8
				30.5	5.39	0.58	1.85	64.1	5.8	23.1
				60.0	5.23	0.53	2.15	62.3	5.3	26.9

Experiment no	Acid Concentration (mM)	Temperature (°C)	SBP Concentration (% w_{drySBP}/v)	Time (min)	L-arabinose concentration ($g.L^{-1}$)	D-glucose concentration ($g.L^{-1}$)	D-Galacturonic acid concentration ($g.L^{-1}$)	L-arabinose yield (% w/w)	D-glucose yield (% w/w)	D-Galacturonic acid yield (% w/w)
16	50	60	4	1.0	7.34	0.77	0.99	87.3	7.7	12.3
				15.0	1.60	0.60	1.98	19.0	6.0	24.8
				30.5	1.94	0.58	1.92	23.0	5.8	24.0
				60.0	2.46	0.56	1.97	29.3	5.6	24.6
17	50	80	4	1.0	0.00	0.00	0.00	0.0	0.0	0.0
				15.0	4.65	0.63	2.60	55.4	6.3	32.5
				30.5	4.61	0.54	1.73	54.9	5.4	21.6
				60.0	5.77	0.60	2.20	68.7	6.0	27.5

Table 4.4. ANOVA results for a 4-factor cf-CCD model of batch SBP pretreatment. Factors (A = H_2SO_4 concentration (mM), B = SBP concentration (% w/v), C = Temperature (°C) and D = Time (min)), combined factors (e.g. BC) and quadratic factors (e.g. A^2) were fitted to models. Their significance with respect to each response is represented by the corresponding p-values. In green are the terms that were deemed significant for each model. Additionally, the overall model significance is shown in the first row of the table.

Variable	p-value Arabinose yield	p-value Glucose yield	p-value Galacturonic acid yield
Model	0.003	0.0017	0.0002
A	0.0001	0.0005	0.0028
B	0.0754	0.0853	< 0.0001
C	0.865	0.9147	0.1111
D	0.0018	0.0062	0.0004
AB	0.317	0.0074	0.9581
AC	0.1094	0.2335	0.0341
AD	0.09	0.1086	0.819
BC	0.5763	0.0389	0.0019
BD	0.5551	0.2374	0.0379
CD	0.5882	0.5363	0.1188
A^2	0.0676		0.2198
B^2	0.7646		0.5814
C^2	0.8726		0.3935
D^2	0.3006		0.0153

$$\log_{10}(\text{L} - \textbf{arabinose yield}) = 1.56 + 0.29 * A - 0.099 * B - 8.853 * 10^{-3} * C + 0.20 * D + 0.056 * AB + 0.093 * AC + 0.100 * AD + 0.031 * BC - 0.033 * BD - 0.030 * CD - 0.27 * A^2 + 0.0410 * B^2 + 0.022 * C^2 - 0.15 * D^2$$ [Equation 4.2]

$$D - glucose\ yield = 5.12 + 0.51 * A + 0.22 * B - 0.013 * C + 0.37 * D + 0.38 * AB - 0.16 * AC + 0.21 * AD - 0.28 * BC - 0.15 * BD + 0.079 * CD$$ [Equation 4.3]

$$\frac{1}{\sqrt{\text{D-galacturonic Acid yield}}} = = 0.22 - 0.032 * A - 0.050 * B + 0.015 * C - 0.041 * D - 4.881 * 10^{-4} * AB - 0.022 * AC + 2.128 * 10^{-3} * AD - 0.036 * BC + 0.021 * BD - 0.015 * CD + 0.029 * A^2 + 0.013 * B^2 - 0.020 * C^2 + 0.064 * D^2$$ [Equation 4.4]

Coded terms equations are equations that model the desired response in terms of the factors, but rather than using the actual units of each factor, such as degrees for temperature and mM for H_2SO_4 concentration, coded equations set the high level of the design as 1 and the lowest as -1 for each factor. For example, since the temperature (factor C) range was 60 °C to 80 °C, 60 °C would equate to -1, 70 °C, the mid-point to 0 and 80 °C to 1. By coding all the terms this way, the equations obtained allow for a quick estimation of which term is most important (the biggest multiplier in front of each term) and how the term affects the response (negative multipliers give a negative correlation between factor and response).

The coded terms equations reveal that the most impactful factors for L-arabinose and D-glucose release are H_2SO_4 concentration and time. A further important factor for L-arabinose is the combination of these two factors. For D-galacturonic acid, on the other hand, release was impacted mostly by SBP concentration, and time. Further, the interaction between temperature and SBP concentration and time squared were also important. Another useful way to interpret the results was by looking at the physical interaction between factors on a 3D plot. Figure 4.5, Figure 4.6, and Figure 4.7 show the 6 possible factor interactions between the 4 factors for L-arabinose, D-glucose and D-galacturonic acid yield, respectively.

Panels (a), (b) and (c) in Figure 4.5 clearly show the effect of H_2SO_4 on L-arabinose release. The effect of time can be seen in panel (d). And although it did not appear to make a significant model term, the effect of lowering SBP concentration at long reaction times (a

reduction in yield) can also be seen in panel (d). Temperature, which was also not seen as a significant term does not appear to have an effect on L-arabinose yields in panels (c), (e) and (f). The graphs appear to suggest that at high acid concentration and temperature L-arabinose yields of 60% w/w can be obtained.

As expected, D-glucose yields were found to be quite low, never exceeding 7% w/w. The effects of the various factors were minimal, and if the D-glucose model was plotted on the same yield axis scale as L-arabinose or D-galacturonic acid the response would appear relatively flat. Further, it was theorised that the D-glucose being released was monomeric D-glucose or a product of sucrose hydrolysis (into D-fructose and D-glucose). Indeed, as discussed earlier, cellulose is depolymerised at much harsher and higher temperatures, than what was used here. A similar finding was made by Hamley-Bennett et al. (2016) when working on selective fractionation of SBP by steam explosion. D-galacturonic acid yields appeared less variable than L-arabinose, with a drastic increase in yield appearing at high temperatures and SBP loading, as shown in Figure 4.7 panel (d). The D-galacturonic acid model had a significant D^2 term, indicating a quadratic relationship between D-galacturonic acid release and reaction time. This may explain the "bump" effect that time appears to have as showcased in panels (c), (e), and (f). H_2SO_4 concentration which appeared to have a large impact on L-arabinose release does not seem to have a similar effect on D-galacturonic acid. This may be caused by the more branched nature of arabinans, which tend to branch from a D-galacturonic acid–rich backbone (Oosterveld *et al.*, 2000; Kühnel *et al.*, 2010). SBP appeared to have a slight effect on D-galacturonic acid release, but this effect appears more prominently when the other factor being studied in the plot is also at its highest level.

The L-arabinose model was found to have a signal to noise ratio of 7.727, deeming it appropriate, as a ratio greater than 4 is desirable. A sufficiently high signal to noise ratio indicates that the model can be used to navigate the design space. Despite this, the predicted R^2 value (0.1288) was found to be too different from the adjusted R^2 value (0.7011); typically, a difference of less than 0.2 is desirable. This large difference indicates a possible block effect or a problem with the model.

The D-glucose model also had a large difference between predicted and adjusted R^2 values (0.0118 and 0.6222, respectively); however its signal to noise ratio was found to be adequate as well at 9.115. The D-galacturonic acid model also had an adequate signal to noise ratio (14.485); additionally, it also had reasonable agreement between predicted and adjusted R^2 values (0.6616 and 0.8228, respectively).

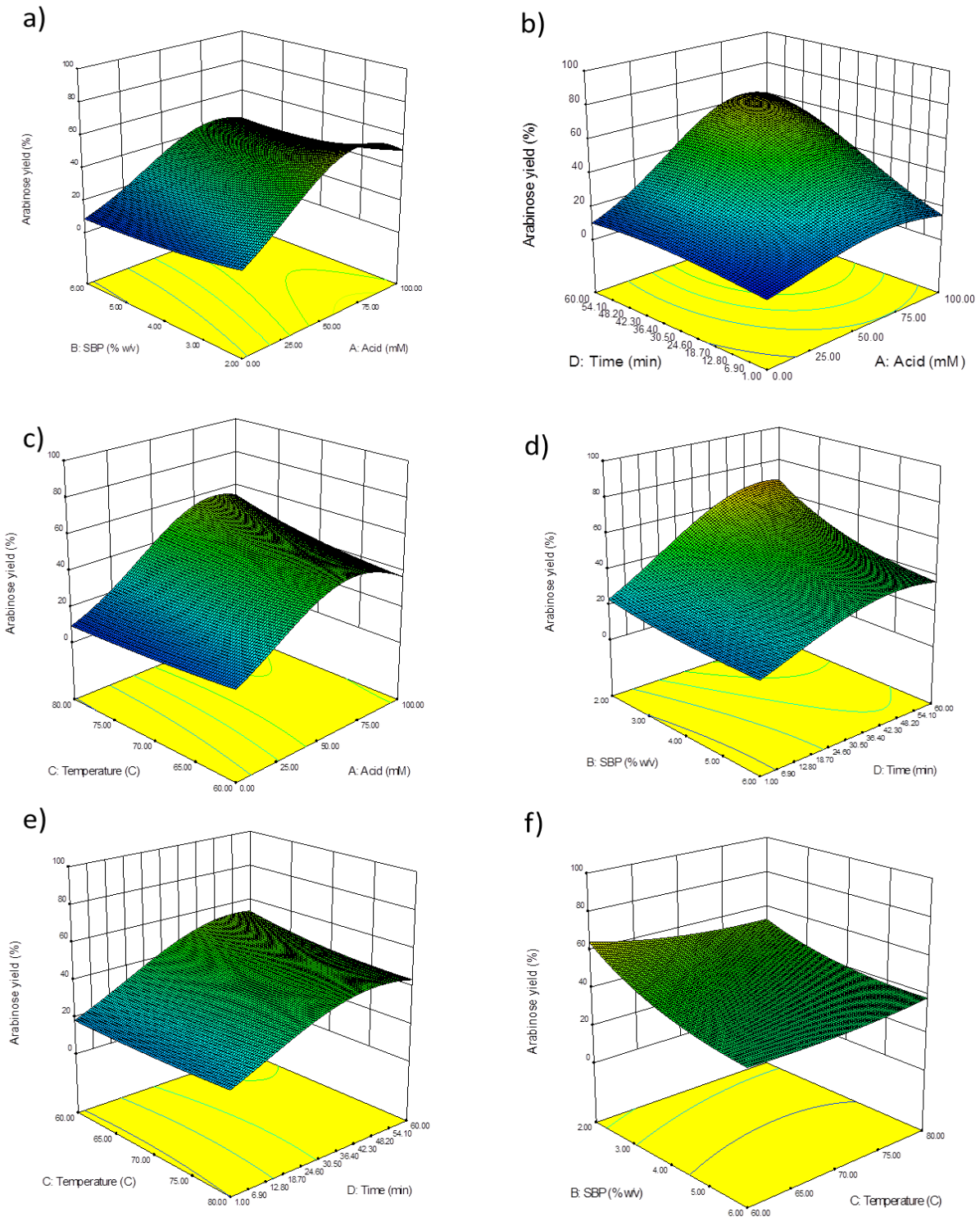

Figure 4.5. Response surface plots illustrating influence of 2-factor interactions on L-arabinose yields. Interactions between acid concentration (factor A), SBP concentration (factor B), temperature (factor C) and time (factor D); and their combined effects on L-arabinose yield is shown. The panels show the following interactions: (a) – AB; (b) – AC; (c) – AD; (d) – BC; (e) – BD; and (f) – CD. Models based on data in Table 4.3 were generated using DesignExpert DoE software as outlined in Section 4.3.2.

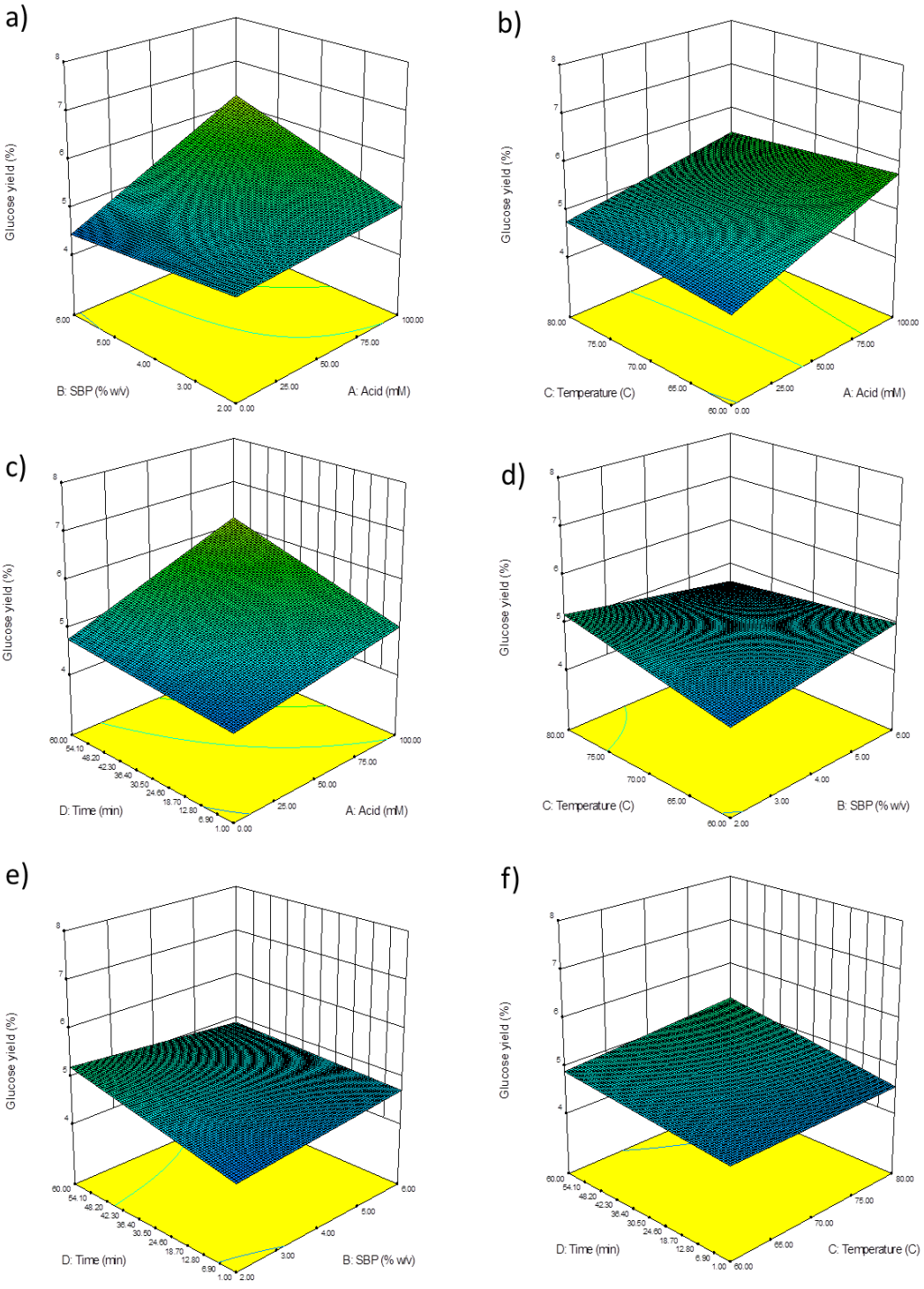

Figure 4.6. Response surface plots illustrating influence of 2-factor interactions on D-glucose yields. Interactions between acid concentration (factor A), SBP concentration (factor B), temperature (factor C) and time (factor D); and their combined effects on D-glucose yield is shown. The panels show the following interactions: (a) – AB; (b) – AC; (c) – AD; (d) – BC; (e) – BD; and (f) – CD. Models based on data in Table 4.3 were generated using DesignExpert DoE software as outlined in Section 4.3.2.

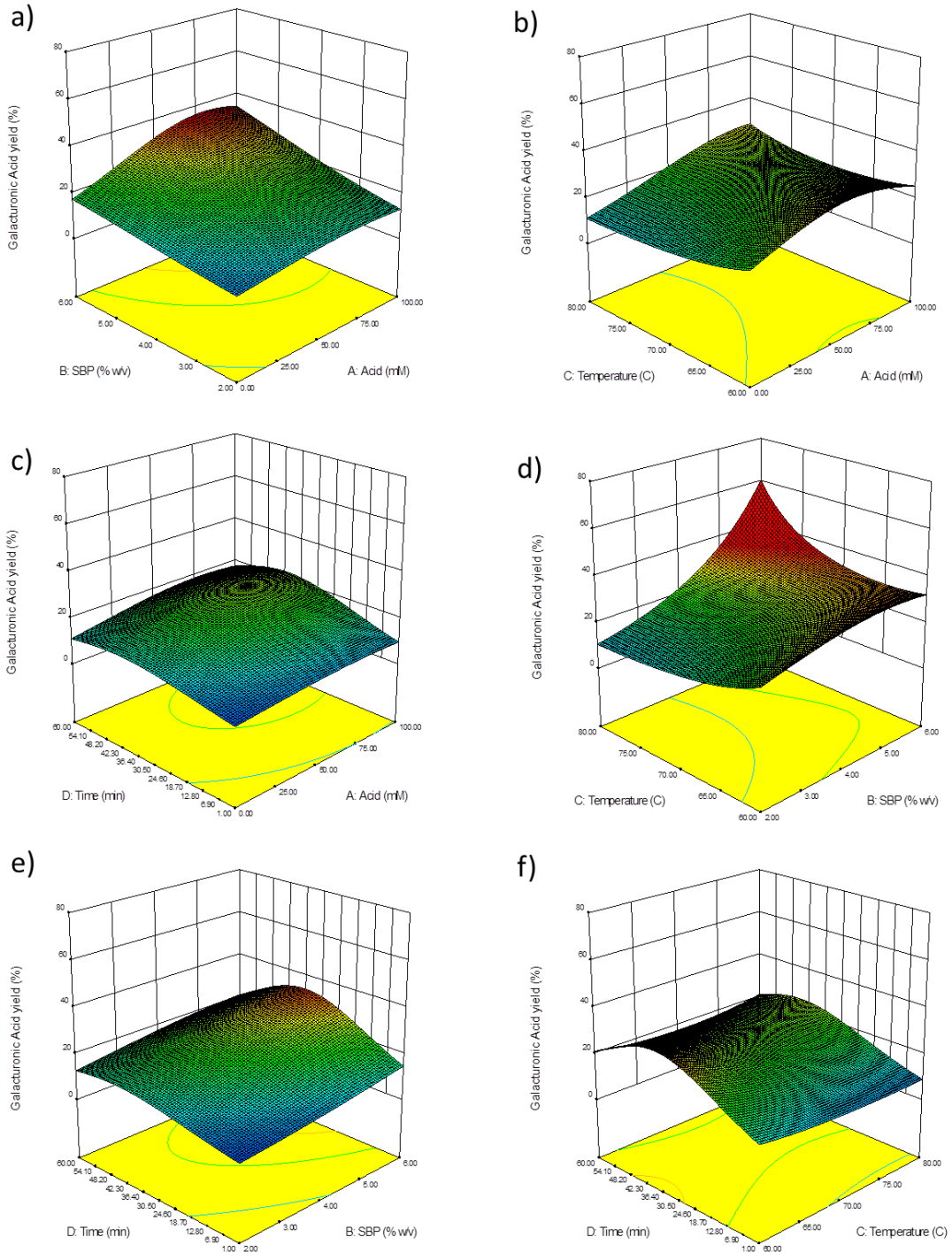

Figure 4.7. Response surface plots illustrating influence of 2-factor interactions on D-galacturonic acid yields. Interactions between acid concentration (factor A), SBP concentration (factor B), temperature (factor C) and time (factor D); and their combined effects on D-galacturonic acid yield is shown. The panels show the following interactions: (a) – AB; (b) – AC; (c) – AD; (d) – BC; (e) – BD; and (f) – CD. Models based on data in Table 4.3 were generated using DesignExpert DoE software as outlined in Section 4.3.2.

4.3.2.3 3-factor DoE ANOVA results and model analysis

The possible blocking effect problems called for a simplification of the models. As mentioned earlier, to reduce the total number of experiments, the same hydrolysis reaction was used to collect more than one data point. It was thought that this could bias the dataset and potentially be causing the blocking effect that was noticed for L-arabinose and D-glucose release. Furthermore, preliminary work on the ACR as well as the work discussed in Chapter 3 set an upper residence time limit at approximately 15 minutes. Thus, 15 min reaction time samples were also taken to build a 3-factor cf-CCD model. The ANOVA on the model terms (A = H_2SO_4 4; B = SBP concentration; and C = Temperature, and their combinations) is shown in Table 4.5. Here different significances were found compared to the 4-factor model. Temperature was found to be a significant model term in the L-arabinose yield model, which had not been the case in the larger, 4-factor design. H_2SO_4 concentration was not found to be a significant model term in the case of D-galacturonic acid yield, though it had been previously. Interestingly the model itself was not found to be significant in the case of D-glucose yield. This may have been because at 15 minutes, D-glucose yields were quite low and not as easily measurable in the HPAEC-PAD detection system.

The models obtained are shown below in their coded terms equations. It can be seen that by removing the time factor, the model for L-arabinose was simplified from a quadratic to a linear model. The coded factors show the H_2SO_4 concentration as the factor with the biggest impact on L-arabinose solubilisation, followed by temperature. SBP, on the other hand, has a slight negative effect on L-arabinose yield. The D-glucose model was not found to be significant, but it did show some slight effects by all three factors. Meanwhile, the D-galacturonic acid yield model shows important temperature and SBP effects, H_2SO_4 concentration also appears to have a positive effect. However, some of these strong positive effects are countered by the quadratic terms of the model (especially the A^2 and B^2 terms that are large and negative).

Table 4.5. ANOVA results for different model terms in the 3-factor cf-CCD model. Factors (A = H_2SO_4 concentration (mM), B = SBP concentration (% w/v) and C = Temperature (°C)), combined factors (e.g. BC) and quadratic factors (e.g. A^2) were fitted to models. Their significance with respect to each response is represented by the corresponding p-values. In green, are the terms that were deemed significant for each model. Additionally, the model significance is shown at the top of the table.

Variable	p-value Arabinose yield	p-value Glucose yield	p-value Galacturonic acid yield
Model	0.0014	0.4335	0.0448
A	0.0005	0.6473	0.2565
B	0.7713	0.1543	0.0068
C	0.0158	0.5266	0.071
AB			0.7234
AC			0.7667
BC			0.1289
A^2			0.1551
B^2			0.0773
C^2			0.2756

$$\sqrt{\mathbf{L-Arabinose\ Yield}} = \mathbf{4.85} + \mathbf{1.52} * \boldsymbol{A} - \mathbf{0.099} * \boldsymbol{B} + \mathbf{0.92} * \boldsymbol{C}$$

[Equation 4.5]

$$\boldsymbol{D-glucose\ Yield} = \mathbf{5.18} + \mathbf{0.14} * \boldsymbol{A} + \mathbf{0.46} * \boldsymbol{B} + \mathbf{0.20} * \boldsymbol{C}$$

[Equation 4.6]

$$\boldsymbol{D-galacturonic\ Acid\ Yield} = \mathbf{24.01} + \mathbf{2.34} * \boldsymbol{A} + \mathbf{7.17} * \boldsymbol{B} + \mathbf{4.03} * \boldsymbol{C} - \mathbf{0.78} * \boldsymbol{AB} + \mathbf{0.65} * \boldsymbol{AC} + \mathbf{3.64} * \boldsymbol{BC} - \mathbf{5.83} * \boldsymbol{A^2} - \mathbf{7.57} * \boldsymbol{B^2} + \mathbf{4.33} * \boldsymbol{C^2}$$

[Equation 4.7]

The linear nature of the L-arabinose model is reflected in the 2-factor surface plots in Figure 4.8 panels (a), (c) and (d). Where it can be seen that temperature and H_2SO_4 concentration have positive effects on L-arabinose yield, and SBP concentration does not appear to affect yields. The D-galacturonic acid yield plots (shown in (b), (d), and (f)), on other hand, reflect the importance of the quadratic terms. H_2SO_4 and SBP concentration have alternate positive and negative model terms (+7.17 * B and – 7.57 B^2), whilst the Temperature factor terms are both positive (+4.03*C and +4.33 * C^2). This effect results in a "bump" for H_2SO_4 and SBP concentration around the mid-point, where the coded terms equal to zero. Conversely, a "trough" can be seen in panels (d) and (f), when temperature is set around the mid-point.

Despite the model being reduced from 4 to 3 factors, the L-arabinose yield still showed a large difference between predicted and adjusted R^2 (0.3708 and 0.6147, respectively). However, the signal to noise ratio was found to be adequate for navigating the design space. For the 3-factor model a signal to noise ratio of 6.095 was found, but the difference between predicted and adjusted R^2 was also too great (0.2555 and 0.6154, respectively). Meanwhile, the predicted R^2 value for the D-glucose yield model was negative; indicating that the overall mean of the various experiments carried out is a better predictor than the derived model. The signal to noise ratio was also too low to navigate the design space.

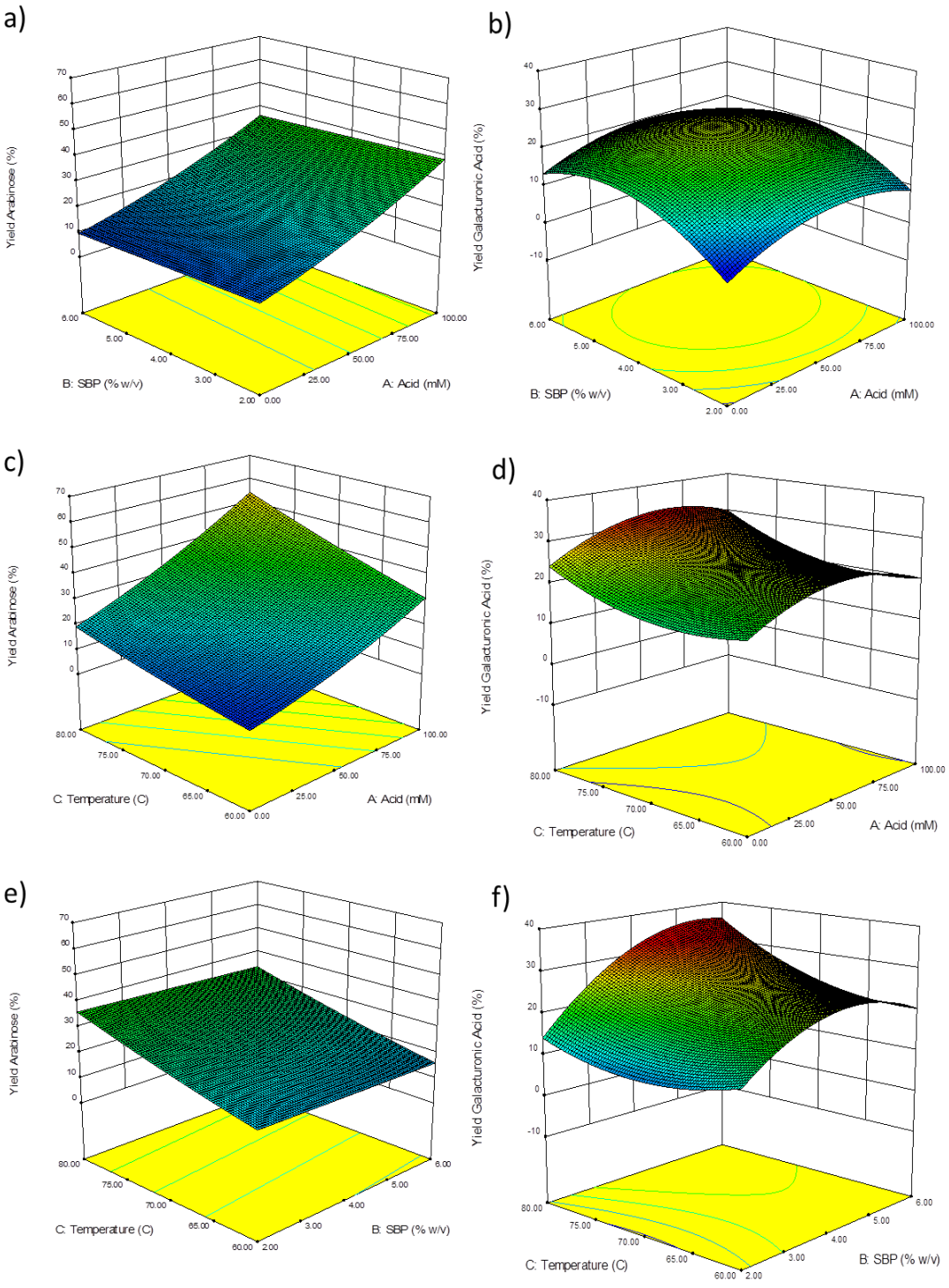

Figure 4.8. Response surface plots illustrating influence of 2-factor on L-arabinose and D-galacturonic acid yields. (a), (c) and (e) show 3 factor interactions for L-arabinose yields, whilst (b), (d) and (f) show factor interactions for D-galacturonic acid yields. (a) and (b) show combined effects of acid and SBP concentration, (c) and (d) show interactions of temperature and acid concentration. And, finally, (e) and (f) show interactions for SBP concentration and temperature. Models based on data in Table 4.3 were generated using DesignExpert DoE software as outlined in Section 4.3.2.

4.3.2.4 Model predictions of optimal DAP conditions and model verification

As stated earlier, the large difference in predicted and adjusted R^2 values can be due to blocking effects, or problems with the model and/or data. Despite this, some confirmation runs were carried out. For this the DesignExpert software allows for targets to be placed on each response. In this case the aim was to maximise L-arabinose and D-galacturonic acid yield and minimise D-glucose yield. This was to obtain DAP conditions that would maximise fractionation by producing a liquid fraction rich in L-arabinose and D-galacturonic acid oligomers and monomers, with little D-glucose carryover. Further, a 15 minute time limit was set on the 4-factor design so that the condition would be optimised for the ACR. The software produced the following conditions to be used as confirmation runs: 85.77 mM H_2SO_4, 6% w/v SBP concentration and 80 °C. Unfortunately, the experimental designs that were tested did not produce predictive models as was hoped. Despite this, the models still gave the possibility of navigating the design space and explore the major interactions between the various factors. The models showed that H_2SO_4 concentration had a large effect on solubilisation of L-arabinose release. This effect was less noticeable on D-glucose and D-galacturonic acid, this is likely due to the highly branched nature of arabinans, compared to the relatively unbranched polygalacturonans and the extremely durable and unbranched D-glucose-containing cellulose (Kühnel, Schols and Gruppen, 2011b). SBP concentration was not found to have a noticeable effect on the release of sugars. Reaction time was found to have an important effect, especially on L-arabinose release. Interestingly, temperature did not appear to have a large impact using the 4-factor model, but when the reduced model was used, its effect on L-arabinose and D-galacturonic acid became larger.

Table 4.6 shows the predicted values for the 4-factor cf-CCD for this condition. Additionally, the table shows the values that were predicted using these same conditions by the 3-factor model. Finally, the actual values found in the confirmation run are shown. The confirmation runs were done in triplicate, and it was found that the models appeared to underestimate L-arabinose release and overestimate the release of D-galacturonic acid.

Unfortunately, the experimental designs that were tested did not produce predictive models as was hoped. Despite this, the models still gave the possibility of navigating the design space and explore the major interactions between the various factors. The models showed that H_2SO_4 concentration had a large effect on solubilisation of L-arabinose release. This effect was less noticeable on D-glucose and D-galacturonic acid, this is likely due to the highly branched nature of arabinans, compared to the relatively unbranched polygalacturonans and the extremely durable and unbranched D-glucose-containing cellulose (Kühnel, Schols and Gruppen, 2011b). SBP concentration was not found to have a noticeable effect on the release of sugars. Reaction time was found to have an important effect, especially on L-arabinose release. Interestingly, temperature did not appear to have a large impact using the 4-factor model, but when the reduced model was used, its effect on L-arabinose and D-galacturonic acid became larger.

Table 4.6. Prediction of maximum solubilisation of sugars using 3- and 4-Factor cf-CCD models and experimental validation for stirred batch DAP. DoE model with 4 and 3 factors were used to predict the optimum values and the actual responses for concentration and yield for L-arabinose, D-galacturonic acid and D-glucose, using a 15 min reaction time. Experimental verification was carried out as described in Section 2.2.2.3. Sugar concentrations were determined by processing samples as described in Section 2.3.3 and analysing resulting monosaccharides by HPAEC-PAD as described in and Section 2.5.

Response	Value Predicted with 4 Factor cf-CCD	Value Predicted with 3 Factor cf-CCD	Actual Value	Standard Deviation
L-arabinose Yield (% w/w)	41.9	34.9	56.2	7.1
D-glucose Yield (% w/w)	4.3	6.0	4.5	1.5
D-galacturonic Acid Yield (% w/w)	48.5	28.3	19.0	2.9

Huang et al. (2010) used a CCD approach on corn cobs acid pretreatment. Although they used higher acid concentrations and did not test corn cob concentration, their design was similar to the present one. The temperature range studied was between 50 °C and 70 °C and it was found that its effect was important at lower temperatures (<60 °C) but less important at higher temperatures. Time also had an impact on other hemicellulosic sugars as formic acid concentration (Huang *et al.*, 2010).

Zheng et al. (2013), on the other hand, tested pretreatment of SBP for simultaneous saccharification and fermentation of bioethanol. Whilst their temperature range was much higher (120 °C – 140 °C), their solid loading was the same and their acid concentration measured as a % w/w was comparable (0% w/w – 1% w/w equivalent to approximately 0 – 100 mM). As in this study, they found that SBP concentration did not affect solubilisation of sugars. Temperature and acid concentration, on the other hand, did have an effect on sugar release. Although, as the SBP pretreatment was used to produce a fermentable slurry rather than a fractionated product, it is worth noting that the amount of D-glucose and D-galacturonic acid solubilised was much higher due to the harsher conditions used (Zheng *et al.*, 2013).

Initially, a centre-faced CCD was selected as it would estimate linear and quadratic interactions; however, the model was not sufficiently significant to fully explore this design space. Possible alternative strategies could have been employed. For example, an initial less detailed screening design could have been planned. This design could have comprised either fewer runs, or more factors such as type of acid. Alternatively, it could have accounted for blocking effects such as the grouping of all the different time points in a single run as was done for the 4-factor model. This initial design would have likely revealed that SBP was not a significant factor. Following this initial screening stage, a more detailed experimental design, such as a full-factorial design, could have been carried out on a system with a reduced number of factors. For example, interactions between acid and temperature using a 15 minute reaction time could have been explored more fully.

To conclude, despite the DoE model not providing very accurate predictions of the arabinans and galacturonans solubilisation, some insights as to what factors could be investigated in continuous mode were still obtained.

4.3.3 Continuous dilute acid pretreatment

4.3.3.1 ACR setup and sugar degradation

Having achieved a better understanding of the various factors affecting pretreatment, continuous DAP was attempted. The reactor was set up as described in Section 2.2.3. Particular attention was given to inlet tubing connecting the feed bottle to the reactor. This was kept at a shallow downwards angle to ensure no blockages or SBP build-up would occur.

The first challenge was the possibility that the acidic conditions inside the reactor might be degrading the sugars obtained. For this, a slightly modified setup was used: a model solution containing monomeric L-arabinose, D-galactose, D-galacturonic acid, D-glucose and L-rhamnose was prepared and passed through the reactor. Different concentrations of H_2SO_4 were pumped through the side entry port at the same flowrate to obtain different final concentrations. The outlet concentration of each sugar was compared to the initial concentration and is reported in Figure 4.9. No sugar degradation was seen for the various initial H_2SO_4 concentrations, corresponding to a final 20, 30, 40, or 50 mM H_2SO_4 in the reactor. Products of degradation that occur during lignocellulosic pretreatment have been reported to have inhibiting effects on fermentative process (Chen *et al.*, 2013; Kim *et al.*, 2014), so the fact that the DAP conditions studied here are mild enough to avoid this is an added advantage of this process over other pretreatment techniques.

4.3.3.2 Flowrate effect on L-arabinose solubilisation

Initial testing on the ACR had revealed that below a pump speed of 10 rpm, SBP particles would settle in the tubing. This speed was equivalent to a 15.2 min residence time in the ACR, and indeed this 15 minute residence time was used as a starting point for the ACR performance characterisation in Chapter 3 and the DoE work presented in the previous section. However, it was important to test the pretreatment reaction at a range of flowrates to test the impact of residence time on sugar release. Along with 10 rpm, the pump speed was also set to 20 and 40 rpm (equivalent to residence times of 7.6 and 3.8 min, respectively). Additionally, it was found that it was possible to attain a residence time of 19.0 min (8 rpm), for short period of times, as the inlet tubing required constant agitation to prevent solid settling.

The pretreatment reaction was tested at 60 °C, using 2% w/v SBP, 50 mM H_2SO_4. The corresponding L-arabinose yield is shown in Figure 4.10. It was found that yields were

increasing with increasing residence time, which followed from the findings of the DoE study. Throughput was calculated by dividing the concentration at the exit of the reactor by the residence time. Here, it appeared that the shortest residence time produced the highest throughput, whilst longer residence times (7.6, 15.2 and 19.0 min) produced comparable throughputs. Despite the higher throughput, the higher flowrates were deemed inappropriate as the yield was considerably lower. The highest yield was obtained with the longest residence time. However, operating the ACR with a pump speed of 8 rpm required constant supervision and was also deemed unfeasible. As such the flowrate equivalent to a 15.2 min residence time was used for further investigations.

4.3.3.3 Effect of temperature on solubilisation of sugars

The DoE setup investigating 3 factors, showed the importance of reaction temperature on L-arabinose release. To investigate this further and confirm that this effect was present in the continuous setup, DAP was tested at different temperatures, by keeping H_2SO_4 concentration, residence time and SBP concentration constant at 50 mM, 15.2 min and 2% w/v. Yields for L-arabinose, D-galacturonic acid, D-glucose, D-galactose and L-rhamnose were monitored and are shown in Figure 4.11. Interestingly, temperature did not seem to have a big effect on yield of D-galacturonic acid and D-glucose. L-arabinose release, on the other hand, increased quite considerably from below 10% w/w at temperatures lower than 60 °C all the way to above 40% w/w at 83 °C. D-galactose yield also increased with temperatures. This, too, was expected, as D-galactose is also part of the branched hemicellulose structure within the SBP structure and is therefore more heat labile than pectin and cellulose (Kühnel, Schols and Gruppen, 2011b). The low yields at low temperatures also reiterate what was already thought, namely that below 60 °C (the temperature used for sucrose extraction in the sugar refinery) yields are very low and release is minimal. As stated in Section 4.3.1.1, the yields reported here include both monosaccharides and oligosaccharides solubilised during the process. In this work, the amount of monosaccharides released during the pretreatment reaction (i.e. before the analytical acid hydrolysis that converted all oligosaccharides into monosaccharides) was not measured, but it is possible that harsher conditions led not only to increased yield, but also an increased proportion of monosaccharides (Kühnel, Schols and Gruppen, 2011b).

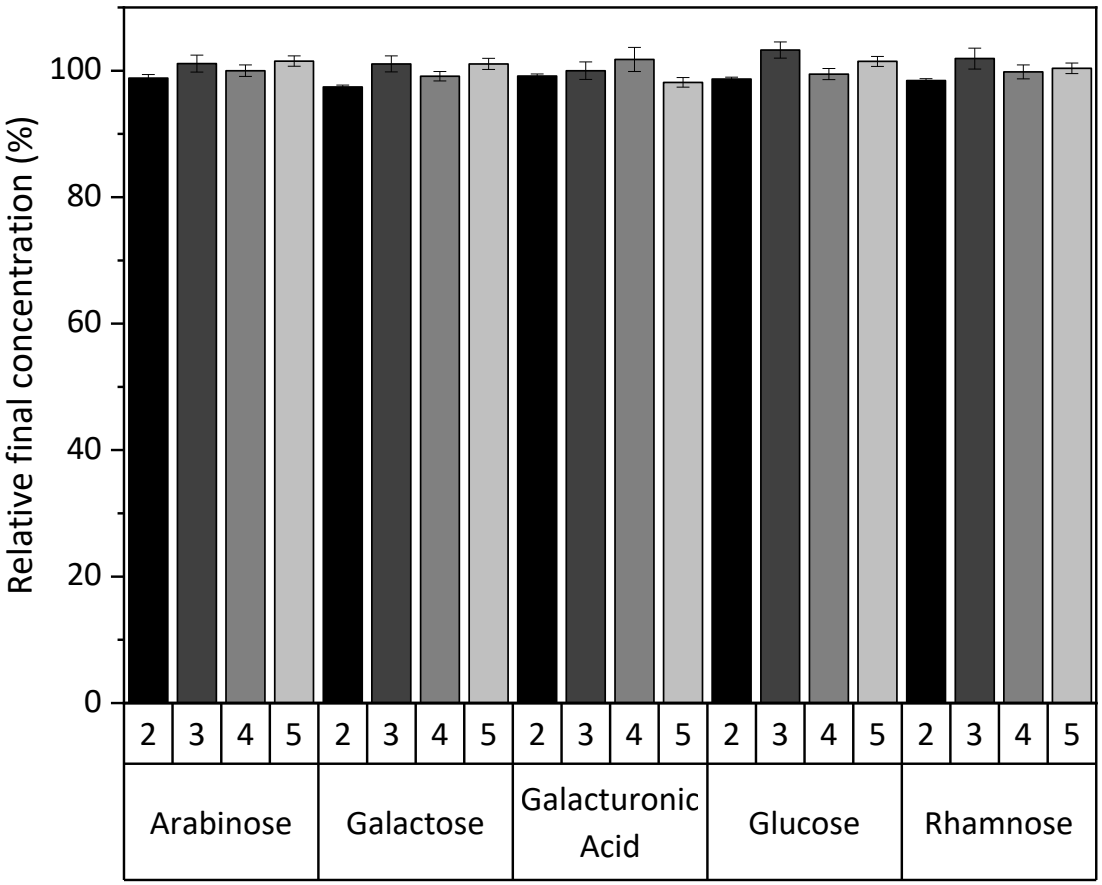

Figure 4.9. Control experiment showing lack of degradation of monomeric SBP sugars in the continuous flow reactor. A mix containing 5 different sugars was pumped through the ACR with a 15.2 min residence time at 80 °C. Different acid concentrations (2, 3, 4, and 5 M H_2SO_4) were injected through the side-entry port at 10 mL.hour^{-1}. Concentration at the outlet was measured via HPAEC-PAD as outlined in 2.5. Error bars represent SEM (n=3).

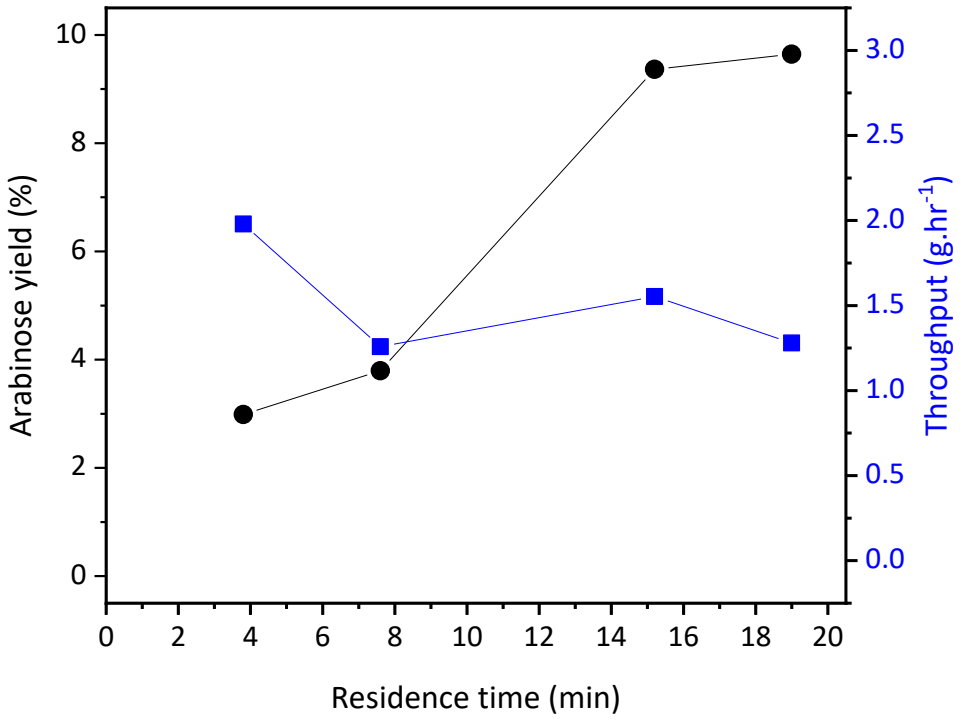

Figure 4.10. Effect of residence time on L-arabinose release during DAP of SBP in the ACR. L-arabinose yield (●) and L-arabinose throughput (■) were obtained for varying residence times. The ACR was operated at 6 Hz, with a 15.2 min residence, 2% w/v SBP, 50 mM H_2SO_4, and 60 °C. Error bars represent SEM (n=3). ACR was operated as described in 2.2.3.

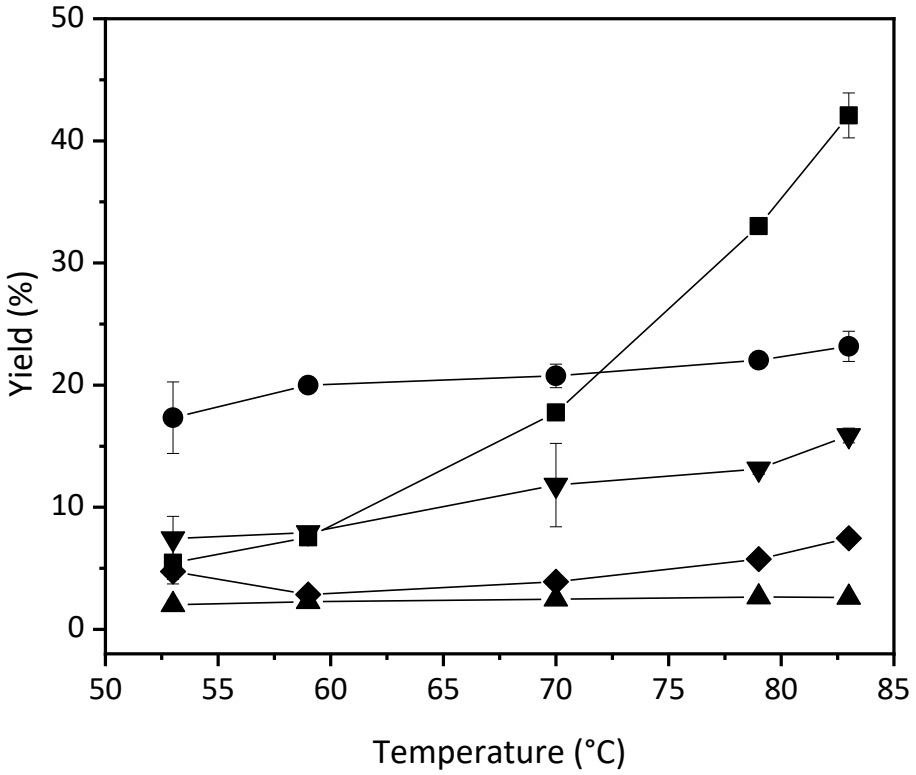

Figure 4.11. Effect of temperature on individual sugar release during DAP of SBP in the ACR. L-arabinose (■), D-galacturonic acid (●), D-glucose (▲), D-galactose (▼) and L-rhamnose (◆) yields are shown for varying temperatures. 2% w/v SBP was pretreated with a 15.2 min residence time, 50 mM acid concentration and 6 Hz agitation rate. Error bars represent SEM (n=3). ACR was operated as described in 2.2.3.

4.3.3.4 Effect of H_2SO_4 concentration on solubilisation of sugars

After looking at temperature, H_2SO_4 concentration was investigated, as this was found to have a large effect in the preliminary batch experiment and the DoE screening. In the ACR, SBP was pretreated at two temperature levels: high and low temperature, 80 °C and 60 °C, respectively. Further, the high temperature experiment had a higher SBP concentration of 4% w/v compared to 2% w/v at 60 °C. In Figure 4.12 (a) it is possible to see how, without any acid addition, the release of sugars was very low, with some 20% w/w L-arabinose and 5% w/w D-galactose being released. With higher H_2SO_4 concentration, D-galacturonic acid solubilisation increased, reaching almost 30% w/w at 75 mM H_2SO_4. In this experiment D-glucose and L-rhamnose were released in too low concentrations to be detected.

A yield of 70% w/w, corresponding to 5.9 $g.L^{-1}$ of L-arabinose; and 30% yield or 2.4 $g.L^{-1}$ of D-galacturonic acid were obtained at 75 mM H_2SO_4 concentration when operating the ACR under a high temperature level (80 °C). In panel (b) L-arabinose yields are relatively lower due to the lower temperature, as was also seen in Section 4.3.2. D-galacturonic acid solubilisation, which in Figure 4.11 appeared to be less affected by temperature, was only slightly lower at the lower temperature level. A steep increase in L-arabinose yield can be seen in both panels suggesting that H_2SO_4 has an important effect even at lower temperatures. Both temperature levels showed that D-galacturonic acid yield remained constant across the range of acid concentrations studied, suggesting that D-galacturonic acid in SBP is more resistant to acid solubilisation.

Interestingly, it appears that L-rhamnose and D-glucose yields are higher in panel (b) than in panel (a). Whilst it is possible that L-rhamnose and D-glucose are released more at lower temperatures; the more likely explanation is due to sample processing. Given that the main sugars of interest were L-arabinose and D-galacturonic acid, samples for HPAEC-PAD analysis were prepared and diluted to ensure that these two sugars were in the quantification range of the HPAEC-PAD. As such when the concentration of L-arabinose and D-galacturonic acid were high, samples required large dilutions. Conversely, samples that had low yields of these two sugars required smaller dilutions to be within the quantification range. D-glucose solubilisation was low across the design space investigated, meanwhile overall L-rhamnose content within SBP was also low. This resulted in these two sugars being below the quantification range when dilutions were large, whereas they appeared at the lower end of

the quantification range when reactions conditions were not as severe and small dilutions were required for L-arabinose and D-galacturonic acid quantitation.

4.3.3.5 Effect of SBP loading in the ACR on solubilisation of sugars

In the preliminary batch experiments in Section 4.3.1 and Figure 4.3, mass transfer limitations in the DAP reaction had been noticed. However, in the well mixed DoE batch setup SBP concentration did not appear to have an effect on sugar release. Further, in Section 3.3.3, the ACR's ability to handle solids was discussed, and whilst no blockages and no visible issues appeared when operating the ACR with solids, it was not certain whether the ACR could provide a level of mass transfer similar to the batch system. To ensure that there was no negative effect of additional SBP loading, different concentrations of SBP (1, 2, 3 and 4% w/v at 80 °C; and 1, 2, 3, 4, and 5% w/v at 60 °C) were loaded on the ACR as described in Section 2.2.3. Figure 4.13 (a) and (b), show that SBP loading had little effect on sugar release. Indeed, the findings in panel (a) reflect what was found earlier, good release of L-arabinose, some release of D-galacturonic acid and D-galactose and little release of D-glucose and L-rhamnose. The low temperature experiment also appeared consistent with previous findings with lower L-arabinose yields (~10%) and relatively higher D-galacturonic acid yields (15-20%). Additionally, the low temperature experiment suggested that the ACR could be operated effectively up to 5% w/v loading with no impediments.

In a continuous system, increasing solid loading has the direct advantage of increasing the final throughput. In this instance, throughput for L-arabinose (in grams per hour, as shown in Table 4.7) almost doubles from 1.61 to 3.07 $g.hr^{-1}$ when switching from a 2% w/v SBP loading to a 4% w/v loading. Table 4.7 also compares the throughput of different conditions explored in the ACR. For example, it highlights the importance of acid concentration, since L-arabinose and D-galacturonic acid throughputs increase dramatically when going from 0 mM to 75 mM at 4% w/v loading at 80 °C, from 0.78 and 0.03 $g.hr^{-1}$ to 3.07 abd 1.17 $g.hr^{-1}$, respectively.

4.3.3.6 Comparison of ACR DAP to other pretreatment methods

Continuous pretreatment of SBP is not yet widely researched, likely due to the cost of large scale continuous equipment. Stoppok and Buchholz published work on continuously fed SBP in a digester to produce biogas, finding that 85% of the carbon was successfully converted to biogas; however, the reactor residence time varied from 10 to 30 days (Stoppok and Buchholz, 1985). On the other hand, other lignocellulosic waste streams have been studied in continuous reactors. As mentioned in Section 4.1, these reactors tend to be rotating screw reactors that can handle solids. Chen et al. (2013) used a pilot scale screw reactor for rice straw pretreatment, for final use of sugars in bioethanol production. As such, acid catalysed steam explosion was employed with the aim of solubilising D-glucose as well as hemicellulose and pectin. The group also reported operating this reactor for several days. Indeed, ensuring operation of a continuous reactor over a long period of time is an important aspect in the final reactor choice (Chen *et al.*, 2013). In this work, once the ACR was set up and operational, several experimental conditions were tested in sequence, meaning that, though the reactor was never left unattended for long periods of time, it operated smoothly over periods of 8-10 hours.

Furthermore, barley straw pretreatment was attempted in a continuous twin screw reactor by Han and coworkers. (2013) In this instance, alkaline pretreatment was attempted, using a DoE setup to investigate the effects of flowrate, temperature and NaOH concentration. The effectiveness of the pretreatment was evaluated based on a biomass to ethanol ratio; and it was revealed that NaOH concentration was important as was temperature (which in this study was 60 °C to 90 °C, comparable to what was used in this work). Additionally, at harsher conditions (higher temperatures and NaOH concentration) higher flowrates were more favourable, which may have been due to a lower production of inhibitors with lower residence times in the reactor. Makishima et al. (2009) used a different type of reactor for pilot scale pretreatment of corn cobs. In their work they simply used an inch-wide tube that could be heated. Interestingly, the flowrate imparted on the system by a slurry pump at the inlet of the “reactor” provided sufficient mixing to avoid blockages and material build-up, bypassing the need for agitation.

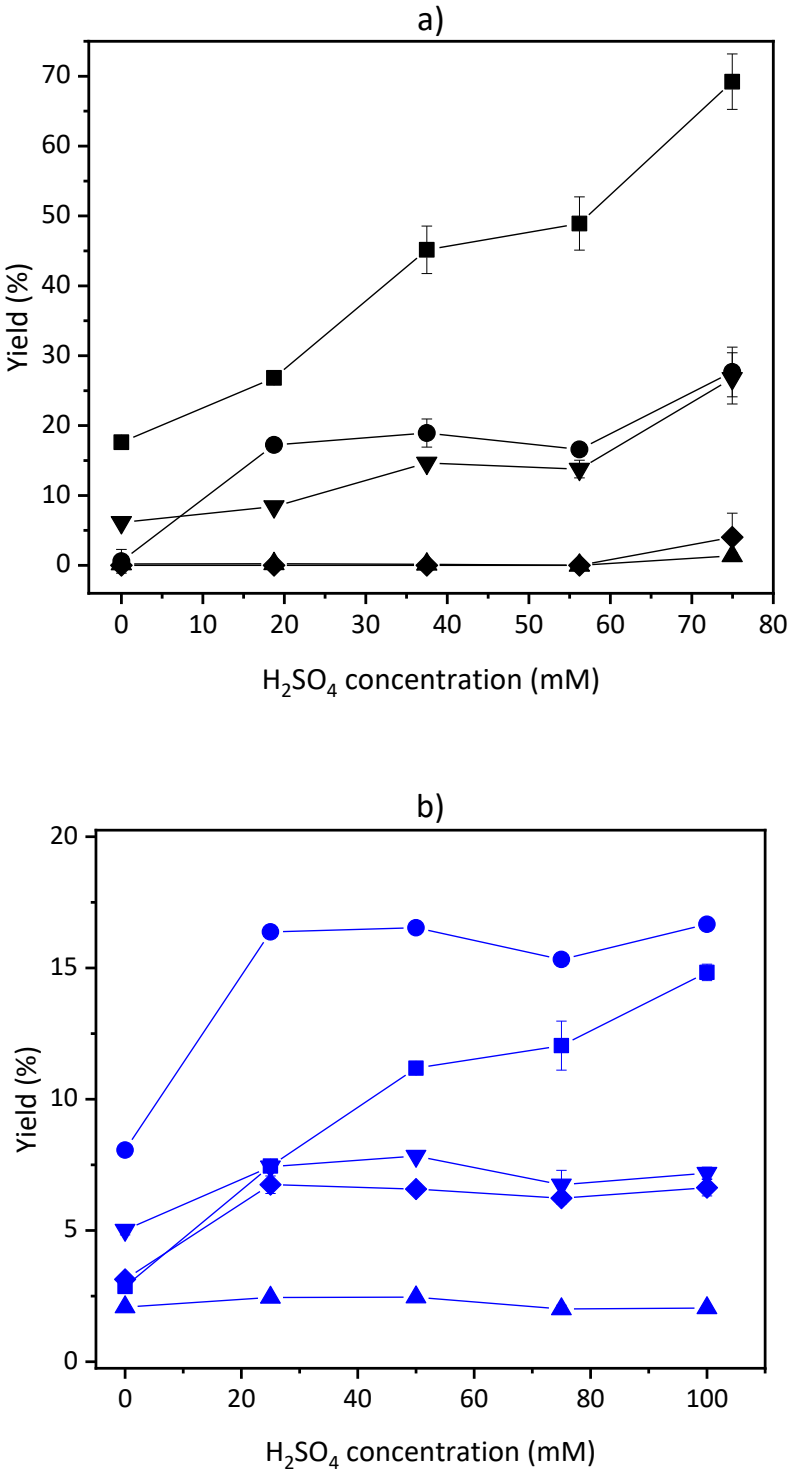

Figure 4.12. Effect of H_2SO_4 concentration on sugar release during DAP of SBP in the ACR. L-arabinose (■), D-galacturonic acid (●), D-glucose (▲), D-galactose (▼) and L-rhamnose (◆) yields are shown for varying H_2SO_4 levels using a 15 min residence time. In panel (a) 4% w/v SBP was pretreated at 80 °C, whilst panel (b) shows the same reaction with 2% w/v at 60 °C. A 15.2 min residence time and 6 Hz agitation rate were used for both conditions. Error bars represent SEM (n=3). ACR was operated as described in 2.2.3.

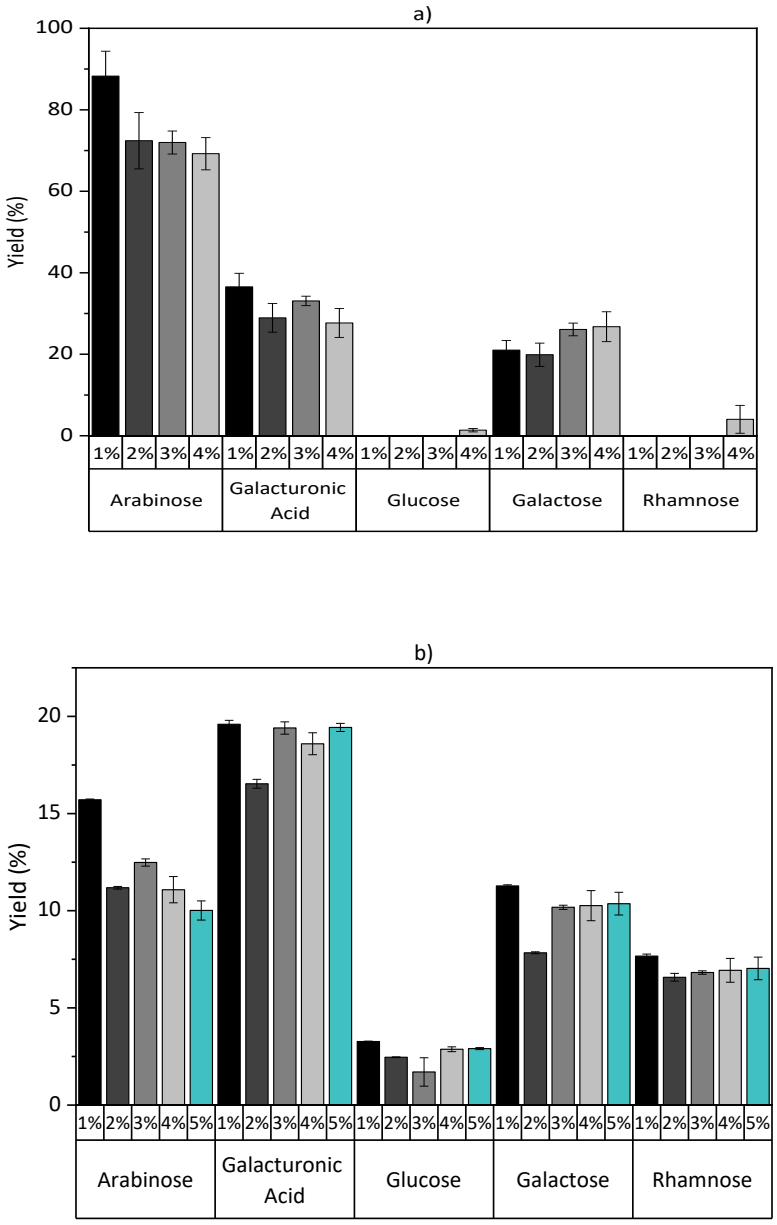

Figure 4.13. Effect of SBP concentration on sugar release during DAP of SBP in the ACR. In (a) using 75 mM H_2SO_4, and 80 °C, SBP at loadings of 1% w/v (black bars), 2% w/v (dark grey bars), 3% w/v (medium grey bars) and 4% w/v (light grey bars) were tested at; whilst in (b) at 50 mM H_2SO_4, and 60 °C, SBP loadings of 1% w/v (black bars), 2% w/v (dark grey bars), 3% w/v (medium grey bars), 4% w/v (light grey bars), and 5% w/v (turquoise bars) were tested. A 15.2 min residence time and 6 Hz agitation rate were used for both conditions. Error bars represent SEM (n=3). ACR was operated as described in 2.2.3.

As mentioned previously, Hamley-Bennett et al (2016). used the same batch of SBP for their steam explosion work. Their reaction was optimised in a 1L Parr batch reactor, using 50 grams of SBP per batch. At a pressure of 5 bar and 24 min the reaction solubilised 83% w/w of the arabinans available. Table 4.8 compares the best condition found in this work with the optimised conditions obtained by Hamley-Bennett. Additionally, an assumed scenario was proposed as well: 5% w/v SBP loading at 80 °C and 75 mM H_2SO_4. As shown in Figure 4.13, 5% w/v SBP loading was achievable with the ACR; and little change in yield between 4% w/v and 5% w/v was noticed at 60 °C. As such, a 65% w/w L-arabinose yield was assumed for pretreatment at a higher temperature and acid concentration (80 °C and 75 mM as in Figure 4.13 (a)). The table shows throughput, calculated as the final concentration or exit concentration divided by the residence time in hours. For this it can be seen that the three scenarios analysed are quite similar. This follows from the fact that, whilst the steam explosion yield is slightly higher than the DAP yield, the reaction time is shorter in the ACR. The real advantage of DAP in a continuous reactor is seen in the difference in productivity, a measure of the reactor efficiency. Productivity is calculated by dividing the throughput by the reactor volume (~120 mL vs 1 L). In this instance, productivities that are almost an order of magnitude greater than the steam explosion in batch reactors can be seen. This calculation does not even account for the additional time it would take to heat and cool the batch reaction mix. Zheng et al. (2013), also using an analogous 1L Parr batch reactor, heated the reaction components (SBP slurry and acid) separately to 100 °C before mixing them in the reactor.

Their reaction temperature range was 120-160 °C and heating times of 30 to 32 minutes were reported, making batch pretreatment an even less favourable option, especially when considering the production-scale heating and cooling requirements. From a process safety standpoint, the argument for a continuous reactor such as the ACR is even clearer: at any one point only <130 mL of material is heated and acidified, reducing the potential hazards if some containment mechanisms fail. The above work focused on moving a DAP reaction from a benchtop batch system to a scalable continuous system. At large scale not only could high yields be achieved, but the productivities obtained in the ACR could rival other well established pretreatment techniques.

Table 4.7 Mass balance and throughput calculations during DAP of SBP in the ACR. Inlet SBP (based on SBP loading) and individual sugars (based on SBP composition) flowrates are reported next to outlet flowrate or throughput for L-arabinose, D-galacturonic acid and D-glucosese. Throughput was calculated on the basis of a 15.2 min residence time and an 8.8 mL.min^{-1} flowrate. Experiment was carried out as described in Section 2.2.3

Conditions				**Flowrate in (based on SBP composition)**			**Sugar flowrate out (throughput)**			
Temperature (°C)	**H_2SO_4 (mM)**	**SBP (% w/v)**	**SBP processed per hour (g.hr^{-1})**	**L-arabinose inlet (g.hr^{-1})**	**D-galacturonic acid inlet (g.hr^{-1})**	**D-glucose inlet (g.hr^{-1})**	**Solubilised L-arabinose (g.hr^{-1})**	**Solubilised D-galacturonic acid (g.hr^{-1})**	**Solubilised D-glucose (g.hr^{-1})**	**Reference**
80	**75**	**1%**	5.28	1.11	1.06	1.32	0.98	0.39	0.00	Figure 4.13 (a)
80	**75**	**2%**	10.56	2.22	2.11	2.64	1.61	0.61	0.00	Figure 4.13 (a)
80	**75**	**3%**	15.84	3.33	3.17	3.96	2.40	1.05	0.00	Figure 4.13 (a)
80	**75**	**4%**	21.12	4.44	4.22	5.28	3.07	1.17	0.07	Figure 4.13 (a)
80	**0**	**4%**	21.12	4.44	4.22	5.28	0.78	0.03	0.01	Figure 4.12 (a)
60	**50**	**1%**	5.28	1.11	1.06	1.32	0.17	0.21	0.04	Figure 4.13 (b)
60	**50**	**2%**	10.56	2.22	2.11	2.64	0.25	0.35	0.07	Figure 4.13 (b)
60	**50**	**3%**	15.84	3.33	3.17	3.96	0.42	0.61	0.07	Figure 4.13 (b)
60	**50**	**4%**	21.12	4.44	4.22	5.28	0.49	0.79	0.15	Figure 4.13 (b)
60	**50**	**5%**	26.4	5.54	5.28	6.60	0.55	1.02	0.19	Figure 4.13 (b)
60	**75**	**2%**	10.56	2.22	2.11	2.64	0.27	0.32	0.05	Figure 4.12 (b)

Table 4.8. Comparison of SBP throughput using the ACR compared to steam explosion pretreatment by Hamley-Bennet et al (2016). The amount of L-arabinose that can be solubilised into the liquid fraction per hour (throughput) and productivity (throughput divided by reactor volume) was calculated for three different pretreatment options. ACR 1 was the most favourable DAP condition found (80 °C, 75 mM H_2SO_4, 4% w/v SBP); ACR 2 is a realistically achievable DAP with an assumed L-arabinose yield of 65%; and the steam explosion literature values were obtained from a pretreatment reaction at 5 bar, 24.4 min, and 5% w/v loading in a 1 L vessel, following a DoE optimisation (Hamley-Bennett, Lye and Leak, 2016).

	ACR 1	ACR 2	Steam Explosion
SBP concentration (% w/v)	4.0	5.0	5.0
Arabinose yield (% w/w)	69.2	65.0	83.0
Reaction time (min)	15.0	15.0	24.4
Throughput ($g_{ara}.hr^{-1}$)	3.1	3.6	3.5
Productivity ($g_{ara}.hr^{-1}.L_{reactor}^{-1}$)	25.6	30.0	3.5

4.3.4 Enzymatic pretreatment and depolymerisation

4.3.4.1 Batch enzymatic pretreatment

An alternative to DAP could be the direct use of enzymes in the breakdown of SBP. The challenge lies in the complex structure of lignocellulosic materials. Different linkages between various polymers mean a range of enzymes are needed for depolymerisation. Indeed, commercially available and suitable enzymatic products typically comprise of arabinases, polygalacturonoases, cellulases enzyme and other enzymes. One such enzyme mix is Viscozyme®L, typically used to reduce viscosity of lignocellulosic slurries, containing arabanases, cellulases, and xylanases amongst others (Mes-Hartree, Dale and Craig, 1988; Kühnel *et al.*, 2010; Leijdekkers *et al.*, 2013).

To see if enzymatic pretreatment could be considered a viable alternative, and especially to verify if it could be translated to continuous mode, the work by Leijdekkers et al. (2013) was used as a starting point. The conditions, described in Section 2.3.1, were similar with the exception that in this study, the flasks were agitated to keep the pulp well mixed and also a lower SBP loading was tested as well. As summarised in Figure 4.14, the difference in yields in the first hours of the experiment shows the importance of mixing. In a mixed system, regardless of the loading, the reaction plateaus at around 50% w/w yield of L-arabinose after 15 hours, whilst the static pretreatment does not appear to reach above 30% in the 48 hours of the experiment. The drop in concentration seen in Figure 4.14 (b) for the 7.5% w/v loading is likely an error that occurred during analysis.

Despite the good release of the key sugars, such as D-galacturonic acid and L-arabinose; enzymatic pretreatment was not studied further as it seemed challenging to translate the process to a continuous reactor such as the ACR. Firstly, the enzymatic pretreatment reaction was too slow, since a 15 min residence time in the ACR was already at the limit of what was practically achievable when handling SBP solids. Secondly, the breakdown by the commercial mix was not selective and produced a large amount of monosaccharides, and therefore would not allow for fractionation making downstream operations in a biorefinery concept more complicated.

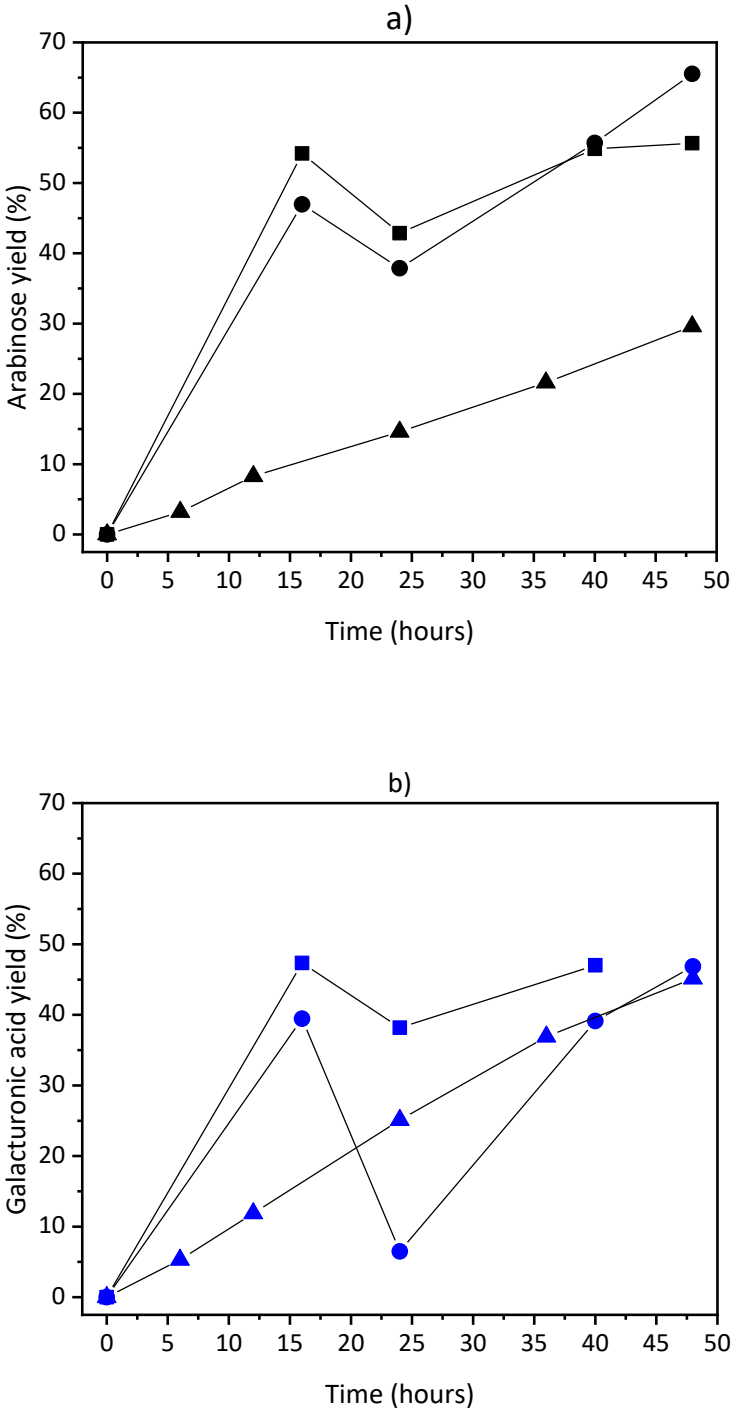

Figure 4.14. Enzymatic pretreatment of whole SBP in static vessel with commercial pectinase enzyme kit. L-arabinose yields, panel (a), in black; and D-galacturonic acid yield, panel (b), in blue for 2.5% w/v (■) and 7.5% w/v (●) of whole dried, SBP. Experiment was carried out as outlined in Section 2.3.1. Results are compared to literature values using the same enzymatic mix, in an unstirred vessel using the same Viscozyme®L loading at 7.5% w/v of dry SBP (▲) by Leijdekkers et al (2013).

4.3.4.2 Fractionation through enzymatic depolymerisation

One such depolymerisation step was the utilisation of an L-arabinofuranosidase (AraF, EC 3.2.1.55) isolated from a thermostable *Geobacillus thermoglucosidasius* (Cárdenas-Fernández *et al.*, 2017). L-arabinofuranosidases are an exo-type glycosidase that catalyse the successive removal of L-arabinose residues from the non-reducing termini of α-1,2-, α-1,3-, α-1,5- and α-4,6-linked arabino- furanosyl residues (Saha, 2000). This thermostable AraF was found to be able to treat steam exploded SBP and selectively depolymerise oligomeric and polymeric arabinans. Here, it was studied in batch, at 60 °C, for the depolymerisation of dilute acid pretreated SBP. A 2% w/v SBP slurry was pretreated in the ACR with a 15.2 min residence time and 75 mM H_2SO_4 concentration. These conditions lead to the release of 72.4% L-arabinose, 28.9% galacturonic aicd and 21.0% D-galactose, corresponding to concentrations of 3.04 $g.L^{-1}$, 1.16 $g.L^{-1}$ and 0.25 $g.L^{-1}$, respectively. No D-glucose was detected using this pretreatment. It is important to note that these concentrations, are reported in the same manner as the DAP results; namely, they include both mono- and polymeric forms of the sugars.

The AraF depolymerisation reaction was run on the pretreated material over a 60-minute period and is shown in Figure 4.15. The samples were tested for monomeric sugars concentrations, meaning that no analytical hydrolysis as described in Section 2.3.3, was carried out. The yield of L-arabinose is given in terms of monomeric L-arabinose produced divided by total L-arabinose available.

Panel (a) clearly shows that AraF acts quite selectively and rapidly on arabinans, obtaining yields close to 100% at the highest AraF concentration within 30 minutes. The reaction begins to plateau within 20 minutes of the start of the reactions. Enzyme loading also appears to have a clear effect on the initial rate of reaction. Unfortunately, no samples were taken between 0 and 5 minutes to obtain a better idea of the real initial rate of reaction. However, increasing the enzyme loading ten-fold only lead to a doubling of the apparent initial reaction rate; as calculated by the L-arabinose depolymerised in the first five minutes (2.1 $g.L^{-1}$ for 50 $U.mL^{-1}$ against 1.0 $g.L^{-1}$ for 5 $U.mL^{-1}$).

Following this initial batch AraF work, a proof-of-concept ACR pretreatment work was carried out. SBP pretreated by dilute acid hydrolysis, was passed through the ACR. Cell lysate or whole *E. coli* cells were pumped through the side-entry port. The total residence time in the reactor was set as 30 minutes. For this experiment it was not possible to measure the activity of the AraF cell lysate and a final ratio of lysate:pretreated material of 1:400 was used. This concentration was quite low to obtain meaningful arabinan depolymerisation, as shown by the low yields obtained in Table 4.9.

This set of preliminary experiments did show; however, that continuous degradation of arabinans with AraF is possible. However, especially when the product of the reaction is a low value compound such as a sugar, an important factor to consider is enzyme retention. Work by Cardenas-Fernandez et al. (2018), within the Sustainable Chemical Feedstocks group (Section 1.2.3) on depolymerisation of steam pretreated SBP arabinans showed the possibility of carrying out depolymerisation in continuous mode. In their work, AraF was immobilized on an epoxy resin and was continuously recycled through a diafiltration unit with the continuous addition of the liquid fraction of steam pretreated SBP. Monomeric L-arabinose was recovered in the filtrate along with some 10% w/w of the oligo-and polymeric D-galacturonic acid. Interestingly, the pretreated SBP was found to foul the epoxy resin very quickly, so a decolourisation step was implemented to adsorb the colouring agents which reduced the lifetime and performance of the immobilized AraF.

DAP was found to release lower amounts of D-galacturonic acid than the steam explosion pretreatment optimised by Hamley-Bennet et al. (2016). Further, the preliminary work on AraF presented here shows that despite the addition and subsequent neutralisation of an acid, good conversion of arabinans into monomeric L-arabinose was possible. As such, it is possible to envisage a fully continuous system that releases arabinans in the ACR, followed by a diafiltration unit as presented by Cardenas-Fernandez et al. (2018). to produce relatively pure monomeric L-arabinose to use in biocatalytic applications.

Table 4.9. Production of monomeric L-arabinose from AraF depolymerisation of pretreated SBP in flask and continuous mode. L-arabinose concentration and yield were obtained for an AraF depolymerisation using *E. coli* cell lysate. A static 200 mL flask, an agitated 200 mL flask (250 rpm, 2.5 cm orbital shaking diameter), and the ACR agitated at 6 Hz with a 30 minute residence time. Reaction was carried out at 50 °C as outlined in Section 2.3.2**.**

Reactor	Type of mixing	D-arabinose concentration ($g.L^{-1}$)	Yield (% w/w)
Flask	Static	0.11	5.95
Flask	Agitated	0.17	8.95
ACR	6 Hz	0.16	8.69

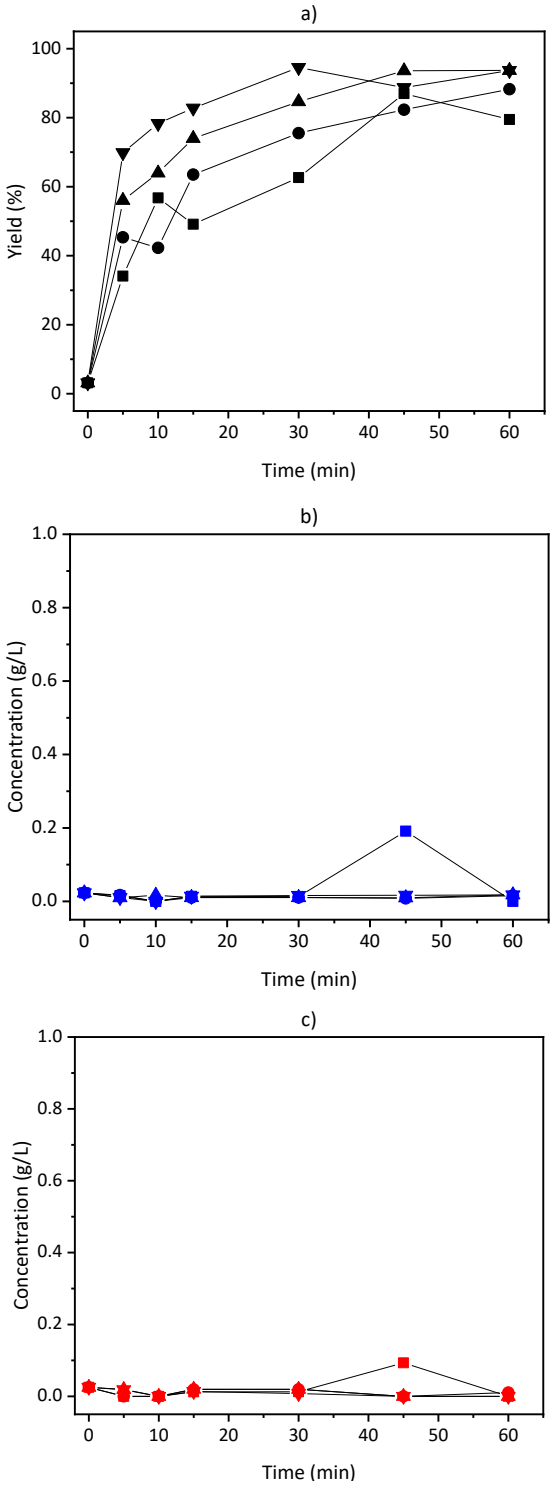

Figure 4.15. Monomeric sugar production through Arabinofuranisidase (AraF) depolymerisation of DAP SBP. Batch fractionation reactions were carried out at 60 °C in shaken test tubes, using dilute acid pretreated SBP as described in Section 2.3.2 Monomeric L-arabinose yield (in black, panel (a)), D-glucose concentration (blue, panel (b)) and D-galactose concentration (red, panel (c)) were measured over time for the following AraF concentrations: 5 (■), 10 (●), 20 (▲) and 50 $U.mL^{-1}$ (▼). Experiment was carried out as described in Section 2.3.2

4.4 Summary

The pretreatment of lignocellulosic biomass is a necessary step into ensuring the full utilisation of agricultural waste resources. Many different types of pretreatment are available, and it is important to select a pretreatment option that best suits the needs of the final application. Whilst most types of pretreatment have focused on releasing as many monomeric sugars at once for fermentative biofuel production, here a DAP step was selected to allow for the selective fractionation of the pretreated SBP to obtain monomeric L-arabinose for use in biocatalytic applications.

DAP was first studied in batch. SBP, which was finely ground for use in the continuous reactor, was found to be more resistant to pretreatment with coarser grinds. Interestingly, however, it was found that pretreatment on the whole, dried SBP led to more solubilised L-arabinose than the coarsest particles tested (Section 4.3.1.3), showing promise for larger scale applications, where smaller particle size may not be required. A DoE study, in Section 4.3.2, revealed the importance of both acid concentration and temperature.

In the ACR, an ideal residence time of 15.2 min was selected, providing a good balance between yield and throughput (Section 4.3.3.2). Then it was found that temperature increase led to better solubilisation of L-arabinose and D-galactose, but improvements in D-galacturonic acid was not as noticeable (Section 4.3.3.3). Section 4.3.3.4 discussed the positive effect of increasing acid concentration on L-arabinose and D-galactose solubilisation, with 70% w/w of arabinans being released at 75 mM H_2SO_4, with a 15 minute residence time. SBP loading, was found to have little effect on yield, creating a compelling case for utilising a dynamically stirred continuous reactor such as the ACR (Section 4.3.3.5). L-arabinose throughput in the ACR was found to be comparable to batch steam explosion pretreatment. When accounting for heating and cooling requirements of batch reactors, the ACR's advantages became even clearer. Productivity, however, was found to be almost an order of magnitude higher compared to steam explosion: a promising finding for continuous pretreatment options (Section 4.3.3.6).

Enzymatic pretreatment and depolymerisation was briefly investigated. A commercial mix showed good release of sugars; however, its reaction time was deemed too long for continuous application (Section 4.3.4.1). Meanwhile, AraF was found to produce monomeric L-arabinose from SBP pretreated material. AraF catalysed depolymerisation also worked in a proof-of-concept study in the ACR as well. A possible setup combining continuous DAP in the

ACR, followed by selective depolymerisation by AraF in a diafiltration reaction was proposed (Section 4.3.4.2).

Future efforts in the pretreatment of SBP could focus on scaling up DAP to larger reactors able to accept whole SBP and studying the continuous depolymerisation by AraF in flow mode, using immobilized enzymes.

5

Enzyme expression, recovery and purification for application in continuous flow biocatalytic reactors

5.1 Introduction

In Chapter 4, the use of the ACR for SBP pretreatment and enzymatic hydrolysis of arabinans into L-arabinose was described. Recently there has been considerable interest in flow biocatalysis and specifically for the operation of multi-step, cascade reactions (Lozano *et al.*, 2002; Britton, Majumdar and Weiss, 2018). It is therefore interesting to consider the use of the ACR for continuous conversion of the released SBP monosaccharides into value-added products.

In Section 1.4.5 the conversion of monomeric L-arabinose into L-gluco-heptulose was discussed. The reaction described by Bawn et al. (2018) involved a thermostable transaminase (TAm) and transketolase (TK). The TK mediated the carboligation step, the addition of a C-C group, to produce L-gluco-heptulose from L-arabinose and hydroxypyruvic acid (HPA). The TAm step mediated the conversion of L-serine and α-ketoglutaric acid to L-glutamate and HPA, an expensive and heat labile intermediate (Dickens and Williamson, 1958). Figure 1.6 shows the mechanism of action of the TAm and TK enzymes. Figure 6.3 on the other hand shows the proposed one-pot two-step production of L-gluco-heptulose. The mechanism of action of TAm and TK enzymes are discussed in further detail in Chapter 6, and the rationale for utilizing a one-pot two-step reaction system over a stand-alone TK reaction to produce L-gluco-heptulose is also outlined in Section 6.3.1.

The TAm and TK enzymes were successfully isolated from *Deinococcus geothermalis* host and expressed with a His-tag in an *E. coli* BL21 (DE3) host cell line. These cell lines were grown in shake flasks and the enzymes obtained were used in the small scale batch production of L-gluco-heptulose. However, continuous bioconversion studies in the ACR would require large amounts of biocatalysts, making shake flask cultures unsuitable for the production of TAm and TK enzymes.

Furthermore, crucial aspects for the successful adoption of enzymatic conversions in a biorefinery context are the cost and scale of enzyme production. Common techniques for the production and purification of enzymes found at lab scale, are often not suitable for large scale operations. In a typical biochemistry or biotechnology laboratory, cells are grown in shake flasks, lysed via sonication or with the addition of lysis enzymes. If required, enzyme purification is typically obtained through Immobilized Metal Affinity Chromatography (IMAC), by exploiting the affinity between a His-tag, engineered onto the C or N terminus of the enzyme, and a Nickel chelated support. Whilst these techniques have advantages at small

scale, alternative processing options need to be found for production of enzymes at a larger, commercial scale in order to decrease the cost of the enzyme in the overall Cost of Goods (CoGs).

Typically, to scale up the production of enzymes, a fermenter or Stirred Tank Reactor (STR) is used to support enhanced microbial cell growth. This offers many advantages over shake flasks: better aration and control of pH and dissolved oxygen (DO) through the use of on-line measurements; better mixing; the possibility of feeding the culture as well as increased scalability. Indeed, whilst the largest shake flasks can have working volumes in the litre scale, the largest STRs can reach tens of cubic metres in operating volume (Knocke *et al.*, 2016; Zhou *et al.*, 2019).

After harvesting the biomass from the culture, via centrifugation or filtration, a cell disruption step is required to release an intracellular protein product. At laboratory scale, techniques such as enzymatic and detergent lysis, and ultrasound treatment are widely used. However, these are challenging and costly to scale up (Costa-Silva *et al.*, 2018). Conversely, whilst high pressure homogenisation is commonly employed in industrial bioprocesses, it is less common in laboratory settings. Indeed the smallest homogenisers have working volumes of tens of millilitres (e.g. the APV Gaulin Lab40 homogeniser has a 40 mL working volume) making them unsuitable for benchtop applications (Chisti and Moo-Young, 1986; Harrison, 1991; Jenning, Lippacher and Gohla, 2002).

Following the release of intracellular enzymes, bioconversions can either be carried out using a clarified cell lysate or the enzymes can be further purified. At small scale, affinity chromatography using His-tag/Nickel affinity is often used; alternatively, techniques such as ion exchange chromatography or size exclusion chromatography can be used in conjunction with, or instead of, affinity chromatography (Gräslund *et al.*, 2008). The utilisation of one or more chromatography steps can often produce a relatively pure product. Furthermore, some chromatographic methods are also widely used in large scale production of a range of products such as biopharmaceuticals, chemicals and foods. Despite this, their operation is both resource and capital intensive (Kelley, 2007; Liu *et al.*, 2013).

Indeed, as titres and scales increase further, protein precipitation, with its more easily scalable parameters, could be seen as an alternative to chromatography for applications like those envisaged in this work (Titchener-Hooker, Dunnill and Hoare, 2008). Precipitation steps take advantage of changes in the relative solubility of the enzyme of interest compared to

other proteins released during cell disruption. This change in solubility can occur in several ways. Often, proteins are precipitated by addition of ammonium sulfate or polyethyleneimine; however, other precipitation methods can be used. Amongst these is thermal precipitation, whereby the thermal stability of an enzyme of interest can be exploited by heating the cell lysate, thus denaturing and causing to precipitate the host cell proteins (HCPs), leaving a soluble protein of interest (Burgess, 2009).

5.2 Chapter aim and objectives

The aim of this chapter is to explore options for the scalable production and purification of the TAm and TK enzymes required for the proposed catalytic upgrading of SBP-derived L-arabinose. This is critical enabling work to facilitate the flow biocatalysis studies envisaged in Chapter 6. The work described here should also lay the groundwork for future large-scale production of these thermostable enzymes beyond the gramme quantities required for ACR operation. In particular, this chapter will investigate more scalable and cost-effective enzyme purification techniques than lab scale affinity chromatography. The specific objectives for this chapter are outlined below.

- To investigate optimisation of enzyme production during shake flask microbial fermentation through choice of growth media and induction strategy.
- To produce TAm and TK enzymes in STRs under the optimised cultured conditions to facilitate larger scale enzyme production.
- To evaluate the effectiveness of scalable cell disruption and purification methods compatible with biorefinery process economics.

5.3 Results

5.3.1 Increasing enzyme production scale

5.3.1.1 Cell culture growth medium selection

To carry out enzymatic reactions at larger scale and in continuous mode, considerable amounts of enzymes were required. To diminish batch to batch variability, the possibility of using enzymes produced from fewer, larger cultures, in a STR was investigated. This work will also provide a foundation for possible later fermentations at even larger, commercial scales. The original culture protocol as employed by Bawn et al. (2018) employed a 1L shake flask with a 200 mL working volume using LB broth as growth media. Induction was carried out after 7 hours using 1 mM IPTG for induction. The temperature was then lowered to 25 °C and the fermentation was left overnight before harvest. Possible improvements to this original cell growth and protein expression method were therefore investigated.

The first modification was to change the growth media. LB was exchanged for TB, a complex medium with improved buffering abilities provided by the addition of phosphates (Lessard, 2013). Figure 5.1 describes the effects of this switch on the Optical Density (OD) measurements taken at a wavelength of 600 nm (OD_{600}). The OD_{600} measurements show that despite the same initial starting optical density, TB cultures with TK-expressing *E. coli* grew more quickly and to approximately twice as high ODs than LB cultures. Mid-exponential induction occurred at the same time, after four hours. Aside from the higher final OD_{600} it can also be noticed that cell growth appeared to plateau at approximately the same time and so twice as many cells are produced in the same time period.

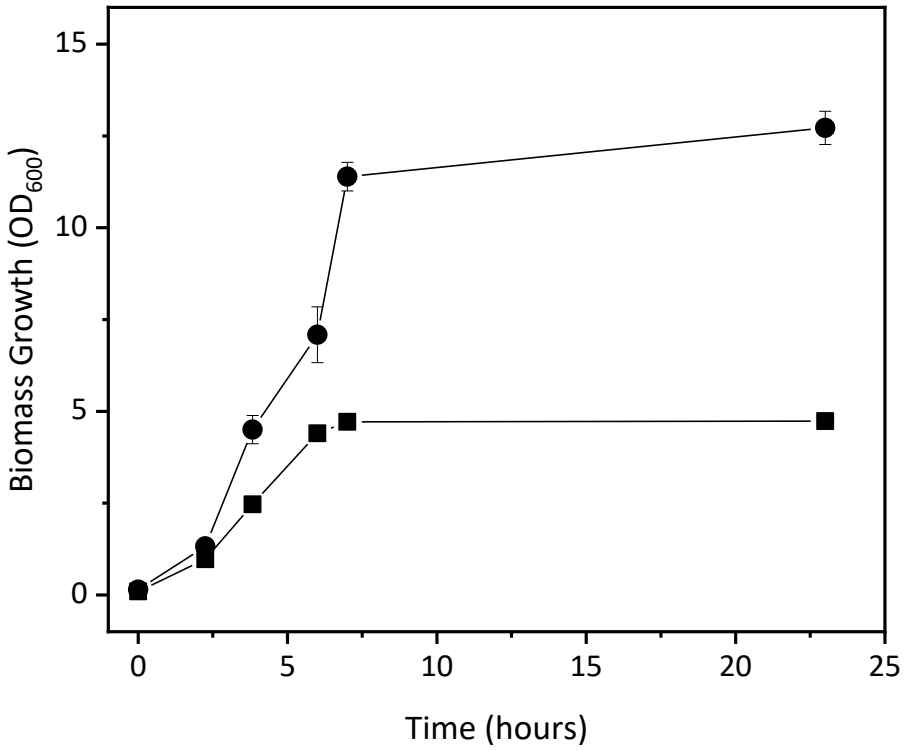

Figure 5.1. Comparison of LB and TB growth media for TK production by *E. coli* BL21 (DE3)-TK in 250 mL baffled flasks. Biomass growth indicated by OD_{600} measurements for LB (■) and Terrific broth, (TB), (●) cultures over time. Induction occurred after 4 hours for both cultures. Error bars denote SEM (n=2). Experiments performed as described in Section 2.4.2.

5.3.1.2 Induction strategy selection

Following the choice of growth medium, the impact of enzyme induction time was also investigated. Figure 5.2 compares the OD_{600} readings of two different induction strategies: mid-exponential and late exponential induction on both TK and Tam production. The OD_{600} of the TAm strain does not appear to be influenced by the induction strategy over the course of the entire fermentation. On the other hand, the TK-producing strain appears to be affected by the different induction timings, with later induction resulting in a lower final OD.

Additional off-line measurements were carried out on end-of-run samples. Figure 5.3. highlights these and corroborates the findings shown in Figure 5.1 and Figure 5.2. SDS-PAGE analysis on the end-of-run samples also revealed the effect of induction on expression. Earlier induction resulted in a larger concentration of TK (lanes 4 and 5). This effect was not as noticeable for TAm expression. For comparison, LB samples (lanes 1 and 2) were loaded at an equivalent volume basis (i.e. band thickness corresponds to concentration of protein in flask), and showed very low expression of both total protein and TK.

The change from LB to TB studied in Figure 5.1, Figure 5.2, and Figure 5.3 matches well with what is suggested in literature: LB and TB are both widely used nutrient-rich, complex broths; however, TB's increased nutrient concentration and buffering abilities allow cells to grow to higher densities (Lessard, 2013). Since the primary goal of this work was to produce sufficient material for continuous flow reactions to be performed in the ACR (Chapter 6), further investigation into media selection was not carried out. However, for larger scale operations defined media, such as mineral salts media, are usually preferred over complex media for having more reproducible growth, allowing higher cell density cultures to be attained, and for giving clearer supernatants (Korz *et al.*, 1995; Thiry, Cingolani and Thiry, 2002; Zhou *et al.*, 2019).

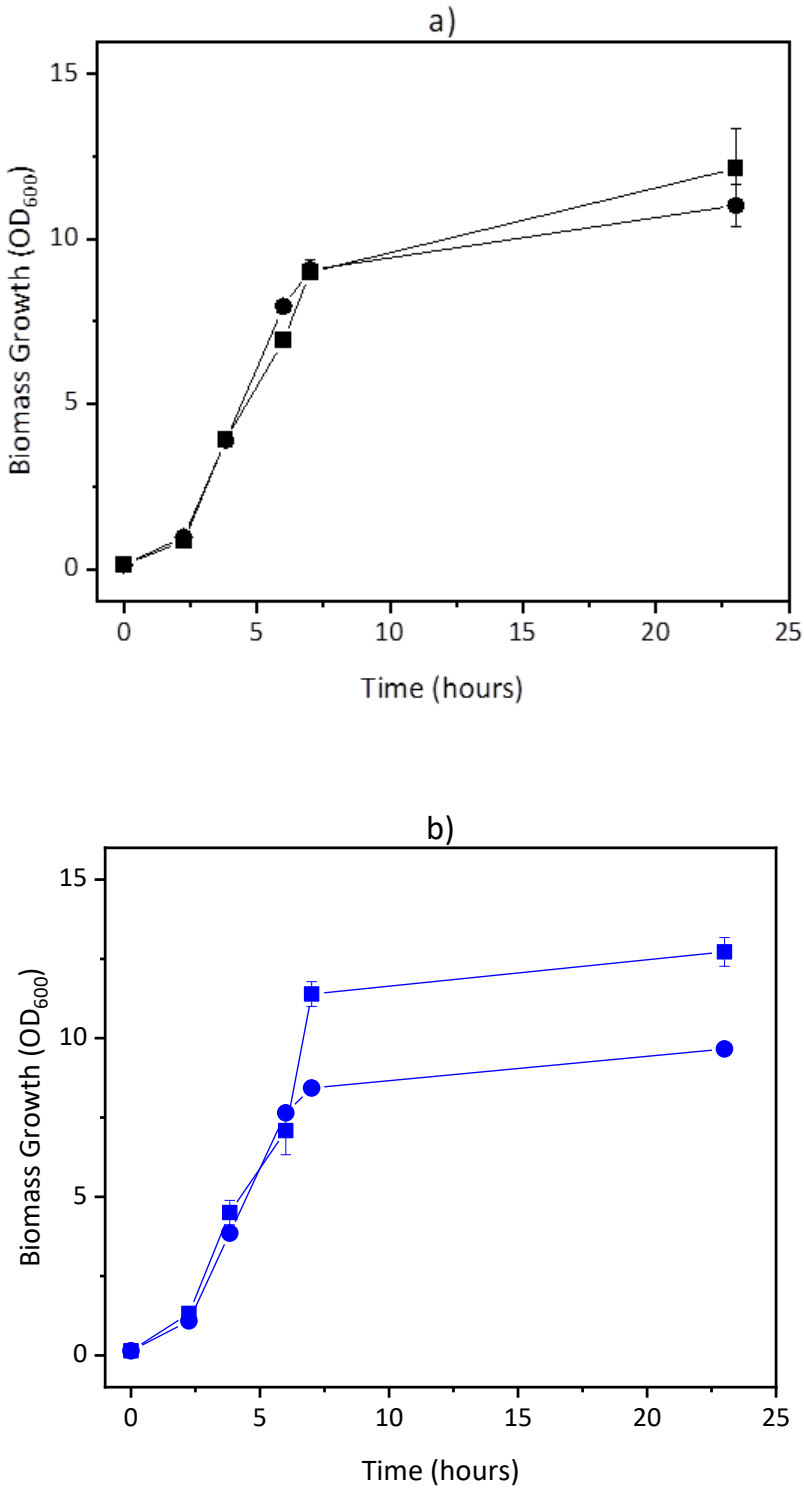

Figure 5.2. Effect of induction strategies on the OD_{600} of *E.coli*-BL21 (DE3)-TAm and *E.coli*-BL21 (DE3)-TK. Mid-exponential phase induction occurred 4 hours after inoculation, and late exponential phase induction occurred after 6 hours; just prior to reducing the incubator temperature to 25 °C. A) compares OD_{600} in mid- and late exponential phase induction for TAm strain (■ and ●, respectively), whilst B) compares OD_{600} in mid- and late exponential phase induction for TK strain (■ and ●, respectively). Error bars denote SEM (n=2). Experiments performed as described in Section 2.4.1.1.

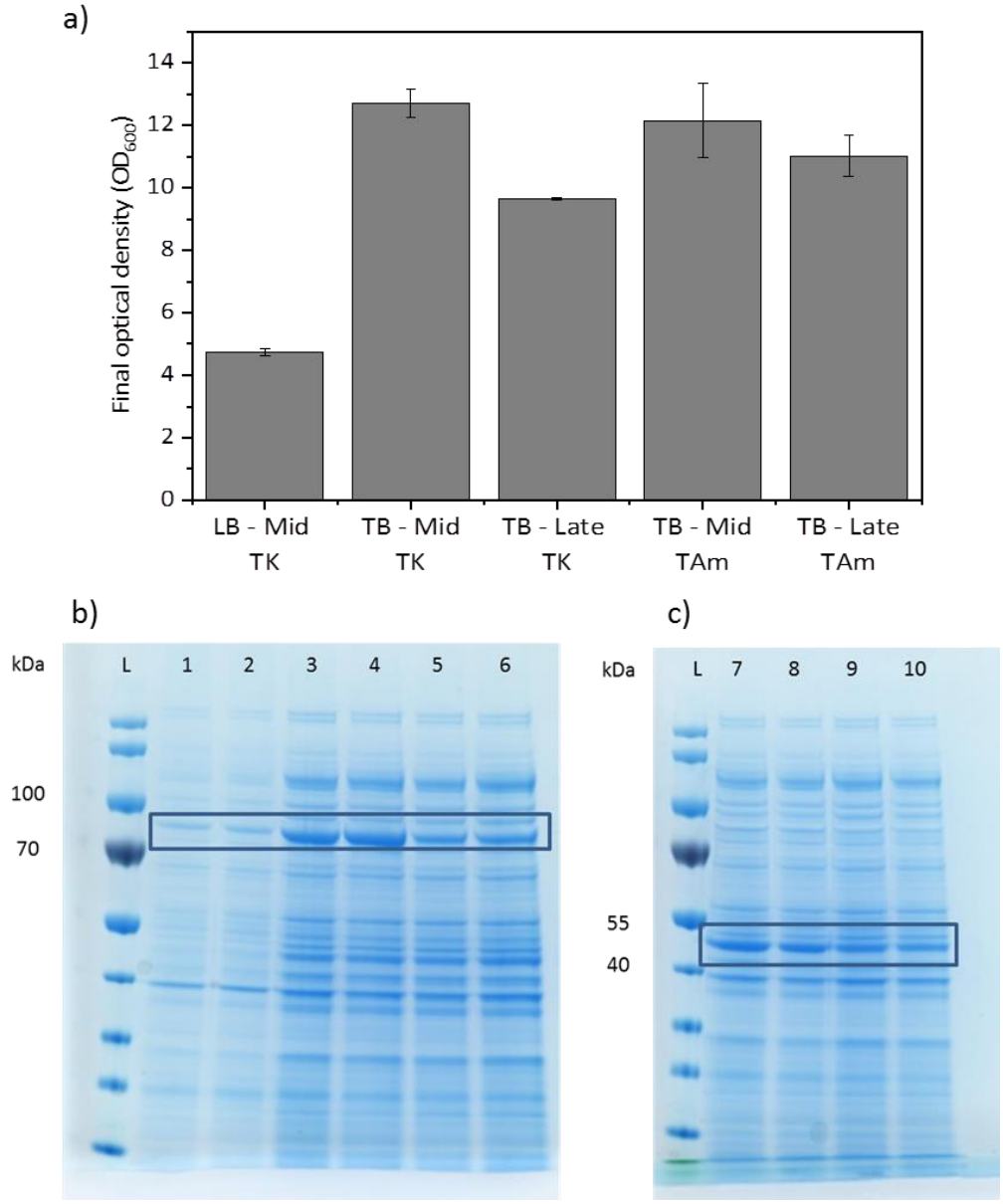

Figure 5.3. Final optical density measurements and SDS-PAGE analysis of small scale fermentation studies. (a) Column chart represents final OD measurement at harvest. Labels indicate: growth media (LB or TB); induction strategy (Mid: mid-exponential; or Late: late-exponential) and expressed enzyme (TK or TAm). Error bars denote SEM (n=2). SDS-PAGE analysis in (b) and (c) was carried out on the soluble fraction of end-point samples for the fermentations indicated in Figure 5.1 and Figure 5.2. Lanes represents the following fermentation (media, induction strategy, expressed enzyme and biological repeat number): LB, Mid, TK, 1 (1); LB, Mid, TK, 2 (2); TB, Mid, TK, 1 (3); TB, Mid, TK, 2 (4); TB, Late, TK, 1 (5); TB, Late, TK, 2 (6); TB, Mid, TAm, 1 (7); TB, Mid, TAm, 2 (8); TB, Late, TAm, 1 (9); and TB, Late, TAm, 2 (10). L represents the standard protein ladder. Boxes highlight the enzyme band (TK on the left image and TAm on the right). SDS-PAGE gels and analysis were performed as described in Section 2.4.1.8.

Selecting the best induction strategy is important for obtaining high levels of active enzyme expression. The most common induction method is the addition of IPTG to the medium during the fermentation for proteins expressed under the control of a T7 lac operator promoter (Hannig and Makrides, 1998; Dvorak *et al.*, 2015). Tuning IPTG concentration for induction is often recommended as IPTG can be toxic and hinder cell growth, despite this, Dvorak et al. (2015) showed no toxic effect on *E. coli*-BL21 (DE3) cells in an IPTG concentration range of 0 to 1 mM (Dvorak *et al.*, 2015). Induction is often recommended either during the mid or late phase of the exponential growth before the cells enter stationary phase (Gräslund *et al.*, 2008). Although the present work, aimed to test mid- and late-exponential phase induction, it is possible to see that the latter occurred as the cells were entering stationary phase at the point of induction. Despite this, expression of the enzyme of interest occurred regardless, and very little difference between the induction strategies was noticed in the *E. coli*-BL21 (DE3)-TAm strain.

5.3.1.3 Fermentation scale-up to a 30L pilot scale STR

After the initial small-scale optimisation studies, a larger scale production run was carried out using a 30 L STR Sartorius Stedim vessel with a 15 L working volume set up as described in Section 2.4.1.2. Although the reactor has the potential for fed-batch operation, the fermentation was run in batch with pH control. Dissolved oxygen control was also possible and set to DOT = 30%. Induction occurred after 4 hours, and in the same manner as the small-scale studies, the temperature was lowered to 25 °C overnight following induction.

The OD measurements of the STR fermentation are compared to the flask performance in Figure 5.4. It appears that the TAm producing strain performed in a very similar way to the flask cultures. Surprisingly, the TK strain did not reach the same optical density as achieved in the shake flask cultures. The lower OD could possibly be due to a contamination or the *E. coli* cells could have also grown overnight but entered death phase more quickly in the morning. Nonetheless, collected biomass was tested and TK activity was detected (successful conversion of L-arabinose into L-gluco-heptulose), and so, the biomass was retained and utilised. Whilst the TAm-strain performed better than the TK-strain, it still only achieved an OD of 10.5 as seen in Figure 5.4. One of the main driving forces for the use of STRs over flasks is that higher cell densities can be achieved. In this instance the STR cultures performed similarly to the flask. The likely explanation for this is that the growth-limiting factor in both instances was the available nutrients, rather than oxygen and mass transfer limitations or pH

variability. This would suggest the implementation of fed-batch fermentations in future, although they were considered beyond the scope of the current investigation.

As mentioned in Section 5.3.1.1, the goal of scaling-up enzyme production from flasks to STRs was to obtain a single consistent batch of biomass for both enzymes that would provide sufficient material for the enzymatic reactions. Despite producing sufficient material, higher cell densities could have been achieved. Indeed, *E. coli* fermentations have routinely been able to reach over 100 $g_{WCW}.L^{-1}$ for many years (Korz *et al.*, 1995; R. Hobbs *et al.*, 1996). As previously mentioned, large scale production is typically carried out by replacing complex growth media with defined culture media such as minimal salts media. The growth rate using defined media is typically smaller but in some cases it can produce better folded enzymes (Gaciarz *et al.*, 2017). Additionally, the TAm strain appeared to be nutrient limited suggesting that an effective feeding strategy after the 'DO spike' (the moment where DO increases because cell growth slows down) could increase cell densities.

Cost is an important concern when producing enzymes for biorefineries and as such decreasing the CoGs is an important aspect to consider as mentioned in Section 6.1. Literature on alternative strategies for the induction of enzyme expressions is widespread, with some work on BL21 (DE3) *E. coli* investigating thermoinduction (increasing temperature for expression) or feeding lactose to induce the promoter (Hoffman *et al.*, 1995; Caspeta *et al.*, 2013). The former, however, causes inhibition to growth; whilst care must be taken when utilising lactose due to concerns with Transmissible Spongiform Encephalopathies (Mad Cow disease) linked to usage of animal products (Thiry, Cingolani and Thiry, 2002).

Another cost reduction possibility is utilisation of other side-product or waste streams in biorefineries as carbon source for fermentations. For example, cellulose produced in the pretreatment of SBP can be used as a source of D-glucose in the fermentation of yeast (with the aid of cellulases) (Hamley-Bennet et al., unpublished). Further, vinasse from the bioethanol production plant in the sugar refinery was diluted and mixed with yeast extract to be used in the production of Arabinofuranosidase (AraF) and a Transaminase enzyme by *E. coli* BL21 (DE3). It was also found that D-galactose within the vinasse caused the enzyme to auto-induce, thus removing the need for IPTG (Cárdenas-Fernández *et al.*, 2017; Suhaili *et al.*, 2019).

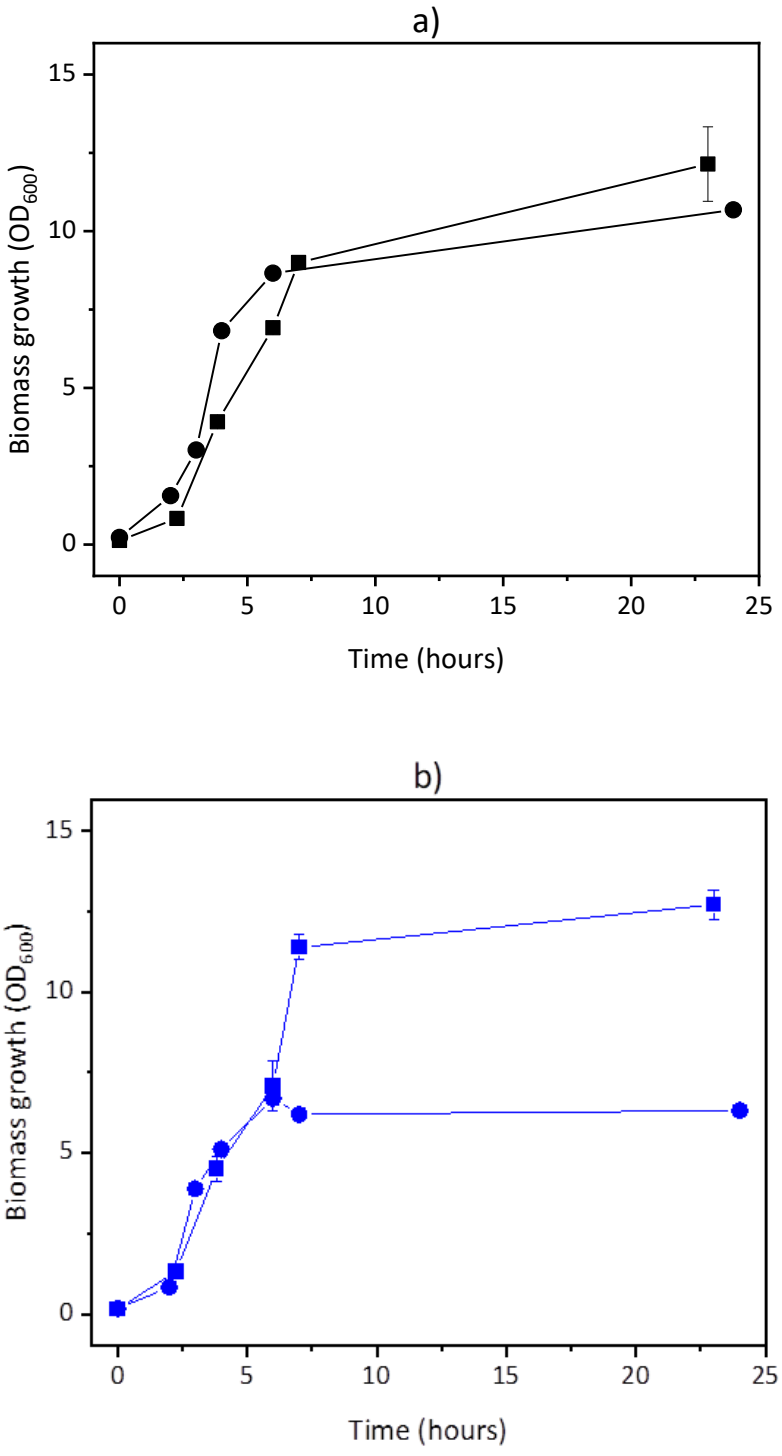

Figure 5.4. Comparison of small and pilot scale fermentations of *E.coli*-BL21 (DE3)-TAm and *E.coli*-BL21 (DE3)-TK. Panel (a) shows OD measurements for TAm-producing strain. It compares shake flask fermentation (■) with a 15 L STR batch fermentation (●). Panel (b) shows OD measurements for TK-producing strain. It compares shake flask fermentation (■) with a 15 L STR batch fermentation (●). Error bars denote SEM (n=2) for flask cultures, whilst for the 15 L fermentations no repeats were carried out. Fermentations were performed and analysed as described in Section 2.4.1.2.

5.3.2 Homogenisation as a scalable alternative to sonication for enzyme release

After fermentation, the biomass was harvested by centrifugation and stored in 50 mL Falcon tubes prior to cell lysis. To evaluate the effectiveness of cell disruption techniques, enzymatic bioconversions were carried out. As stated in Section 5.1, the mechanisms of the enzymes are discussed further in Chapter 6; but here the TAm and TK enzymes activities were measured separately. For the bioconversions, 10% v/v of either clarified homogenate or clarified sonicated lysate were used in 1.2 mL reactions as described in Section 2.4.2. For the TAm reaction 10 mM of L-serine and α-ketoglutaric acid were used and HPA concentration was monitored. Meanwhile, the TK reaction employed 33 mM of HPA and L-arabinose, for the production of L-gluco-heptulose. As stated in Section 2.4.2.2 and Section 2.4.2.3 both reactions were carried out at 50 °C, over a 24-hour period.

Although sonication can be easy to implement at small scale, it cannot be scaled effectively, so as an alternative, high pressure homogenisation was investigated. The APV Gaulin Lab40 homogeniser has a working volume of 40 mL, but operating conditions can be easily scaled up to larger homogenisers (Bláha *et al.*, 2018). Homogenised cell lysate samples of TAm and TK were used in enzymatic reactions to compare with the effectiveness of sonication. Additionally, the number of homogenisation passes, $N_{H,}$ was compared to provide insight into the release of enzymes throughout the homogenisation process.

Interestingly, the individual, or stand-alone, TAm and TK reactions in did not perform as well when utilising the same volume (10% v/v) of clarified sonicated or homogenised material as shown in Figure 5.5. Indeed, HPA production (by TAm) and L-gluco-heptulose production (by TK) were noticeably lower when the homogeniser was used. For the TAm reaction, the formation of HPA at 24 hours is more than 4 times lower (5.0 mM for the sonicated sample versus approximately 1.2 mM for the homogenised samples). Similarly, L-gluco-heptulose concentration for the sonication reaction (4.0 mM) is more than twice larger than the homogenised samples (1.8 mM). The initial rate of the reaction also appears to be much slower for both enzymes. Additionally, although the material was homogenised with 3 passes, panels (a) and (b) in Figure 5.5 show that even a single pass would be sufficient.

The most likely explanation for the lower homogenate activity is that the sonication and homogenisation steps required different dilutions of the same amount of cells. Pellets were resuspended in 15 mL of buffer for sonication and in 40 mL for homogenisation, making the sonicated lysate 2.67 times more concentrated. If the amount of enzymes released using

either technique were similar, this would explain why the homogenised samples appear to have much lower activity. Further evidence corroborating this theory was provided by SDS-PAGE analysis of samples of equal volume. The SDS-PAGE gels in Figure 5.6 show that very little difference in band thickness was seen between homogenisation number of passes (Lanes 2-4 for TAm, and 6-8 for TK). However, sonicated lysates appear to have more visible enzyme bands. They also appeared to have more total protein content in general.

To test if the lower conversions obtained by the homogenised lysates was due to the larger dilution used in the homogeniser, different homogenate proportions of the total volume of the reaction mix were compared. Homogenised lysates were used in: 10% v/v; 20% v/v; 26.7% v/v; and 40% v/v of the total reaction mix volume. These reaction mixes were compared to sonicated lysate reactions run at 10% v/v loading as described in Section 2.4.2.2 and 2.4.2.3.

Predictably, higher lysate concentration, and therefore enzyme loading resulted in better conversions as shown in Figure 5.7. Panels (a) and (b) show that almost 10 mM HPA, and 5 mM L-gluco-heptulose can be obtained, with 40% v/v lysate loading. Panels (c) and (d), which highlight the first 6 hours of the reaction, show that higher enzyme concentrations result in faster reactions. For TAm, the 26.7% v/v loading of homogenised lysate and the sonicated material match very closely throughout the reaction. In the case of TK, the final L-gluco-heptulose concentration for the 26.7% v/v homogenised lysate sample and the sonicated lysate are very close (both approximately 4.5 mM). The sonicated material appeared to be slower at the beginning of the reaction (as highlighted in panel (d)) but did not reach a plateau until later than the 26.7% v/v homogenised sample allowing them to reach similar 24-hours concentration.

The comparison between homogenisation and sonication shows that using the current resuspension methods sonication performs better on a volumetric basis. However, once the different dilution is accounted for, this effect disappears. This work also found that at 800 bar the number of passes had no impact on the enzyme released and the enzyme activity.

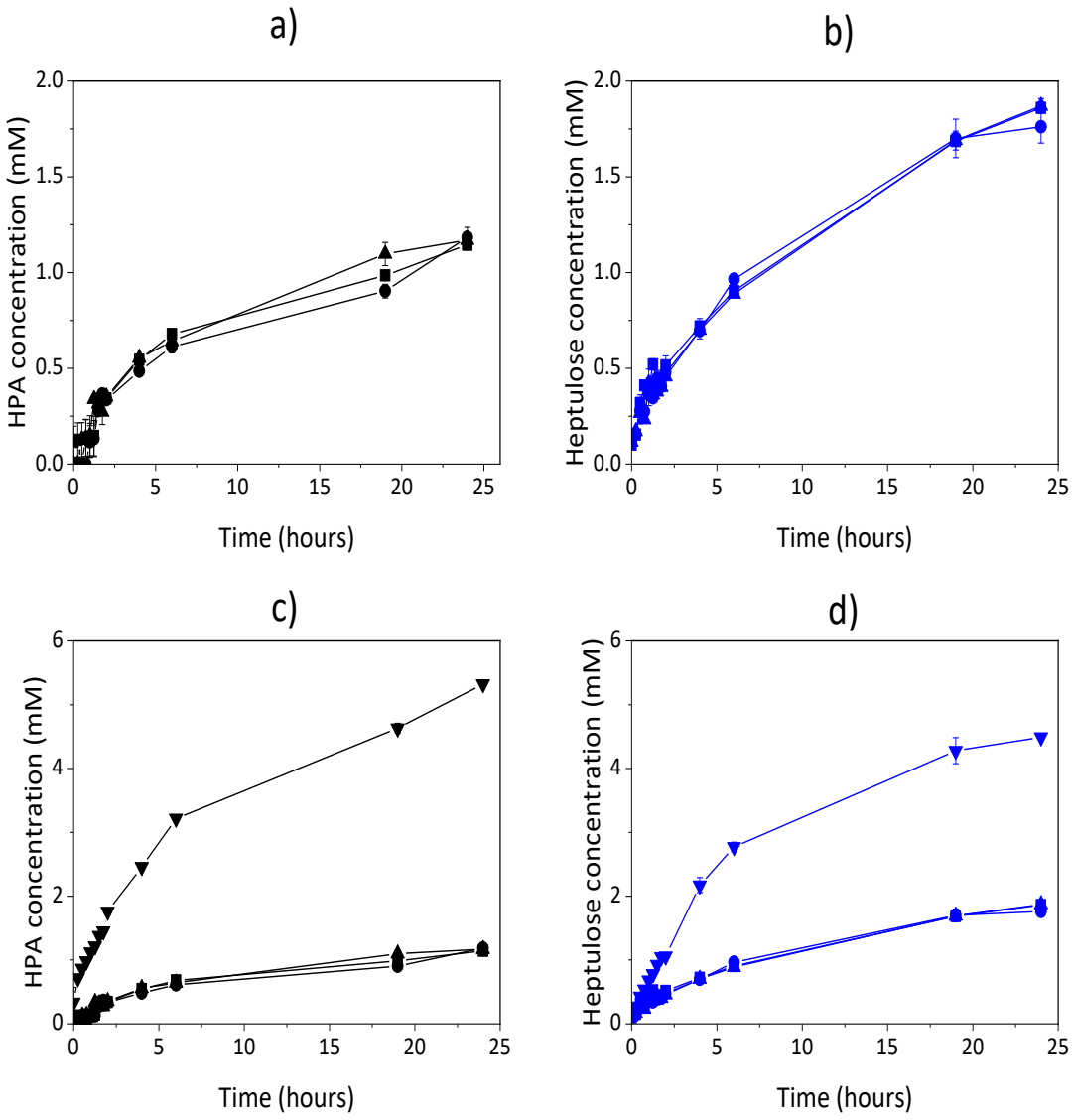

Figure 5.5. Effect of number of homogenisation passes (N_H) on bioconversion performance of TAm and TK as indication by HPA and L-gluco-heptulose production respectively. Panels (a) and (b) show the effect of N_H, whilst panels (c) and (d) show the performance of the homogenate compared to the same volume of sonicated samples. Panels (a) and (c) look at the production of HPA by TAm (■ for N_H = 1; ▲ for N_H = 2; ● N_H = 3; and ▼ for sonicated lysate), whilst (b) and (d) look at the production of L-gluco-heptulose by TK (■ for N_H = 1; ▲ for N_H = 2; ● N_H = 3; and ▼ for sonicated lysate). Error bars denote SEM (n=2). Cell lysis through sonication and homogenisation was carried out as described in Sections 2.4.1.3 and Section 2.4.1.5 and bioconversions were carried out as described in Section 2.4.2.

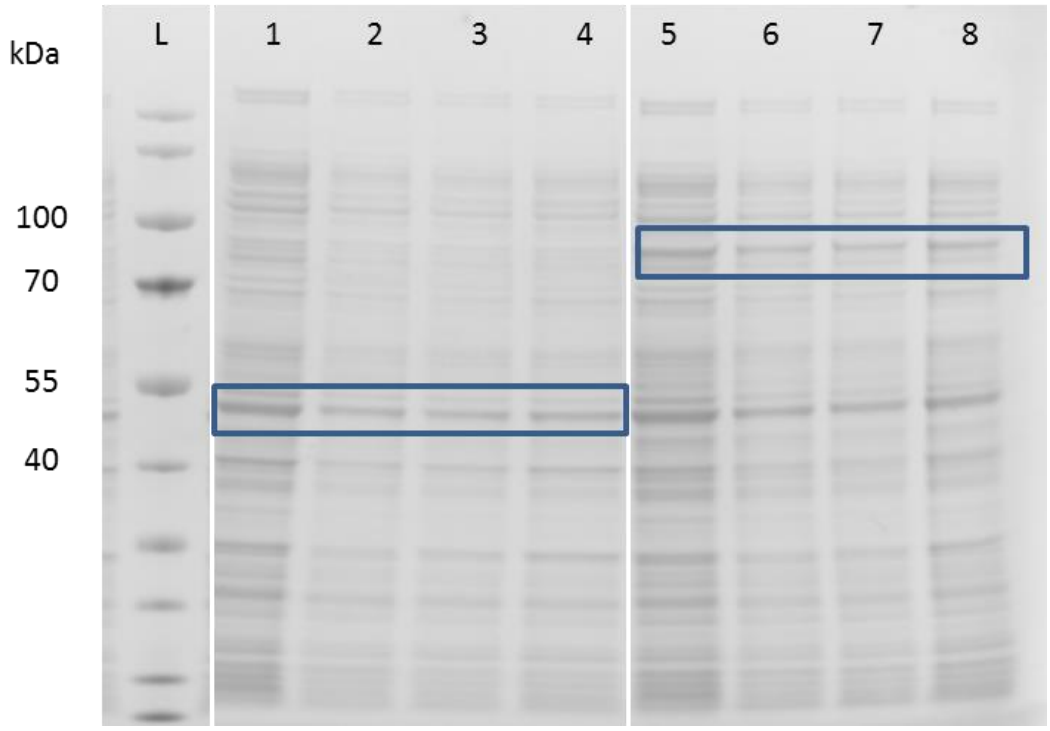

Figure 5.6. SDS-PAGE analysis of homogenised and sonicated *E.coli*-BL21 (DE3)-TAm and *E.coli*-BL21 (DE3)-TK lysates. The same volume of each sample was loaded to allow comparison. Rectangles highlight the TAm and TK bands. Lanes correspond to: TAm sonicated sample (1); TAm homogenate N_H = 1 (2); TAm homogenate N_H = 2 (3); TAm homogenate N_H = 3 (4); TK sonicated sample (5); TK homogenate N_H = 1 (6); TK homogenate N_H = 2 (7); and TK homogenate N_H = 3 (8). L represents the standard protein ladder. SDS-PAGE gels and analysis were performed as described in Section 2.4.1.8.

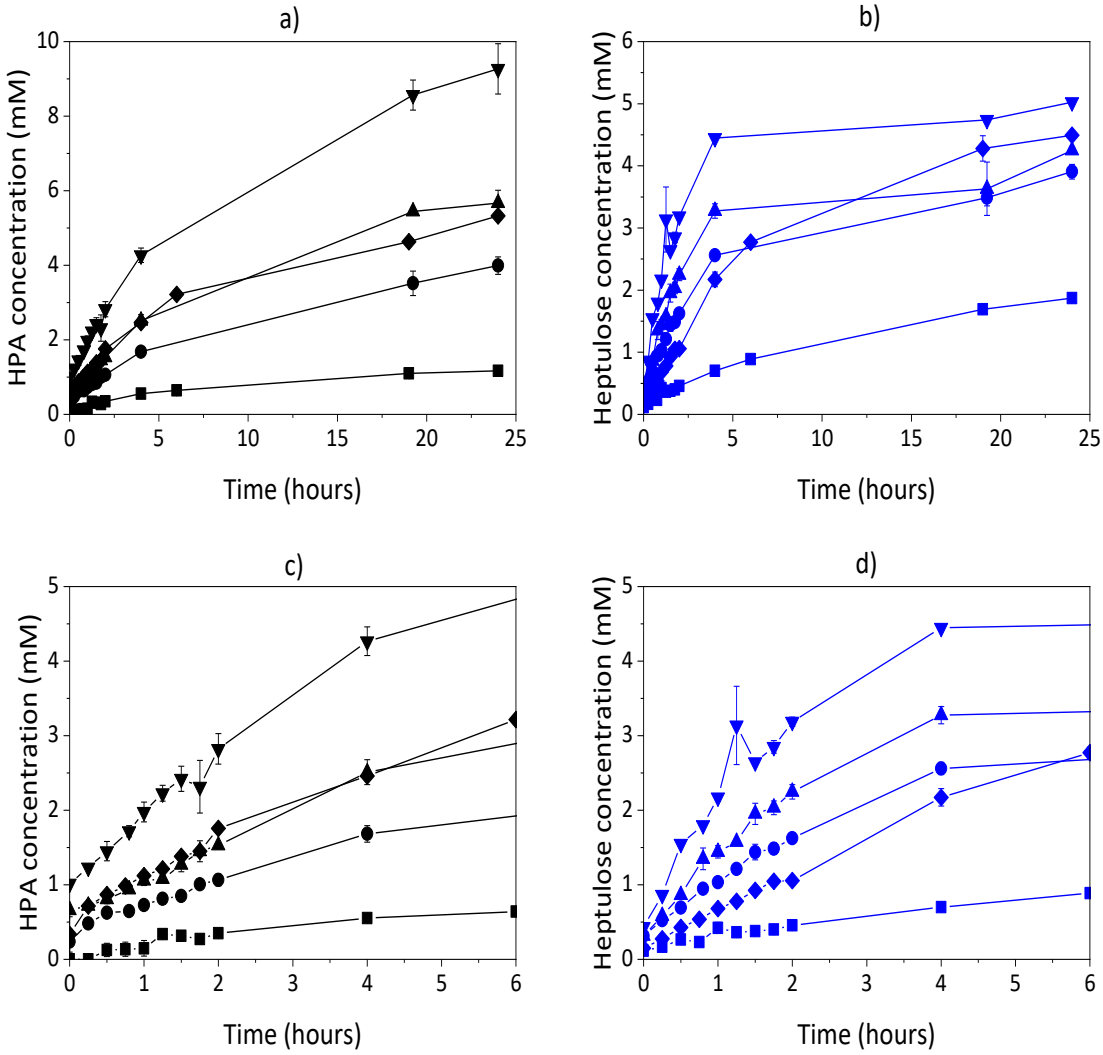

Figure 5.7. Effect of cell lysate concentration on TAm and TK batch reaction kinetics. Panels (a) and (b) show the product of the reactions over a 24-hour period, whilst panels (c) and (d) focus solely on the first six hours of the reactions. Panels (a) and (c) show the change in HPA concentration from the TAm reaction, for varying homogenised cell lysate concentrations. Panels (b) and (d) show the production of L-gluco-heptulose from the TK reaction. As an additional comparison the sonicated cell lysate was also used. Cell lysate concentrations used: 10% (■); 20% (●); 26.7% (▲); 40% (▼); and sonicated material at 10% v/v (◆). Symbols and lines in black represent the TAm reaction, and in blue the TK reaction. Error bars denote SEM (n=2). Cells were produced as described in Section 2.4.1.2; and lysed as described in Section 2.4.1.5. Reactions were carried out as described in Section 2.4.2.

The issue with keeping the current resuspension method is that the enzyme preparation would be too dilute. At large scale this could increase costs and become cumbersome, since most of the reaction volume would ideally be taken up by the substrate obtained from the SBP pretreatment. As such, increasing the enzyme concentrations in the homogenate would be an important step in scaling up this process further. In the current process the harvested cells are resuspended to about 10% w/v prior to homogenisation, but it has been shown that biomass concentrations has little effect on homogenisation, albeit at concentration of less than 17% w/v (Harrison, 1991; Bláha *et al.*, 2018). Nonetheless, if increasing concentrations in the homogeniser does negatively affect cell disruption it would be possible to use more homogenisation passes to release more enzyme. When Hobbs et al. (1996) homogenised TK-expressing *E.* coli they showed that only 60% of the total intracellular protein was released after 1 pass at 500 bar, but almost 100% was released after 3 passes. Interestingly the active enzyme concentration dropped in further passes (R. Hobbs *et al.*, 1996). Some homogenisers could also be set up in a semi-continuous mode by rerouting the homogeniser outlet to an inlet feed tank (Li *et al.*, 2013). Furthermore, homogenisers able to reach ultra-high pressures (over 1000 bar) have been employed in the food industry for steps such as bacterial inactivation, and could also be applied for cell lysis for protein release (Wuytack, Diels and Michiels, 2002; Briñez *et al.*, 2007).

5.3.3 Purification of TAm and TK enzymes

5.3.3.1 Heat-precipitation as a partial purification technique

The purification of proteins or enzymes involves one or more steps that can be implemented to obtain a pure or partially pure protein or enzyme preparation. In this work enzymes were purified to be used in immobilization protocols. Purification is carried out by exploiting a particular attribute of a protein or enzyme of interest (e.g. a His-tag, or a particular net charge at a certain pH). In this section, heat precipitation is investigated as a partial and rapid purification technique. Due to the stability of the TAm and TK enzymes used in this Thesis at relatively elevated temperatures (Bawn et al. (2018)), it was theorised that by heating cell lysate, other proteins could be precipitated whilst the enzymes of interest would remain in the soluble fraction.

The partial purification through thermal precipitation (also referred to as heat purification, or HP) was performed as described in Section 2.4.1.6. The screened purification conditions are shown in Figure 5.8 for TAm and Figure 5.9 for TK. The TAm band on the SDS-PAGE

becomes less visible at 50 °C with longer incubation time. This indicates that the TAm likely precipitated with longer incubations. The band appears almost fully faded after 20 minutes. At 55 °C a TAm band is present after 5 minutes but thereafter it is much less noticeable. The TK protein band in Figure 5.9 appears slightly less affected by the heat treatment, being noticeable throughout the timepoints studied at 50 °C and only fading after 20 minutes at 55 °C. The overall band intensity of the heat purified samples is much lower than the intensity of the cell lysates indicating that a reduction of overall protein concentration can be seen. The centrifugation tubes pictured on the right of Figure 5.8 for TAm and Figure 5.9 for TK show that the size of the precipitate after centrifugation increases with longer treatment times. This study also showed that the TAm seemed to be less able than the TK cell lysate to withstand harsher heat treatment conditions.

The activity of heat purified TAm and TK samples were monitored over the initial 2 hours of the purification process using standard bioconversion reaction conditions (10% v/v enzyme loading, 1.2 mL reaction volume, 50 °C and 10 mM L-serine and α-ketoglutaric acid for TAm and 33 mM of L-arabinose and HPA). Product concentrations measured over the first 2 hours of the reactions were then used to obtain initial reaction rates for HPA and L-gluco-heptulose production and are summarised in Table 5.1.

In the case of TAm it appears that, aside from the first sample, activity increased compared to the cell lysate reaction. The TK activity remained unaffected compared to the cell lysate, except after 20 minutes at 55 °C when the activity dropped by 25%. The TK finding reflects the protein gel findings (Figure 5.9, lanes 1-8) where the TK band did not disappear until the 55 °C and 20-minute timepoint. Conversely, whereas TAm activity seemingly increased, within the TAm SDS-PAGE gel the corresponding band became fainter with longer incubation and higher temperatures. It is possible that a different protein with similar molecular weight, or an inactive version of TAm, was removed during the heat treatment, but whilst this may explain a conservation of activity, it does not explain an increase in activity. Since samples were taken over the first 2 hours, the 24-hour reaction data was not available to corroborate either the gel or the activity work. Despite this, the SDS-PAGE analysis was used to select 50 °C and 10 min incubation time as the HP conditions used in subsequent studies.

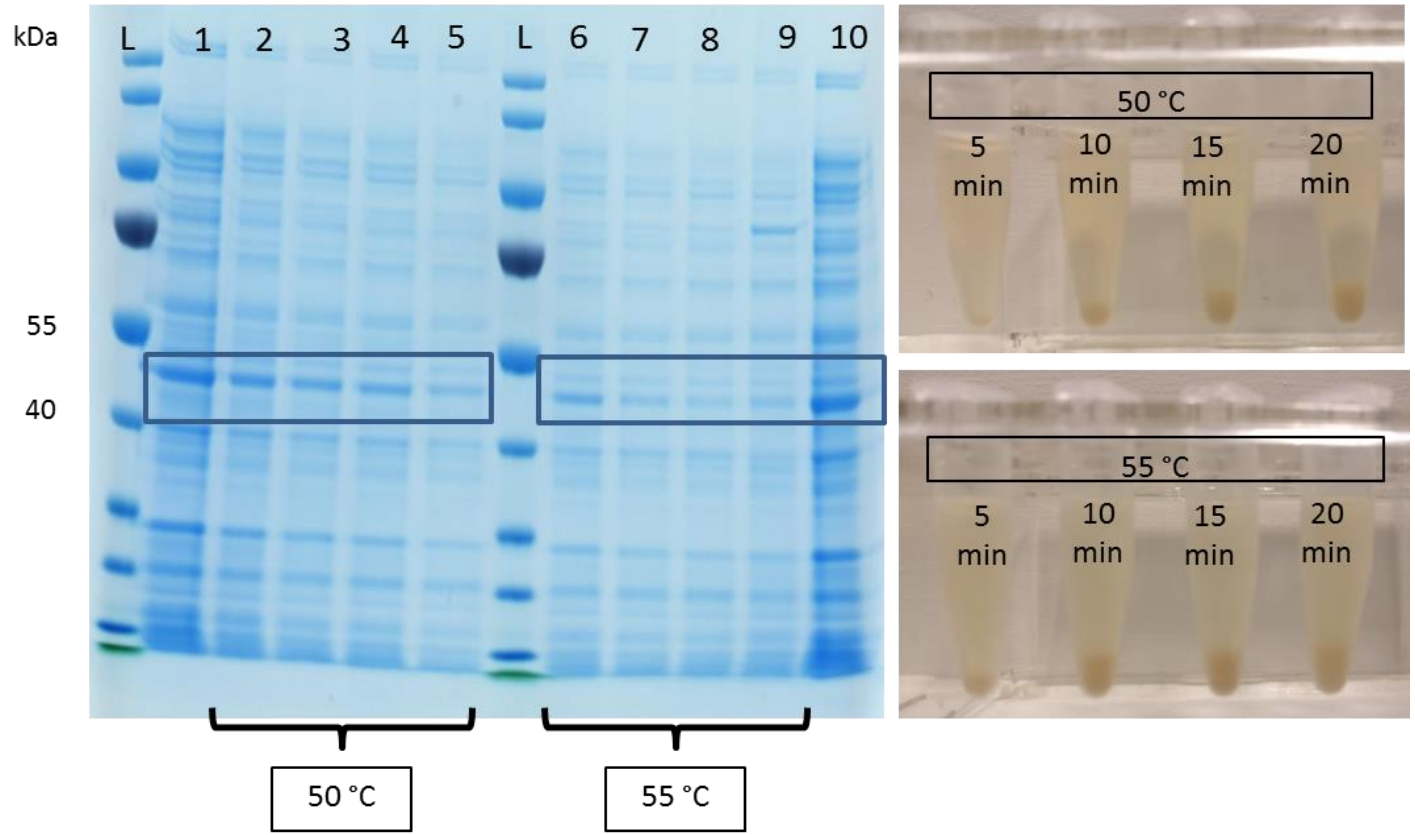

Figure 5.8. SDS-PAGE analysis of TAm heat precipitation (HP) and images of the precipitate formed. Left, is an SDS-PAGE gel displaying samples of TAm cell lysate at various stages of HP. Gel lanes correspond to various time points and temperatures of HP: protein standard ladder (L); TAm cell lysate (1); 50 °C – 5 min (2); 50 °C – 10 min (3); 50 °C – 15 min (4); 50 °C – 20 min (5); 55 °C – 5 min (6); 55 °C – 10 min (7); 55 °C – 15 min (8); 55 °C – 20 min (9); and TAm cell lysate (10). On the right are pictures of the heat purified samples after being spun down (20 min, 21,130g) as described in Section 2.4.1.6; SDS-PAGE were analysed as described in Section 2.4.1.8.

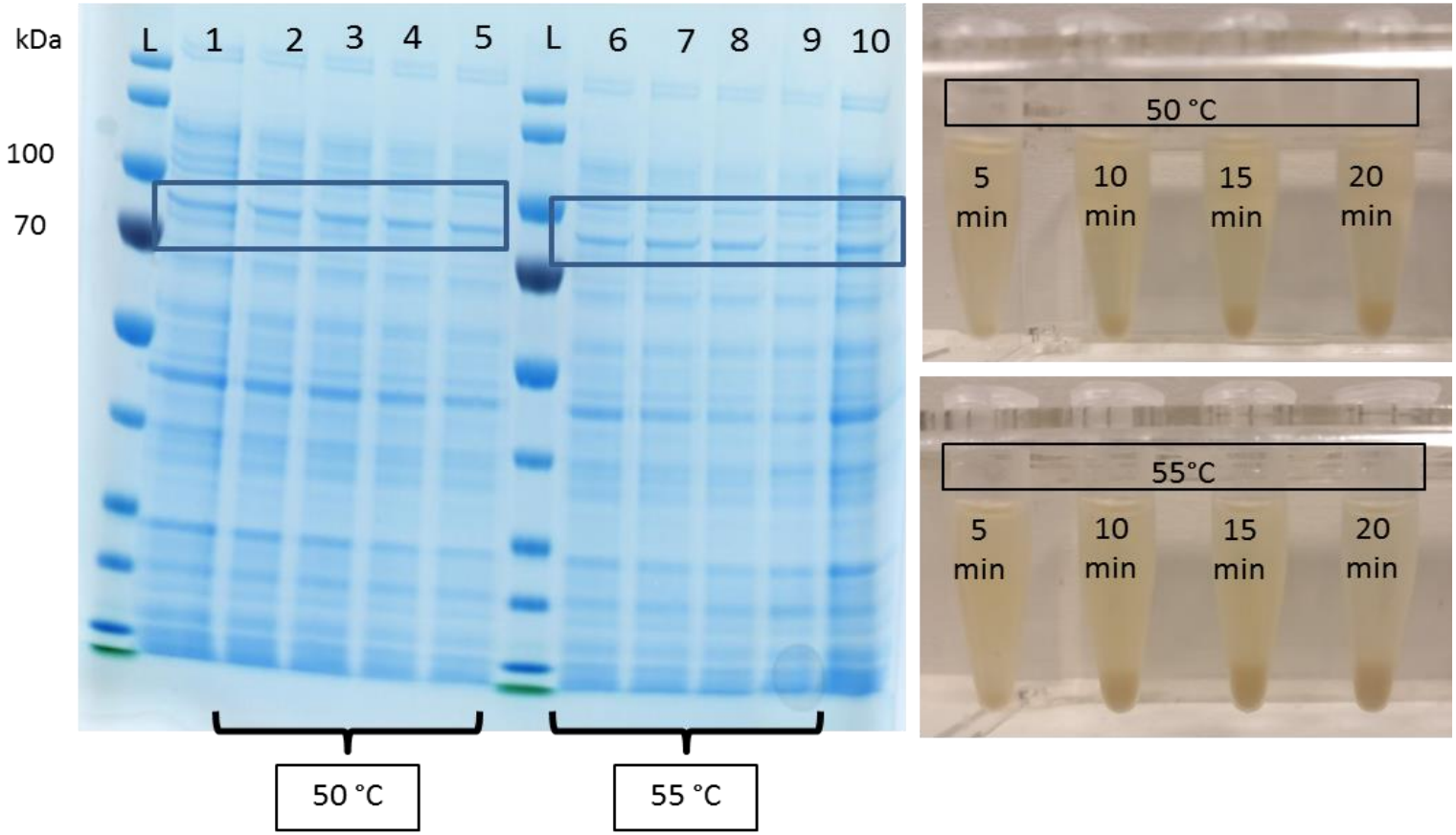

Figure 5.9. SDS-PAGE analysis of TK HP and images of precipitate formed. Left, is a SDS-PAGE gel image displaying samples of TK cell lysate at various stages of HP. Gel lanes correspond to varying time points and temperatures of HP:, Protein standard ladder (L); TK cell lysate (1); 50 °C – 5 min (2); 50 °C – 10 min (3); 50 °C – 15 min (4); 50 °C – 20 min (5); 55 °C – 5 min (6); 55 °C – 10 min (7); 55 °C – 15 min (8); 55 °C – 20 min (9); and TK cell lysate (10). On the right, pictures of the heat purified samples after being spun down (20 min, 21,130g) as described in Section 2.4.1.6; SDS-PAGE were analysed as described in Section 2.4.1.8.

An SDS-PAGE analysis coupled with a Bradford total protein measurement (Sections 2.4.1.8 and Section 2.4.1.7) was carried out on the homogenate samples as well as the samples after heat purification at 50 °C for 10 minutes. The first finding is that the protein content does not vary significantly with the number of passes as noted in Section 5.3.2. The additional interesting finding is that the total protein content of the heat purified samples is noticeably reduced (3-fold reduction for TAm and 2.1-fold for TK). The larger total protein reduction for TAm may, however, not be as desirable as it appears. As suggested in Figure 5.10 HCP is removed by heat precipitation but the TAm band also becomes fainter during the purification process.

5.3.3.2 Heat purified and His-tag purified enzyme immobilization comparison

The goal of the partial purification procedure described in Section 5.3.3.1 was to obtain enzyme preparations that could be immobilized to facilitate flow bioconversion using a retained, immobilized enzyme and increase enzyme reuse in an industrial setting. In this case, heat purified TK cell lysate was compared with His-tag purified material (obtained as described in Section 2.4.1.4). The purified enzyme solutions were immobilized following the procedure outlined in Section 2.4.3.2 on an Epoxymethacrylate resin (ECR) support. The details of this techniques are explored further in Section 6.3.3. However to compare the purification techniques, a protein loading concentration of 100 $mg_{totalprotein}.g_{resin}^{-1}$ was used. After the incubation step, the immobilized enzymes were tested at a 5% $w_{resin}.v_{reaction}^{-1}$ using standard reaction conditions as set out in Section 2.4.3.3.

Figure 5.11 shows a comparison of the purification methods and their effect on the production of L-gluco-heptulose by TK bioconversion over time. It can be clearly seen that both the initial rate, and the final product concentration, is higher for the His-tag purified material as opposed to that of heat purified enzymes. Indeed, the final concentration of L-gluco-heptulose is almost 3 times larger for the former and the concentration after 2 hours is almost twice as high (1.2 mM versus 0.6 mM). The likely explanation is that since the heat purification step does not remove all the HCPs, some of it may be binding to the resin during the incubation step leading to a lower concentration of immobilized TK. Despite the indication that the His-tag purification performs better, it is not necessarily the best choice when considering industrial scale up. Protein precipitation can scale better than column chromatography and His-tag purification is not often used at large scale (Titchener-Hooker, Dunnill and Hoare, 2008).

Table 5.1. Initial TAm and TK reaction rates for heat purified samples. Initial reaction rates for stand-alone batch TAm and TK reactions. Initial rates measured as the rate of change of product concentration over time in the reaction mix is shown for the various heat purification conditions. Standard reaction conditions, with 10% v/v of either clarified cell lysate or heat purified lysate were used for all reactions. Initial reaction rates were calculated as outlined in Section 2.4.2.

TAm Heat purification			**TK Heat purification**		
Temperature (°C)	**Time (min)**	**Initial rate ($mM_{HPA}.hr^{-1}$)**	**Temperature (°C)**	**Time (min)**	**Initial rate ($mM_{HEP}.hr^{-1}$)**
50	5	0.41	50	5	0.16
50	10	0.87	50	10	0.17
50	15	0.84	50	15	0.17
50	20	0.81	50	20	0.17
55	5	0.82	55	5	0.16
55	10	0.93	55	10	0.16
55	15	0.93	55	15	0.17
55	20	0.90	55	20	0.12
Cell Lysate		0.42	Cell Lysate		0.17

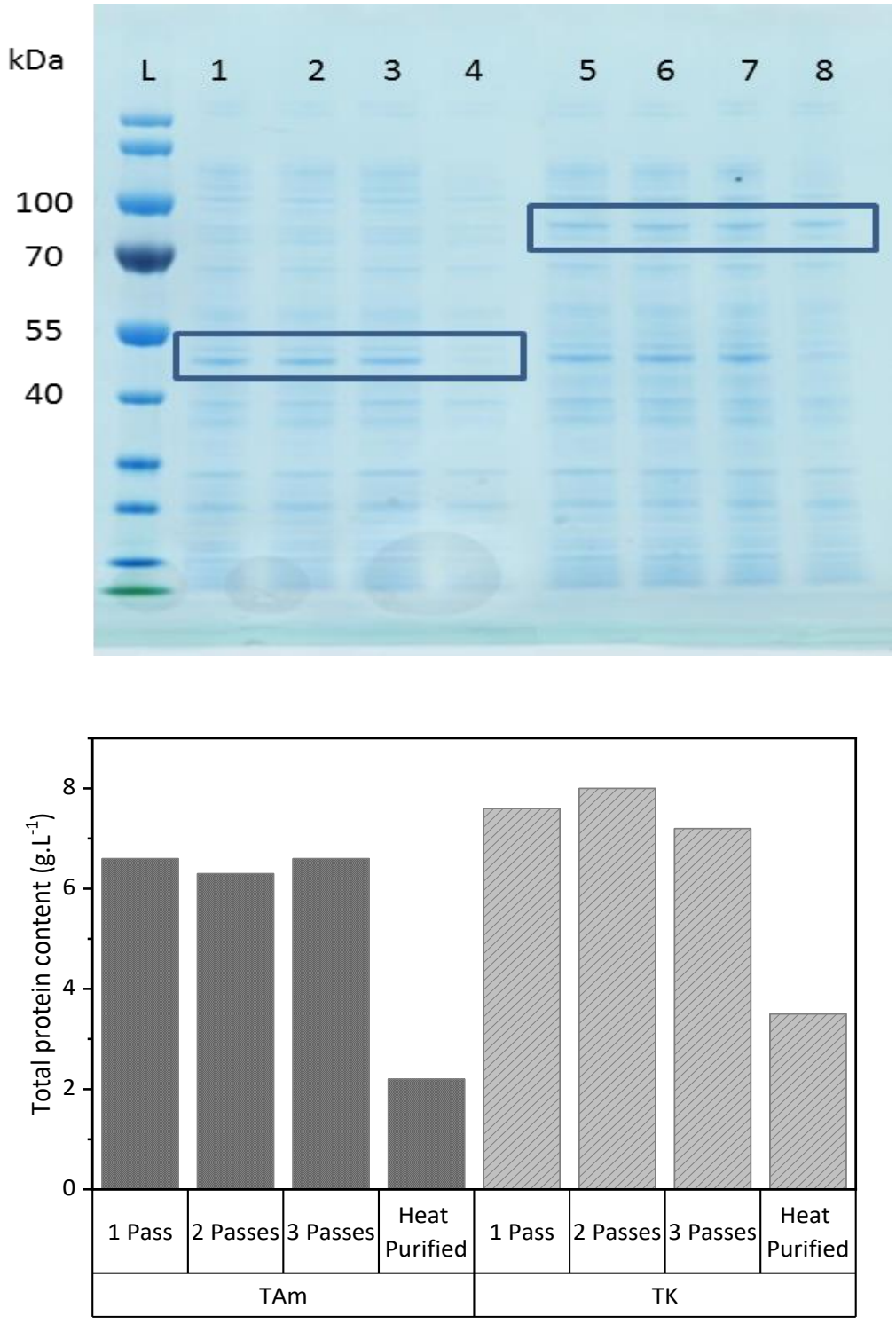

Figure 5.10. SDS-PAGE analysis and total protein content for homogenised and heat purified samples of *E.coli*-BL21 (DE3)-TAm and *E.coli*-BL21 (DE3)-TK. Protein gel lanes correspond to TAm samples (lanes and 1 – 4) and TK samples (5 – 8 =). N_H=1 (1 and 5); N_H=2 (2 and 6); and N_H=3 (3 and 7) are shown next to the heat purified samples (4 and 8). Bar chart shows the total protein content for the same samples as measured by the Bradford assay. Bradford reagent assay and SDS-PAGE gel were performed as described in Sections **2.4.1.7** and 2.4.1.8, respectively.

As seen in Figure 5.7 and discussed in Section 5.3.2, the enzyme concentration affects the initial reaction rate, suggesting that the worse performance by the heat purified material may be due to a lower enzymatic loading. This is in line with what was suggested by the SDS-PAGE analysis in Figure 5.10. The heat purified enzymes recovered were relatively impure. So, it is possible that the same performance as the IMAC purified immobilized enzyme could be obtained by loading more heat-purified immobilized enzyme.

In Figure 5.8 and Figure 5.9, it was possible to see that a considerable amount of material, including HCP, precipitated during the heat treatment purification. Meanwhile, TAm and TK activity was retained after the process, suggesting that this technique could be used for partial purification prior to immobilization. HP, often referred to as heat treatment or thermal precipitation was suggested as an alternative to the more conventional chromatographic purification methods that require large equipment and result in very dilute purified product. Indeed, within this work, the clarified cell lysate did not undergo any dilution during HP, since when using IMAC, the eluted fraction was 3 times more diluted than the lysate. Whereas this posed little challenge at small scale, in an industrial setting this would create additional operational challenges (Hartmann *et al.*, 2009). Examples of HP used in literature are not very common, with the exception of the dairy industry (Castro-Rosas *et al.*, 2013). HP was suggested as an alternative to chromatography for the production of biopharmaceuticals from tobacco leaves (Buyel *et al.*, 2014) and for the purification of HEPb core protein from *E. coli* cell lysate (Ng *et al.*, 2006).

Additionally, using HP for the treatment of thermostable enzymes was implemented as long as three decades ago (Patchett *et al.*, 1989; Takesawa *et al.*, 1990). Regarding purification of TAm and TK enzymes in particular, HP was mentioned in some early TAm work, when the enzymes were obtained from animal sources such as pig liver (Taylor and Jenkins, 1966; Norton and Sokatch, 1970). A thermostable TK, on the other hand, was heat purified recently by Abdoul-Zabar and colleagues (2013). It is worth noting in this instance, that the process appeared to remove most HCPs, suggesting that their conditions (65 °C, 45 minutes) may have been more conducive to HCP precipitation. However, the TK presented in their work was found to be stable up to 70 °C, whilst results discussed in Chapter 6 suggest that the TK used here had little to no activity at 70 °C (Abdoul-Zabar *et al.*, 2013).

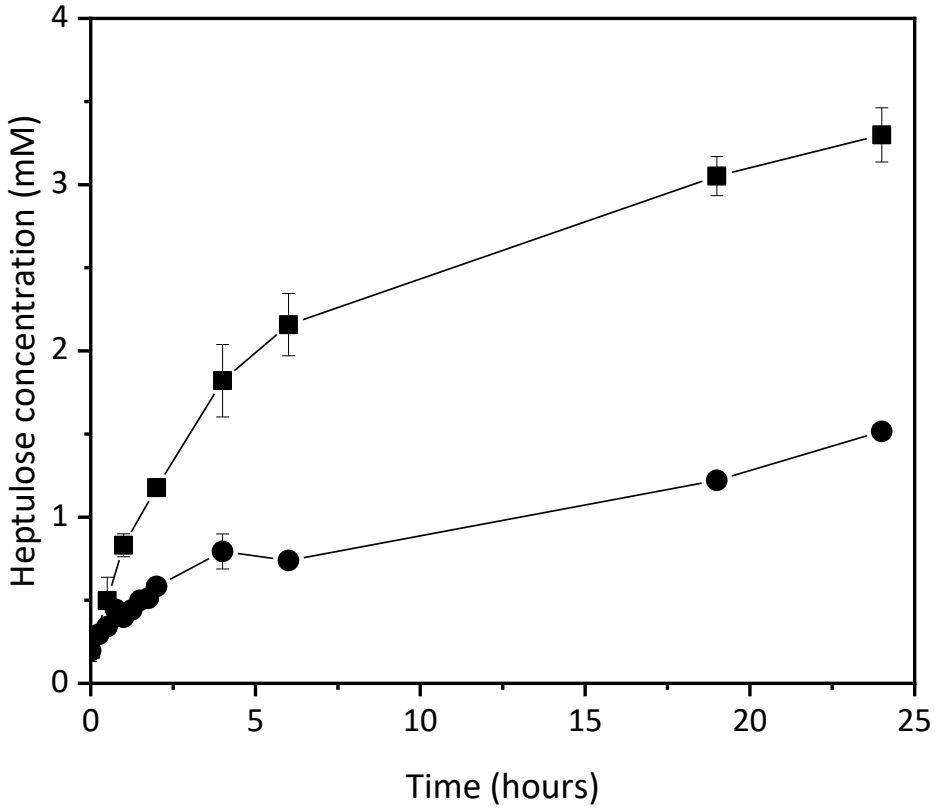

Figure 5.11. Effect of purification strategy on the kinetics of L-gluco-heptulose production by immobilized TK in batch reactions. Either His-tag purified (■) or heat purified (●) TK was immobilized on ECR resin. 5% w/v of resin was used in the reaction mix to evaluate which purification would yield the most effective immobilized enzyme. Error bars denote SEM (n=2). Enzyme purifications were carried out as described in Section 2.4.1.4 and 2.4.1.6, immobilization procedures were outlined in Section 2.4.3.2 and are further discussed in Section 6.3.3.

The disappearance of the enzymes of interest during the purification process clearly highlights the need for further optimisation of the purification step. As the TAm and TK bioconversions can be carried out at 50 °C, the heat is not likely to denature the enzymes. A possible cause for the low purification quality was thought to be the isoelectric point (pI) of the proteins. If the buffer pH is close to the pI of a protein this is likely to precipitate (Castro-Rosas *et al.*, 2013). In this case, however, the buffer pH was 8, whilst the theoretical pIs of TAm and TK are 6.01 and 5.41 respectively. It is possible that some of the TAm and TK enzymes co-precipitated with other proteins, rather than being denatured. As such, a possible improvement that could have been investigated would be the effect of mixing the lysates during the HP step.

5.4 Summary

This chapter explored alternatives to classic laboratory techniques to scale production, lysis and purification of TAm and TK enzymes from bench top experiments to industrially relevant unit operations. This was important work to facilitate subsequent flow bioconversion studies in the ACR (Chapter 6).

Firstly, in Section 5.3.1, the growth *E. coli* and enzyme expression was improved by selecting a more suitable culture media and induction strategy (Figure 5.1 and Figure 5.2). These strains were then, also, grown in a stirred tank reactor in Section 5.3.1.3. The STR cultures gave similar final cell yields as the flask cultures; indicating the need to develop feeding strategies to increase cell mass (Figure 5.4). Next, homogenisation was investigated as a scalable alternative to sonication for the disruption of cells in Section 5.3.2. The disruption methods appeared no different in terms of TAm and TK performance when the dilution prior the disruption was accounted for (Figure 5.7).

The purification of the clarified cell lysates was carried out with both IMAC and heat purification as described in Section 5.3.3. Although the HP step requires further study and optimisation of reaction conditions, it showed a viable alternative for the production of cheaper, partially pure enzymes. Heat purified TK was successfully immobilized and converted L-arabinose into L-gluco-heptulose, albeit to lower final concentrations than His-tag purified material (Figure 5.11). Since the amount of material loaded onto the resin for the immobilization procedure was calculated on a total protein content basis; the higher His-tag yields are likely attributable to more TK being loaded onto the resin.

If the scale up of the production, lysis and purification of TAm and TK is necessary, future work should look into moving from a complex to a defined medium and implementing a feeding strategy in stirred tank reactors. It should then focus on increasing the solid loading during the lysis steps, without compromising protein release, to create a more concentrated enzyme solution. Finally, the HP step could be improved to obtain a purer enzyme solution. In the following chapter, the enzymes produced in this Chapter, will be investigated for use in both batch and continuous reactions with both model solutes and SBP-derived L-arabinose.

6

Continuous production of L-gluco-heptulose via a one-pot two-step enzymatic cascade from Sugar Beet Pulp

6.1 Introduction

Chapter 4 demonstrated how L-arabinose can be obtained from SBP via dilute acid pretreatment (Section 4.3.3). Having produced an L-arabinose-rich feedstock, it is important to find ways to add value to the process stream by utilising the L-arabinose effectively. Fermentation of L-arabinose is challenging, as pentoses are not readily utilised by bacteria or yeast, hence a number of research groups have engineered strains to utilise L-arabinose for biomass growth in conjunction with hexose sugars (Deanda *et al.*, 1996). The target product of L-arabinose fermentations has typically been bioethanol: a low value, high volume side product, making fermentative solution relatively unattractive (Deanda *et al.*, 1996; Richard *et al.*, 2003; Wiedemann and Boles, 2008). As stated in Section 1.4 an alternative to fermentative solutions is the biocatalytic upgrading of L-arabinose into high value-added, speciality products.

Enzymes are naturally occurring catalysts involved in a number of reactions in living organisms. Biocatalytic reactions, on the other hand, make use of enzymes *ex vivo* to yield products or intermediate compounds of interest. Despite one of the oldest examples of biocatalysis dating back to 1815, with the conversion of ethanol into acetic acid through the use of an *Acetobacter* strain immobilized on wood chips, biocatalysis has become increasingly relevant in recent years (Wandrey, Liese and Kihumbu, 2000; Turner, 2012; Torrelo, Hanefeld and Hollmann, 2015). Enzymes tend to operate at near physiological conditions, making them attractive alternatives to typical chemical synthesis steps, by removing the need of extreme temperatures, pressures or the use of harsh or toxic solvents (Schmid *et al.*, 2001; Ringborg and Woodley, 2016). In some instances, enzymes are also the preferred catalyst of choice for reactions requiring a high selectivity, or steps requiring the selection of one enantiomer over another (Schmid *et al.*, 2001; Pollard and Woodley, 2007; Tufvesson *et al.*, 2010).

One potential enzyme for the upgrading of L-arabinose is transketolase (TK) for the production of a ketoheptose: L-gluco-heptulose. As explained in Section 1.4.5, L-gluco-heptulose could have potential therapeutic applications in hypoglycaemia and cancer (Paulsen, Richenderfer and Winick, 1967; Board, Colquhoun and Newsholme, 1995). TKs are widespread enzymes that have a key role in metabolic regulation in living organisms (Section 1.4.5). TKs supply ribose for nucleoside synthesis in *E. coli* and produce erythrose-4-phosphate in the Shikimate pathway for amino acid synthesis. They transfer two carbon

atoms in the form of a ketol group, from one molecule to another through a “ping-pong”, or bi-bi mechanism. This means that the carboligation step occurs in 4 phases: firstly the ketol-donor binds to the enzyme, then the byproduct is released having donated the ketol group, this is followed by the binding of the keto acceptor which accepts the ketol group before being released as the “extended molecule” (Gyamerah and Willetts, 1997; Turner, 2000; Ringborg and Woodley, 2016). Biocatalytic TK reactions can be made irreversible if hydroxypyruvate (HPA) is used as ketol donor. HPA is transformed into CO_2 which evaporates from solution after the removal of the C-C group. The irreversibility of the reaction drives product formation to completion making it a more favourable reaction from an industrial perspective. Despite this, HPA and its lithium salt (Li-HPA) remain expensive, making large scale reactions more challenging. Furthermore, HPA synthesis is complex and HPA has been shown to be heat labile (Dickens and Williamson, 1958; Lorillière *et al.*, 2017).

An emerging aspect of biocatalysis is the coupling of more than one enzymatic reaction together forming multi-step biocatalytic or enzymatic cascades. These cascades can provide shortened synthetic routes and can help overcome issues with unstable reaction intermediates and/or unfavourable reaction equilibria (Patil *et al.*, 2018). Recent work from the Sustainable Chemical Feedstock group proposed a one-pot two-step enzymatic cascade to bypass the need for HPA addition when upgrading L-arabinose. This approach utilised a transaminase (TAm) to deaminate L-serine to produce HPA *in situ* for the subsequent TK bioconversion (Bawn *et al.*, 2018).

TAms are a class of enzymes that were first applied commercially in the production of an agrochemical herbicide in the 1990s (Matcham *et al.*, 1999). Since then, TAms have become of great interest due to their ability to synthesise chiral amino alcohols: an important type of chemicals with a wide range of applications in pharmaceutical, fine chemicals and agro-industries (Villegas-Torres *et al.*, 2015; Guo and Berglund, 2017). TAms catalyse the transfer of an amino group from an amino-donor to an amino acceptor as shown in Figure 1.6. TAms are Pyridoxal 5’ Phosphate (PLP) dependant enzymes that do not require cofactor recycling as within the amine transfer mechanism the cofactor is not degraded (Kara *et al.*, 2014). Similarly to TKs, TAms also employ a ping-pong, or bi-bi reaction mechanism. In this instance the reaction is initiated by the amino donor binding to the enzyme to release the amino donor byproduct. Then the amino acceptor (a keto acid ketone or aldehyde) binds to the enzyme to accept the amino group and is then released from the enzyme complex. TAms are generally divided into two subclasses: α-TAms and ω-TAms. Whilst the former catalyses the

transfer of an amino group from the first carbon that attaches to a functional group, or α carbon, the latter subclass transfers the amine moiety located away from the α carbon and has become, arguably more interesting and more widely studied (Slabu *et al.*, 2017).

TAm conversions are also equilibrium dependent, however, in the proposed one-pot two-step reaction shown in Figure 6.3, the equilibrium would be driven to final product formation by the irreversible TK reaction step. One-pot two-step reactions involving TAm and TK have been reported in various studies. In some instances, a carboligation step using TK was followed by an amino transfer catalysed by TAm. For example, glycolaldehyde was converted into L-erythrulose, with HPA as the ketol donor; this was followed by the aminotransfer reaction to produce (2*S*,3*R*)-2-amino-1,3,4-butanetriol. In another example propionaldehyde was converted into (3*S*)-1,3-dihydroxypenan-2-one through the TK-mediated carboligation, to produce (2*S*,3*R*)-2-aminopentane-1,3-diol (Smith *et al.*, 2010; Rios-Solis *et al.*, 2015; Villegas-Torres *et al.*, 2015). The TAm-mediated production of HPA from L-serine was shown, using thermostable enzymes, by Lorilliere et al. (2017) and Bawn et al. (2018) at the 20 mL and 2 mL scale rescpetively. The latter work, part of the Sustainable Chemical Feedstocks group, used a previously produced library of TAms and a TK isolated from *Deinococcus radiodurans* and *Deinococcus geothermalis*. Of the screened thermostable TAms, two showed activity towards the production of HPA, but only one, isolated from *Deinococcus geothermalis* appeared to work when used in a one-pot two-step system. The thermostable TAm and TK enzymes were also engineered to have a His-tag to facilitate enzyme purification (Bawn *et al.*, 2018).

Due to the small scales used in laboratory settings, enzymes are rarely recycled. However, in cost-sensitive industrial processes, considerable effort goes into developing strategies for the retention and reuse of enzymes in order to minimise their impact on the overall CoGs. Enzyme immobilization is one such retention strategy (Hanefeld, Gardossi and Magner, 2009) . Immobilizing enzymes not only allows the re-use of the biocatalyst but also avoids contamination of the reaction product, enables further control of the reaction conditions and allows different reactor configurations (e.g. packed-bed reactors) (Garcia-Galan *et al.*, 2011). Additionally, the high biocatalyst loadings required for some enzymatic reactions limit the use of free enzyme (Tran and Balkus, 2011). Indeed, a well-immobilized enzyme is often crucial for the success of a bioprocess. For example, the immobilization of glucose isomerase made the isomerisation reaction of D-glucose, in the High Fructose Corn Syrup process cost

competitive; and the successful immobilization of penicillin acylase enabled the development of β-lactam antibiotics (Sheldon, 2007).

As biocatalytic processes are translated from bench-top experiment to commercial settings, scale up and process intensification considerations need to be made. An emerging approach is the use of flow biocatalysis (Britton, Majumdar and Weiss, 2018). As stated in Section 1.5.1, flow reactors can offer better control, shorter downtime and safer operation than batch or fed-batch conversions (Browne *et al.*, 2011; Gasparini *et al.*, 2012; Britton, Majumdar and Weiss, 2018). Indeed, in recent years the number of publications and patents including the term "continuous flow biocatalysis" has increased dramatically, from less than 5 in the year 2000 to over 50 in the year 2017 (Britton, Majumdar and Weiss, 2018).

Various groups have carried out bioconversions using immobilized enzymes. For example, Contente et al. (2017) used a TAm from *Halomonas elongata*, immobilized on an epoxy resin to produce aldehydes in an aqueous solution. For production in two-phase liquid systems, a segmented flow capillary reactor was used to convert 1-heptaldehyde to 1-heptanol. Another study immobilized whole cells expressing ω-TAm on methacrylate beads, placed them in a packed bed reactor, and screened a range of amine acceptors (Karande, Schmid and Buehler, 2011; Andrade, Kroutil and Jamison, 2014; Contente *et al.*, 2017).

Biocatalytic cascades have also been attempted in flow, including some of the aforementioned TK-TAm mediated reactions. (2*S*,3*R*)-2-amino-1,3,4-butanetriol has been produced using both enzymes immobilized using His-tags to His-Select Nickel Affinity agarose beads, as well as free enzymes from cell lysates, in a microreactor (A. Halim, Szita and Baganz, 2013; Gruber *et al.*, 2018). Most of the continuous flow biocatalysis work has focused on using microreactors, and whilst these offer advantages, their laminar flow regimes are not necessarily scalable. Large scale continuous flow biocatalytic reactors are not as widely described. Despite this, the ACR, a scalable, lab-scale flow reactor, has been applied to flow biocatalysis in two published instances. Jones et al. (2012) carried out a D-amino-oxidase reaction in both batch reactors and the ACR, showing that the latter had better gas-liquid mass transfer properties leading to better conversion. Similarly, the ACR characterisation work mentioned in Section 3.3.2 by Toftgaard Pedersen et al. (2017) involved another oxidation reaction that benefitted from enhanced mass transfer in the ACR. To date, there have been no published studies on use of the ACR involving multi-enzymatic cascades.

6.2 Aim and objectives

The aim of this chapter is to demonstrate the potential for the scalable one-pot two-step enzymatic production of L-gluco-heptulose, employing TAm and TK enzymes, in a continuous flow reactor. The free enzymes will first be studied individually, using model solutes at small scale. The two enzymes will then be studied in one-pot two-step reactions at different scales. The immobilization of the enzymes on two different supports will be investigated, in batch mode, both for individual enzymes and the one-pot two-step reaction. Finally, the one-pot two-step reaction will be investigated in a continuous regime using the ACR. Pretreated and depolymerised SBP, will also be used as a source of sustainable L-arabinose in batch and flow reactions and compared to the model solution performance. The one-pot two-step biocatalytic production of L-gluco-heptulose from pretreated SBP will then be demonstrated in the ACR. The specific objectives are outlined below.

- To characterise TAm performance in terms of HPA production using model solutes.
- To characterise TK performance in terms of L-gluco-heptulose production using model solutes.
- To investigate production of L-gluco-heptulose, via a one-pot two-step reaction bediated by TAm and TK, in batch, at different scales.
- To investigate TAm and TK immobilization it terms of individual, and one-pot two-step reactions.
- To demonstrate continuous production of L-gluco-heptulose in the ACR using pure and SBP-derived L-arabinose.

6.3 Results

6.3.1 Single enzyme characterisation

6.3.1.1 Reaction selection

As discussed in Section 6.1 the production of L-gluco-heptulose by enzymatic means could be a possible avenue for the utilisation of L-arabinose produced from pretreated SBP. **Figure 6.1**, highlights the proposed reaction. Firstly, the pyranose form of L-arabinose in solution spontaneously linearizes. This L-arabinose form can then react with HPA. HPA acts as the ketol donor, extending L-arabinose length by two carbon units, thus forming L-gluco-heptulose. Under atmospheric conditions, CO_2, the byproduct of the carboligation step, then evaporates, making the reaction irreversible. The L-gluco-heptulose could then take its favoured pyranose form, thereby driving the reaction equilibrium forward.

In Chapter 4, L-arabinose stability had been tested at high acidity and temperatures (Figure 4.9); however, it was important to determine if HPA would also be stable under the proposed reaction conditions. To investigate this, an initial experiment was carried out to test HPA stability at high temperature (50 °C). Figure 6.2 clearly shows that HPA quickly degraded over the course of a 24-hour reaction period. In the first 4 hours it appeared to be decrease to ~30% w/w of the initial concentration, stabilising at around 25%-30% w/w thereon.

The HPA employed in *in vitro* biocatalytic reactions is typically a lithium salt. This was first isolated by Dickens and Williamson (1958), who also observed degradation caused by heat. Previous groups working on thermostable TKs showed that temperature had an effect on increased degradation of HPA. Additionally, high TK cofactors concentration (2.4 mM ThDP and 9 mM $MgCl_2$, approximately twice as much as what was used in this study, 1.3 mM and 5.1 mM) appeared to promote HPA degradation (Lorillière *et al.*, 2017).

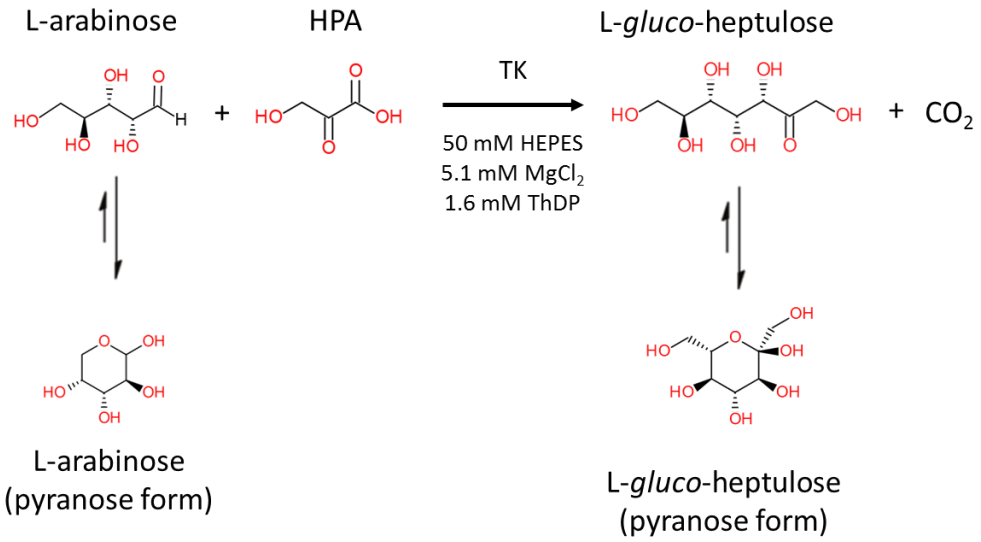

Figure 6.1. Reaction scheme for L-gluco-heptulose production from L-arabinose and HPA as catalysed by TK. Sugars such as L-arabinose and L-gluco-heptulose are typically found in their pyranose form however in solution they are in equilibrium with their linear forms. Reaction scheme adapted from Subrizi et al. (2016).

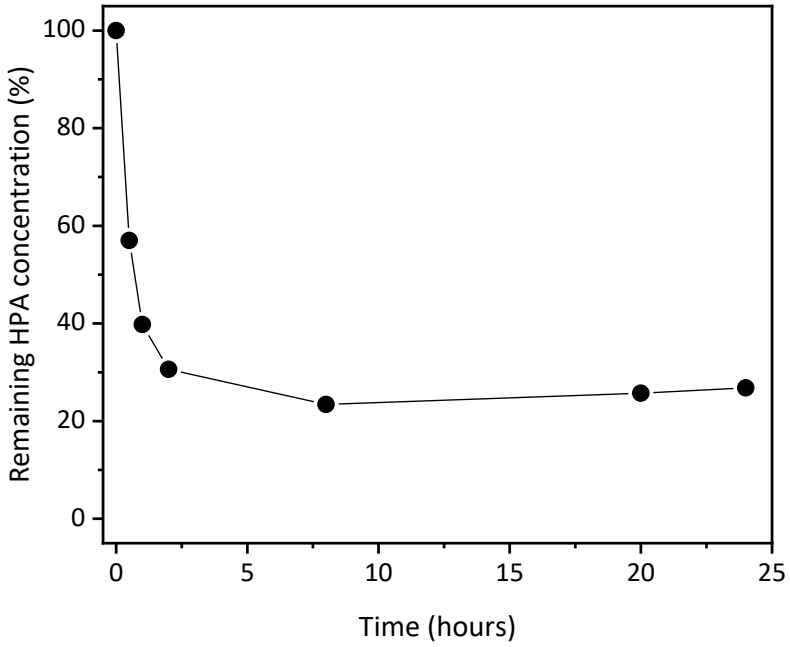

Figure 6.2. Kinetics of HPA degradation at 50 °C. The HPA solution was incubated over a 24-hour period at 50 °C in 50 mM HEPES pH 8. Experiment performed as described in Section 2.4.2.3.

In addition to the heat degradation of HPA, the production of the lithium salt in house is time consuming, requiring the use of bromine, handling toxic wastes and several purification steps (Dickens and Williamson, 1958; Subrizi *et al.*, 2016; Bawn *et al.*, 2018). Whilst purchasing HPA is achievable in small scale studies, it is not a feasible solution when scaling up, as shown by its high price in Table 6.1.

Previous work by Bawn et al. (2018), has established a one-pot two-step reaction, using thermostable TAm and TK where HPA was produced from the deamination of L-serine *in situ*. The HPA could then be used in the L-arabinose carboligation reaction (Bawn *et al.*, 2018). The two-enzyme reaction scheme is shown in Figure 6.3. With reaction A being the amine transfer from L-serine to α-ketoglutaric acid to produce HPA and L-glutamate and reaction B, displaying the TK-catalysed reaction to produce L-gluco-heptulose. Figure 6.4 offers a simplified schematic of the same reaction and displays how the product of the TAm mediated deamination of L-serine, HPA, is used with L-arabinose, which could be SBP derived, to produce L-gluco-heptulose and CO_2. With the reaction system defined, it was important to characterise the enzymes to better understand how they may behave in continuous applications using SBP derived sugars.

Table 6.1. Comparison of substrates and product costs. Prices for substrates and products of comparable purity and grade were sourced from the SigmaAldrich website. Prices for L-gluco-heptulose were not found, so L-gluco-heptulose isomer, D-seduheptulose, price is shown instead (accessed August 2019).

Chemical	Quantity (g)	Price (EUR)	Specific Price (EUR.g^{-1})	Advertised Purity
L-serine	100	118	1.2	>99%
α–ketoglutaric acid	100	96.4	1.0	>99%
L-arabinose	100	144	1.4	>99%
Li-HPA	5	655	131.0	>97%
D-sedoheptulose	0.05	1010	20,200.0	>95%

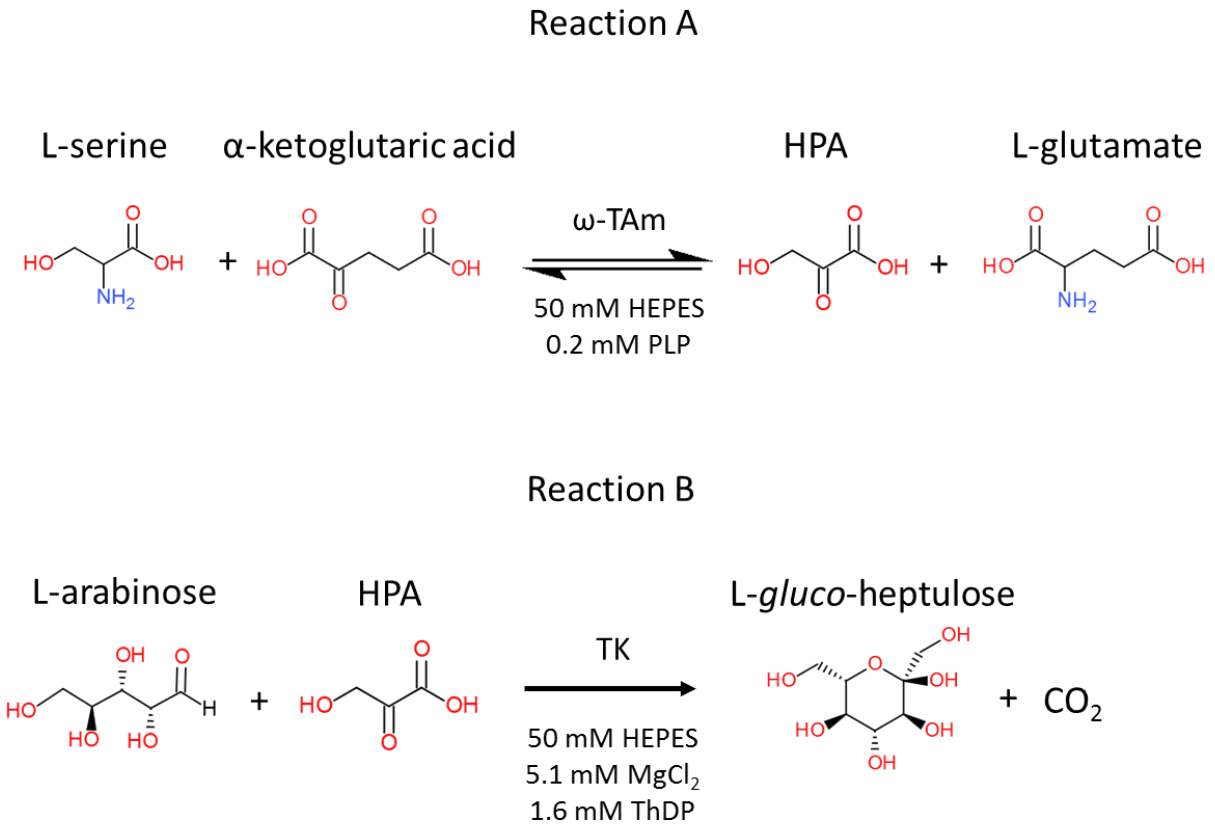

Figure 6.3. Proposed reaction scheme for the one-pot two-step production of L-gluco-heptulose. Reaction A shows the production of HPA catalysed by TAm via the deamination of L-serine, whilst reaction B shows the TK catalysed ketol group addition from HPA to L-arabinose, resulting in the production L-gluco-heptulose and CO_2. Schematic adapted from Bawn et al. (2018).

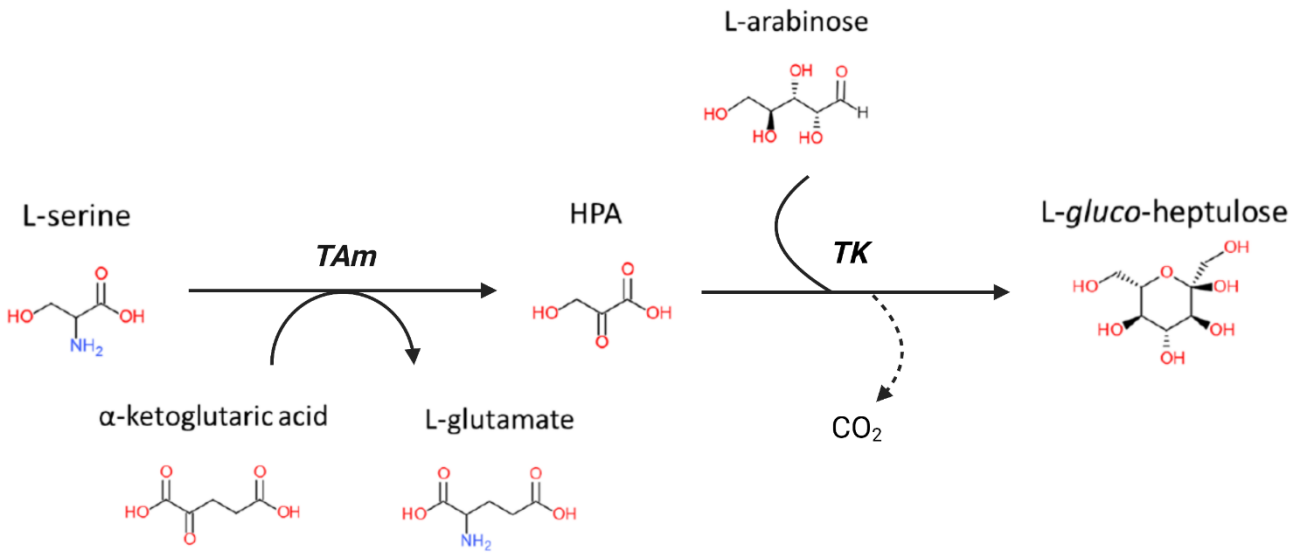

Figure 6.4. Simiplified one-pot two-step reaction mechanism. Schematic adapted from Bawn et al. (2018).

6.3.1.2 Effect of temperature on bioconversion

TAm was not screened for thermal stability as both work by Bawn et al. (2018) and previous publication suggested that this particular TAm strain was thermostable and able to selectively deaminate L-serine (Sayer *et al.*, 2012; Deszcz *et al.*, 2015; Villegas-Torres *et al.*, 2015; Bawn *et al.*, 2018). On the other hand, the stability of TK was tested by carrying out single-enzyme conversions of HPA and L-arabinose to L-gluco-heptulose. Both substrates were used with a starting concentration of 33 mM. Temperatures tested were: 37 °C; 50 °C; 60 °C and 70 °C. Further reaction conditions are outlined in Section 2.4.2.3. As shown in Figure 6.5, 70 °C appeared too high a temperature to obtain meaningful conversion. Temperatures in the range of 37 - 60 °C all showed similar level of conversion after 24 hours; however, the reaction rate at 37 °C was significantly slower. The apparent activity of the cell lysate preparations used in these experiments was calculated as described in Section 2.4.2. In Table 6.2 it can be seen that the highest activities and final concentrations of L-gluco-heptulose were obtained at 50 °C and 60 °C, whilst 70 °C appeared to be the lowest. These findings corroborate the studies of Bawn et al. (2018), who found good activity and conversion at 50 °C and 60 °C, and lower activity at 37 °C. Further, they also found that despite observing the presence of initial enzyme activity, very low conversion was obtained at 70 °C. Further, a disadvantage of operating a reaction at 37 °C would be that a substrate solution made from treated SBP would likely have a range of sugars present which could be conducive to bacterial growth and contamination.

The final L-gluco-heptulose concentration reached between 3.5 and 4.5 mM, or 11 to 14% $mol.mol^{-1}$ conversion. This poor conversion is offset by the aforementioned HPA degradation. Indeed, if assuming only 30% of HPA was available due to heat degradation, the conversion yields obtained range from 35 to 45%.

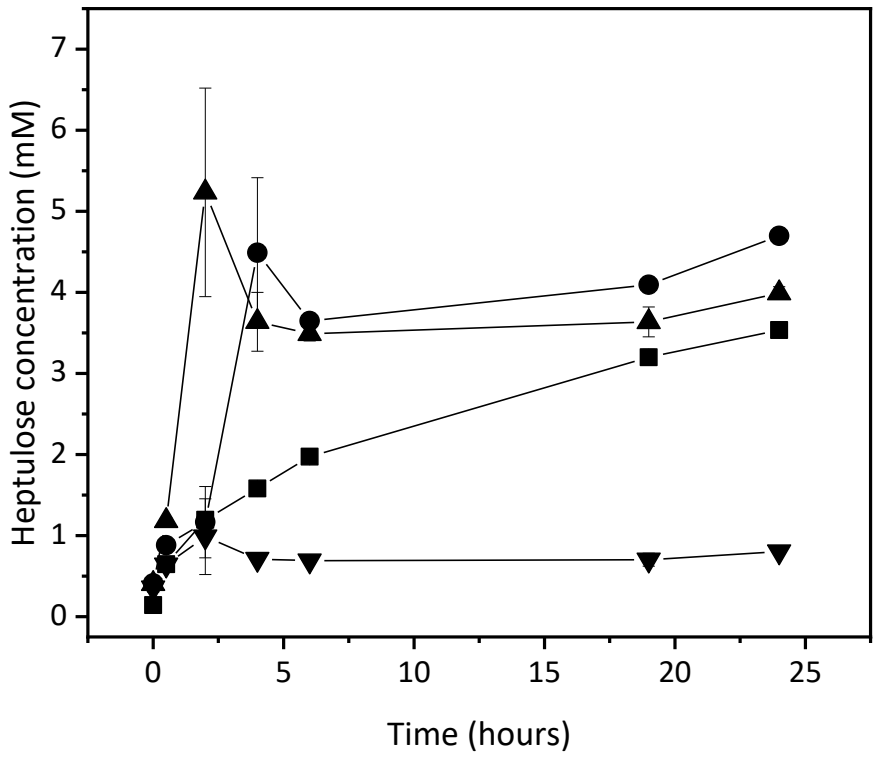

Figure 6.5. L-gluco-heptulose production over a 24-hour period at different temperatures. Reactions were carried out at 37 °C (■), 50 °C (●), 60 °C (▲), and 70 °C (▼). Error bars represent SEM (n=2). Experiment was performed using 10% v/v clarified TK cell lysate as described Section 2.4.2.3.

Table 6.2. Apparent TK activity at different temperatures and final, 24-hour L-gluco-heptulose titre. Activity values calculated based on initial rate data shown in Figure 6.5.

Temperature (°C)	Act_{app} ($mM.hr^{-1}$)	SEM	Final L-gluco-heptulose concentration (mM)
37	0.45	0.00	3.54
50	1.02	0.22	4.70
60	1.26	0.11	3.99
70	0.25	0.05	0.80

6.3.1.3 Effect of buffer pH on bioconversion

Following the investigation into the effect of temperature on TK, the stability of the separate TAm and TK reactions at different pH was examined. The buffering range of HEPES (pH 6.8 to pH 8.2) was screened by testing pH 6.5, 7.0, 7.5, 8.0 and 8.5. The other conditions used are outlined in Section 2.4.2.2 and Section 2.4.2.3.

As highlighted in panels (c) and (d) in Figure 6.6 the initial activity of the enzymes (over a period of 6 hours) show little difference between the various pH levels. The 24-hour final conversion values also revealed little effect of pH. The small difference between activities at different pH is beneficial as it provides a broader range of operation for a successful industrial process.

HPA concentrations of up to 6 mM were achieved. The initial L-serine and α-ketoglutaric acid concentrations were 10 mM each, demonstrating the viability of the enzymatic production of HPA. A further conclusion of this work was the highlighted need of more measurements in the initial phase of the reaction to obtain a better picture of the enzymatic activity.

Native *E. coli* TK has a maximum activity between pH 8.0 and pH 8.5, whilst thermostable TK obtained from *Geobacillus stearothermophilus* was found to have a pH stability between pH 7.0 and pH 8.0. This is also in line with the results of Bawn et al. (2018) who showed greatest activity between 8.0 (using HEPES) and 8.5 (using sodium borate).

Similarly, work on thermostable ω-TAms had shown that they appear to be stable at similar pH values. For example Mathew et al. (2016) studied a TAm from *Sphaerobacter thermophiles* showed an optimum pH between 8.0 and 8.5 with rapid activity decrease above and below this range (Sprenger, 1995; Abdoul-Zabar *et al.*, 2013). Furthermore, a TAm isolated from *Geobacillus thermodenitrifcans* had a highest activity at pH at 9.0. The same study showed that the TAm employed in this work offered good activity at a range of 8.0 to 9.0 (Chen *et al.*, 2016; Mathew *et al.*, 2016; Bawn *et al.*, 2018). However, based on the work carried out by Bawn et al. (2018) and the trends that could be seen in Figure 6.6, a pH of 8.0 was selected for the subsequent biocatalytic reactions, as this would provide a suitable overlap between the two enzymes in a one-pot two-step reaction.

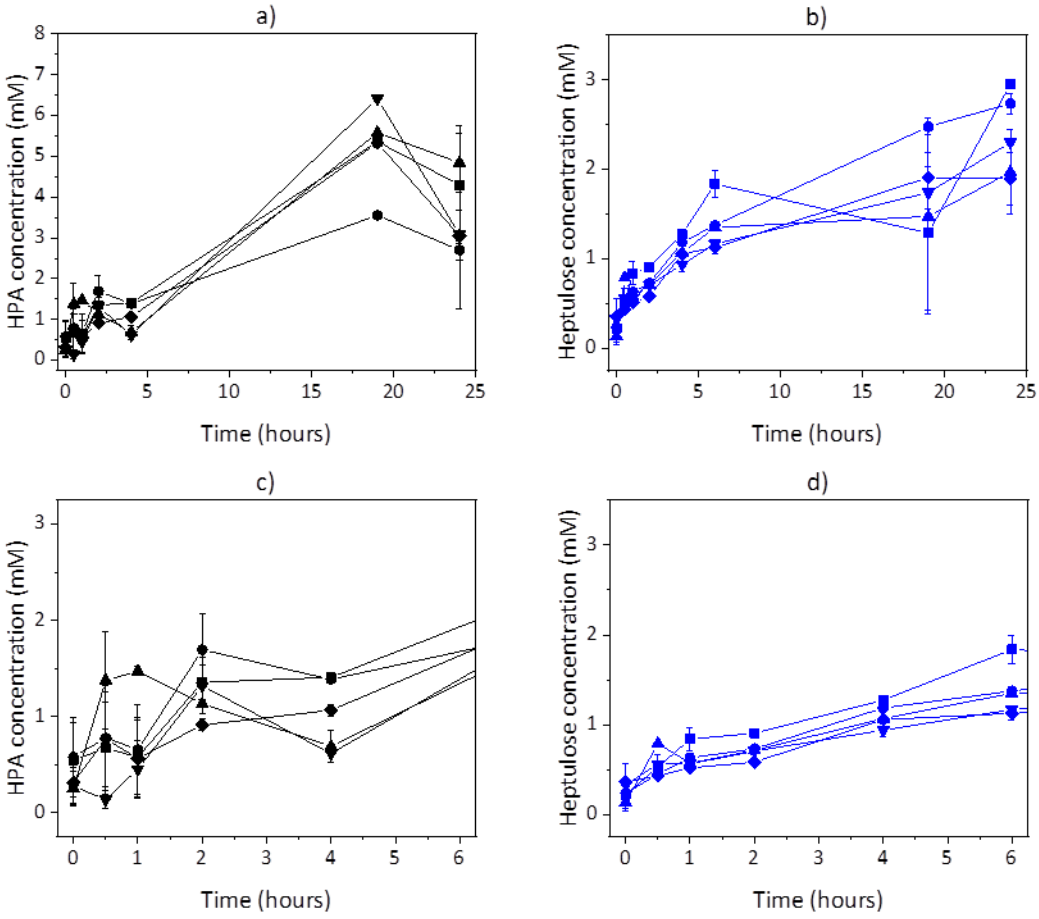

Figure 6.6. TAm and TK reaction performance at different pH values. Single enzyme reactions were carried out. Panels (a) and (c) show the production of HPA by TAm. Panels (b) and (d) show (in blue) the production of L-gluco-heptulose by TK. Further, the upper panels show the reaction over the entire 24-hour period, whilst the bottom panels highlight the first 6 hours of the reaction period. Reaction pH values investigated: 6.5 (■); 7 (●); 7.5 (▲); 8 (▼); and (◆) 8.5. Error bars represent SEM (n=2). Reactions were performed as described in Section 2.4.2.2 and in Section 2.4.2.3

6.3.1.4 Effect of substrate concentration on TAm and TK performance

The next step in the characterisation of the enzymes was the effect of substrate concentration on bioconversions. For this, substrate concentrations were changed one at a time as outlined in Table 6.3 and Table 6.4, where initial rates of reaction and final HPA and L-gluco-heptulose concentrations were also reported. The substrate concentration effect on HPA bioconversion and the TAm initial rates of reaction are reported in Figure 6.7 and Table 6.3, respectively. Panels (a) and (c) in Figure 6.8 look at the effects of changing L-serine concentration with constant α-ketoglutaric acid at 10 mM. It can be observed that higher concentrations of L-serine such as 50 mM and 100 mM produce faster initial reaction rates as well as higher final HPA concentration. With the highest serine concentration, 10 mM of HPA are produced after 19 hours. This indicates a total conversion of α-ketoglutaric acid into HPA. Increasing α-ketoglutaric acid, as shown in panels (b) and (d), on the other hand, appears to have a negative effect on initial rates and final concentrations, both of which are lower than at lower concentrations. Despite other studies with TAm using 10 mM each of L-serine and α-ketoglutaric acid, this experiment appeared to reveal that a slightly lower concentration was more beneficial (Bawn *et al.*, 2018). From a stoichiometric perspective, however, the maximum amount of HPA that could be produced from a 5 mM starting α-ketoglutaric acid concentration is 5 mM, suggesting a sampling error, or that an additional amino-acceptor is present in the cell lysate.

The individual TK substrates for the production of L-gluco-heptulose were also evaluated, as outlined in Section 2.4.2.3. One substrate concentration was set at 33 mM, whilst the other was changed from 5 mM to 100 mM. Panels (a) and (c) in Figure 6.8 show the effects of changing L-arabinose concentration from 5 mM to 100 mM, whilst panels (b) and (d) show the effects of changing HPA concentrations. Table 6.4 shows the apparent activity for both substrates at the various conditions listed.

L-arabinose concentration appears to have a positive effect on L-gluco-heptulose production and apparent activity. HPA, on the other hand, shows little effect on activity beyond a certain concentration (as shown by panel (d) in Figure 6.8). Indeed, increasing HPA concentration beyond 33 mM does not increase apparent activity.

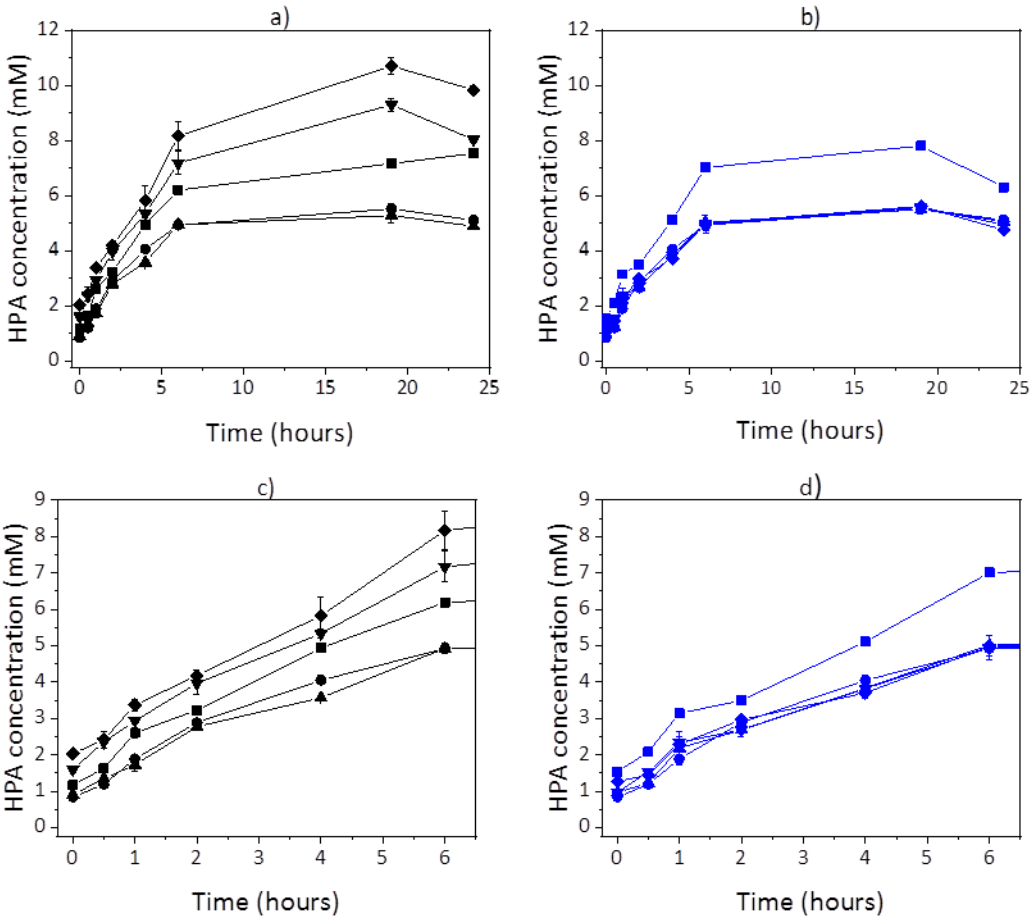

Figure 6.7. Effect of TAm substrate concentration on HPA production. Panels (a) and (c) show in black the effects of changing L-serine concentration with α-ketoglutaric acid fixed at 10 mM. Meanwhile effects of changing α-ketoglutaric acid concentration against fixed L-serine at 10 mM are shown in panels (b) and (d) in blue. Additionally, panels (c) and (d) highlight the initial 6 hours of the reaction. The varying substrates concentrations used were: 5 mM (■); 10 mM (●); 20 mM (▲); 50 mM (▼); and 100 mM (◆). Error bars represent SEM (n=2). TAm reactions were performed as described in Section 2.4.2.2

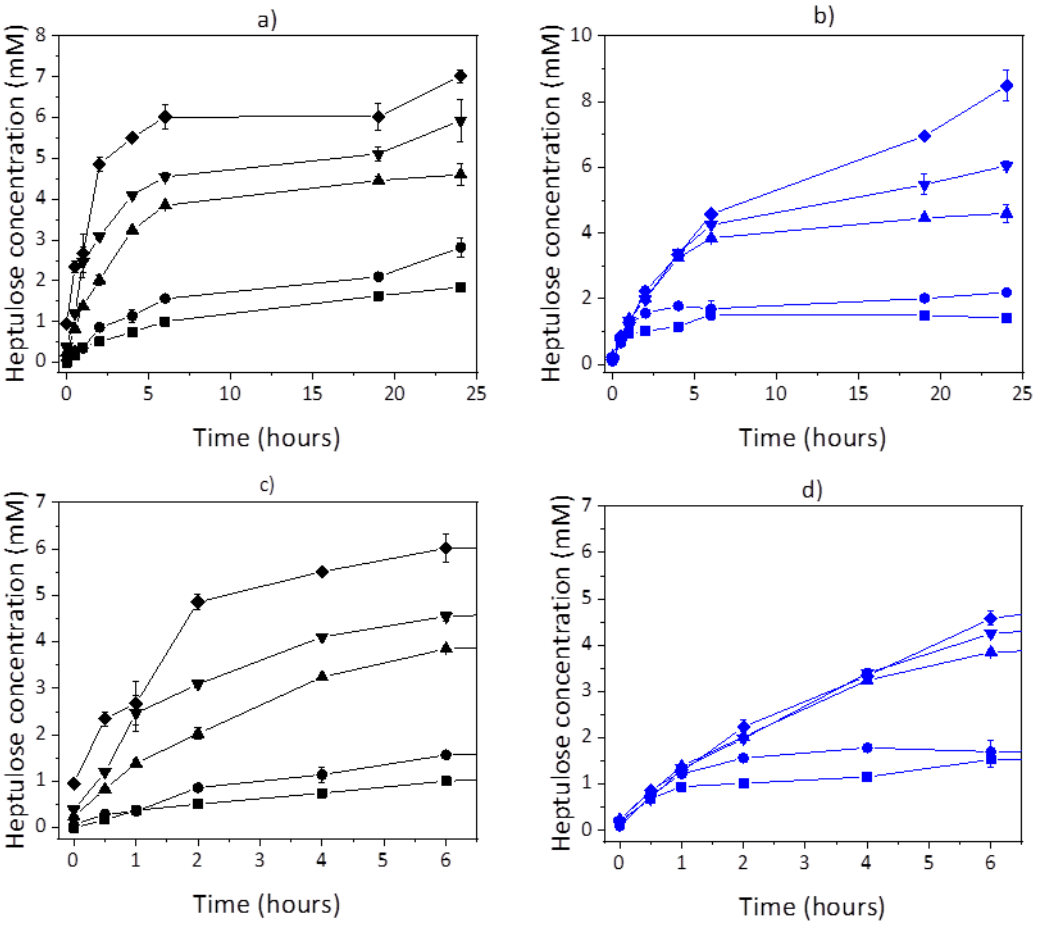

Figure 6.8. Effect of TK substrates concentration on L-gluco-heptulose production. Panels (a) and (c) show in black the effects of changing Ara concentration against HPA fixed at 10 mM. Meanwhile effects of changing HPA against fixed Ara 10 mM are shown in panels (b) and (d) in blue. Additionally, panels (c) and (d) highlight the initial 6 hours of the reaction. The varying substrates concentrations used were: 5 mM (■); 10 mM (●); 33 mM (▲); 50 mM (▼); and 100 mM (◆). Error bars represent SEM (n=2). TK reactions were performed as described in Section 2.4.2.3.

Table 6.3. Apparent activity for TAm at different substrates concentrations and final, 24-hour HPA titre obtained. Activity values calculated based on initial rate data shown in Figure 6.7.

L-serine (mM)	A-ketoglutaric acid (mM)	Act_{app} ($mM_{HPA}.hr^{-1}$)	Final HPA concentration (mM)	L-serine (mM)	A-ketoglutaric acid (mM)	Act_{app} ($mM_{HPA}.hr^{-1}$)	Final HPA concentration (mM)
5	10	1.88	7.52	10	5	2.13	6.30
10	10	1.57	5.11	10	10	1.57	5.11
20	10	1.52	4.89	10	20	1.56	5.06
50	10	2.30	8.03	10	50	1.62	4.94
100	10	2.47	9.83	10	100	1.70	4.75

Table 6.4. Apparent activity for TK at different substrates concentrations and final, 24-hour L-gluco-heptulose titre obtained. Activity values calculated based on initial rate data shown in Figure 6.8.

L-arabinose(mM)	HPA (mM)	Act_{app} ($mM_{hep}.hr^{-1}$)	Final L-gluco-heptulose concentration (mM)	L-arabinose (mM)	HPA (mM)	Act_{app} ($mM_{hep}.hr^{-1}$)	Final L-gluco-heptulose concentration (mM)
5	33	0.28	1.84	33	5	0.63	1.42
10	33	0.42	2.82	33	10	0.90	2.19
33	33	1.11	4.60	33	33	1.11	4.60
50	33	1.76	5.93	33	50	1.08	6.05
100	33	2.58	7.02	33	100	1.18	8.49

Despite the noticeable effects of changing concentration in the case of L-arabinose, the final L-gluco-heptulose yield is quite low. The rapid degradation of HPA that will occur in these single-step batch reactions, as discussed in Section 6.3.1.1, likely explains both the low yield despite large changes in starting HPA concentration.

6.3.1.5 Effect of TAm and TK concentration on bioconversion

Following the substrate concentration effect characterisation, the effect of increasing catalyst concentration was studied. For this section it is important to note that rather than using 10% v/v of sonicated material in the reaction mix, as is the case in the rest of the work in this chapter, homogenised material was used instead (Section 2.4.1.5). As seen in Chapter 5, Figure 5.7, 26.7% v/v of homogenised cell lysate was equivalent to 10% v/v sonicated cell lysate.

Different concentrations of homogenised TAm and TK cell lysate were used: 10% v/v; 20% v/v; 26.7% v/v; and 40% v/v. TAm reactions were performed with 10 mM each of L-serine and α-ketoglutaric acid, whilst the TK reaction was run with 33 mM each of L-arabinose and HPA. Figure 6.9 (a) and (c) show the clear effects of increasing enzyme concentration on HPA production. The initial rate of production, in Table 6.5, and the final HPA concentration are much greater for the higher enzyme loading. The highest loading appears to have almost full conversion at 24 hours. Similar results were obtained for the TK reaction. Higher enzyme loadings obtained better conversion and faster initial phases. In this experiment more samples were taken over the first 2-hour period to obtain a more accurate picture of the very beginning of the reaction. This is also reflected in Table 6.5 with a noticeable increase in activity for both TAm and TK. In panel (c) product formation can be seen already at time 0. This is because time 0 represents a sample taken between 1 and 2 minutes after the reaction start (to allow all the substrates, enzymes and buffers to mix).

This experiment highlighted that increasing enzyme concentration in the reaction significantly improves the final conversions. One of the advantages of enzyme immobilization is that it enables higher catalyst concentrations to be achieved in the reactor (Sheldon and van Pelt, 2013). Future work into reaction optimisation should therefore reinvestigate TAm immobilization (Section 6.3.3) in order to facilitate this.

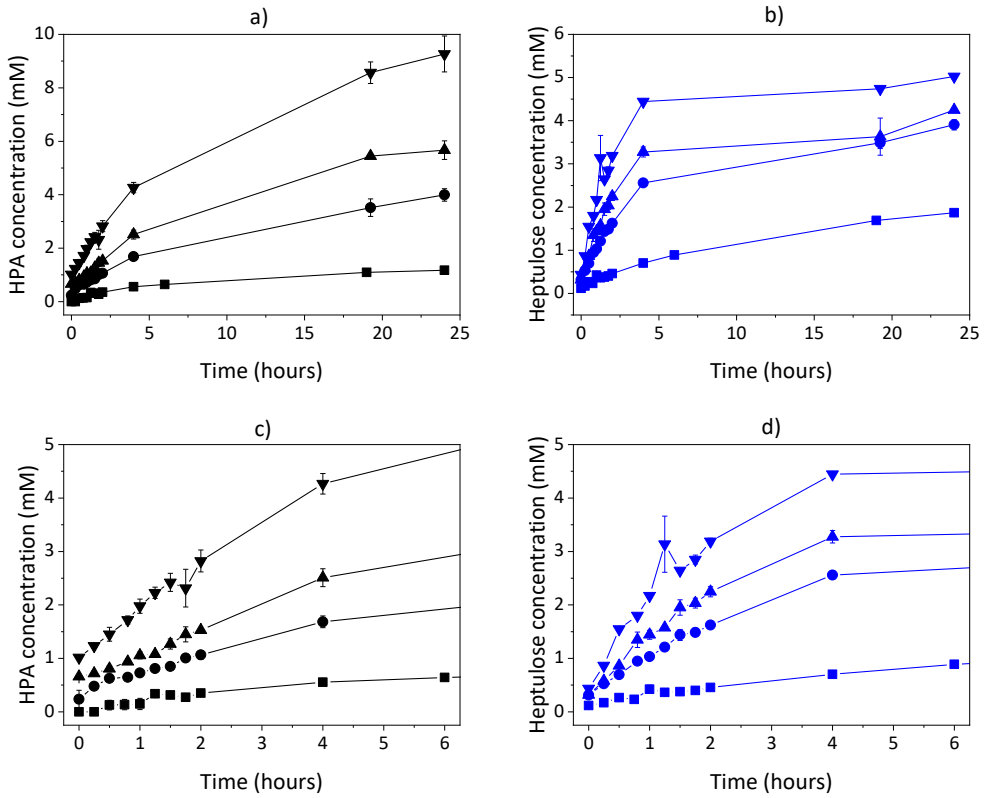

Figure 6.9. **Effect of TAm and TK concentration on HPA and L-gluco-heptulose production, respectively.** Panels (a) and (c) show the effect of increasing TAm loading on HPA production, whilst panels (b) and (d) show the effect of increasing TK loading on L-gluco-heptulose production. Bottom panels highlight the first 6 hours of the reaction. Lysate concentrations used were: 10% v/v (■); 20% v/v (●); 26.7% v/v (▲); and 40% v/v (▼). Error bars represent SEM (n=2). Clarified cell lysate was obtained by homogenisation rather than sonication (as described in Section 2.4.1.5).

Table 6.5. Activity measurements for varying enzyme loadings and final, 24-hour HPA and L-gluco-heptulose titre obtained. Activity values calculated based on initial rate data shown in Figure 6.9.

Enzyme Loading (% v/v)	TAm activity ($mM_{HPA}.hr^{-1}$)	Final HPA concentration (mM)	TK activity ($mM_{Hep}.hr^{-1}$)	Final L-gluco-heptulose concentration (mM)
10.0	0.19	1.09	0.28	1.82
20.0	0.61	3.99	0.92	3.91
26.7	0.88	5.67	1.25	4.25
40.0	1.60	9.27	1.86	5.03

In summary, the study of the individual enzyme reactions, as described in Sections 6.3.1.1 to Section 6.3.1.5, highlighted a few important benefits and challenges of these reactions. Firstly, it described the success in using relatively inexpensive materials to make a valuable product with potentially important pharmaceutical applications. Despite this success, the yields were low due to the observed degradation of the HPA. A one-pot two step approach whereby HPA is produced throughout the reaction instead of just being added at the beginning of the reaction might benefit the overall conversion.

The relatively elevated reaction temperature at 50 °C also showed promise as it would prevent bacterial contamination and optimum production of L-gluco-heptulose. α-ketoglutaric acid concentration increases did not lead to faster reactions or higher production, owing, probably, to the unfavourable reaction equilibrium of TAms. Finally, the enzyme loading proved very important in the increase of initial reaction yields, and whilst, in the following experiments the concentration was kept at 10% v/v of each enzyme future work could focus on concentrating the enzymes further.

6.3.2 One-pot two-step reaction characterisation

6.3.2.1 Changing substrate concentration of a one-pot two step TAm-TK reaction

Having better understood the kinetics of the stand-alone, batchwise enzymatic reactions, the TAm and TK enzymes were used together in a one-pot two-step reaction. As discussed in Section 6.3.1.1, the two-enzyme system sought to bypass the need for the expensive and heat-labile HPA. As such, the substrates used in these reactions were L-serine, α-ketoglutaric acid, and L-arabinose. Furthermore, placing a second enzyme after TAm could provide the added benefit of shifting the TAm reaction equilibrium toward product formation.

The starting concentration of substrates was a combination of the amounts used for the characterisation of the stand-alone reactions, namely, 10 mM of L-serine and α-ketoglutaric acid, and 33 mM of L-arabinose. However, since the substrates should react with each other in 1 : 1 : 1 ratio, the first investigation was to rapidly determine the effects of changing substrate concentration. To test the substrate concentrations, the one-pot two-step reaction was performed using 10% v/v each of TAm and TK clarified cell lysate. The reaction conditions are outlined in Section 2.4.2.4.

The results of reactions performed with different substrate concentration are depicted in Figure 6.10, and the final concentrations for HPA and L-gluco-heptulose are reported in Table 6.6. It can be seen that the one-pot two-step reaction successfully produced L-gluco-heptulose without requiring the addition of HPA. The different starting substrate concentrations had little effect on HPA production over time, with HPA concentration achieved after 24 hours being slightly over 10 mM across the range. This concentration is higher than was observed at comparable L-serine and α-ketoglutaric acid concentrations in the stand-alone TAm reaction (Figure 6.7). at the lowest substrate concentration level, more HPA is produced than aIt also suggests almost complete utilisation of L-serine and α-ketoglutaric acid at the lowest concentration of 10 mM. This confirms that the addition of TK shifted the equilibrium of the TAm reaction to product formation in the one-pot reactions.

Concentrations of the desired product, L-gluco-heptulose were lower than HPA. Additionally, a difference was seen between the lowest and highest concentration obtained in 24 hours, with the 10 mM substrate concentration resulting in 5.7 mM and the 100 mM and 200 mM reactions reaching approximately 7.7 and 9.0 mM, respectively. The fact that different concentrations of L-gluco-heptulose were obtained, whilst the HPA production appeared unaffected by substrate concentration, suggest that more HPA was being formed in the experiments with high substrates concentration, but was immediately being used in the TK reaction. It is also possible to see that at the lowest concentration level (10 mM: 10 mM : 33 mM of L-serine, α-ketoglutaric acid and L-arabinose) the final concentrations of HPA (9.8 mM) and L-glucoheptulose (5.7mM). amounts to more than the theoretical maximum of 10 mM. This reiterates what was seen in Section 6.3.1.4, where at low substrate concentrations TAm produced more than the stoichiometric amount of HPA. This is likely due to evaporation during the reaction or the presence of additional substrate coming from the cell lysate.

Initial rates of reaction, shown in Table 6.6, also show increasing activity of TAm (with respect to HPA production) and TK (with respect to L-gluco-heptulose production) with increasing substrate concentration.

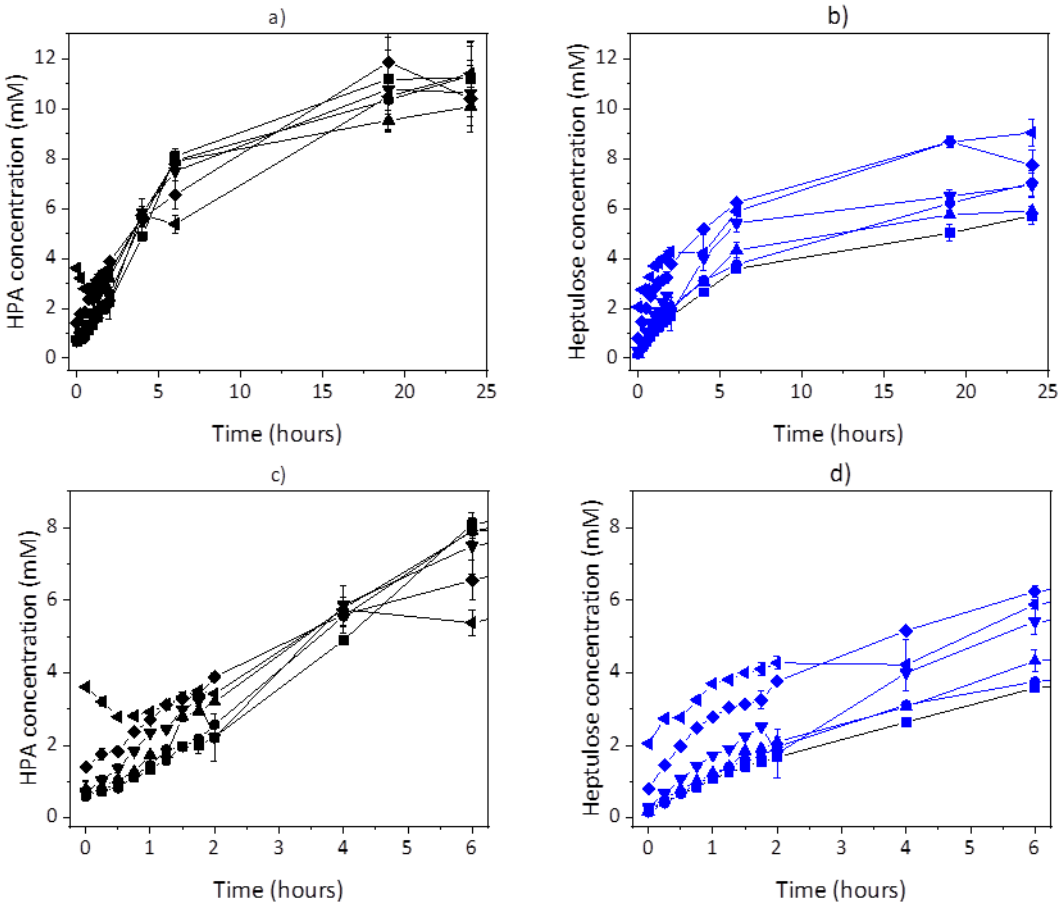

Figure 6.10. Effect of substrate concentrations on the kinetics of a one-pot two-step TAm-TK reaction. Intermediate product HPA production is shown in panels (a) and (c) in black, whilst final L-gluco-heptulose product is shown in (b) and (d) in blue. Panels (c) and (d) show the initial 6 hours of the reaction. Starting concentrations, in mM for L-serine : α-ketoglutaric acid : L-arabinose were: 10:10:33 (■); 20:20:33 (●); 33:33:33 (▲); 50:50:50 (▼); 100:100:100 (◆) and 200:200:200 (◀). Error bars represent SEM (n=2). Reactions were performed as described in Section 2.4.2.4.

Table 6.6. Effect of subtrate concentration on TAm and TK activity for a one-pot two-step reaction and final, 24-hour L-gluco-heptulose titre. Activity values calculated based on initial rate data shown in Figure 6.10.

Symbol in graph	Ser (mM)	Keto (mM)	Ara (mM)	TAm activity ($mM_{HPA.hr^{-1}}$)	TK activity ($mM_{Hep.hr^{-1}}$)	Final HPA concentration (mM)	Final L-gluco-heptulose concentration (mM)
■	10	10	33	**1.24**	**0.93**	**11.21**	**5.71**
●	20	20	33	**1.35**	**1.04**	**11.34**	**7.02**
▲	33	33	33	**1.67**	**1.14**	**10.09**	**5.91**
▼	50	50	50	**1.75**	**1.35**	**10.64**	**6.93**
◆	100	100	100	**2.22**	**2.17**	**10.40**	**7.73**
◀	200	200	200	**2.28**	**2.72**	**11.41**	**9.04**

6.3.2.2 One-pot two-step reaction at different scales

Following the study of substrate effects on production of L-gluco-heptulose, the scale up of the batch reaction was carried out. 10 mM L-serine, 10 mM α-ketoglutaric acid and 33 mM L-arabinose were used in a one-pot two-step reaction at three different scales, with the aim of determining any possible challenges of scaling the reaction up. The one-pot two-step reaction was carried at different volumes and in different reaction vessels. As shown in Figure 6.11, the smallest reaction volume, 1.2 mL appeared to perform similarly, if not slightly better than a 50 mL centrifuge or "Falcon" tube with a 10 mL working volume. The reaction in the shake flask, on the other hand, appeared to attain lower product concentrations after 24 hours; namely, 66% mol.mol^{-1} of HPA and 50% mol.mol^{-1} of L-gluco-heptulose compared to the 1.2 mL reaction.

Observing the initial 4 hours of the reaction, the rates of production of both HPA and L-gluco-heptulose appeared to be matched at the different scales. However, in the later stages of the conversion the larger vessel performs less well, indicating either a change in the substrate availability, product degradation, or catalyst deactivation. Since all the reactors were kept sealed and the Falcon tube reaction and the shake flask reaction were carried out at the same time in the same shaking incubator, the lower yield was likely due to the different mixing environments in the two containers. However, the probable cause of this challenge at scale is discussed further in Section 6.3.4.

In the 1.2 mL reaction, 1 mM of L-gluco-heptulose was obtained. This is much lower than the 5.7 mM of L-gluco-heptulose obtained in the previous experiment (Figure 6.10) using the same conditions. A "control" reaction was usually run with each set of experiment. This was a reaction at standard conditions (1.2 mL well mixed reactor, 10 mM L-serine, 10 mM α-ketoglutaric acid and 33 mM L-arabinose, at 50 °C, with freshly prepared 10% v/v of sonicated cell lysate of each enzyme). In this instance, whilst the TAm reaction appeared to operate well, the TK enzyme appeared to be less active. A possible explanation for this was poor cell lysis efficiency during the enzyme preparation stage. Homogenisation, discussed in Section 5.3.2, could be a robust alternative to sonication and reduce operator error and batch-to-batch variability.

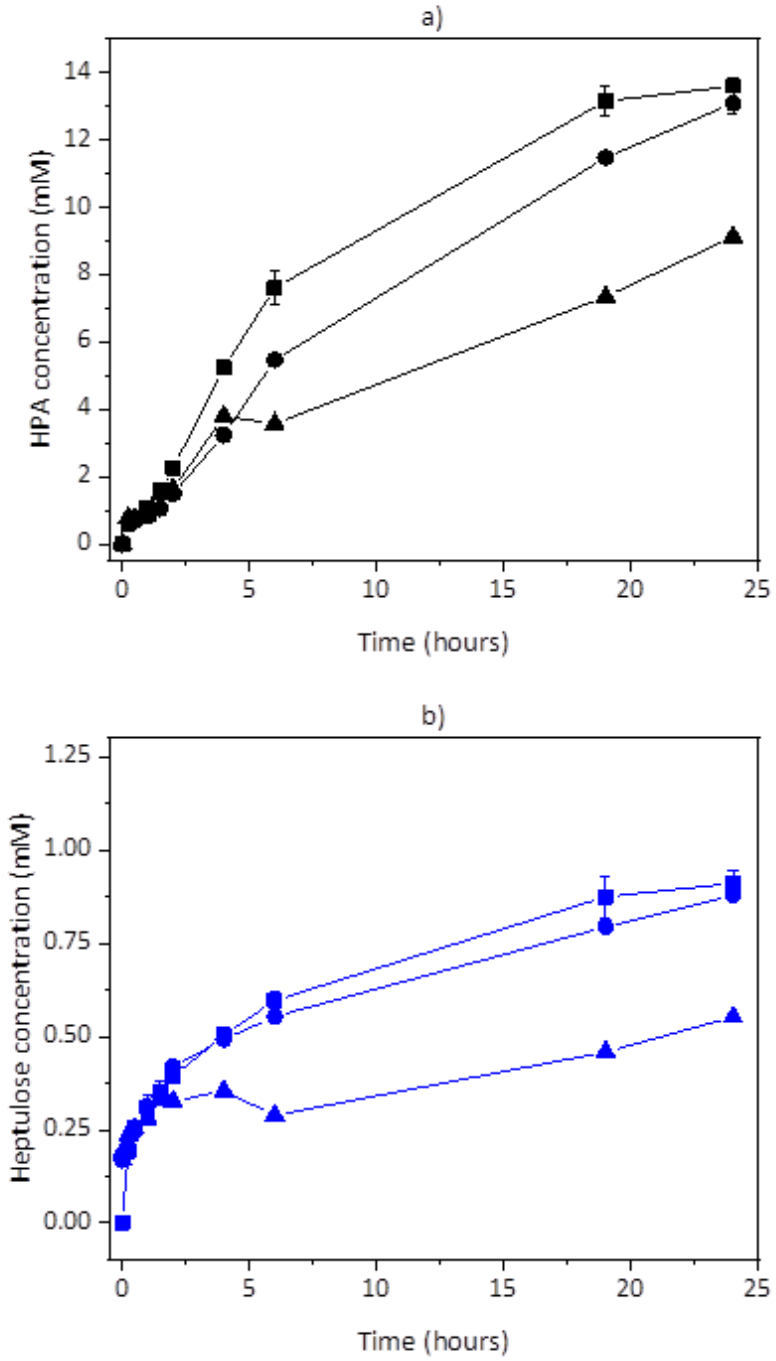

Figure 6.11. Effect of reaction scale on the One-pot two-step synthesis of intermediate product HPA and L-gluco-heptulose by TAm and TK. Conversion of L-serine and α-ketoglutaric acid into HPA (panel (a)), in black, to be used in the subsequent reaction with L-arabinose for production of L-gluco-heptulose (panel (b)), in blue) were tested at different scales: Small tube (1.2 mL, ■); Falcon tube (10mL, ●); and Flask (50 mL, ▲). Error bars represent SEM (n=2). Reactions were performed as described in Section 2.4.2.4.

Lower conversions and initial reaction rates at larger scale, could potentially pose issues for translation of the one-pot two-step reaction to industrial or flow applications. Jones et al. (2012) used the ACR to move an oxidase reaction from batch into continuous flow mode. Within it they compared batch reactor type, reactor mixing, and reactor volume for effects on the performance of this oxygen dependent reaction. Similar to findings shown here, increasing volumes and decreasing mixing in batch reactors led to lower conversions. Interestingly, however, both the ACR and its scaled-up version, the ATR, were compared to vessels of equivalent volume and obtained higher yields than their batch counterparts (Jones *et al.*, 2012). This, alongside the characterisation work shown in Chapter 3 showed promise for the ACR to deliver sufficient mixing to the reaction, and overcome the scaling challenges of the one-pot two-step L-gluco-heptulose production.

6.3.3 Investigation of different immobilization strategies for biocatalyst retention

6.3.3.1 Immobilization of purified enzymes on Ni-NTA resin

Retaining and reusing enzymes could be a compelling cost-saving solution for a biorefinery; and is, therefore, worth investigating. As discussed in Section 6.1 a range of immobilization techniques are available. This work focuses on investigating enzyme immobilized onto solid supports: nickel charged affinity resin (as used at small scale) and an epoxy methacrylate resin (ECR).

The first immobilization method pursued exploiting the same enzyme property used for the affinity purification of TK and TAm, namely their His-tag. It was hypothesised that TAm and TK enzymes could be affinity bound to a Nickel chelated nitriloacetic acid (Ni-NTA) resin. The bound enzymes could then be recovered and utilised in reactions. The advantage of this technique is that the resin would very selectively bind to the engineered TAm and TK enzymes containing a His-tag and would only be eluted at high imidazole salt concentrations.

E.coli-BL21 (DE3)-TAm and *E.coli*-BL21 (DE3)-TK biomass was resuspended and lysed by sonication in N1 buffer (the binding buffer in the His-tag purification process) prior to incubation with Ni-NTA resin as described in the Section 2.4.3.1. The *immobilizing buffer* refers to the enzyme-containing solution which enables enzyme binding or adsorption when placed in contact with the resin. The incubation with Ni-NTA resin was carried out over a period of 60 minutes with immobilizing buffer samples taken and retained for SDS-PAGE analysis, reported in Figure 6.12. It was anticipated that, as the enzyme binds to the column,

the concentration in the immobilizing buffer would decrease and therefore, the bands on the gel would fade over time. This, however, was not observed, either signifying poor enzyme binding or, alternatively, excess enzyme in the immobilizing buffer preventing a trend to be visible in the SDS-PAGE. The latter hypothesis is supported by work on IMAC purification (not shown in this Thesis) which showed enzyme bands in the flow through of the columns, indicating large amounts of unbound enzymes.

The subsequent bioconversion reaction using TAm and TK immobilized on Ni-NTA resin was carried out using 5% w/v loading instead of the 10% v/v which was used for clarified cell lysate reactions. The substrate concentration and reaction conditions were kept as described in Section 2.4.3.3. The kinetics of product formation during the stand-alone bioconversion reactions are shown in Figure 6.13. As is shown in panels (a) and (b) HPA is produced in very small amounts after the start of the TAm reaction. However, it quickly peaks and disappears thereafter. On the other hand, panels (c) and (d) show that immobilized TK operates well, with the reaction plateauing after 6 hours at approximately 2 mM L-gluco-heptulose concentration.

Production of L-gluco-heptulose through the TAm-TK, one-pot two-step reaction also appeared successful. Bawn et al (2018) had successfully shown the one-pot two-step reaction with free enzymes. Unpublished work on the individual immobilized enzymes also proved activity, but Figure 5.13 shows production of L-gluco-heptulose using immobilized enzymes for the first time. The HPA concentration profile follows what was found in the stand-alone TAm reaction. Despite this, L-gluco-heptulose concentration reached 4.73 mM, almost twice as much as the stand-alone TK reaction which only obtained 2.41 mM after 24 hours. This finding further substantiates that the one-pot two-step biocatalytic reaction system not only provides an alternative to the chemical synthesis of HPA, but actually provides an improved system for the production of L-gluco-heptulose even using immobilized enzymes.

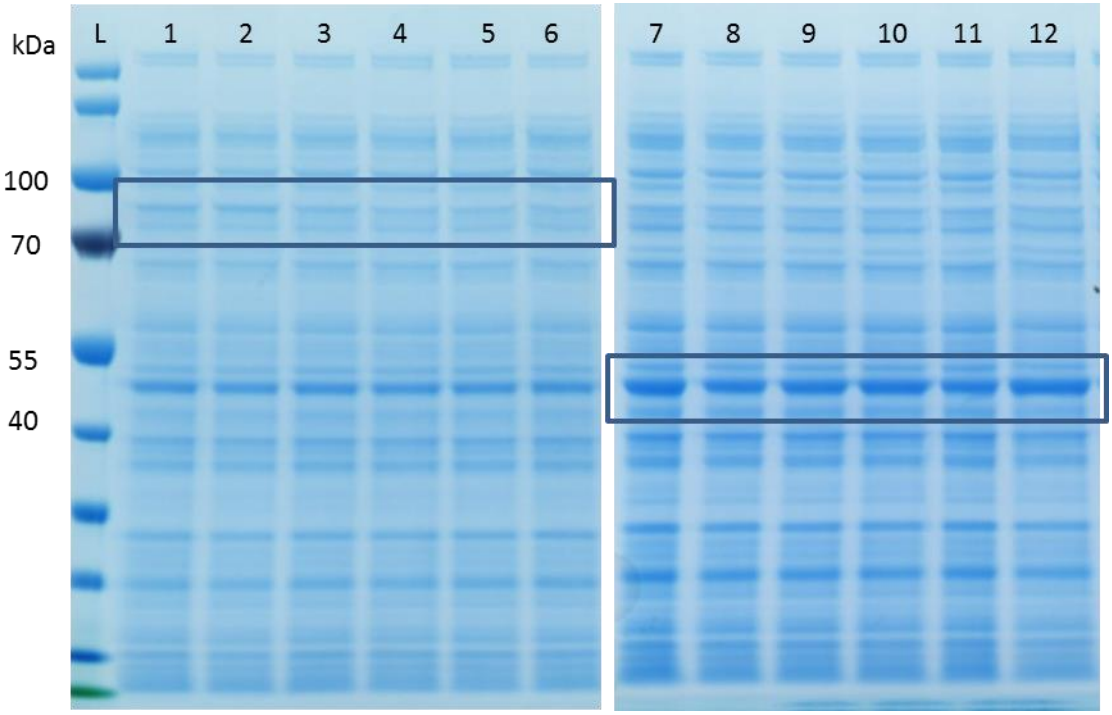

Figure 6.12. SDS-PAGE analysis of supernatant from His-tag immobilization of TK and TAm. Clarified cell lysate containing either TK (lanes 1 to 6) or TAm (lanes 7 to 12) were placed in contact with Ni-NTA resin. Supernatant samples (without Ni-NTA resin) were taken to be analysed at various time intervals: Starting material (TK lane 1 and TAm lane7); 5 min (2 and 8); 10 min (3 and 9); 20 min (4 and 10); 30 min (5 and 11); and 60 min (6 and 12). Ni-NTA immobilization was performed as outlined in Section 2.4.3.1 and SDS-PAGE analysis was carried out as described in Section 2.4.1.8.

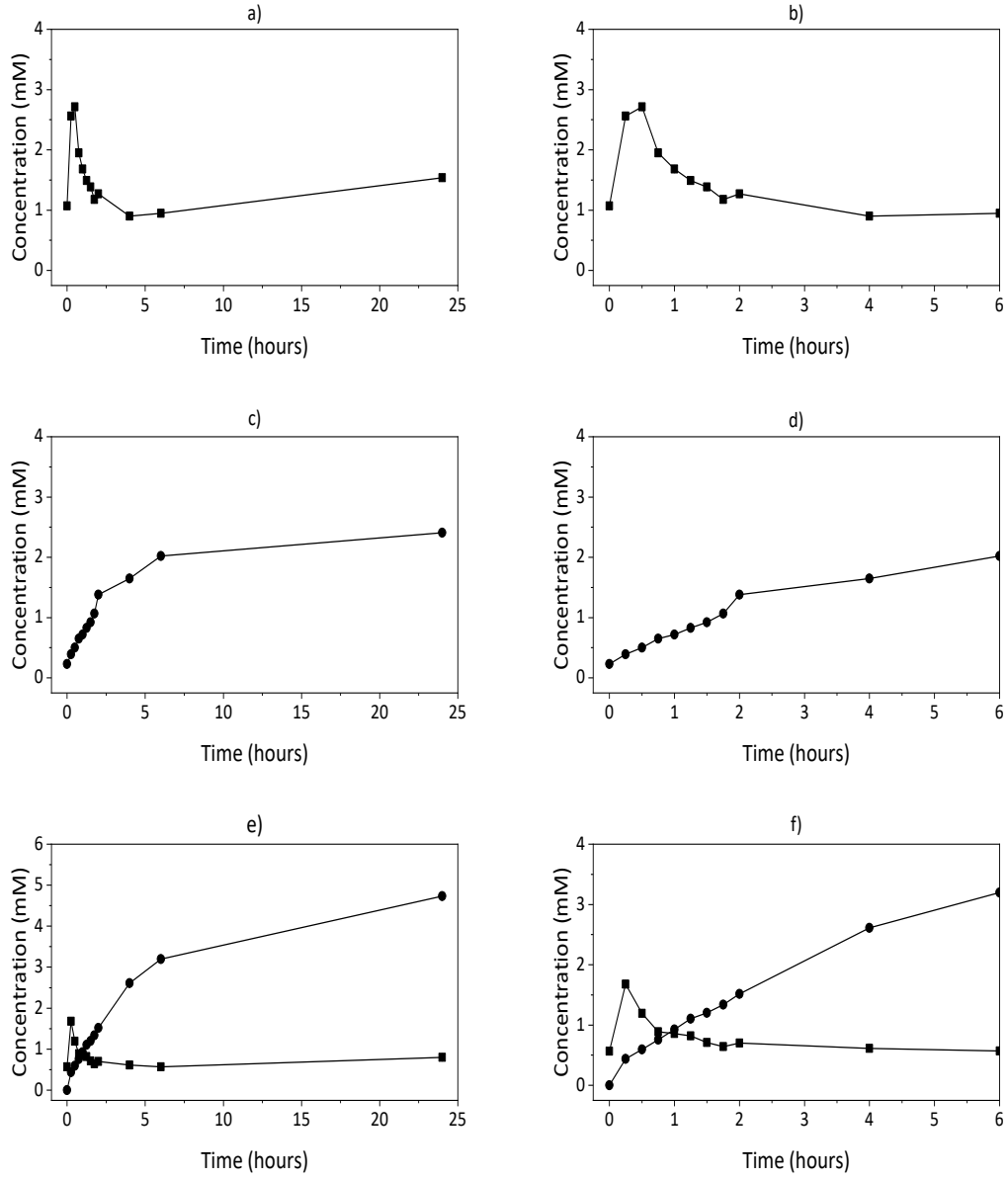

Figure 6.13. Kinetics of L-gluco-heptulose and HPA production for stand-alone and one-pot two step batch reactions using Ni-NTA immobilized enzymes. Panels (a), (c) and (e) monitor the entire 24-hour duration of the reaction, whilst panels (b), (d) and (f) focus on the initial 6 hours of the reaction. Panels (a) and (b) show HPA concentration (■, for all panels) for the immobilized TAm reaction. Panels (c) and (d) show L-gluco-heptulose concentration (●, for all panels) for the immobilized TK reaction. Panels (e) and (f) show HPA and L-gluco-heptulose concentrations for the one-pot two-step reaction with immobilized TAm and TK. Error bars show SEM (n=2 for single enzyme reaction, n=3 for one-pot two-step reaction). Ni-NTA immobilized enzymes were prepared as described in Section 2.4.3.1 and tested using a 5% w_{resin}/v loading of each immobilized enzyme.

6.3.3.2 Immobilization of purified enzymes onto epoxymethacrylate resin

Despite its straightforward application, immobilization of TAm and TK onto Ni-NTA beads poses some challenges. Ni-NTA resin can be quite expensive, imidazole is toxic and the beads are very small making retention of the enzyme in the ACR challenging. To overcome these challenges, use of an epoxymethacrylate resin (ECR) was investigated. ECRs covalently bind to exposed amine groups in an enzyme, facilitating multipoint immobilization (Hanefeld, Gardossi and Magner, 2009). For this work ECR8204F and ECR8204M resins from Purolite, UK were investigated. These epoxy resins have similar pore size (300-600 Å) but have different particle size distributions as shown in Figure 6.14. From the laser diffraction work it appears that ECR8204M had an approximate average particle size of 400 µm whilst ECR8204F had an average particle size of 250 µm. One of the goals of this immobilization study was to develop a procedure that could be implemented using the ACR catalyst baskets shown in Figure 3.10, which have a 400 µm mesh size. To fulfil this, the larger resin was chosen (pictured placed inside the catalyst basket in Figure 6.14). All subsequent findings discussed here were obtained using ECR8204M, referred from here on simply as ECR (Brady and Jordaan, 2009; Hanefeld, Gardossi and Magner, 2009; Purolite, 2015).

The first round of immobilizations was carried out using pure enzymes obtained through His-tag purification as described in Section 2.4.3.1. The recommended 100 $mg_{protein}.g_{resin}^{-1}$ enzyme concentration in the immobilizing buffer was used and 5% w/v of each immobilized enzyme was used in subsequent batch bioconversion reactions. 33 mM of HPA was mistakenly added in the one-pot two-step reaction. The concentrations of the reaction products are shown in Figure 6.15. The concentration profile of HPA produced by TAm follows a profile that was already noticed with the Ni-NTA-immobilized TAm (Figure 6.13), namely an early peak in HPA concentration followed by a sharp decline thereafter. Panels (c) and (d) show that TK, on the other hand, performed as expected with a final L-gluco-heptulose concentration of 3.3 mM. This concentration was higher than was obtained with the Ni-NTA immobilized bioconversion (Figure 6.13). This suggests that the ECR is an effective immobilization technique. The one-pot two-step reaction shown in panels (e) and (f) depict a similar early peak and decline of HPA as was observed in the stand-alone TAm reaction.

As shown in Figure 6.16, the L-gluco-heptulose concentration obtained in the one-pot two-step reaction was 4.8 mM, a 45% increase with respect to the stand-alone reaction. This

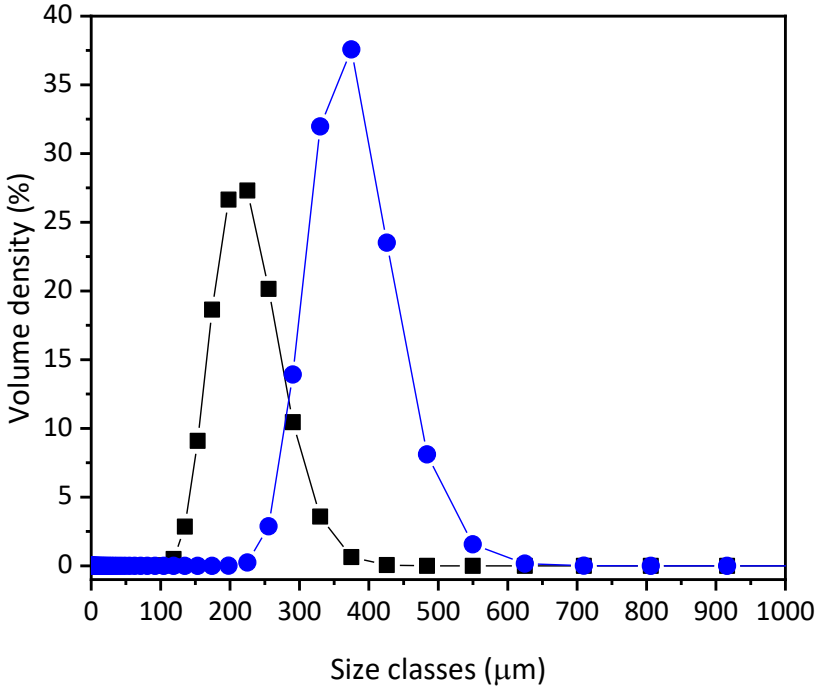

Figure 6.14. Particle size distribution of ECR8204F and ECR8204M enzyme immobilization resins and photograph of the resin in an ACR catalyst basket. Resins were analysed by laser diffraction as described in Section 2.4.3.2. The catalyst baskets have a mesh with an approximate pore size of 400 μm and are approximately 2.5 cm across.

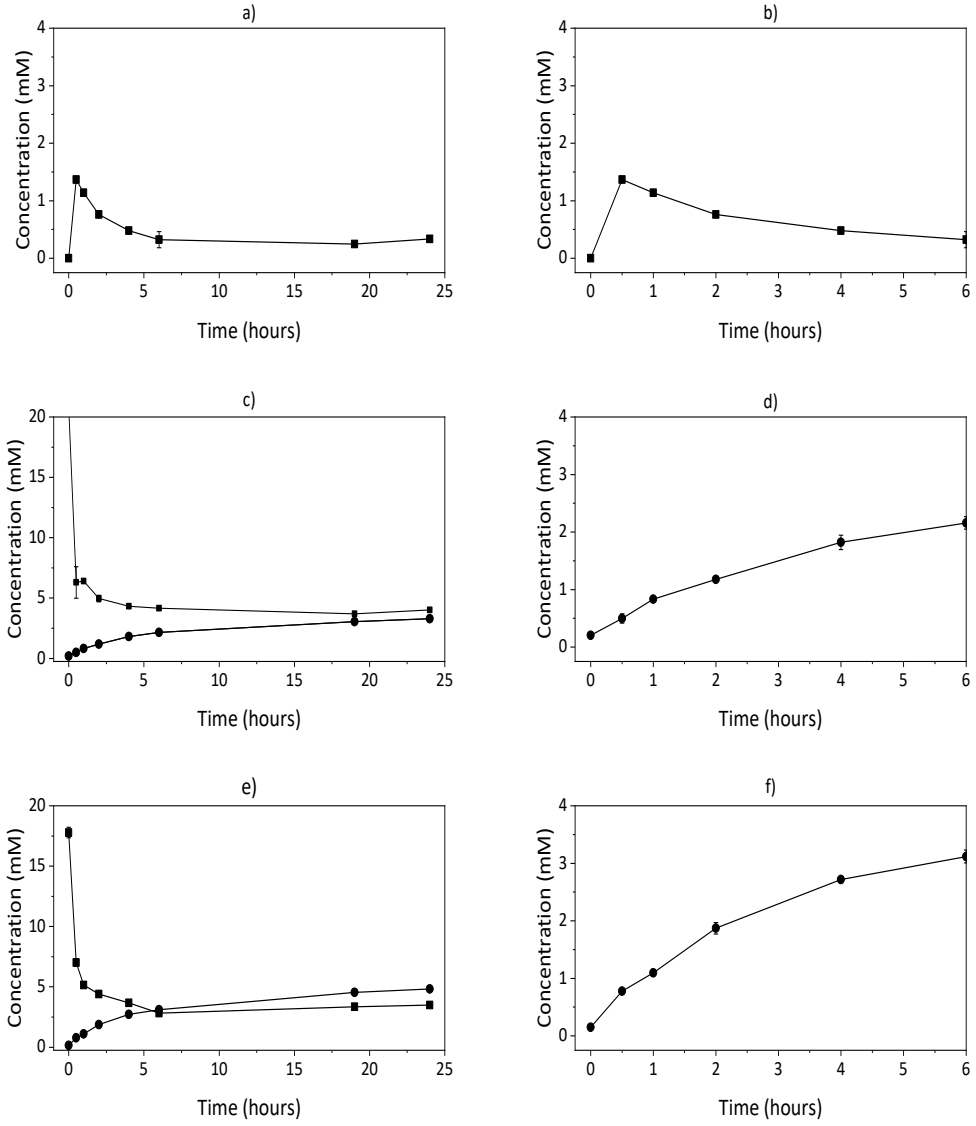

Figure 6.15. Kinetics of L-gluco-heptulose and HPA production for stand-alone and one-pot two-step batch reactions using His-Tag purified and ECR immobilized TAm and TK. Panels (a), (c) and (e) monitor the entire 24-hour duration of the reaction, whilst panels (b), (d) and (f) focus on the initial 6 hours of the reaction. Panels (a) and (b) show HPA concentration (■) for the immobilized TAm reaction. The course of the TK reaction is shown in panels (c) and (d); with production of L-gluco-heptulose (●) and degradation of HPA (■, not shown in panel (d)). The one-pot two-step reaction with immobilized enzyme (panels (e) and (f)) for the production of L-gluco-heptulose (●) was carried out with the addition of HPA (■) the degradation of which is shown in panel (e). Error bars represent SEM (n=2). Immobilized TAm and TK were prepared as described in Section 2.4.1.4 and, 5% w/v of total reaction mix of each enzyme was used in the reaction. Reaction performed as described in Section 2.4.3.3.

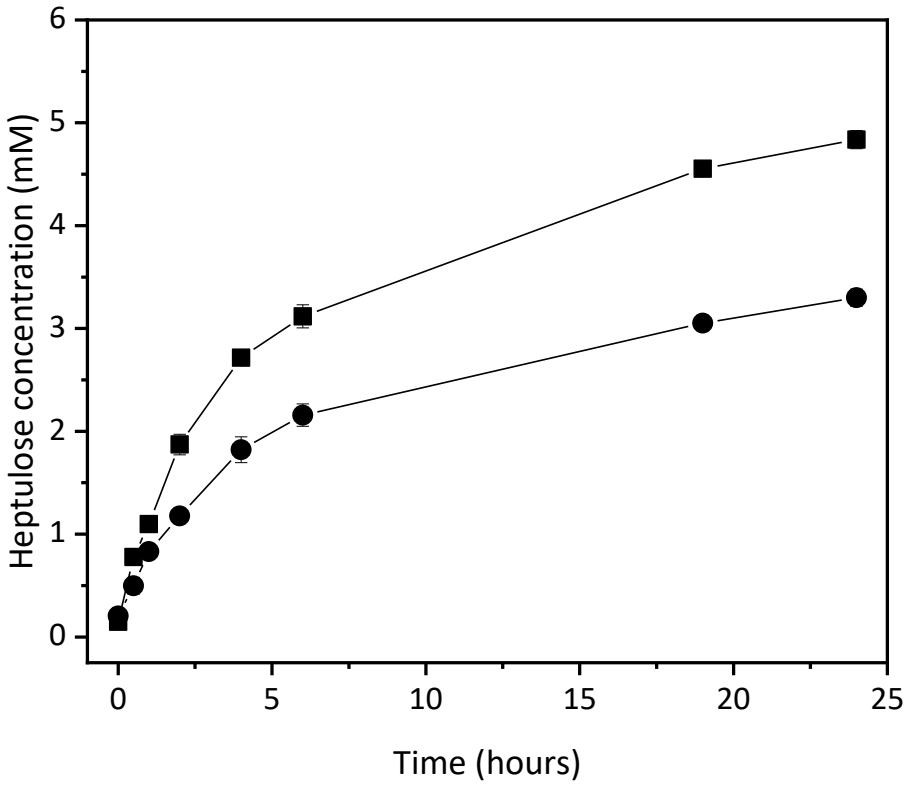

Figure 6.16. Kinetics of L-gluco-heptulose production for one-pot two-step and stand-alone TK reaction. The conversion of L-arabinose into L-gluco-heptulose by immobilized TK alone (●) was compared to the one-pot two-step reaction (■). In both cases 33 mM of HPA was added at the start of the reaction. Error bars represent SEM (n=2). Immobilization of TAm and TK was carried out as described in Section 2.4.1.4 and reactions were set up as presented in 2.4.3.3.

highlights that despite the same initial HPA concentration (33 mM of HPA was added to both reactions) the TAm helped increase the yield of the reaction This corroborates the finding that the one-pot two-step allows the enzymes to act synergistically and aids in overall yields, discussed in Section 6.3.2.1.

6.3.3.3 Epoxymethacrylate immobilization of partially purified TAm and TK

As discussed in Section 5.1, purifying enzymes through IMAC is time consuming, costly and not widely employed at large scale. The heat purification step studied in Section 5.3.3.1 was therefore used to prepare partially purified enzymes for further immobilization studies. Here, different protein concentrations, as determined by Bradford reagent assay (Section 2.4.1.7), in the immobilizing buffer were tested to see if there was the potential for improvement of the immobilization process of the individual Tam and TK enzymes. 3 different protein loadings were examined: 10; 50; and 100 $mg_{protein}.g_{resin}^{-1}$. Additionally, a co-immobilization was performed. This involved incubating the resin with an immobilization buffer which contained both partially purified TAm and TK in a ratio of 1:1 (in terms of total protein content). The initial and final concentration of the immobilizing buffer was measured during the immobilization procedure and is shown in Figure 6.17.

The concentration process, which employed an ammonium sulfate precipitation and resuspension step (as detailed in Section 2.4.3) can likely explain the variation in measured initial protein concentration between the 3 immobilizing buffers (TAm; TK; and TAm and TK together) and why the starting concentrations of the 10 $mg_{protein}.g_{resin}^{-1}$ loading could barely be detected by the Bradford total protein assay. On the other hand, 50 and 100 $mg_{protein}.g_{resin}^{-1}$ were detected, and more importantly showed a considerable reduction in the protein concentration in the immobilizing buffer at the end of the immobilization process. Additionally, it can be seen that the 100 $mg_{protein}.g_{resin}^{-1}$ loading had some small amounts of protein left. This suggests that most of the protein is bound to the resin and that the 100 $mg_{protein}.g_{resin}^{-1}$ loading is very close to the optimal loading.

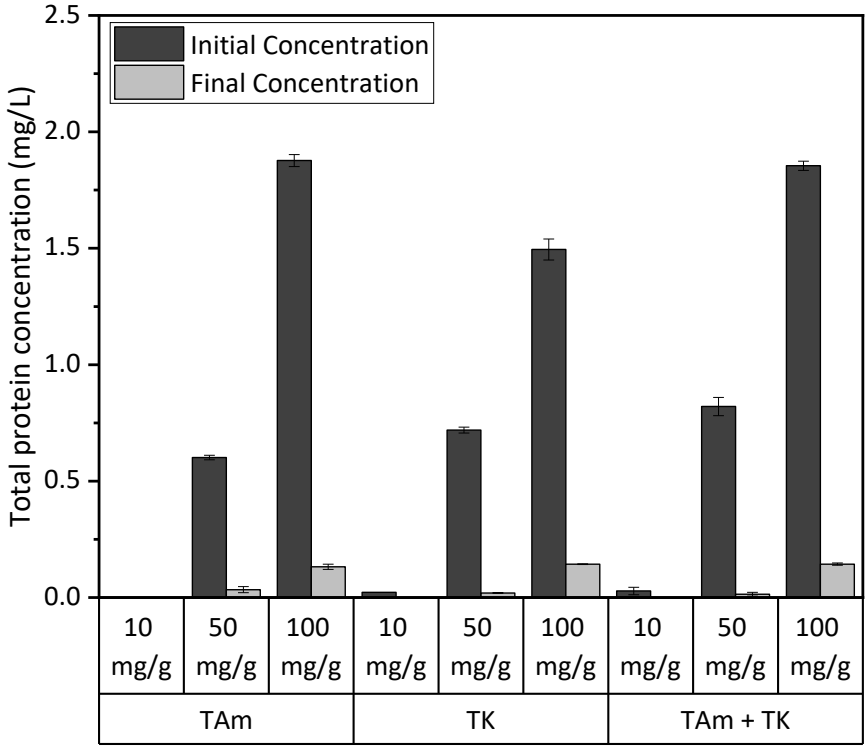

Figure 6.17. Initial and final concentrations of soluble protein in the immobilization buffer during the ECR immobilization process. Error bars indicate SEM of the protein assay procedure (n=3). Immobilizing buffer was incubated with ECR resin overnight as described in Section 2.4.3.2 Initial and final total protein concentrations of immobilizing buffer as measured by Bradford reagent assay (Section 2.4.1.7).

The subsequent bioconversion reactions using the heat purified, immobilized enzyme preparations, are shown in Figure 5.18; only very small quantities of HPA were produced which were not quantifiable by HPAEC-PAD. This was not unexcepted as TAm had not performed well in previous immobilization studies using the His-tag purified enzyme (Section 6.3.3.2). The immobilized TK, on the other hand, did show L-gluco-heptulose formation. From panel (a) it appears that the the loading condition that appears to yield the highest amount of L-gluco-heptulose is: 100 $mg_{protein}.g_{resin}^{-1}$. In comparison to the studies described in Section 5.3.3.2, L-gluco-heptulose synthesis using the IMAC purified material however yielded higher concentrations (3.3 mM), albeit after 24 hours rather than 19, than the heat purified material (1.9 mM). As discussed in Section 5.3.3.2, the lower activity of the heat purified material is likely due to the presence of other proteins in the immobilization buffer. This highlights the importance of identifying a selective purification technique.

The one-pot two step enzyme reaction which employed co-immobilized TAm and TK enzymes gave very poor production of HPA and L-gluco-heptulose. In Figure 5.18, panel (b) it is possible to see how increasing protein content in the immobilization buffer led to higher final L-gluco-heptulose concentrations, but the absolute amount of L-gluco-heptulose produced by the one-pot two-step reaction is considerably lower than the TK reaction on its own. This suggests that the TAm reaction is not producing sufficient intermediate product (HPA) due to the low activity of the TAm.

6.3.3.4 Immobilization and co-immobilization of TAm and TK in the presence of PLP

In all bioconversion reactions presented in this work, TAm was incubated with PLP for 20-30 minutes prior the addition of the substrates. Thus, it was theorised that the poor conversions obtained with immobilized TAm could be due to the lack of PLP during the immobilization procedure. To prevent this from happening, a modified immobilization protocol was performed in which PLP was added into the immobilizing buffer, extending the contact time between TAm and cofactor from 20 minutes to an overnight incubation. Furthermore, findings discussed in Section 6.3.1, Table 6.3 suggested that the initial rate of the TAm reaction was lower than that for TK. Consequently, to favour the production of HPA, rather than co-immobilizing TAm and TK in a 1:1 ratio, a 9:1 (TAm:TK) ratio was used.

The stand-alone batch TAm and TK reactions depicted in Figure 6.19 show that some HPA is produced in the TAm reaction, albeit at very low concentrations. Nonetheless, this is better than the trace amounts obtained for immobilization in the absence of PLP addition using

heat purified TAm. TK, on the other hand, appears to convert L-arabinose into L-gluco-heptulose at a comparable rate, obtaining, after 24 hours, 1.5 mM in this instance; compared to 1.7 mM of in the immobilization described in Figure 6.18.

The one-pot two-step reactions as shown in Figure 6.20 indicate little production of L-gluco-heptulose (only approximately 0.2 mM). When compared to the stand-alone TK reaction, Panel (a), which depicts the two separately immobilized enzymes loaded each at 5% w/v, highlights how the poor production of HPA leads to poor performance of the one-pot two-step system. The 9_{TAm}:1_{TK} co-immobilized setup was theorised to favour the production of HPA and so drive the production of the intermediate to create a more favourable reaction equilibrium. Both HPA and L-gluco-heptulose were produced. However, L-gluco-heptulose concentrations obtained were lower than both the stand-alone TK reaction and the separately immobilized TAm and TK working in the one-pot two-step reaction. The likely explanation for this is that the total resin loading for the co-immobilized reaction was 5% w/v. This means that the amount of TK loaded is less and work in Section 5.3.2 has shown how important enzyme loading is with regard to final product yield. In both one-pot two-step reactions shown here, a peak in HPA concentration shortly after the start of the reaction was also detected. Indicating a possible, short-lived, residual TAm activity which is followed by HPA degradation (Section 6.3.1.1).

The immobilization and co-immobilization work presented in Figure 6.20 showed that production of HPA and L-gluco-heptulose using immobilized TAm and TK is possible. However, the purity of the enzyme in the immobilizing buffer is clearly important, as shown by the comparison of His-Tag and HP materials in Figure 5.11. This is especially true when using the ECR resin which employs a non-selective binding method (Purolite, 2015). This highlights the importance of optimising the purification process so that it can be scalable and provide pure enzymes at a low cost.

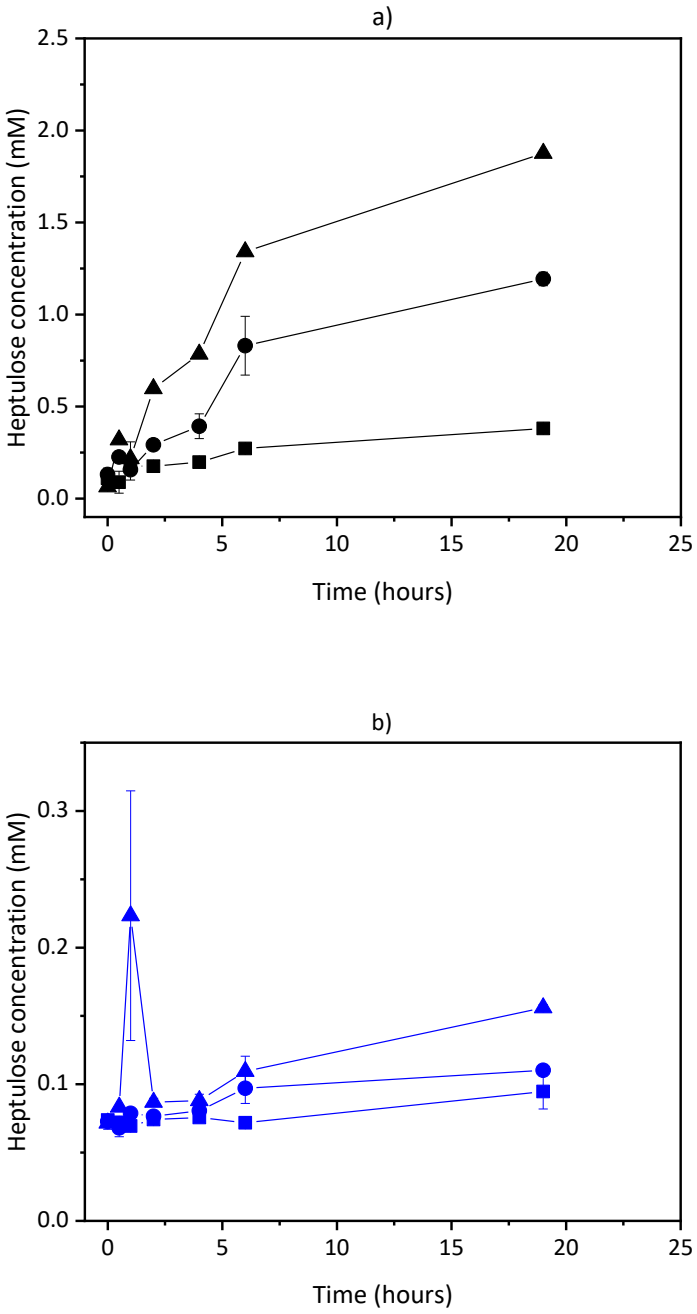

Figure 6.18. Batch bioconversion kinetics showing L-gluco-heptulose production for stand-alone immobilized TK reaction and one-pot two-step reaction with immobilized TAm and TK. Enzymes were immobilized using different immobilization loadings (10, 50 and 100 $mg_{total\ protein}.g_{resin}^{-1}$). Panel (a) shows L-gluco-heptulose production from immobilized TK reaction (■= 10 $mg_{total\ protein}.g_{resin}^{-1}$; ●= 50 $mg_{total\ protein}.g_{resin}^{-1}$; and ▲= 100 $mg_{total\ protein}.g_{resin}^{-1}$). Panel (b) shows L-gluco-heptulose concentration for the one-pot two-step reaction with immobilized TAm and TK (■= 10 $mg_{total\ protein}.g_{resin}^{-1}$; ●= 50 $mg_{total\ protein}.g_{resin}^{-1}$; and ▲= 100 $mg_{total\ protein}.g_{resin}^{-1}$). Error bars represent SEM (n=2). Immobilized enzyme loading was 5% w/v for each enzyme and standard reaction conditions were used. Immobilization on ECR support procedure is described in Section 2.4.3.2.

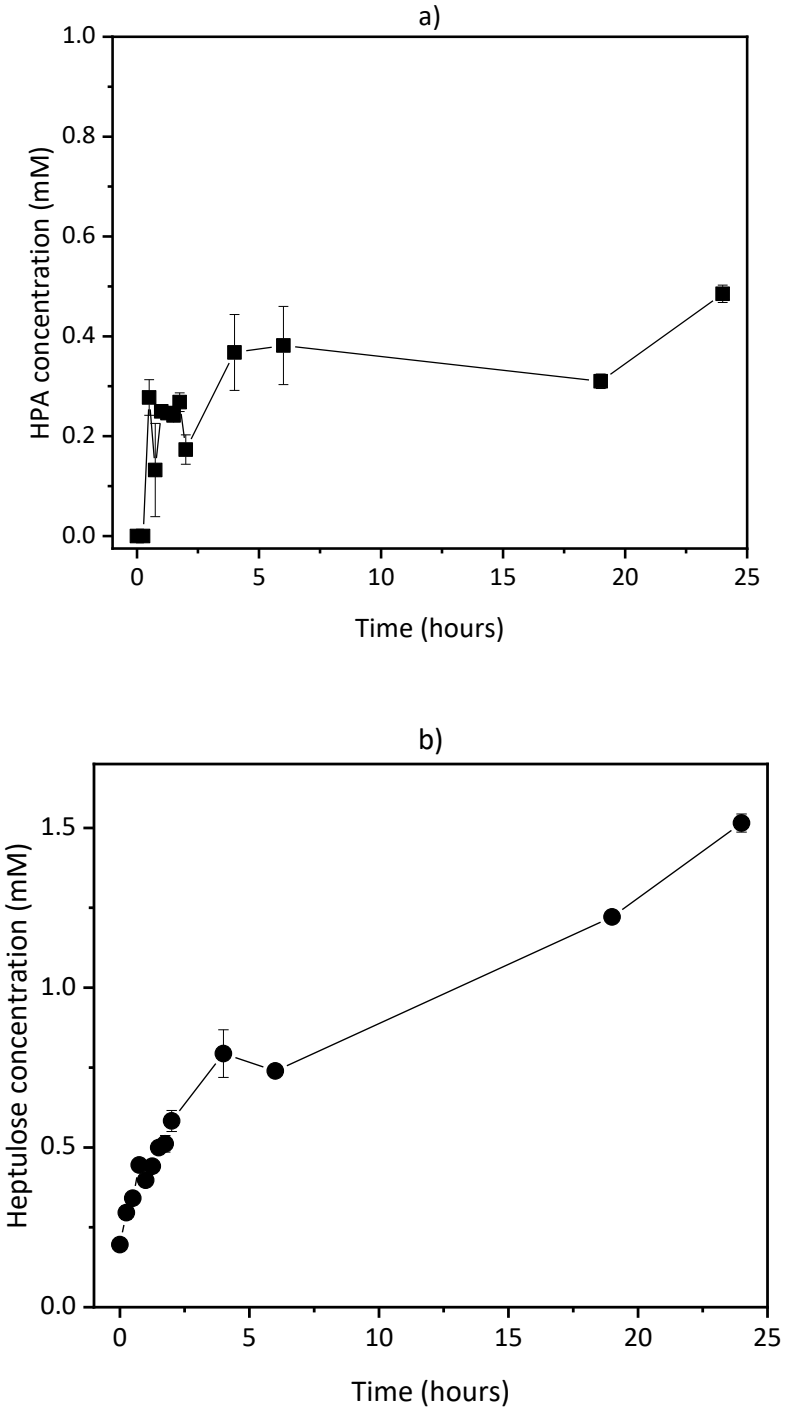

Figure 6.19. Batch bioconversion kinetics of stand-alone immobilized TAm and TK batch reactions with overnight PLP incubation (for TAm only). Panel (a) shows HPA concentration (■) over time for the immobilized TAm reaction under standard conditions, with 5% w/v enzyme loading, using a PLP-bicarbonate immobilizing buffer. Panel b) shows the production of L-gluco-heptulose (●) over time for the stand-alone immobilized TK reaction, under standard condition, with 5% w/v enzyme loading. Error bars denote SEM (n=2). TAm and TK immobilization procedures are outlined in Section 2.4.3.2.

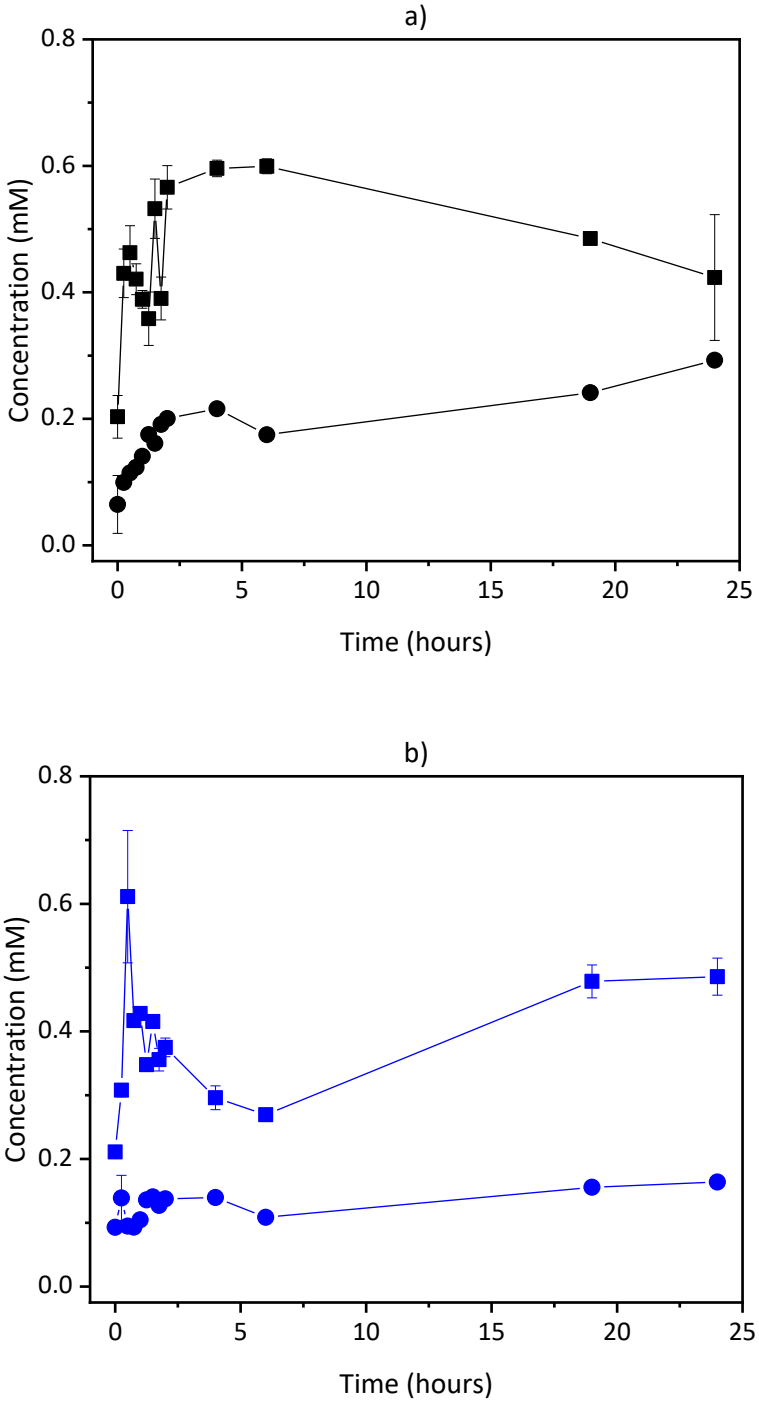

Figure 6.20. One-pot two-step batch bioconversion kinetics showing HPA and L-gluco-heptulose production using separately immobilized and co-immobilized TAm and TK. Immobilization of TAm took place in presence of PLP overnight. Intermediate product formation, HPA (■) and L-gluco-heptulose concentration over time (●) are shown for the two separately immobilized enzymes (panel (a)), and for the co-immobilized enzyme reaction (panel (b)), in blue). Enzyme loading was 5% w/v each of the separate TAm and TK enzymes and 5% w/v for the co-immobilized enzymes. Error bars denote SEM (n=2). TAm and TK immobilization procedures are outlined in Section 2.4.3.2.

Additionally, it was found that the one-pot two-step reaction often worked better than the stand-alone reactions. This makes a compelling case for the utilisation of biocatalytic routes to produce intermediates over chemically synthesised substrates. In this instance, the rapid degradation of HPA, discussed further in Section 6.3.1.1, led the real concentration of HPA in stand-alone TK reaction to be much lower than the starting concentration (33 mM). In the case of the one-pot two-step reaction system the HPA was produced *in situ* and rapidly used up, limiting thermal degradation. Although it was hypothesised that co-immobilizing the two enzymes onto the ECR support would further drive this synergistic effect by reducing mass transfer limitations between the TAm and TK active sites, the co-immobilization methods used were not developed enough to provide improved production of L-gluco-heptulose.

Despite the clear advantage of using the two enzymes together, TAm immobilization proved less successful than TK immobilization. The main findings regarding the immobilization of TAm were that HP TAm performance is not as good as IMAC purified TAm, and that the HPA yield could be slightly improved by the co-incubation with the PLP cofactor during the immobilization procedure. In literature, efforts at immobilizing TAm, have given reduced residual activity, indicating that this class of enzymes may be a challenging class to immobilize (Shin, Kim and Shin, 2001; Neto *et al.*, 2015). Future immobilization efforts could focus on utilising a purer enzyme solution, and testing different resin supports. However, Cárdenas-Fernández and coworkers successfully immobilized an ω-TAm on an amino epoxy resin, using a method not dissimilar to the ECR immobilization procedure in this work, with the added step of blocking exposed epoxy groups with 2-mercaptoethanol. (Cárdenas-Fernández *et al.*, 2015). Additionally, a higher concentration of PLP could be used in the immobilizing buffer. In this work 0.2 mM PLP was added during TAm reactions and immobilizations, but concentrations of up to 1.4 and 2 mM PLP have been reported (Neto *et al.*, 2015; Petri, Colonna and Piccolo, 2019).

6.3.4 Continuous production with model solutes

6.3.4.1 ACR and system setup

The ultimate aim of this project (Section 1.7) was to demonstrate the feasibility of a one-pot two-step reaction in continuous mode, using pretreated SBP as an L-arabinose feedstock. Firstly, however, the one-pot two-step reaction in the ACR was operated with a preparation of model solutes, and buffer salts, rather than pretreated and depolymerised SBP. In addition, due to the high price of Li-HPA required as substrate for the stand-alone TK reaction, only the one-pot two-step TAm-TK reaction was studied under flow conditions.

The reactor setup shown in Figure 6.21 details how the substrates and enzymes were mixed together and how the reaction was monitored by sampling at the outlet. To ensure the substrates and enzymes would mix and react in the ACR and not before, two preparations or *feeds* were created. The *enzyme feed*, which consisted of 30% v/v of the total flowrate; and the *substrate feed*, which made up the remaining 70% v/v. The *enzyme feed* consisted of the two clarified cell lysates (10% of the total flowrate each), the cofactors and HEPES buffer. The *substrate feed* contained HEPES buffer and the substrates, L-serine, α-ketoglutaric acid and L-arabinose to produce L-gluco-heptulose. The substrate concentrations in the *substrate feed* was higher than the final desired concentration to account for the dilution that would occur when *substrate* and *enzyme feeds* would combine.

The tubing connecting the syringe pump containing the *enzyme feed* to the ACR was sized to allow a 25-minute residence time leading into the ACR, thereby ensuring that enzymes had enough time to incubate with their cofactors. The *substrate feed*, on the other hand, was fed to the ACR via a peristaltic pump to the main inlet port. The reaction was monitored by taking samples at the outlet. As described in Section 2.4.2.6, approximately 6.5 $mL.hr^{-1}$ of each lysate was required, equating approximately to 130 $mL.hr^{-1}$ of cell culture broth. Furthermore, the sonication step to produce sufficient amounts of lysate required for this reaction was time consuming. The amount of time required to produce the quantities of enzymes required can help to contextualize the need for the development work explored in Chapter 5.

6.3.4.2 One-pot two-step reaction with fixed substrate concentration

The ACR run was performed with 10 mM L-serine and α-ketoglutaric acid, and 33 mM L-arabinose. To maximise the amount of L-gluco-heptulose produced, a 2-hour residence time was selected, as this was the largest residence time the ACR manufacturer recommended beyond which diffusion effects across the reactor would be too great.

Figure 6.22 displays the successful production of L-gluco-heptulose in a one-pot two-step system run in continuous mode. The concentrations of HPA and L-gluco-heptulose were monitored over a period of 6.5 hours where it can also be seen that both products appear to reach steady state approximately 3-4 hours after the initiation of the reaction. The steady state concentrations were calculated as the average of the samples between 4 and 6.5 hour and were 4.75 mM HPA and 1.15 mM L-gluco-heptulose, respectively.

The RTD characterisation explored in Section 3.3.2 did not study residence times of 2 hours. However, Figure 6.22 shows the modelled step change for a theoretical 10 tanks-in series reactor, as calculated in Section 3.3.2.1, using Equation 3.9. The HPA concentration step change curve appears steeper than the N=10 step change, suggesting a slightly larger N value for the ACR at the flowrate used in this reaction. Furthermore, the modelled step change curve appears shifted to the right of the real curve obtained by monitoring HPA concentration. This observed shift suggests that the actual residence time inside the reactor is slightly less than two hours. A possible reason for this, is that the peristaltic pump used to feed the *substrate feed* had only discrete speed settings for the pump rotations speed. As such a pump speed of 13 rpm instead of a 12.5 rpm was selected (as calculated in Appendix 9.1), which would have led to a slightly shorter residence time in the reactor).

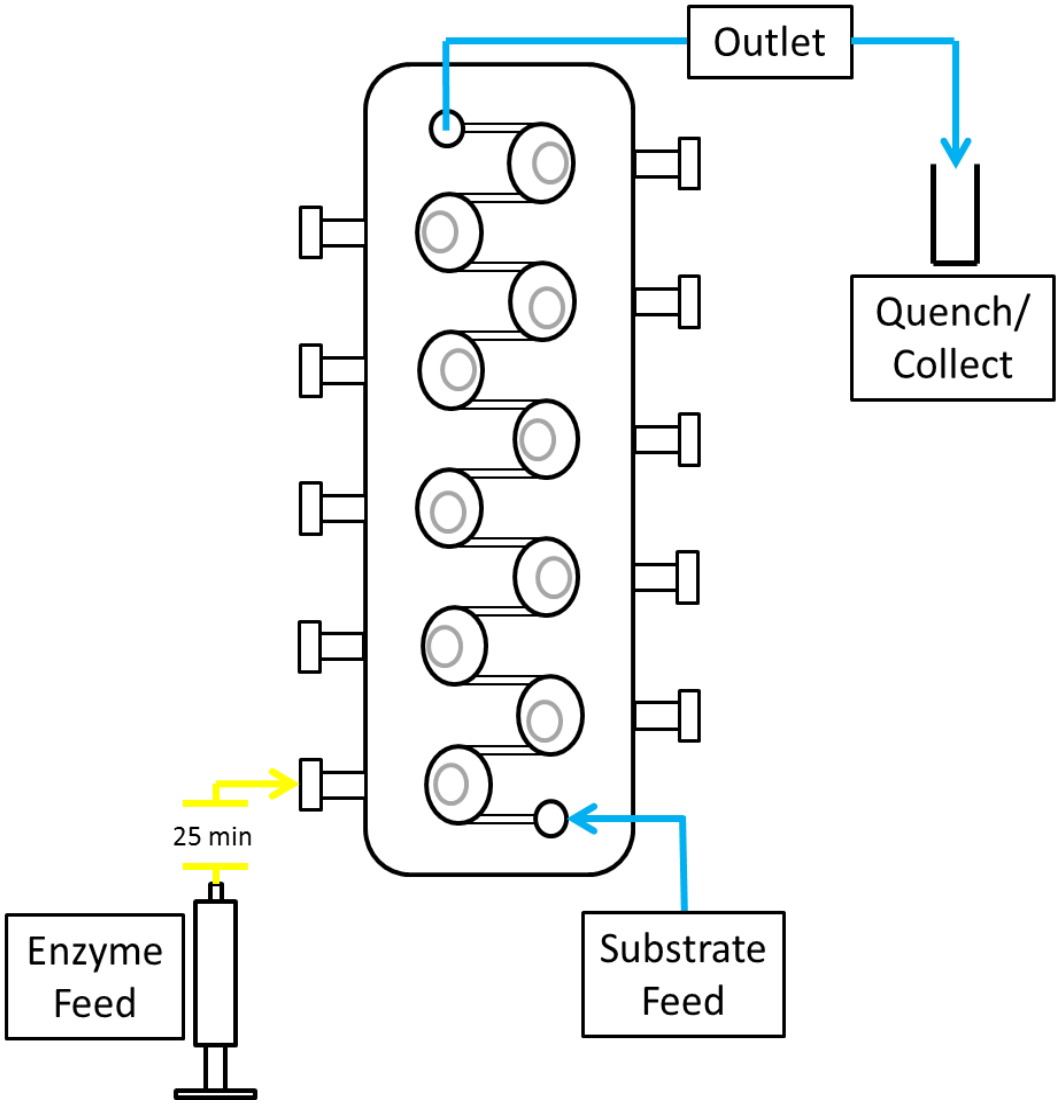

Figure 6.21. ACR setup for continuous L-gluco-heptulose production. A substrate feed was pumped via a peristaltic pump from the main inlet port, whereas the enzyme feed was pumped via syringe pump from side inlet point. Samples at the outlet were collected and quenched with 0.5% v/v TFA. Substrate and enzyme feeds were prepared as outlined in Section 2.4.2.6.

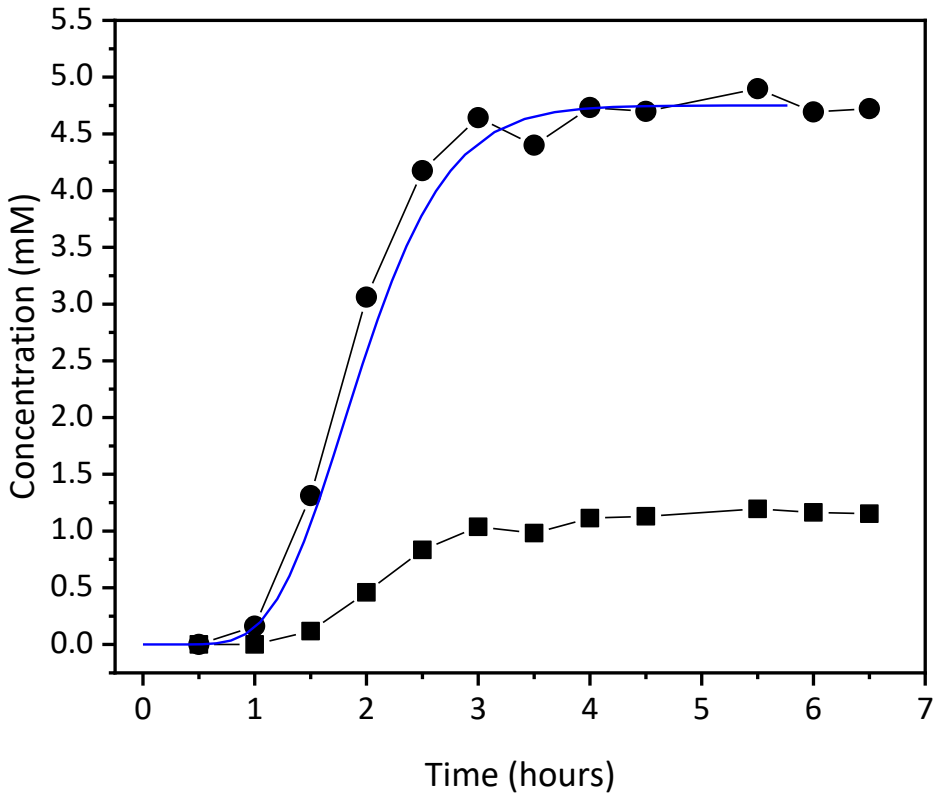

Figure 6.22. Continuous production of L-gluco-heptulose from L-serine, α-ketoglutaric acid and L-arabinose, in a one-pot two-step TAm-TK reaction system. HPA (■) and L-gluco-heptulose (●) concentrations are shown. 10 mM L-serine, 10 mM α-ketoglutaric acid were used with 33 mM L-arabinose with a 2-hour residence time. In blue is the step change response obtained by assuming an equivalent of 10 CSTRs in series. Reactor and reaction set up are outlined in Section 2.4.2.6. Equation 3.6 was used for the derivation of the step change response.

6.3.4.3 Continuous one-pot two-step reaction with a step change

The work discussed in Section 6.3.2.1 showed that higher substrate concentrations led to improved initial rates as well as higher final, 24-hour, concentrations (as highlighted in Figure 6.10). To obtain an improved bioconversion in the ACR, a continuous run was performed in which two separate conditions were tested. During the initial period of operation the same concentrations of 10 mM L-serine; 10 mM α-ketoglutaric acid; and 33 mM L-arabinose were used. After a first steady state was reached, a step-change in the substrate feed concentration was introduced i.e. 100 mM each of L-serine, α-ketoglutaric acid and L-arabinose. The purpose of switching between conditions was to observe the ability of the ACR to respond to step changes in feed concentrations.

Figure 6.23 shows the course of this two-stage experiment. Highlighted in pink is the steady state period at the low concentration conditions. Highlighted in green is the steady state period for the high concentration conditions.

The steady state values obtained are outlined in Table 6.7. L-gluco-heptulose and HPA reached 1.17 mM and 4.84 mM, respectively, in the first stage. This is very close to the conditions obtained in the previous ACR run, where concentrations reached 1.15 mM and 4.75 mM, showing good robustness and repeatability of the continuous flow biocatalysis. The second stage which employed higher substrate concentrations yielded 2.1 times as much L-gluco-heptulose (2.44 mM) and 2.5 times as much HPA. The intermediate and final reaction product concentration are shown on separate axis to highlight how closely the kinetics of the intermediate and final product synthesis are matched. Increasing the initial substrate concentration led to an increase in the production of both products.

Contrary to the findings in the ACR, the same increase in substrate concentration examined in batch mode (Figure 6.10) showed small effects on the HPA produced. L-gluco-heptulose production, on the other hand, did see a 1.6-fold increase from 5.7 mM to 9.0 mM after 24 hours. Rather than comparing outlet concentrations of the reactions in flow to the final 24-hour concentrations obtained in batch, a more apt comparison would be to examine the concentrations obtained in batch reactions after 2 hours.

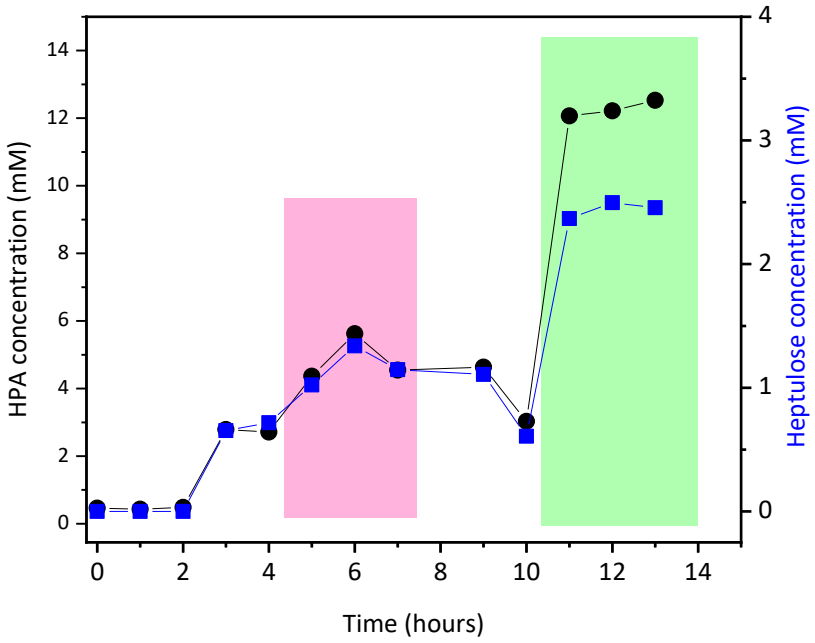

Figure 6.23. Continuous production of L-gluco-heptulose from L-serine, α-ketoglutaric acid and L-arabinose in a one-pot two-step TAm-TK reaction system with a step change in substrate concentration. HPA (●, in black) and L-gluco-heptulose (■, in blue) concentrations are shown on separate y-axes. Two sets of concentrations were used for the reaction: 10 mM L-serine, 10 mM α-ketoglutaric acid, and 33 mM L-arabinose; and 100 mM L-serine, 100 mM α-ketoglutaric acid, and 100 mM L-arabinose. The steady state concentrations obtained with the first set of conditions are shown in the pink rectangle, whilst the green rectangle shows the concentrations obtained from the second sets of conditions. Reaction performed as outlined in Section 2.4.2.6.

Table 6.7. Steady state product concentration and throughputs for the one-pot two-step continuous reaction. L-gluco-heptulose and HPA concentrations and throughputs for the first stage and second stage of the reaction, calculated from values obtained from values in Figure 6.23.

	First Stage		Second Stage	
	L-gluco-heptulose	**HPA**	**L-gluco-heptulose**	**HPA**
Average (mM)	1.17	4.84	2.44	12.27
SEM	0.075	0.321	0.031	0.111
Throughput ($\mu M.hr^{-1}$)	76.10	311.61	158.71	790.00

To ensure that any difference between batch and flow reactions was due to the mode of operation, samples of the *enzyme feed* were kept and 1.2 mL batch reactions were carried out for comparison over the entire 24-hour reaction period as shown in Figure 6.24. Over a 24 hour period a clear effect of increasing substrate concentration could be seen for L-gluco-heptulose concentration, but this was less pronounced for HPA. Further in panel (a), showing HPA concentration the initial rate for the two concentration levels appears very similar. The effects of increasing substrates concentration on the stand-alone TAm reaction discussed in Figure 6.7 did show only limited effects of increasing substrate concentrations. Indeed, over a 24-hour period increasing L-serine concentration led to increases in HPA; but increasing α-ketoglutaric acid concentration had little effect on HPA production. The stand-alone TK reaction studied in Figure 6.8, conversely, showed an increase in initial rate and final L-gluco-heptulose concentrations with increasing L-arabinose concentrations; a finding, in line with what was observed in Figure 6.24.

The conversions obtained in the ACR at steady state and in batch after 2 hours are compared in Table 6.8. The first ACR reaction and the first stage of the second ACR run which used 10 mM L-serine and α-ketoglutaric acid and 33 mM of L-arabinose showed very similar concentrations of both HPA and L-gluco-heptulose, indicating good repeatability of the process. The second batch reaction, which employed the same batch of lysate as the second ACR run, obtained very similar L-gluco-heptulose concentrations after 2 hours. The HPA concentrations obtained in the ACR were higher than in batch. With 4.8 mM instead of 3.2 mM for the first stage and 12.3 mM instead of 3.8 for the second stage, being obtained. The first batch reaction (data obtained from Figure 6.10) appeared to obtain higher product concentration than the second batch reaction. However, it still did not predict the HPA concentration obtained in flow.

The difference between the first and second batch reactions could be due to variability in the cell lysis process used for enzyme production. However, the difference between the HPA concentration obtained in batch and in continuous mode is less clear, but given that L-gluco-heptulose is produced at the same level in batch and continuous modes, it appears that the ACR provides an advantageous environment for HPA production. Possible reasons for this could be more favourable mixing conditions, reversibility of the reaction or reactor configuration.

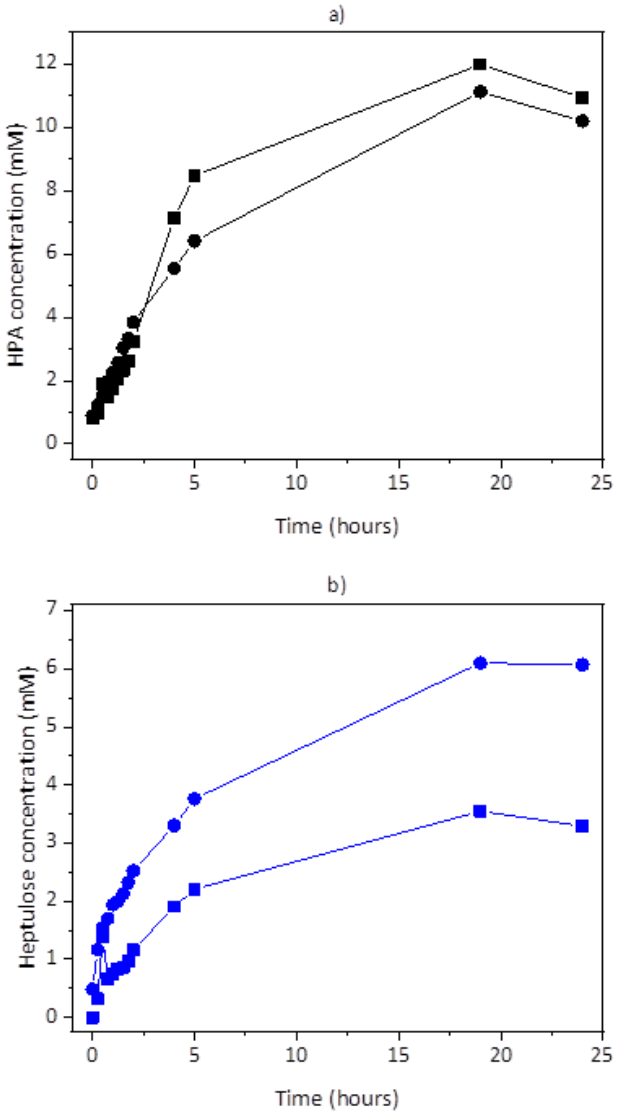

Figure 6.24. One-pot two-step batch production mimicking ACR conditions. Samples of the TAm and TK cell lysates used for the ACR experiment in Figure 6.23 were used for 1.2 mL batch reactions to evaluate batch conversion kinetics. 10 mM of L-serine and α-ketoglutaric acid with 33 mM of L-arabinose (■) and 100 mM each of L-serine, α-ketoglutaric acid, and L-arabinose (●). Panel (a) shows HPA concentrations obtained, whilst panel (b) shows concentrations for L-gluco-heptulose. Batch reactions were performed as described in Section 2.4.2.4.

Table 6.8. Comparison of ACR steady-state product concentrations with those obtained in a batch bioconversion after 2 hours. Batch conversion data are compared to the ACR values obtained for the low and high substrate concentration. The figure from which the values are obtained is also indicated.

Concentration	**10 mM L-serine** **10 mM α-ketoglutaric acid** **33 mM L-arabinose**				**100 mM L-serine** **100 mM α-ketoglutaric acid** **100 mM L-arabinose**		
Experiment	**ACR 1**	**ACR 2**	**Batch 1**	**Batch 2**	**ACR 2**	**Batch 1**	**Batch 2**
Reference	Figure 6.22	Figure 6.23	Figure 6.10	Figure 6.24	Figure 6.23	Figure 6.10	Figure 6.24
L-gluco-heptulose (mM)	1.15	1.17	1.67	1.16	2.44	3.77	2.52
HPA (mM)	4.75	4.84	2.23	3.23	12.27	3.88	3.84

In Section 6.3.2.2 where different production scales were compared, mixing appeared to affect 24-hour L-gluco-heptulose conversions in batch. However, as is shown in Figure 6.11, these difference between scales are less pronounced in the first hours of the reaction and became more prominent over time. Translating a 1.2 mL batch reaction to a 120 mL continuous setup in the ACR did not seem to affect L-gluco-heptulose concentrations.

The reactor configuration could explain the increased HPA concentration in the ACR when compared to the batch bioconversion. Some inhibitory effects from α-ketoglutaric acid were observed in the stand-alone batch reaction (Figure 6.7). By having 10 interconnected cells in the ACR, only 1 tenth of the total enzyme amount is ever in contact with the highest (initial) α-ketoglutaric acid concentration, this could result in higher conversions. Further, HPA was proposed as a ketol donor for TK reactions because the carboligation step produces CO_2 which in a batch reaction at atmospheric conditions would evaporate and drive the equilibrium towards the product. However, in a closed continuous reaction the CO_2 would only be allowed to escape at the outlet and not in the middle of the reaction. This could lead to higher HPA accumulation in the ACR. The L-gluco-heptulose concentration, on the other hand, remained comparable to the batch reaction as increasing HPA concentration had little effect on final concentrations in the stand-alone TK reactions discussed in Section 6.3.1.4, Figure 6.8. Although possible, these hypotheses were not tested and further work should focus on identifying and addressing the root cause of the HPA overproduction and attempt to increase L-gluco-heptulose concentration.

6.3.5 Continuous one-pot two-step bioconversion with hydrolysed SBP

6.3.5.1 ACR set-up and comparison to batch system

Having demonstrated the feasibility of L-gluco-heptulose production through a one-pot two-step reaction in continuous mode, attention was focused on implementing the same reaction using pretreated SBP as the source of L-arabinose rather than working with model solutes.

In Chapter 4, the acid hydrolysis of SBP was successfully performed in flow mode (4.3.3). Additionally, preliminary work using AraF for the selective depolymerisation of arabinans in the ACR was also demonstrated (Section 4.3.4.2). Despite this, the full SBP-to-feedstock system had not been sufficiently characterised to be employed as a source of L-arabinose for its one-pot two-step conversion into L-gluco-heptulose. Instead, steam exploded SBP provided by Hamley-Bennett et al. (2016) and discussed in Section 4.3.3.6 was used for this

study. Following steam explosion for release of the arabinans, these were depolymerised using the continuous process described by Cardenas-Fernandez et al. (2018) as discussed in Section 4.3.4. The resulting feedstock material was analysed through HPAEC-PAD and was found to contain 21.5 mM of L-arabinose.

The current ACR set-up shown in Figure 6.21, divided the total flowrate in the ACR in two streams: the *enzyme feed* making up 30% of the total flowrate; and the *substrate feed* making up the remaining 70% of the total flowrate. As discussed in Section 6.3.4.1, and shown in Figure 6.8 and Table 6.4, L-arabinose concentration had an impact on the measured initial rate of reaction and there was no evidence of substrate inhibition. It was thus important to obtain as high a reaction rate as possible by keeping the L-arabinose concentration high and avoid unnecessary dilutions of the substrate stream. On this basis, the pretreated feedstock was set to comprise 65% of the total flowrate feeding into the ACR. In practice the ACR inputs were: enzyme feed (30% of the total flowrate); depolymerised, L-arabinose-rich SBP (65% of the total flowrate); L-serine, α-ketoglutaric acid and concentrated HEPES buffer (together accounting for 5% of the total flowrate). This meant that the inlet concentration of L-arabinose into the reactor would be 14 mM. The final reaction conditions were then based on using equimolar concentrations of all substrates (i.e. 14 mM of L-arabinose, α-ketoglutaric acid and L-serine).

Prior to carrying out ACR studies, bioconversion of L-arabinose in the real pretreated process solution was tested using the one-pot two-step reaction in batch mode. A reaction using model solutes instead of depolymerised SBP was performed as well to examine the effects that the pretreatment liquor would have on the enzyme kinetics. Finally, a reaction in a shake flask was also set up, to further investigate the effect of scale L-gluco-heptulose production. The HPA and L-gluco-heptulose concentrations obtained by this set of experiments are reported in Figure 6.25. Panels (a) and (c) show the small-scale reaction (1.2 mL) which had previously (Figure 6.11) shown to be the most effective reaction vessel. Panels (b) and (d), on the other hand, show the reaction carried out at flask scale (50mL). HPA and L-gluco-heptulose concentration are shown in the top and bottom panels, respectively, over a 24-hour reaction period.

Panels (a) and (c) show how at 1.2 mL scale, enzymes appear to perform similarly regardless of the source of L-arabinose. At scale however, final concentrations as well as initial reaction rates appear slower than at small scale corroborating what was observed in Section 6.3.2.2. Despite this, TK activity did not seem to be affected by the pretreated material; TAm, on the other hand, appears to have a slightly faster reaction with pretreated material. However, the initial concentration was also higher, possibly caused by slightly later sampling

Whilst model solutes were resuspended in a pure solution of buffer, the pretreated material was pH neutralised using KOH (Cárdenas-Fernández *et al.*, 2018) leading to a higher salt concentration. Indeed increased salt concentration can be detrimental to enzymatic performance; however an argument for thermostable enzymes is that beyond tolerating high heat they also are stable in harsher reaction conditions (Mathew *et al.*, 2016; Ferrandi *et al.*, 2017). For example, a thermostable TAm from *Halomonas elongata* was found to not only be stable at 50 °C but also handle up to 20% cosolvents. The taurine-pyruvate TAm mentioned in Section 6.1 from *Geobacillus themodenitrificans* also shows good stability in solvents. Lorilliere and coworkers (2016) showed that their TK, isolated from *Geobacillus stearothermophilus* was also stable in ionic liquids as well as high temperatures (Cerioli *et al.*, 2015; Chen *et al.*, 2016; Lorillière *et al.*, 2017).

Figure 6.26 also identifies the likely cause of the lower conversion in shake flask: cell lysate precipitation. Since the thermostable enzymes were not purified, the clarified cell lysates used contained a range of other proteins and cell debris which likely denatured and aggregated at 50 °C. Within this process the active enzymes could have likely precipitated out as well. In a well-mixed environment, such as the small centrifuge tubes used for the 1.2 mL reactions, the extent of the precipitation may have been lower, leading to better dispersion, and hence more active enzymes. Indeed, no precipitate was seen in the small-scale reactors or the ACR. At the end of the 24-hour reaction, it appeared that using the depolymerised SBP feed led to more precipitation. It could be that the presence of additional salts from the pretreatment and enzymatic steps prior to the bioconversion lead to increased precipitation. However, this effect was not quantified, and the reaction employing depolymerised SBP appeared to achieve only marginally lower L-gluco-heptulose yields (Figure 6.25, panel (d)). This possible increased precipitation could be a further argument for utilising a well-mixed reaction system at production scale.

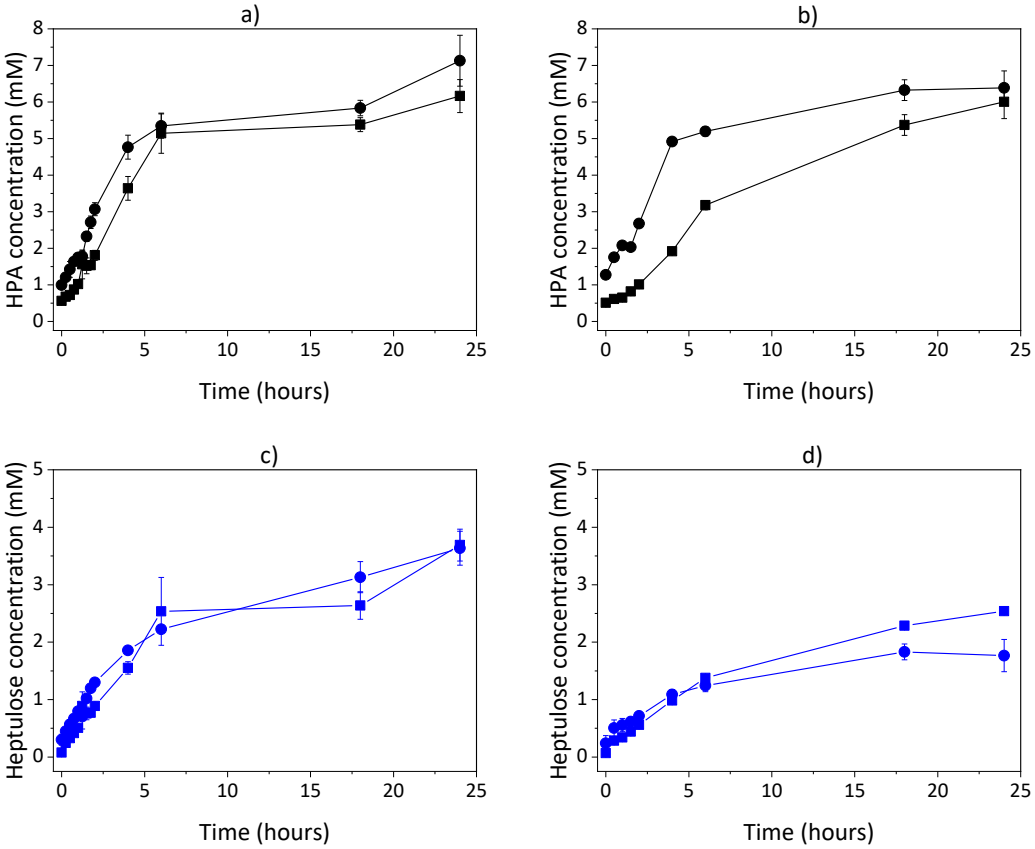

Figure 6.25. Comparison of batch reaction kinetics using depolymerised SBP and model solutes for the one-pot two-step L-gluco-heptulose production reaction.HPA concentration, in black in panels (a) and (b), and L-gluco-heptulose concentration, in blue in panels (c) and (d) were obtained for the one-pot two-step reaction using Model solutes (■) or the depolymerised SBP (●). Reactions were performed either at 1.2 mL scale, in panels (a) and (c) or 50 mL scale, in panels (b) and (d). Error bars denote SEM (n=2). Experiments performed as described in Section 2.4.2.4

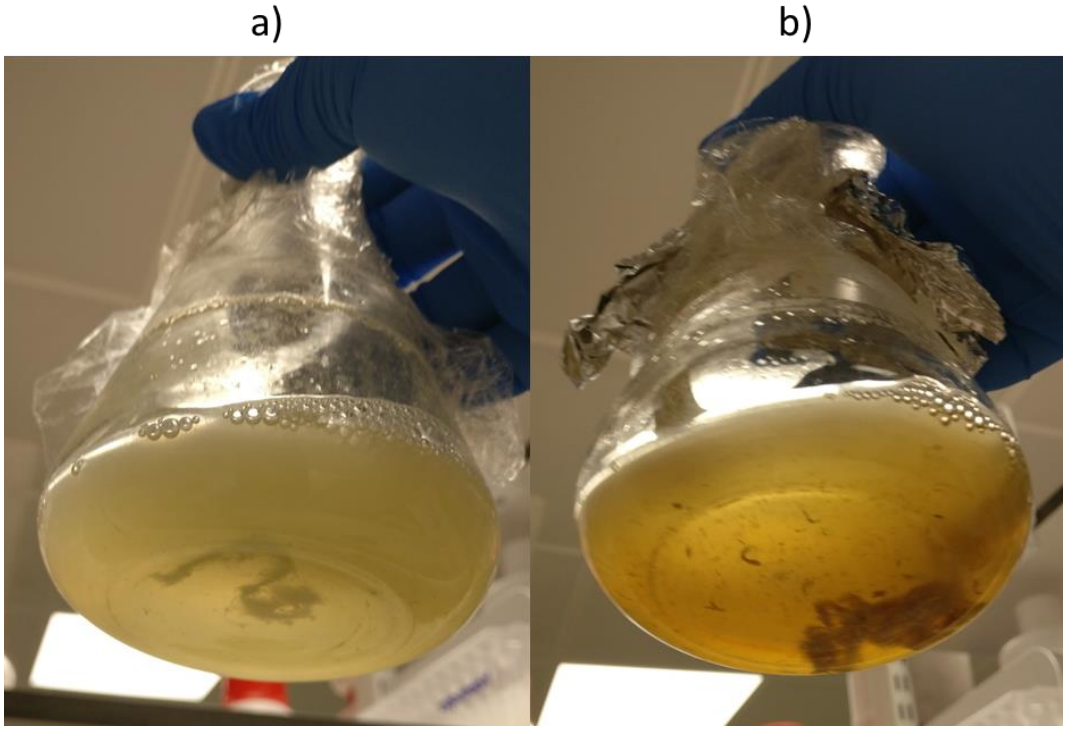

Figure 6.26. Photograph of the shake flasks used for large scale, one-pot two-step production of L-gluco-heptulose. Appearance of the reaction mix for the one-pot two-step reaction using model solutes (a) and pretreated SBP (b) is shown side by side indicating increased precipitation in the reaction containing the SBP material. Pictures were taken at the end of the 24-hour reaction period. Experiments performed as described in Section 2.4.2.4

6.3.5.2 Continuous production of L-gluco-heptulose from SBP-derived L-arabinose

Having established that employing the pretreated and depolymerised SBP as an L-arabinose feedstock did not appear to hinder the individual or combined activities of TAm and TK, the bioconversion was established in continuous mode in the ACR. As stated in Section 6.3.5.1, the substrate feed stream was composed of pretreated and depolymerised SBP supplemented with HEPES buffer salts, L-serine and α-ketoglutaric acid. The model solutes were pumped through the ACR first, and after steady state was reached the model solutes stream was switched with the pretreated SBP material.

Figure 6.27 shows the time-course of a representative experiment from the initial injection of enzyme feed at time 0 to the final sampling point. The pink rectangle highlights the steady state HPA and L-gluco-heptulose concentrations obtained with model solutes; and the green rectangle highlights the concentrations obtained with the pretreated material at the same initial substrate concentrations. Figure 6.27, displays the successful production of L-gluco-heptulose from a renewable L-arabinose feedstock in continuous mode. The system performed over several hours without blockages or visible precipitation. This suggests that the ACR provided a mixing regime able to prevent precipitation, a challenge that reduced bioconversion yields in larger scale batch reactions (Section 6.3.2.2). Interestingly, product concentration appears to increase when the model solutes are switched to pretreated materials. The averaged (over 5 steady-state time-points) HPA and L-gluco-heptulose concentrations were 1.21 mM (SEM =0.054) and 2.62 mM (SEM = 0.062), whilst L-gluco-heptulose were 0.31 (SEM = 0.015) mM and 0.60 (SEM = 0.014) mM for the model solutes and pretreated material, respectively.

The increase in conversion seen in pretreated SBP was not observed in the batch work described in Figure 6.25, where the model solute performance matched quite closely with the pretreated material both in the initial rate of reaction and the final concentration. Table 6.10 shows how the HPA and L-gluco-heptulose batch conversions after 2 hours compared with the flow reaction. Both the 1.2 mL well mixed, as well as the 50 mL reaction, that showed considerable precipitation, are included. Despite this, the batch reactions, which had previously predicted L-gluco-heptulose ACR conversions, did not appear to successfully match the conversions obtained in this ACR run.

The L-gluco-heptulose concentration in the ACR reaction was lower than the flask reactions, whilst HPA was more closely matched with the batch reactions, whilst in previous experiments, the ACR outperformed the batch reactions (Table 6.8). However, it is important to note that the batch reaction work was carried out with enzymes prepared on a different date and some variability between batches has been noted as demonstrated by the different results obtained as shown in Table 6.8.

The ACR reaction outlined in Figure 6.27 demonstrated how it is possible to produce in continuous mode a high value compound derived from a sustainable feedstock. The concentrations obtained, although higher than the model solutes version, were lower than what was obtained in previous ACR experiments. Indeed, with a starting concentration of 14 mM of L-serine, α-ketoglutaric acid and L-arabinose only 2.62 mM and 0.60 mM of HPA and L-gluco-heptulose was obtained; resulting in yields of 18.7% $mol.mol^{-1}$ of HPA on L-serine and 4.3% $mol.mol^{-1}$ of L-gluco-heptulose on L-arabinose. In future runs, a number of improvements could be applied to the reaction system to result in better yields and final higher product concentrations.

Figure 6.9 showed how increasing the concentration of enzymes led to faster reaction rates. Higher concentrations of catalyst were not employed in the ACR to limit the proportion of the total flowrate rate taken up by the *enzyme feed*. However, it is possible to obtain more concentrated enzyme solutions. This can be achieved by improving the enzyme production stage or by implementing a series of purification and concentration steps. These solutions are discussed to a greater extent in Section 6.3.3. A solution to increasing the enzyme concentration of the clarified cell lysate used in this study could have been the implementation of a vacuum evaporation step, or an ultrafiltration step. The latter option would also allow the possibility of running a diafiltration stage which could exchange the lysis buffer with a reaction buffer, thereby removing some cell debris, which was linked to some precipitation in Figure 6.26.

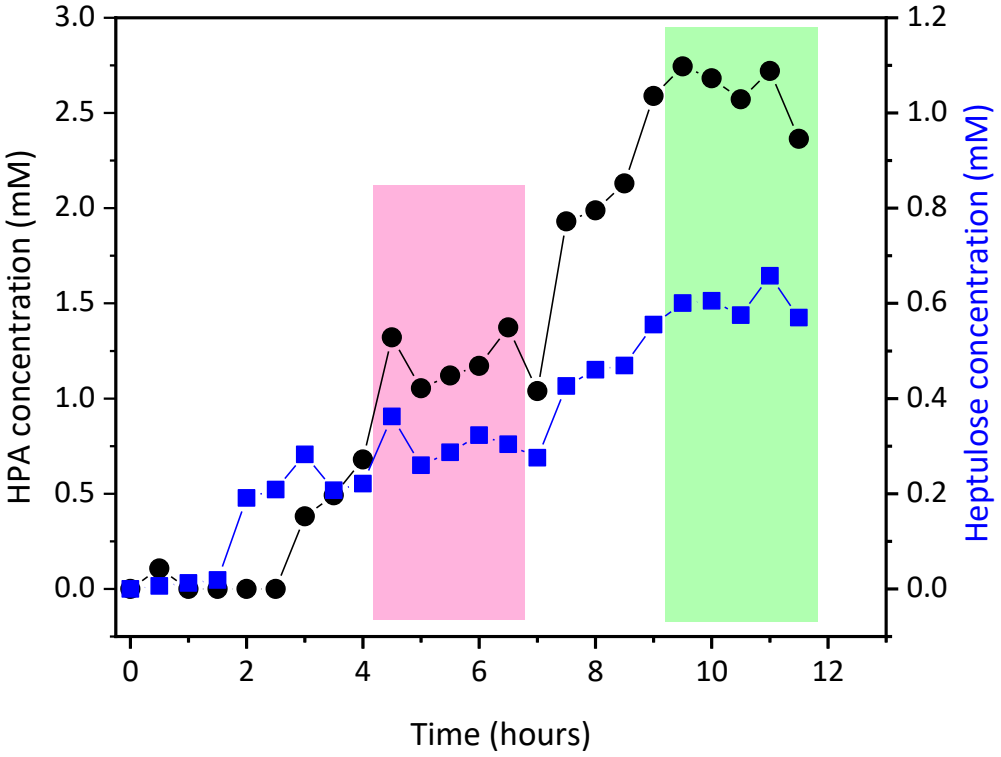

Figure 6.27 Continuous production of L-gluco-heptulose from one-pot two-step TAm-TK reaction system using model solutes and pretreated SBP. HPA (●, in black) and L-gluco-heptulose (■, in blue) concentrations are shown on separate y-axes. Two substrate feeds were used consecutively: model solutes consisting of 14 mM L-serine, 14 mM α-ketoglutaric acid, and 14 mM L-arabinose; and steam pretreated and depolymerised SBP with the addition of 14 mM L-serine and 14 mM α-ketoglutaric acid. The concentrations obtained with the first set of conditions are shown in the pink rectangle, whilst the green rectangle shows the concentrations obtained from the second set of conditions. Reaction performed as outlined in Section 2.4.2.6.

Table 6.9 Steady state HPA and L-gluco-heptulose concentrations using model solutes and pretreated and depolymerised SBP. Values calculated based on product concentration obtained in Figure 6.27.

Model solutes			Pretreated and depolymerised SBP		
	L-gluco-heptulose (mM)	**HPA (mM)**		**L-gluco-heptulose (mM)**	**HPA (mM)**
Average	0.31	1.21	**Average**	0.60	2.62
SEM (n=5)	0.015	0.054	**SEM** (n=5)	0.014	0.062

Table 6.10 Comparison of ACR steady state product concentrations with those obtained in a batch bioconversion after 2 hours. Batch conversion data, at 1.2 mL and 50 mL scale, are compared to the ACR values obtained for the bioconversions utilising model solutes and depolymerised SBP.The figure from which the values are obtained is also indicated.

	Model Solutes			Pretreated SBP		
Experiment	ACR	Batch 1.2 mL	Batch 50 mL	ACR	Batch 1.2 mL	Batch 50 mL
Reference	Figure 6.27	Figure 6.25	Figure 6.25	Figure 6.27	Figure 6.25	Figure 6.25
HPA (mM)	1.21	1.81	0.71	2.62	3.07	2.67
L-gluco-heptulose (mM)	0.31	0.89	0.56	0.60	1.30	1.01

Alternatively, increasing the concentration of substrates employed could lead to better bioconversions. Despite the ACR experiment in Section 6.3.5.2, using 14 mM of L-serine and α-ketoglutaric acid instead of the 10 mM used in the first and second ACR reactions, the amount of HPA and L-gluco-heptulose produced was reduced. Indeed, as shown in Section 6.3.1.4 increasing α-ketoglutaric acid concentration could be detrimental, whilst increased L-serine concentration did not impact the initial reaction rate for the production of HPA. Increasing L-arabinose concentration is, on the other hand, likely to increase the final L-gluco-heptulose concentration. To do this, the pretreated and depolymerised L-arabinose stream would have to be more concentrated. This could be done via vacuum evaporation, whereby water is boiled off at reduced pressure. The advantage of this technique is that vacuum pans are widely used in the Wissington sugar refinery already (Section 1.2.2). Alternatively, a membrane concentration step using a nanofiltration or reverse osmosis step could be employed (Malmali, Stickel and Wickramasinghe, 2014). The challenge of these techniques is that they would concentrate the L-arabinose as well as any other salts or process impurities present in the depolymerised SBP stream. However, these compounds could be removed, if required, via purification through ion exchange chromatography, activated charcoal adsorption or carbonatation. The last of these options, is a precipitation step which is also already employed in sugar refineries as outlined in Section 1.2.2.

6.4 Summary

The aim of this final results chapter was to demonstrate the potential for the scalable one-pot two-step enzymatic production of L-gluco-heptulose, employing TAm and TK enzymes, in a continuous flow reactor. This was achieved for ACR operation both with model substrate solutions (Figure 6.23) and a real SBP-derived feed stream (Figure 6.27).

To avoid microbial contamination in the sugar rich feeds from agricultural waste utilisation, thermostable enzymes, able to operate above physiological temperatures, were investigated for use in a one-pot two-step reaction system (Section 6.3.1.1). Thermostable TAm and TK enzymes were initially characterised in individual bioconversion reactions (Section 6.3.1). TAm used L-serine and α-ketoglutaric acid to produce L-glutamate and HPA, whilst TK employed HPA and L-arabinose to yield L-gluco-heptulose and CO_2. Stability across temperature (37 °C – 60 °C) and a range of pHs (6.5-8.5) was shown for both enzymes. Increasing L-serine and L-arabinose concentrations 10-fold (from 10 to 100 mM) lead to 1.7

and 6.1 times faster initial reaction rates. Increases in α-ketoglutaric acid and HPA concentrations, on the other hand, did not appear to be beneficial to conversions.

Following study of the individual bioconversions, a one-pot two-step reaction in batch was demonstrated (Figure 6.10), successfully bypassing the need for expensive and heat labile HPA addition. In reactions carried out at 50 mL scale, aggregation of the cell lysate was observed, leading to lower conversion than in the well-mixed 1.2 mL reaction system.

Immobilization of the enzymes was then studied on two different supports: Ni-NTA and ECR resins. The clarified cell lysate loaded directly onto Ni-NTA resin showed good conversion of TK and showed that one-pot two-step reaction in presence of HPA, performs better than the stand-alone TK reaction, suggesting a synergistic effect between the enzymes. This was shown, despite the stand-alone TAm reaction yielding only trace amounts of HPA (Figure 6.13). His-tag purified TK, immobilized onto ECR produced higher concentrations of L-gluco-heptulose than the TK immobilized directly onto the Ni-NTA support, indicating that purity of the enzyme was an important aspect in the success of the immobilization procedure (Figure 6.15 (c) and Figure 6.13 (c)). The immobilization of Tam onto ECR proved challenging, with additional incubation with TAm cofactor PLP giving only marginal improvements in TAm performance (Figure 6.19).

The one-pot two-step reaction was successfully translated from batch to continuous flow mode in the ACR in Section 6.3.4. The L-gluco-heptulose concentration obtained in the ACR, using a 2-hour residence time matched the batch bioconversions after 2 hours of reaction. The ACR HPA concentrations that were obtained were higher than in batch systems. This suggested that the ACR configuration improved HPA yields without hindering final L-gluco-heptulose yields (Section 6.3.4.3). In a biorefinery context, HPA production could become a further product stream so increases in yield of both intermediate and final product were desirable.

Reactions with the pretreated materials performed similarly to the model solutes, demonstrating the ability of the thermostable enzymes to handle the presence of salts and pretreatment byproducts.

Finally, pretreated and depolymerised SBP was used for the first time in the upgrading of L-arabinose, both in batch (Figure 6.25) and in a continuous flow enzymatic reactor (Figure 6.27). The ACR operation was stable and moved between different steady states with step

changes in substrate concentration. Final yields were 18.7% mol.mol^{-1} of HPA on L-serine and 4.3% mol.mol^{-1} of L-gluco-heptulose on L-arabinose.

A discussion on how to improve final L-gluco-heptulose yields was presented in Section 6.3.5.2. Possible solutions revoled around increasing enzyme or L-arabinose loading in the reaction. A possible alternative to a concentration step would be to obtain a more concentrated pretreated feed material. This would be the most preferable solution as it would bypass the need for additional unit operations. Work in Chapter 4, Section 4.3.3.5 showed how the ACR was able to handle solids effectively, up to 50 $g_{SBP}.L^{-1}$. Potentially the ACR and its larger versions such as the ATR and RTR could handle even higher SBP concentrations without sacrificing L-arabinose release yields, resulting in a more concentrated arabinan stream, which could then be depolymerised by AraF and then used in the one-pot two-step conversion of L-arabinose into L-gluco-heptulose.

Future work could focus on increasing final L-gluco-heptulose concentrations by increasing enzyme loading and increasing initial L-arabinose concentration in the pretreated material. These are discussed further in Chapter 7.

7

General conclusions and future work

7.1 General Conclusions

Increased interest in sustainably produced and sourced chemical feedstocks has spurred work in the effective pretreatment of agricultural waste such as SBP (Section 1.1). There is also growing interest in the utilisation in biocatalytic reactions for creation of higher value-added products due to their advantages over chemical catalysts (Section 1.4). With the use of biocatalysts, however, comes the need for developing more intensified continuous processes compatible for use in a biorefinery context (Section 1.5). The aim of this work was to establish a scalable process for the pretreatment of SBP and the conversion of one of SBP's most abundant sugars, L-arabinose, into higher value product (Section 1.6). This has been achieved through creation of a continuous acidic pretreatment step and a two-step enzymatic conversion of L-arabinose into L-gluco-heptulose. Key findings related to the objectives outlined in Section 1.7 and their importance are detailed in the following subsections.

7.1.1 System and continuous flow reactor characterisation

As mentioned in Section 1.5, translating operations from batch to flow mode could provide advantages such as reduced hazards and increased productivity. However, prior to studying specific reactions the first objective involved the engineering characterisation of the experimental system to be studied and the reactor being used.

In Section 3.3.1.1, the SBP slurry rheology was characterised to determine potential challenges in continuous pretreatment operations. It was found that higher solids concentrations up to 10% w/v led to rapid increases in viscosity from 0.0011 Pa.s to 0.0339 Pa.s. It was also determined that the slurry exhibited shear thinning behaviour, which was especially noticeable at larger solids concentrations. A series of quadratic correlations were developed that enabled the viscosity to be predicted from SBP loading and shear rate (Figure 3.2).

Next, the ACR, a continuous reactor made up of 10 inter-connected cells, was characterised as described in in Section 3.3.2. An RTD study using a solid-free system was employed. It was found that the equivalent number of tanks, N, a measure of plug flow characteristics in the reactor, increased with agitation rate (Section 3.3.2.3). At the optimized agitation rate of 6 Hz the ACR appeared to operate as 13 CSTRs in series. Flowrate, on the other hand, was not

found to affect N significantly (Table 3.1). Viscosity which was matched to SBP slurry viscosities equivalent to up to 10% w_{SBP}/v did not appear to have an effect on N, either, suggesting that the reactor would provide a satisfactory flow regime to the liquid-solid slurry used in pretreatment reactions (Table 3.4).

It was then shown for the first time that the ACR could be operated with a slurry of up to 2% w/v SBP solids, in Section 3.3.3. No blockages or challenges in the solid handling of the reactor were noticed. Interestingly, novel data obtained using laser diffraction, suggested that small particles in the slurry could exit the reactor more rapidly than large particles (Figure 3.15). Despite this, steady state operation with constant PSD was observed over a longer usage time as shown in Figure 3.16.

Overall, Chapter 3 demonstrated that despite the challenges present in handling viscous slurries, the ACR could deal with them effectively making it a suitable reactor for study of SBP pretreatment.

7.1.2 SBP pretreatment options and kinetics

In Chapter 4 dilute acid pretreatment for the solubilisation of SBP sugars was investigated. Initial experiments, in Section 4.3.1, established the importance of acid concentration and temperature for the solubilisation of polymeric and monomeric L-arabinose and D-galacturonic acid from SBP. Furthermore, they showed the importance of the particle size on the solubilization of sugars (Figure 4.4). Interestingly, it was found that whole SBP released more sugars than the coarsely ground powders, suggesting the action of the ball mill on the SBP cossettess reduced the accessibility of the acid to the polysaccharide structure to be solubilised.

Initial studies focused on batch reactions and the use of DoE to study the experimental design space (Section 4.3.2). This revealed the importance of acid concentration and temperature, as well as highlighting the effect of time. It was also found that, whilst in some conditions more than 70% w/v of L-arabinose (e.g. 73% w/w and 84% w/w at 100 mM H_2SO_4, 2% w/v SBP, 80 °C at 30 and 60 min respectively) and 36% w/v D-galacturonic acid (50 mM H_2SO_4, 4% w/v SBP, 70 °C and 30 min) could be solubilised, D-glucose was hardly released (always less than < 8% w/w) into the liquid fraction within the parameters in the design range. This was attributed to the more rigid structure of cellulose compared to arabinans and polygalacturonans (Section 1.3.1). The selective solubilisation of arabinans and

polygalacturonans could be employed to fractionate the SBP material and create multiple product streams to be used in different valorisation reactions.

The batch reactions were then translated into continuous hydrolysis operations in the ACR as described in Section 4.3.3. This is the first example of any agricultural byproduct being processed in the ACR. Here it was found that temperature and acid concentration had an effect on solubilisation of L-arabinose and D-galactose (Figure 4.5 and Figure 4.8). Only traces of D-glucose were obtained, whereas D-galacturonic acid yields remained more constant at around 20-25% w/w across the range studied, SBP concentration did not appear to have an effect on yields in the range of 1-5% w/v demonstrating again good mixing of the ACR. At 4% w/v, 80 °C and and 75 mM H_2SO_4 approximately 70% w/w yield of L-arabinose was obtained (Figure 4.12).

The continuous pretreatment results were compared with steam explosion results from Hamley-Bennett et al. (2016). The two pretreatment methods, which used the same batch of SBP, had a comparable L-arabinose throughput. However, when accounting for reactor productivity, the ACR appeared to be almost an order of magnitude better (Table 4.8); highlighting again the effectiveness of the ACR as a pretreatment reactor.

Preliminary enzymatic depolymerisation work in the ACR, discussed in Section 4.3.4.2, showed that AraF was capable of selectively hydrolysing arabinans into L-arabinose. Within 30 minutes, 90% w/w of arabinans had been hydrolysed (Figure 4.15). This reaction showed promise especially, if coupled with AraF immobilization techniques developed by Cardenas-Fernandes et al. (2018) (Section 1.3.4).

7.1.3 Large scale production and purification of enzymes

The next objective was to investigate the scalable production, recovery and purification of TAm and TK enzymes to be used in subsequent continuous ACR biocatalytic upgrading of L-arabinose. In Section 5.3.1, *E. coli*-BL21 (DE3)-TAm and *E. coli*-BL21 (DE3)-TK strains were studied. The TAm and TK enzymes production was improved by optimising the medium (Figure 5.1) and the induction time (Figure 5.2). This resulted in fermentations with 50-fold increase in biomass production (from 400 mL to 20 L). Enzyme production was also scaled from flasks to a 30L fermenter in an attempt to make a first step towards an optimised large scale production process (Figure 5.4).

In Section 5.3.2, two cell disruption techniques, sonication and homogenisation, were found to be comparable at equivalent enzyme loadings in both initial rate and final bioconversion; producing 5.3 mM and 5.7 mM of HPA and 4.5 mM and 4.2 mM of of L-gluco-heptulose for sonication and homogenisation, respectively (Figure 5.7). Heat precipitation was studied as a scalable and cheaper alternative to His-tag purification. A 10 minute incubation at 50 °C resulted in partially purified preparations. The heat purified TAm had 2.1 times less total protein than the clarified cell lysate, whilst TK had a 3.1-fold protein reduction (Figure 5.10). When heat and His-tag purified TK was immobilized on the same resin support, the His-tag material performed better, obtaining 3.3 mM and 1.75 m of final L-gluco-heptulose (Figure 5.11), respectively. The lower conversion yield was attributed to the presence of other proteins in the HP material. Despite this, the more scalable heat treatment step could provide a source of cheap partially purified enzymes.

Overall, this chapter highlighted some important aspects of the biocatalyst production, an important step in the translation of a project from laboratory to industrial setting.

7.1.4 One-pot two-step production of L-gluco-heptulose

The final objective was to characterize the upgrading of SBP-derived L-arabinose into L-gluco-heptulose via a one-pot two-step TAm and TK reaction (Section 6.3.1.1 and reaction scheme in Figure 6.3). Thermostable TAm and TK enzymes were selected. Firstly, in a continuous industrial operation, this would allow the L-arabinose upgrading without requiring excessive cooling. Secondly, operating at higher temperatures would minimise microorganism contamination in the sugar-rich pretreated fractions. Initial work on the single enzyme reactions showed that the TK enzyme appeared to have a temperature optimum between 50 °C and 60 °C, and indeed showed some microbial contamination at 37 °C (Figure 6.5).

It was found that the synthetic HPA, needed for a single enzyme TK upgrading of L-arabinose which was heat labile and disappeared quickly after the start of the reaction (Figure 6.2). To overcome this, a TAm reaction was studied instead for its *in-situ* production based on the conversion of L-serine and α-ketoglutaric acid into HPA and L-glutamate. It was found that increasing L-arabinose and L-serine concentration had no inhibitory effects on the reaction kinetics, whilst α-ketoglutaric acid and HPA concentration increases did not yield higher product concentration to the respective reactions beyond concentrations of 10 mM and 33 mM, respectively (Figure 6.7 and Figure 6.8).

In Section 6.3.2 , the one-pot two-step system was studied in batch at small scale where it was revealed that increasing substrate concentration from 10 mM L-serine, 10 mM α-ketoglutaric acid and 33 mM L-arabinose to 100 mM of each substrate led to an 1.8-fold increase in TAm reaction rate and 2.3-fold increase in TK reaction rate (Figure 6.10 6.10), and the increase in final L-gluco-heptulose yield was 2-fold.

As described in Section 6.1, enzyme immobilization enables the reuse of catalyst and could enable higher enzyme loadings in a continuous reactor. Here, immobilization of TAm and TK was studied on two supports as described in Section 6.3.3. Immobilization onto Ni-NTA resin, by exploiting the His-tags on the TAm and TK enzymes showed a successful production of L-gluco-heptulose (2.4 mM after 24 hours). HPA was produced in the initial phases of the reaction (up to 2.7 mM), but its concentration quickly diminished over time. Most notably the one-pot two-step reaction with immobilised enzymes (Figure 6.15), , produced more L-gluco-heptulose than the stand-alone TK reaction (4.7 mM instead of 2.4 mm after 24 hours). This highlights the potential synergies of the two enzymes over the utilization of synthetic Li-HPA. Immobilization of His-tag purified TAm and TK on an epoxymethacrylate resin was attempted next (Section 6.3.3.2). Immobilized TK successfully converted L-arabinose to L-gluco-heptulose (3.1 mM after 24 hours). However, no detectable amount of HPA was produced by the TAm reaction (Figure 6.15). Small amounts of HPA (0.5 mM at 24 hours) could be detected when the TAm cell lysate was incubated with the resin in presence of TAm cofactor, PLP. The immobilization studies showed that TK was successfully immobilized, but TAm could only be immobilized with very low levels of retained activity. Consequently, the decision was taken to focus on the use of soluble enzymes to demonstrate the continuous one-pot two-step production of L-gluco-heptulose from SBP derived L-arabinose.

The one-pot two-step reaction was performed in continuous mode in the ACR without the use of immobilized enzymes. The residence time was set to 2 hours. The increase in HPA concentration at the beginning of the reaction was fitted to model for 10 tanks-in-series model, showing good comparability and suggesting good flow characteristics (Figure 6.22). HPA and L-gluco-heptulose were successfully produced from model solutes. L-gluco-heptulose concentrations reached 2.4 mM and 1.2 mM, respectively, with a starting concentration of 10 mM L-serine, 10 mM α-ketoglutaric acid and 33 mM L-arabinose. Increasing the concentration of substrates to 100 mM each of L-serine, α-ketoglutaric acid and L-arabinose resulted in a final L-gluco-heptulose concentration of 2.4 mM and a concentration of intermediate HPA of 12.3 mM. The throughputs for L-gluco-heptulose and

HPA were 76.1 μM.hr^{-1} and 311.6 μM.hr^{-1} at the lower substrate concentration level and 158.7 μM.hr^{-1} and 790.0 μM.hr^{-1} at the higher substrate level. L-gluco-heptulose concentration was very closely predicted by 2-hour batch bioconversions. It was found that HPA, on the other hand, was underpredicted by the batch reaction. The likely cause of HPA overproduction in the ACR was attributed to the reactor configuration preventing CO_2 release and driving the equilibrium towards HPA (Figure 6.23 and Table 6.8).

In Section 6.3.5, steam exploded and AraF depolymerised SBP was used as an L-arabinose feed and L-gluco-heptulose was produced from SBP derived L-arabinose for the first time. The feed solution resulted in substrate concentrations of 14 mM of each L-serine, α-ketoglutaric acid and L-arabinose. In batch, the TAm and TK enzymes appeared to perform equally well using model solutes at the same initial concentration level and real SBP derived feed (Figure 6.25). Finally, a continuous reaction was carried out with the real SBP feed in the ACR. This experiment successfully demonstrated the possibility of using an agricultural byproduct to produce value added compounds through a combination of physicochemical and enzymatic treatments. 2.62 mM of HPA and 0.60 mM of L-gluco-heptulose were obtained. This was higher than the 1.25 mM of HPA and 0.31 mM of L-gluco-heptulose obtained for the same reaction using model solutes (Figure 6.27 and Table 6.10).

Overall, this Thesis demonstrated the feasibility of using the ACR and enzymatic means to produce valuable fine chemicals from sustainably sourced chemical feedstocks.

7.2 Future work

Initial suggestions for future work focus on studies to further investigate some of the specific findings reported in this Thesis. These are listed and discussed below.

- Attempt further characterisation of the ACR, in terms of studying the RTD of SBP particles of differing sizes. Furthermore, the characterization work was limited to SBP loadings of 2% w/v (Figure 3.12) and the DAP studies used a maximum concentration of 5% w/v (Figure 4.13). Exploring higher SBP loading would enable more complete specification of the operating range of the continuous pretreatment process.
- The rheological properties of the pretreated SBP slurry could be characterized and compared to the untreated SBP slurry that was characterized in Section 3.3.1.1. Understanding the change in the rheology after pretreatment would expand the understanding of the reaction mechanism and allow for a greater understanding of the agitation requirements in the ACR. Pretreatment is likely to reduce viscosity but it may change the rheology of the liquid (Stickel *et al.*, 2009; Liu *et al.*, 2012)
- The ACR pretreatment system was limited by maximum allowable temperatures. However, more severe pretreatment conditions could be investigated both in terms of temperature and SBP concentration. If temperatures above 100 °C are desired, a backpressure regulator for the ACR, such as the one described by Deadmant et al. (2011) should be implemented.
- Once optimal pretreatment conditions are established the pretreatment reaction could be scaled up and performed in the ATR or the RTR (Section 1.5.2) using whole SBP. This would provide good insight into the scalability of the process.
- Investigate and optimise the use of immobilized AraF, as described by Cardenas-Fernandes et al. (2018), on pretreated SBP in continuous mode. This step would allow for the effective translation of all they processes into continuous mode, by using the ACR.
- Improve production of biocatalysts by exploring fermentation optimisation through the use of a more defined medium and an effective feeding strategy. A characterisation of the oxygen and nutrient requirements could also help improve the production of enzyme as described by Zhou et al. 2019.
- TAm and TK heat purification presented in Section 5.3.3.1 showed that some activity loss occurred. Similarly, some HCPs remained. Developing this step further by

examining factors such as buffer and salt type and concentration to aid in the selective precipitation would produce a more fractionated product stream.

- Explore different enzyme immobilization techniques specifically for TAm in order to obtain an active immobilized TAm preparation. This would enable the study of more intensive flow reactions by facilitating greater enzyme loading within the the ACR.
- Characterise the TAm and TK catalysed reactions further. This includes possible characterizing product and substrate inhibitions as well as obtaining K_m and k_{car} parameters for both enzymes. His-tag purification could be used to study the enzymes in their purified form. Knowing their Michaelis-Menten kinetic parameters as well as inhibitory effect would enable modelling of the reaction in both batch and continuous mode.
- Carry out one-pot two-step reaction using immobilized TAm and TK in continuous flow mode. Include within this study the possibility of retaining enzymes within the catalyst basket agitators (Figure 3.10) and characterise ACR performance in terms of its RTD and mixing as discussed in Sections 3.3.3.

In addition, it is interesting to explore the wider context of the research. Some possible topics to be investigated are listed and discussed below:

- Utilize reaction systems such as the Bourne reaction to characterize the micromixing environment in the ACR (Section 3.3.2.5), to choose operational conditions that provide good plug flow characteristics as well as good mixing.
- Use the same pretreatment techniques developed here to pretreat other lignocellulosic material. SBP was of particular interest due to its low lignin content so it could be beneficial to understand the effect that increased lignin content could have on DAP effectiveness in the ACR.
- Explore different biocatalytic reactions for the upgrading of other SBP components such as D-galacturonic acid. For example D-galacturonic acid could be used in a TAm mediated reaction to produce polyhydroxyazepanes (as shown Figure 1.8) (Andreana *et al.*, 2002).
- The ACR reactor is supplied with side-entry ports in each of the ten reaction cells. This allows for addition of material throughout the reaction. By furthering the understanding of the kinetics of the reaction studied here it could be possible to design a continuous reaction where depleted substrates are added throughout the reactor length.

- Couple the reactor RTD model with pretreatment and enzyme reaction kinetics to develop a computational model of the various steps of the process. This would enable optimization of the process *in silico* prior to real experimentation.
- For implementation of the reactions described in this Thesis it is important to carry out a techno-economic analysis of the proposed process. Within it, aspects such yields and conversions and possible revenues from side products (such as glutamate, as a byproduct of HPA formation), should be investigated. Alongside the techno-economic analysis a life cycle assessment could be carried out to ascertain the various environmental impacts of the whole process.

8

Evaluation of the scalability and commercialisation potential of this work[†]

[†] This chapter is included as part of the UCL requirements for award of the EngD in Biochemical Engineering.

8.1 Introduction

The work presented in this Thesis aimed to investigate the utilization of SBP sugars and the translation of relevant processes from batch to continuous mode. Briefly, in Chapter 3 the wide operational range of the ACR, employing the Coflore® mixing technology was established. In Chapter 4 the continuous pretreatment of SBP for the release of monosaccharides such as L-arabinose from agricultural waste streams was demonstrated. Finally, Chapter 6 demonstrated the ability to use the L-arabinose obtained from SBP in a two-enzyme biocatalytic cascade for the synthesis of a value-added pharmaceutical precursor.

This Chapter discusses how the work presented in this Thesis could find commercial applications and outlines the steps required to ensure a successful translation from laboratory research to industrial settings.

In Chapter 6 (Table 6.1) a case is made for studying the bioconversion of L-arabinose to L-gluco-heptulose. Namely, L-gluco-heptulose has potential therapeutic applications (Section 6.1) and its price at point of sale could be upwards of 10,000 EUR/g. Whilst demand for L-gluco-heptulose and 7-carbon sugars in general is modest, the pretreatment of SBP to obtain separate L-arabinose and D-glucose fractions is still of interest; other fermentative processes and some bulk chemical production processes may require cheap and renewable sources of monosaccharides e.g. D-glucose for bioethanol production. Further, the application of the Coflore® reactors (shown in Figure 8.1) for bioconversion of L-gluco-heptulose at different scales would prove useful to Active Pharmaceutical Ingredient (API) and fine chemical manufacturers, as the learnings obtained from the scaling of one biocatalytic reaction could be applied to other bioprocesses.

As such, the discussion on the scale-up and commercialisation of the work presented in this Thesis, will be divided into three sections: (1) Scaling and commercializing the continuous dilute acid and depolymerization reaction; (2) enzymatic upgrading of L-arabinose to L-gluco-heptulose; and (3) enzymatic production of platform and specialty chemicals from sugars derived from agricultural biomass or industrial waste streams.

Figure 8.1 Coflore® range of reactors. ACR (left, 100 mL volume), ATR (middle, 1-10L volume) and rotating tube reactor (right, 100L). Images taken from AM technology website (www.amt.uk).

8.2 Scaling and commercialization of the pretreatment process

The volumes of SBP handled by a sugar refinery would require pretreatment and subsequent utilization of the SBP to be carried out at large scale. As such, it is worthwhile considering the steps required to translate the SBP pretreatment work performed in the ACR to a full-scale commercial operation. As discussed in Section 7.2 further improvements to the reaction could be investigated at the ACR scale. Following optimisation, translation of the process to larger Coflore® reactors would provide additional insights to ensure a successful commercialization of the technology.

A main advantage of the dilute acid pretreatment, studied in 4.3.3, is that a good separation of arabinans and cellulose was obtained. An effective separation, with minimal carryover in the respective fractions, is desired as it would reduce downstream processing requirements. To achieve an even better separation and yield, specific reaction conditions such as acid concentration, temperature and time could be investigated further. Indeed, across the design space in the DoE work presented in Section 4.3.2, D-glucose carryover was minimal, indicating that the reaction severity could likely be increased further with increased fractionation efficiency. However, use of extreme pre-treatment conditions could lead to the production of inhibitors which could restrict the types of applications for the released sugars (Larsson *et al.*, 1999). Further it would also increase CoGs, and initial capital expenditure as sturdier equipment will be required to handle the more corrosive conditions.

Accessibility of the cellulosic fraction to enzymatic hydrolysis would also require investigation. Cellulose is harder to solubilise than pectin or hemicellulose, necessitating the use of cellulases (Sun and Cheng, 2002; Wildschut *et al.*, 2013). Within the Sustainable Chemical Feedstock group, some initial cellulose hydrolysis for bioethanol production was performed on steam exploded SBP, but further characterization of the process for the utilization of the insoluble SBP fraction from dilute acid pretreatment would have to be carried out. Processes for the hydrolysis of cellulose to D-glucose are well established in the literature hence good hydrolysis of the SBP-derived cellulose would be expected.

A further point of investigation for process improvement is the reaction throughput achievable in the ACR. Section 4.3.3.5 showed how increasing SBP loading from 2% w/w to 5% w/w had very little impact on yield, thus further increases in SBP concentration would improve throughput. This is of particular interest in a biorefinery context where minimising

water utilisation is imperative, due to the costs associated with treatment of process water (Modenbach and Nokes, 2012). Ultimately, increasing solid loading could result in an increase in throughput and simultaneously a lowering in costs through reduced waste-water treatment costs.

Once optimal conditions have been determined in the ACR at lab scale these could be translated to the ATR and RTR shown in Figure 8.1. The ACR presented some limitations however, such as the maximum temperature that was achievable in the laboratory setting (80 ° C) as well as the maximum particle size to flow through the reactors (particles were passed through a 212 µm sieve before use). Section 4.3.1.2 showed that smaller, milled particles led to better solubilisation of the L-arabinose. It also showed that the dried unmilled SBP cossettes also resulted in favourable yields, more so than coarsely milled particles. The dimensions of the ATR and RTR would permit studying the pretreatment reaction with whole cossettes, which would remove the energy requirements for drying and milling altogether. Reaction conditions would then have to be optimized again, given the different condition of the starting feedstock.

Similar steps could be carried out for the Arabinofuranosidase-mediated reaction to convert arabinans into L-arabinose (Section 4.3.4.2). This reaction was demonstrated in both the ACR and in a membrane reactor (Cárdenas-Fernández *et al.*, 2018) and could potentially be scaled up in both reactors. The downside of employing Coflore® reactors would be the limit on reaction times (as discussed in Section 6.3.5) which could be overcome by implementing higher enzyme loadings. Whilst it is likely that this would drive up costs, enzyme immobilization techniques such as those studied in Section 6.3.3, to enable long-term enzyme reuse could be considered to circumvent this.

A major challenge to commercial application of the SBP-to-sugars process is the possible high price of the final sugars at the end of the process. This can be determined by a techno-economic analysis following a successful translation of the pretreatment and depolymerisation steps to larger scale reactors. Successfully fractionating and valorising each stream, increasing throughput, reducing waste-water production, and reducing downstream cleaning requirements could all work to make the process financially sustainable. Following a successful assessment, scale up to the 100 L (working volume) system offered by AM Technology is plausible. However, to meet the demand of the hundreds of thousands of tons of SBP produced each year (Section 1.2.2) a larger reactor employing similar mixing would have to be developed for the commercial application.

8.3 Commercial application of enzymatic L-gluco-heptulose production

As discussed in Section 8.1 there would likely be a considerable difference in the production scale between a process to obtain sugars from biomass and the process to make a speciality chemical with possible pharmaceutical applications, such as L-gluco-heptulose, from L-arabinose. Further, the purity and hygienic production requirements for a fine chemical or an API may differ greatly from the upstream steps in a biomass fractionation process.

The smaller volume of biocatalytic reactions could be advantageous for possible commercial translation of the work presented here, as the current Coflore ® range would likely be able to fulfil demand for fine chemicals production. Thus, for the successful commercialization of the one-pot two-step production of L-gluco-heptulose several steps should be taken: optimize the reaction further; establish the demand for the product and possible by-products and validate production at the required scale.

Firstly, the reaction optimization should focus on increasing yields. This can be achieved through a wider screen of reaction conditions. For example, Section 6.3.1.5 discussed how increasing concentrations could lead to positive or negative effects on final yield and reaction rate depending on the substrate. Another avenue to improve the reaction is to increase reusability of the enzyme, thereby driving operating costs down and allowing higher enzyme concentrations to be used. Enzyme recycling could be obtained through further investigation of immobilization strategies (Section 6.3.3) or utilizing protein recovery systems such as ultrafiltration membranes. Another possible avenue is the possibility of using the side-entry ports present in the reactors to create a 'fed-continuous' system whereby the reaction conditions (such as pH or substrate concentrations) are kept at the optimum along the reactor. Indeed, as seen in Figure 6.7 increasing substrate concentration has a deleterious effect, so the gradual addition along the length of the reactor would prevent excessively high concentrations of substrates that are inhibitory. As discussed in Section 6.1 the one-pot two-step system was intended to avoid the expensive intermediate (such as HPA), as such the one-pot two-step reaction could also be scaled to the ATR and RTR as proof of concept without the need for large quantities of expensive substrates.

Further technical challenges to address are the purification of the final product, and the potential valorisation of the side products. Improving the conversion yield would reduce the need to separate the products from the substrates. However, it is likely that complete conversion may not be achieved and substrate and intermediate products such as HPA and

L-glutamate would likely be present in the product stream. These intermediate products are valuable themselves and could therefore be separated from L-gluco-heptulose. Substrates could also be recovered and recycled.

Table 8.1 shows all the components present in the one-pot two-step reaction. Based on the properties of the individual components, separation techniques can be used to obtain a pure L-gluco-heptulose stream. As shown in the proposed process in Figure 8.2, after exiting the ACR the enzymes involved in the reaction could be recovered and reused. Electrodialysis could be used to separate neutral compounds such as sugars and L-serine from charged compounds such as salts, L-glutamate and α-ketoglutaric acid. The charged components could also be valuable side-products and further chromatographic steps could separate and purify them. Residual salts and charged compounds remaining in the L-gluco-heptulose stream could then be run through a demineralisation step consisting of a Cation and Anion Exchange columns operated in flow through mode. These are widely used in the sugar industries to remove coloured compounds and minerals (Lutin, Bailly and Bar, 2002; Elmidaoui *et al.*, 2006). As discussed in Section 1.2.3, a chromatographic ion exchange step could then be used to separate the sugars. Commercially continuous technologies such as simulated moving bed can be used to separate molecules with very similar physicochemical properties such as D-fructose and D-glucose (Azevedo and Rodrigues, 2001; Lutin, Bailly and Bar, 2002; Aniceto and Silva, 2014). Alternatively, techniques such as continuous centrifugal partition chromatography, explored within the SCF group could also be employed to separate L-gluco-heptulose from L-arabinose and L-serine (Ward *et al.*, 2015). Finally, the purified and isolated L-gluco-heptulose could then be processed and formulated further depending on the final application.

Whilst developing and delivering a sound production process is important for the commercial translation of L-gluco-heptulose, a demand needs to be established for this product. Working with key industrial partners, as was done with the SCF group, could help find possible applications and markets for this product, as well as assess demand for any intermediates. Further, partners could provide insights into purity and hygienic requirements. Industrial collaborators could also have access to facilities and know-how to operate scale-up trials observing the required manufacturing standards.

For a successful commercialization of L-gluco-heptulose and its production process, the technical and business development aspects would have to be carried out simultaneously with insights from one helping shape the other. Since the commercial landscape for L-

Table 8.1. Properties of the components present in the conversion of L-arabinose to L-gluco-heptulose and possible methods for their recovery.

Component	Role	Description	Method of separation from main product	Reference
L-gluco-heptulose	Main product	Neutral, seven carbon sugar	-	-
L-glutamate	Side product	Positively charged amino acid	Electrodialysis, ion chromatography	(Lutin, Bailly and Bar, 2002; Tugtas, 2011)
HPA	Side product	Organic acid	Electrodialysis, ion chromatography	(Lutin, Bailly and Bar, 2002; Tugtas, 2011)
L-serine	Substrate	Neutral amino acid	Strong cation exchange	(Azevedo and Rodrigues, 2001; Lutin, Bailly and Bar, 2002; Ward, 2017)
α-ketoglutaric acid	Substrate	Organic acid	Electrodialysis, ion chromatography	(Lutin, Bailly and Bar, 2002; Tugtas, 2011)
L-arabinose	Substrate	Neutral, 5 carbon sugar	Strong cation exchange	(Azevedo and Rodrigues, 2001; Lutin, Bailly and Bar, 2002; Ward, 2017)
Enzymes	Catalyst	Large molecules composed of many amino acids	Ultrafiltration, centrifugation (if immobilized)	(Spagnuolo *et al.*, 1999)
Cofactors	Catalyst aid	Magnesium chloride and Phosphate coenzymes	Demineralisation	(Holzer, Goedde and Ulrich, 1961; Elmidaoui *et al.*, 2006)
Buffer salts	pH stabilisation	Buffer exchange	Demineralisation	(Elmidaoui *et al.*, 2006)

.

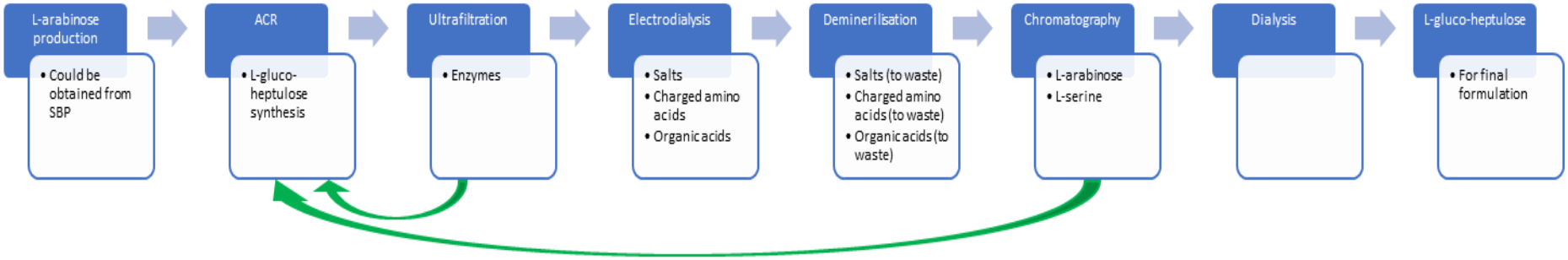

Figure 8.2. Proposed process for the purification of L-gluco-heptulose following biocatalytic synthesis in the ACR and methods for the recovery or reuse of the other reaction components. Green arrows indicate possible recycling routes.

gluco-heptulose is limited and uncertain, the next section will discuss a commercialization approach for a more general reaction scheme that uses sugars from sustainable feedstocks as building blocks for enzymatic reactions or fermentation processes.

8.4 Commercial application of upgrading of sugars from lignocellulosic materials

A critical aspect when considering the commercialization of the techniques developed in this Thesis is to consider the balance between the supply of raw material and demand of the final products. The work by the SCF group demonstrated that SBP can be effectively fractionated into a cellulose, a pectin and an arabinan stream. These polymers could then be monomerised chemoenzymatically to produce monomers. A suitable process would investigate the utilization of all the main components into specialty chemicals, for which there is a large demand.

D-glucose utilization is widely reported in the literature as the starting carbon source for cellulosic ethanol fermentation. On the other hand, L-arabinose and D-galacturonic acid have been less investigated (Section 1.4.5). These sugars could be either fermented or converted in enzymatic reactions. For example, Garcia Sanchez et al. (2010) genetically engineered a *Saccharomyces cerevisiae* to utilize L-arabinose, as a carbon source and produce ethanol. L-arabinose can also be converted through a fermentative process or a chemical hydrogenation to arabitol: a sweetener and a chemical building block (McMillan and Boynton, 1994; Kordowska-Wiater, 2015; Subrizi, Hailes and Lye, 2015). Similarly, D-galacturonic acid could also be used in fermentative or chemical reactions. A *Saccharomyces cerevisiae* strain and an edible strain of *Aspergillus* fungus have been engineered to accept D-galacturonic acid as a carbon source (Protzko *et al.*, 2018). This sugar acid could be converted to *meso*-galactaric acid, which have applications as sequestering agents and binders, corrosion inhibitors, biodegradable chelators for pharmaceuticals and pH regulators (Mehtiö *et al.*, 2015).

A proposed process for the complete transformation of SBP sugars into such platform chemicals is shown in Figure 8.3. SBP is first pretreated and fractionated as discussed in Chapter 4. This results in a solid cellulose fraction and a solubilised fraction consisting of arabinans and polygalacturonans. The cellulose can then be hydrolysed through the use of

cellulases resulting in D-glucose, which can then be used in the current bioethanol production facility within the sugar refinery on the ABSugar Wissington site (Section 1.2.2) to yield ethanol. A possible alternative could be the use of simultaneous saccharification and fermentation, whereby the cellulose hydrolysis and ethanol production occur in the same reactor. The solubilised stream is treated with AraF enzyme as discussed in Section 4.3.4.2, resulting in easily separated polygalacturonans and monomeric L-arabinose (Spagnuolo *et al.*, 1999; Cárdenas-Fernández *et al.*, 2018). D-galacturonic acid can then be obtained through the use of polygalacturonases. L-arabinose can then be used in either fermentative process to produce ethanol or enzymes, or for the production of arabitol. Similarly, D-galacturonic acid can be utilised in fermentative processes to obtain fungi, enzymes or ethanol, or for the production of *meso*-galactaric acid.

Some of the reactions within the proposed process could be carried out in continuous mode, for example the pretreatment and hydrolysis as well as biochemical or chemical means of producing arabitol or *meso*-galactaric acid. On the other hand, fermentation steps are more likely to be batch or semi-batch steps. Conversely, the edible fungus used in the commercial meat-replacement Quorn™ is a strain of *Fusarium venatum* and is grown in a continuous process (Finnigan *et al.*, 2019).

The specific steps in establishing a biorefinery process such as this one are similar to the steps discussed in previous sections. Namely, reaction conditions would have to be optimised, then reactions would have to be scaled. Meanwhile, demand for the products would need to be established and industrial partners that can help with the scaling and commercialization would have to be brought on board.

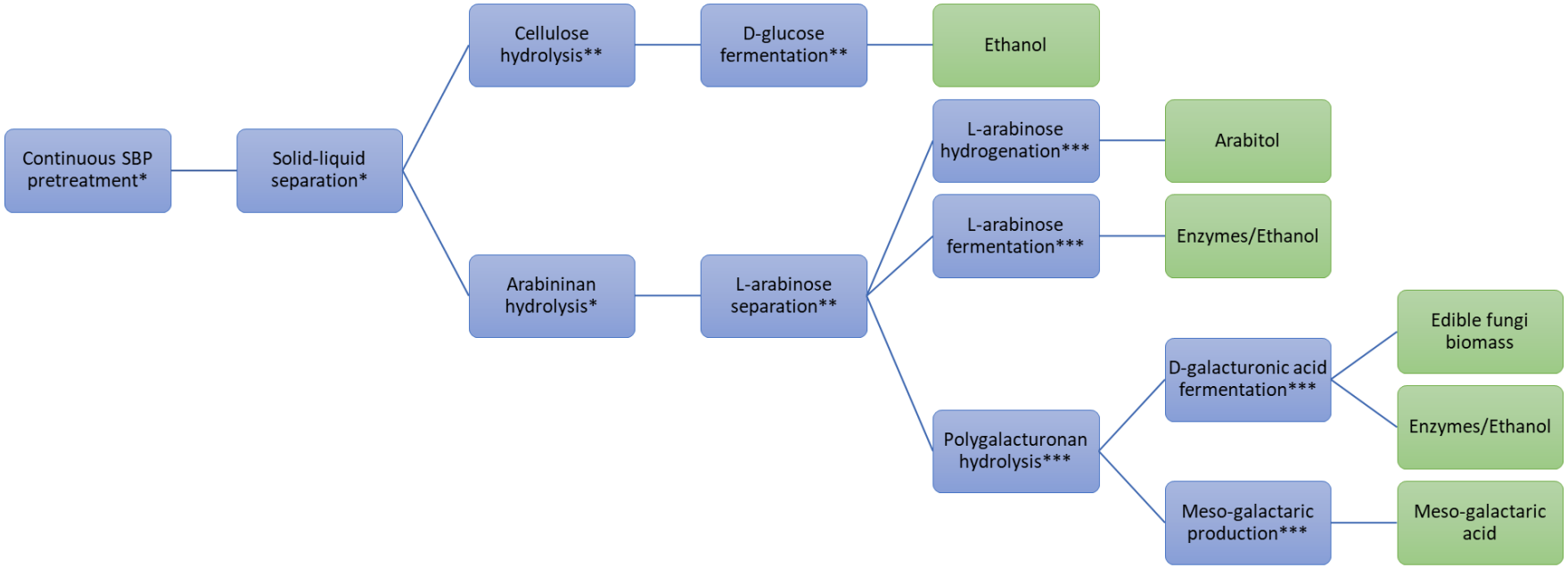

Figure 8.3 Proposed process for complete SBP fractionation and sugar utilisation to produce platform and specialty chemicals, and edible fungal biomass. Blue boxes represent the process steps, whilst green boxes represent final products. Boxes marked with * indicate work presented in this Thesis, whilst those marked with ** indicate work presented by the SCF and those showing *** indicate work presented in the wider literature

8.5 Conclusions

The original work presented in this Thesis has demonstrated that SBP solids could be continuously pretreated. The sugars released from this treatment could then be utilised in enzymatic reactions to produce valuable compounds such as L-gluco-heptulose. Moreover, this work presented a whole process, starting from raw material to a final value-added product, and demonstrated the feasibility of this process in a flexible and scalable continuous reactor.

Various aspects of the commercial value and potential of this research have been considered in this chapter. The main challenge in the successful translation of the biorefinery process remains the same challenge that has affected many other biorefinery projects. Namely, the size of byproduct streams that are produced in modern agricultural practices require value added products that can be produced and sold in large quantities. This often means that bulk chemicals that can be used as building blocks are targeted. However, these chemicals typically have low price points and therefore reduce profit margins, highlighting the importance of developing processes that can ensure the complete utilisation of a feedstock to add financial value to the biorefinery. A process that can valorise all streams, ensuring complete utilisation of feedstock.

The narrow profit margins and complicated processing expected in biorefineries is why flexible and scalable technologies and processes such as the one discussed in this Thesis are important.

9 References

Abdoul-Zabar, J. *et al.* (2013) 'Thermostable transketolase from Geobacillus stearothermophilus: Characterization and catalytic properties', *Advanced Synthesis and Catalysis*, 355(1), pp. 116–128. doi: 10.1002/adsc.201200590.

Ademark, P. *et al.* (1998) 'Softwood hemicellulose-degrading enzymes from Aspergillus niger: Purification and properties of a β-mannanase', *Journal of Biotechnology*, 63(3), pp. 199–210. doi: 10.1016/S0168-1656(98)00086-8.

Alberts, B. *et al.* (2012) *Molecular Biology of the Cell*. 5th edn. Garland Science.

Allen, S. G. *et al.* (1996) 'Fractionation of Sugar Cane with Hot, Compressed, Liquid Water', *Industrial & Engineering Chemistry Research*, 35(8), pp. 2709–2715. doi: 10.1021/ie950594s.

Andrade, L. H., Kroutil, W. and Jamison, T. F. (2014) 'Continuous flow synthesis of chiral amines in organic solvents: Immobilization of E. coli cells containing both ω-transaminase and PLP', *Organic Letters*, 16(23), pp. 6092–6095. doi: 10.1021/ol502712v.

Andreana, P. R. *et al.* (2002) 'Chemo-enzymatic synthesis of polyhydroxyazepanes', *Tetrahedron Letters*, 43(37), pp. 6525–6528. doi: 10.1016/S0040-4039(02)01465-X.

Aniceto, J. P. S. and Silva, C. M. (2014) 'Simulated Moving Bed Strategies and Designs: From Established Systems to the Latest Developments', *Separation & Purification Reviews*, 44(1), pp. 41–73. doi: 10.1080/15422119.2013.851087.

Ashe, R. and Wühr, M. (2012) *Wie sich Feststoffe in Durchflussreaktoren richtig handhaben lassen*.

Azevedo, D. C. S. and Rodrigues, A. E. (2001) 'Fructose--glucose separation in a SMB pilot unit : Modeling , simulation , design , and operation', *AICheE Journal*, 47(9), pp. 2042–2051.

Barnes, H. A. (1995) 'A review of the slip (wall depletion) of polymer solutions, emulsions and particle suspensions in viscometers: its cause, character, and cure', *Journal of Non-Newtonian Fluid Mechanics*, 56(3), pp. 221–251. doi: 10.1016/0377-0257(94)01282-M.

Bawn, M. *et al.* (2018) 'One-pot, two-step transaminase and transketolase synthesis of L-gluco-heptulose from L-arabinose', *Enzyme and Microbial Technology*, 116(May), pp. 16–22. doi: 10.1016/j.enzmictec.2018.05.006.

Bhusarapu, S., Al-Dahhan, M. and Dudukovic, M. P. (2004) 'Quantification of solids flow in a gas-solid riser: Single radioactive particle tracking', *Chemical Engineering Science*, 59(22–23), pp. 5381–5386. doi: 10.1016/j.ces.2004.07.052.

Bláha, B. A. F. *et al.* (2018) 'Development of a high-throughput microscale cell disruption platform for Pichia pastoris in rapid bioprocess design', *Biotechnology Progress*, 34(1), pp. 130–140. doi: 10.1002/btpr.2555.

Board, M., Colquhoun, A. and Newsholme, E. A. (1995) 'High Km Glucose-phosphorylating (Glucokinase) Activities in a Range of Tumor Cell Lines and Inhibition of Rates of Tumor Growth by the Specific Enzyme Inhibitor Mannoheptulose', *Cancer Research*, 55(15), pp.

3278–3285.

Bobleter, O., Niesner, R. and Röhr, M. (1976) 'The hydrothermal degradation of cellulosic matter to sugars and their fermentative conversion to protein', *Journal of Applied Polymer Science*, 20(8), pp. 2083–2093. doi: 10.1002/app.1976.070200805.

Bommarius, A. S. and Riebel-Bommarius, B. R. (2004) 'Introduction to Biocatalysis', in *Biocatalysis: Fundamentals and Applications*. Wiley-Blackwell.

Bommarius, A. S. and Riebel, B. R. (2004) 'Protein Engineering', in *Biocatalysis*. Weinheim, FRG: Wiley-VCH Verlag GmbH & Co. KGaA.

Bornik, M.-A. and Kroh, L. W. (2013) 'D-Galacturonic acid as a highly reactive compound in nonenzymatic browning. 1. Formation of browning active degradation products.', *Journal of agricultural and food chemistry*, 61(14), pp. 3494–500. doi: 10.1021/jf303855s.

Bouchard, J. *et al.* (1991) 'Analytical methodology for biomass pretreatment. Part 2: Characterization of the filtrates and cumulative product distribution as a function of treatment severity', *Bioresource Technology*, 36(2), pp. 121–131. doi: 10.1016/0960-8524(91)90169-K.

Bourne, J. R., Kozicki, F. and Rys, P. (1981) 'Mixing and Fast Chemical Reaction - I - Test reactions to determine segregation', 36(10), pp. 1643–1648.

Bradford, M. M. (1976) 'A Rapid and Sensitive Method for the quantitation of Microgram Quantities of Protein Utilizing the Principle of Protein-Dye Binding', *Analytical Biochemistry*, 72, pp. 248–254. doi: 10.1016/j.cj.2017.04.003.

Brady, D. and Jordaan, J. (2009) 'Advances in enzyme immobilisation', *Biotechnology Letters*, 31(11), pp. 1639–1650. doi: 10.1007/s10529-009-0076-4.

Brandon, S. K. *et al.* (2008) 'Hydrolysis of Tifton 85 bermudagrass in a pressurized batch hot water reactor', *Journal of Chemical Technology & Biotechnology*, 83(4), pp. 505–512. doi: 10.1002/jctb.1824.

Breuer, M. *et al.* (2004) 'Industrial methods for the production of optically active intermediates.', *Angewandte Chemie (International ed. in English)*, 43(7), pp. 788–824. doi: 10.1002/anie.200300599.

Briñez, W. J. *et al.* (2007) 'Inactivation of Staphylococcus spp. strains in whole milk and orange juice using ultra high pressure homogenisation at inlet temperatures of 6 and 20 °C', *Food Control*, 18(10), pp. 1282–1288. doi: 10.1016/j.foodcont.2006.09.002.

Brink, D. L. (1993) 'Two stage hydrolysis or depolymerization of polysaccharide material as cellulose, hemicellulose and lignocellulose to monosaccharides using nitric acid'. US.

Brink, D. L. (1994) 'Method of treating biomass material'.

British Sugar (2010) *How our factory operates*.

Britton, J., Majumdar, S. and Weiss, G. A. (2018) 'Continuous flow biocatalysis', *Chemical Society Reviews*, 47(15), pp. 5891–5918. doi: 10.1039/c7cs00906b.

Browne, D. L. *et al.* (2011) 'Continuous Flow Processing of Slurries: Evaluation of an Agitated Cell Reactor', *Organic Process Research & Development*, 15(3), pp. 693–697. doi: 10.1021/op2000223.

Brunhuber, N. M. W. and Blanchard, J. S. (2008) 'The Biochemistry and Enzymology of Amino Acid Dehydrogenases'.

Burgess, R. R. (2009) 'Protein Precipitation Techniques Chapter 20', in *Methods in Enzymology*. 1st edn. Elsevier Inc., pp. 331–342. doi: 10.1016/S0076-6879(09)63020-2.

Buyel, J. F. *et al.* (2014) 'Rational design of a host cell protein heat precipitation step simplifies the subsequent purification of recombinant proteins from tobacco', *Biochemical Engineering Journal*, 88, pp. 162–170. doi: 10.1016/j.bej.2014.04.015.

Cahela, D. R., Lee, Y. Y. and Chambers, R. P. (1983) 'Modeling of percolation process in hemicellulose hydrolysis.', *Biotechnology and bioengineering*, 25(1), pp. 3–17. doi: 10.1002/bit.260250103.

Cai, X. and Stieger, K. W. (2014) 'Market Analysis of Ethanol Capacity', *International Food and Agribusiness Management Review2*, 17(1).

Cárdenas-Fernández, M. *et al.* (2015) 'Co-immobilised aspartase and transaminase for high-yield synthesis of l-phenylalanine', *Biochemical Engineering Journal*, 93, pp. 173–178. doi: 10.1016/j.bej.2014.10.010.

Cárdenas-Fernández, M. *et al.* (2017) 'An integrated biorefinery concept for conversion of sugar beet pulp into value-added chemicals and pharmaceutical intermediates', *Faraday Discussions*, 202, pp. 415–431. doi: 10.1039/c7fd00094d.

Cárdenas-Fernández, M. *et al.* (2018) 'Continuous enzymatic hydrolysis of sugar beet pectin and L-arabinose recovery within an integrated biorefinery', *Bioresource Technology*, 269(August), pp. 195–202. doi: 10.1016/j.biortech.2018.08.069.

Caspeta, L. *et al.* (2013) 'Enhancing thermo-induced recombinant protein production in Escherichia coli by temperature oscillations and post-induction nutrient feeding strategies', *Journal of Biotechnology*, 167(1), pp. 47–55. doi: 10.1016/j.jbiotec.2013.06.001.

Castro-Rosas, J. *et al.* (2013) 'Optimization of thermal protein precipitation from acid whey', *Journal of Food Processing and Preservation*, 37(5), pp. 924–929. doi: 10.1111/j.1745-4549.2012.00728.x.

Cázares, A. *et al.* (2010) 'Non-alpha-hydroxylated aldehydes with evolved transketolase enzymes.', *Organic & biomolecular chemistry*, 8(6), pp. 1301–9. doi: 10.1039/b924144b.

Cerioli, L. *et al.* (2015) 'Characterization of a novel amine transaminase from Halomonas elongata', *Journal of Molecular Catalysis B: Enzymatic*, 120, pp. 141–150. doi: 10.1016/j.molcatb.2015.07.009.

Chamy, R. *et al.* (1994) 'Acid hydrolysis of sugar beet pulp as pretreatment for fermentation', *Bioresource Technology*, 50(2), pp. 149–152. doi: 10.1016/0960-8524(94)90067-1.

Chen, W. H. *et al.* (2013) 'Pilot-scale study on the acid-catalyzed steam explosion of rice straw using a continuous pretreatment system', *Bioresource Technology*, 128, pp. 297–304. doi: 10.1016/j.biortech.2012.10.111.

Chen, Y. *et al.* (2016) 'Identification of novel thermostable taurine–pyruvate transaminase from Geobacillus thermodenitrificans for chiral amine synthesis', *Applied Microbiology and Biotechnology*, 100(7), pp. 3101–3111. doi: 10.1007/s00253-015-7129-5.

Cheng, J. *et al.* (2009) 'An efficient synthesis of d-mannoheptulose via oxidation of an olefinated sugar with potassium permanganate in aqueous acetone', *Carbohydrate Research*, 344(15), pp. 2093–2095. doi: 10.1016/j.carres.2009.06.020.

Cheng, J. (2010) *Biomass to Renewable Energy Processes*. Boca Raton: CRC Press.

Chisti, Y. and Moo-Young, M. (1986) 'Disruption of microbial cells for intracellular products', *Enzyme and Microbial Technology*, 8(April), pp. 194–204. doi: 10.1016/0003-9861(64)90174-2.

Choi, C. H. and Oh, K. K. (2012) 'Application of a continuous twin screw-driven process for dilute acid pretreatment of rape straw', *Bioresource Technology*, 110, pp. 349–354. doi: 10.1016/j.biortech.2012.01.075.

Christen, P. and Metzler, D. E. (1985) *Transaminases*, *FEBS Letters*. Wiley-Interscience. doi: 10.1016/0014-5793(85)80462-2.

Chundawat, S. P. S., Venkatesh, B. and Dale, B. E. (2007) 'Effect of particle size based separation of milled corn stover on AFEX pretreatment and enzymatic digestibility', *Biotechnology and Bioengineering*, 96(2), pp. 219–231. doi: 10.1002/bit.21132.

Contente, M. L. *et al.* (2017) 'Highly Efficient Oxidation of Amines to Aldehydes with Flow-based Biocatalysis', *ChemCatChem*, 9(20), pp. 3843–3848. doi: 10.1002/cctc.201701147.

Costa-Silva, T. A. *et al.* (2018) 'Microbial cell disruption methods for efficient release of enzyme L-asparaginase', *Preparative Biochemistry and Biotechnology*, 48(8), pp. 707–717. doi: 10.1080/10826068.2018.1487850.

Costa, J. A. V. and de Morais, M. G. (2011) 'The role of biochemical engineering in the production of biofuels from microalgae.', *Bioresource technology*, 102(1), pp. 2–9. doi: 10.1016/j.biortech.2010.06.014.

Cox, R. D. and Reid, N. (2000) *The Theory of Designs of Experiments*.

Deadman, B. J. *et al.* (2015) 'Back pressure regulation of slurry-forming reactions in continuous flow', *Chemical Engineering and Technology*, 38(2), pp. 259–264. doi: 10.1002/ceat.201400445.

Deanda, K. *et al.* (1996) 'Development of an arabinose-fermenting Zymomonas mobilis strain by metabolic pathway engineering', *Applied and Environmental Microbiology*, 62(12), pp. 4465–4470.

Deszcz, D. *et al.* (2015) 'Single active-site mutants are sufficient to enhance serine:pyruvate α-transaminase activity in an ω-transaminase', *FEBS Journal*, 282(13), pp. 2512–2526. doi: 10.1111/febs.13293.

Dickens, F. and Williamson, D. H. (1958) 'The preparation and properties of lithium hydroxypyruvate and hydroxypyruvic acid', *Biochemical Journal*, 68(1), pp. 74–84. doi: 10.1042/bj0680074.

Doran, P. M. (2012) *Bioprocess Engineering Principles*. Second. Academic Press.

Draycott, A. P. (2006) *Sugar Beet*. Blackwell Publishing Ltd.

Duraisam, R., Salelgn, K. and Berekete, A. K. (2017) 'Production of Beet Sugar and Bio-ethanol from Sugar beet and it Bagasse: A Review', *International Journal of Engineering*

Trends and Technology, 43(4), pp. 222–233. doi: 10.14445/22315381/ijett-v43p237.

Dvorak, P. *et al.* (2015) 'Exacerbation of substrate toxicity by IPTG in Escherichia coli BL21(DE3) carrying a synthetic metabolic pathway', *Microbial Cell Factories*, 14(1), pp. 1–16. doi: 10.1186/s12934-015-0393-3.

Elmidaoui, A. *et al.* (2006) 'Demineralisation for beet sugar solutions using an electrodialysis pilot plant to reduce melassigenic ions', *Desalination*, 189(1-3 SPEC. ISS.), pp. 209–214. doi: 10.1016/j.desal.2005.06.026.

Esteghlalian, A. *et al.* (1997) 'Modeling and optimization of the dilute-sulfuric-acid pretreatment of corn stover, poplar and switchgrass', *Bioresource Technology*, 59(2–3), pp. 129–136. doi: 10.1016/S0960-8524(97)81606-9.

Fang, H., Deng, J. and Zhang, X. (2011) 'Continuous steam explosion of wheat straw by high pressure mechanical refining system to produce sugars for bioconversion', *BioResources*, 6, pp. 4468–4480.

FAO (2009) *Sugar Beet - Agribusiness Handbook*.

Ferrandi, E. E. *et al.* (2017) 'Novel thermostable amine transferases from hot spring metagenomes', *Applied Microbiology and Biotechnology*, 101(12), pp. 4963–4979. doi: 10.1007/s00253-017-8228-2.

Ferreira, A. G. M. *et al.* (2017) 'The viscosity of glycerol', *Journal of Chemical Thermodynamics*, 113(June 2016), pp. 162–182. doi: 10.1016/j.jct.2017.05.042.

Ferrer, a *et al.* (2013) 'Acetosolv pulping for the fractionation of empty fruit bunches from palm oil industry.', *Bioresource technology*, 132, pp. 115–20. doi: 10.1016/j.biortech.2012.12.189.

Filipponi, P., Gioiello, A. and Baxendale, I. R. (2016) 'Controlled Flow Precipitation as a Valuable Tool for Synthesis', *Organic Process Research and Development*, 20(2), pp. 371–375. doi: 10.1021/acs.oprd.5b00331.

Finkenstadt, V. L. (2013) 'A Review on the Complete Utilization of the Sugarbeet', *Sugar Tech*, 16(4), pp. 339–346. doi: 10.1007/s12355-013-0285-y.

Finnigan, T. J. A. *et al.* (2019) 'Mycoprotein: The Future of Nutritious Nonmeat Protein, a Symposium Review', *Current Developments in Nutrition*, 3(6), pp. 1–5. doi: 10.1093/cdn/nzz021.

Foster, B. L., Dale, B. E. and Doran-Peterson, J. B. (2001) 'Enzymatic Hydrolysis of Ammonia-Treated Sugar Beet Pulp', *Applied Biochemistry and Biotechnology*, 91–93, pp. 269–282.

Gaciarz, A. *et al.* (2017) 'Efficient soluble expression of disulfide bonded proteins in the cytoplasm of Escherichia coli in fed-batch fermentations on chemically defined minimal media', *Microbial Cell Factories*, 16(1), pp. 1–12. doi: 10.1186/s12934-017-0721-x.

Gao, Y., Muzzio, F. J. and Ierapetritou, M. G. (2012) 'A review of the Residence Time Distribution (RTD) applications in solid unit operations', *Powder Technology*, 228, pp. 416–423. doi: 10.1016/j.powtec.2012.05.060.

Garcia-Galan, C. *et al.* (2011) 'Potential of different enzyme immobilization strategies to improve enzyme performance', *Advanced Synthesis and Catalysis*, 353(16), pp. 2885–2904.

doi: 10.1002/adsc.201100534.

Gargulak, J. D., Lebo, S. E. and McNally, T. J. (2015) 'Lignin', in *Encyclopedia of Chemical Technology*. Wiley Online Library.

Gasparini, G. *et al.* (2012) 'Scaling Up Biocatalysis Reactions in Flow Reactors', *Organic Process Research & Development*, 16, pp. 1013–1016.

Gienau, T., Kraume, M. and Rosenberger, S. (2018) 'Rheological Characterization of Anaerobic Sludge from Agricultural and Bio-Waste Biogas Plants', *Chemie-Ingenieur-Technik*, 90(7), pp. 988–997. doi: 10.1002/cite.201700102.

Gómez-Quero, S., Cárdenas-Lizana, F. and Keane, M. a. (2011) 'Liquid phase catalytic hydrodechlorination of 2,4-dichlorophenol over Pd/Al2O3: Batch vs. continuous operation', *Chemical Engineering Journal*, 166(3), pp. 1044–1051. doi: 10.1016/j.cej.2010.07.032.

González Quiroga, A., Costa, A. and MacIel Filho, R. (2010) 'Analysis of conversion and operation strategies for enzymatic hydrolysis of lignocellulosic biomass in a series of CSTRs with distributed feeding', *Bioprocess and Biosystems Engineering*, 33(8), pp. 901–910. doi: 10.1007/s00449-010-0413-y.

Gräslund, S. *et al.* (2008) 'Protein production and purification', *Nature Methods*, 5(2), pp. 135–146. doi: 10.1038/nmeth.f.202.

Gruber, P. *et al.* (2018) 'Enzymatic synthesis of chiral amino-alcohols by coupling transketolase and transaminase-catalyzed reactions in a cascading continuous-flow microreactor system', *Biotechnology and Bioengineering*, 115(3), pp. 586–596. doi: 10.1002/bit.26470.

Guichardon, P. and Falk, L. (2000) 'Characterisation of micromixing effciency by the iodide-iodate reaction system. Part I: experimental procedure', *Chemical Engineering Science*, 55, pp. 4233–4243.

Guo, F. and Berglund, P. (2017) 'Transaminase biocatalysis: Optimization and application', *Green Chemistry*, 19(2), pp. 333–360. doi: 10.1039/c6gc02328b.

Gyamerah, M. and Willetts, A. J. (1997) 'Kinetics of overexpressed transketolase from Escherichia coli JM 107/pQR 700', *Enzyme and Microbial Technology*, 20(2), pp. 127–134. doi: 10.1016/S0141-0229(96)00106-8.

Hailes, H. C. *et al.* (2009) 'Biocatalytic approaches to ketodiols and aminodiols', *Chemistry Today*, 27(August), pp. 28–31.

Halim, A., Szita, N. and Baganz, F. (2013) 'Characterization and multi-step transketolase-ω-transaminase bioconversions in an immobilized enzyme microreactor (IEMR) with packed tube', *Journal of Biotechnology*, 168(4), pp. 567–575. doi: 10.1016/j.jbiotec.2013.09.001.

Hamley-Bennett, C., Lye, G. J. and Leak, D. J. (2016) 'Selective fractionation of Sugar Beet Pulp for release of fermentation and chemical feedstocks; optimisation of thermo-chemical pre-treatment', *Bioresource Technology*, 209, pp. 259–264. doi: 10.1016/j.biortech.2016.02.131.

Han, M. *et al.* (2013) 'High efficiency bioethanol production from barley straw using a continuous pretreatment reactor', *Process Biochemistry*, 48(3), pp. 488–495. doi: 10.1016/j.procbio.2013.01.007.

Hanefeld, U., Gardossi, L. and Magner, E. (2009) 'Understanding enzyme immobilisation', *Chemical Society Reviews*, 38(2), pp. 453–468. doi: 10.1039/b711564b.

Hannig, G. and Makrides, S. C. (1998) 'Strategies for optimizing heterologous protein expression in Escherichia coli', *Trends in Biotechnology*, 16(2), pp. 54–60. doi: 10.1016/S0167-7799(97)01155-4.

Harris, A. T., Davidson, J. F. and Thorpe, R. B. (2003) 'Particle residence time distributions in circulating fluidised beds', *Chemical Engineering Science*, 58(11), pp. 2181–2202. doi: 10.1016/S0009-2509(03)00082-4.

Harrison, S. T. L. (1991) 'Bacterial cell disruption: A key unit operation in the recovery of intracellular products', *Biotechnology Advances*, 9(2), pp. 217–240. doi: 10.1016/0734-9750(91)90005-G.

Hartmann, B. M. *et al.* (2009) 'The chromatography-free release, isolation and purification of recombinant peptide for fibril self-assembly', *Biotechnology and Bioengineering*, 104(5), pp. 973–985. doi: 10.1002/bit.22447.

Hibbert, E. G. *et al.* (2007) 'Directed evolution of transketolase activity on non-phosphorylated substrates.', *Journal of biotechnology*, 131(4), pp. 425–32. doi: 10.1016/j.jbiotec.2007.07.949.

Hibbert, E. G. *et al.* (2008) 'Directed evolution of transketolase substrate specificity towards an aliphatic aldehyde.', *Journal of biotechnology*, 134(3–4), pp. 240–5. doi: 10.1016/j.jbiotec.2008.01.018.

Hinman, N. D. *et al.* (1992) 'Preliminary estimate of the cost of ethanol production for ssf technology', *Applied Biochemistry and Biotechnology*, 34–35(1), pp. 639–649. doi: 10.1007/BF02920584.

Hoffman, B. J. *et al.* (1995) 'Lactose fed-batch overexpression of recombinant metalloprotein in E. coli BL21 (DE3): Process control yielding high levels of metal-incorporated, soluble protein', *Protein Expression and Purification*, 6, pp. 646–654.

Holtzapple, M. T. *et al.* (1991) 'The ammonia freeze explosion (AFEX) process', *Applied Biochemistry and Biotechnology*, 28–29(1), pp. 59–74. doi: 10.1007/BF02922589.

Holtzapple, M. T., Humphrey, A. E. and Taylor, J. D. (1989) 'Energy requirements for the size reduction of poplar and aspen wood.', *Biotechnology and bioengineering*, 33(2), pp. 207–10. doi: 10.1002/bit.260330210.

Holzer, H., Goedde, H. W. and Ulrich, B. (1961) 'Purification of synthetic 14C-D,L-α-hydrpxyethyl-2-thiamine pyophosphate', *Biochemical and Biophysical Research Communications*, 5(6), pp. 447–451.

Hooper, R. J. and Li, J. (1996) 'Summary of the factors critical to the commercial application of bioenergy technologies', *Biomass and Bioenergy*, 11(6), pp. 469–474. doi: 10.1016/S0961-9534(96)00054-2.

Horecker, B. L. (2002) 'The pentose phosphate pathway.', *The Journal of biological chemistry*, 277(50), pp. 47965–71. doi: 10.1074/jbc.X200007200.

Huang, R. L. *et al.* (2010) 'The optimization of fractionating lignocellulose by formic acid using response surface methodology', *Energy Sources, Part A: Recovery, Utilization and*

Environmental Effects, 32(14), pp. 1282–1292. doi: 10.1080/15567030903076669.

Illanes, A. and Nufiez, L. (1994) 'Acid hydrolysis of sugar beet pulp as pretreatment for fermentation', *Bioresource Technology*, 50, pp. 149–152.

Ingram, C. U. *et al.* (2007) 'One-Pot Synthesis of Amino-Alcohols Using a De-Novo Transketolase and b -Alanine : Pyruvate Transaminase Pathway in Escherichia coli', *Biotechnology and Bioengineering*, 96(3), pp. 559–569. doi: 10.1002/bit.

Israilides, C. J., Grant, G. A. and Han, Y. W. (1978) 'Sugar Level, Fermentability, and Acceptability of Straw Treated with Different Acids', *Appl. Envir. Microbiol.*, 36(1), pp. 43–46.

Jaramillo, O. J., Gómez-García, M. Á. and Fontalvo, J. (2013) 'Prediction of acid hydrolysis of lignocellulosic materials in batch and plug flow reactors.', *Bioresource technology*, 142, pp. 570–8. doi: 10.1016/j.biortech.2013.05.064.

Jenning, V., Lippacher, A. and Gohla, S. H. (2002) 'Medium scale production of solid lipid nanoparticles (SLN) by high pressure homogenization', *Journal of Microencapsulation*, 19(1), pp. 1–10. doi: 10.1080/713817583.

Johansson, A., Aaltonen, O. and Ylinen, P. (1987) 'Organosolv pulping — methods and pulp properties', *Biomass*, 13(1), pp. 45–65. doi: 10.1016/0144-4565(87)90071-0.

Jones, E. *et al.* (2012) 'Biocatalytic oxidase: Batch to continuous', *Chemical Engineering Research and Design*, 90(6), pp. 726–731. doi: 10.1016/j.cherd.2012.01.018.

Kamzon, M. A., Abderafi, S. and Bounahmidi, T. (2016) 'Promising bioethanol processes for developing a biorefinery in the Moroccan sugar industry', *International Journal of Hydrogen Energy*, 41(45), pp. 20880–20896. doi: 10.1016/j.ijhydene.2016.07.035.

Kara, S. *et al.* (2014) 'Recent trends and novel concepts in cofactor-dependent biotransformations', *Applied Microbiology and Biotechnology*, 98(4), pp. 1517–1529. doi: 10.1007/s00253-013-5441-5.

Karande, R., Schmid, A. and Buehler, K. (2011) 'Miniaturizing biocatalysis: Enzyme-catalyzed reactions in an aqueous/organic segmented flow capillary microreactor', *Advanced Synthesis and Catalysis*, 353(13), pp. 2511–2521. doi: 10.1002/adsc.201100394.

Kaulmann, U. *et al.* (2007) 'Substrate spectrum of ω-transaminase from Chromobacterium violaceum DSM30191 and its potential for biocatalysis', *Enzyme and Microbial Technology*, 41(5), pp. 628–637. doi: 10.1016/j.enzmictec.2007.05.011.

Kelley, B. (2007) 'Very large scale monoclonal antibody purification: The case for conventional unit operations', *Biotechnology Progress*, 23(5), pp. 995–1008. doi: 10.1021/bp070117s.

Kharina, M. *et al.* (2016) 'Pretreatment of Sugar Beet Pulp with Dilute Sulfurous Acid is Effective for Multipurpose Usage of Carbohydrates', *Applied Biochemistry and Biotechnology*, 179(2), pp. 307–320. doi: 10.1007/s12010-016-1995-x.

Kim, Y. *et al.* (2014) 'Severity factor coefficients for subcritical liquid hot water pretreatment of hardwood chips', *Biotechnology and Bioengineering*, 111(2), pp. 254–263. doi: 10.1002/bit.25009.

Kindstedt, P. S. (1993) 'Rheological Methods in Food Process Engineering Dais . Science and Technology Vols 1-3', 41(September), p. 1993.

Kleinert, T. N. (1971) 'Organosolv pulping and recovery process'.

Knocke, C. *et al.* (2016) 'Bioprocess scale-up from small to large pilot scale using eppendorf fermentation systems', *New Biotechnology*, 33(306), p. S40. doi: 10.1016/j.nbt.2016.06.862.

Koch, K. *et al.* (2008) 'Enzymatic enantioselective C-C-bond formation in microreactors.', *Biotechnology and bioengineering*, 99(4), pp. 1028–33. doi: 10.1002/bit.21649.

Kochetov, G. a and Solovjeva, O. N. (2014) 'Structure and functioning mechanism of transketolase.', *Biochimica et biophysica acta*, 1844(9), pp. 1608–18. doi: 10.1016/j.bbapap.2014.06.003.

Köhler, V. *et al.* (2013) 'Synthetic cascades are enabled by combining biocatalysts with artificial metalloenzymes', *Nature Chemistry*, 5(2), pp. 93–99. doi: 10.1038/nchem.1498.

Kordowska-Wiater, M. (2015) 'Production of arabitol by yeasts: Current status and future prospects', *Journal of Applied Microbiology*, 119(2), pp. 303–314. doi: 10.1111/jam.12807.

Korz, D. J. *et al.* (1995) 'Simple fed-batch technique for high cell density cultivation of Escherichia coli', *Journal of Biotechnology*, 39(1), pp. 59–65. doi: 10.1016/0168-1656(94)00143-Z.

Kühnel, S. *et al.* (2010) 'Chrysosporium lucknowense arabinohydrolases effectively degrade sugar beet arabinan.', *Bioresource technology*, 101(21), pp. 8300–7. doi: 10.1016/j.biortech.2010.05.070.

Kühnel, S. (2011) *Characterization of cell wall degrading enzymes from Chrysosporium lucknowense C1 and their use to degrade sugar beet pulp*.

Kühnel, S., Schols, H. A. and Gruppen, H. (2011a) 'Aiming for the complete utilization of sugar-beet pulp: Examination of the effects of mild acid and hydrothermal pretreatment followed by enzymatic digestion.', *Biotechnology for biofuels*, 4, p. 14. doi: 10.1186/1754-6834-4-14.

Kulsharova, G. *et al.* (2018) 'Simplified immobilisation method for histidine-tagged enzymes in poly(methyl methacrylate) microfluidic devices', *New Biotechnology*, 47(November), pp. 31–38. doi: 10.1016/j.nbt.2017.12.004.

Kwon, S. J. and Ko, S. Y. (2001) 'Orthogonally Protected, Enantiopure syn -2-Amino-1,3,4-butanetriol: A General Building Block for syn -Amino Alcohols', *The Journal of Organic Chemistry*, 66(20), pp. 6833–6835. doi: 10.1021/jo015886j.

Larsson, S. *et al.* (1999) 'The generation of fermentation inhibitors during dilute acid hydrolysis of softwood', *Enzyme and Microbial Technology*, 24(3–4), pp. 151–159. doi: 10.1016/S0141-0229(98)00101-X.

Lawrence, J. *et al.* (2013) 'Microfluidic multi-input reactor for biocatalytic synthesis using transketolase.', *Journal of molecular catalysis. B, Enzymatic*, 95(100), pp. 111–117. doi: 10.1016/j.molcatb.2013.05.016.

Leijdekkers, a G. M. *et al.* (2013) 'Enzymatic saccharification of sugar beet pulp for the

production of galacturonic acid and arabinose; a study on the impact of the formation of recalcitrant oligosaccharides.', *Bioresource technology*, 128, pp. 518–25. doi: 10.1016/j.biortech.2012.10.126.

Lessard, J. C. (2013) *Growth media for E. coli*. 1st edn, *Methods in Enzymology*. 1st edn. Elsevier Inc. doi: 10.1016/B978-0-12-420067-8.00011-8.

Levenspiel, O. (1999) 'Chapter 13 The Dispersion Model', in *Chemical reaction engineering*. New York, NY, pp. 293–320.

Li, G. *et al.* (2018) 'Comparison of various pretreatment strategies and their effect on chemistry and structure of sugar beet pulp', *Journal of Cleaner Production*, 181, pp. 217–223. doi: 10.1016/j.jclepro.2018.01.259.

Li, Q. *et al.* (2013) 'An ultra scale-down approach to study the interaction of fermentation, homogenization, and centrifugation for antibody fragment recovery from rec E. coli', *Biotechnology and Bioengineering*. doi: 10.1002/bit.24891.

Licari, A. *et al.* (2016) 'Comparison of various milling modes combined to the enzymatic hydrolysis of lignocellulosic biomass for bioenergy production: Glucose yield and energy efficiency', *Energy*, 102, pp. 335–342. doi: 10.1016/j.energy.2016.02.083.

Liu, L. S. *et al.* (2005) 'Biodegradable composites from sugar beet pulp and poly(lactic acid)', *Journal of Agricultural and Food Chemistry*, 53(23), pp. 9017–9022. doi: 10.1021/jf058083w.

Liu, S. *et al.* (2013) 'Designing cost-effective biopharmaceutical facilities using mixed-integer optimization', *Biotechnology Progress*, 29(6), pp. 1472–1483. doi: 10.1002/btpr.1795.

Liu, X. *et al.* (2012) 'Effect of thermal pretreatment on the physical and chemical properties of municipal biomass waste', *Waste Management*, 32(2), pp. 249–255. doi: 10.1016/j.wasman.2011.09.027.

Lorillière, M. *et al.* (2017) 'One-pot, two-step cascade synthesis of naturally rare l-: Erythro (3 S,4 S) ketoses by coupling a thermostable transaminase and transketolase', *Green Chemistry*, 19(2), pp. 424–435. doi: 10.1039/c6gc02015a.

Lozano, P. *et al.* (2002) 'Continuous green biocatalytic processes using ionic liquids and supercritical carbon dioxide', *Chemical Communications*, 7, pp. 692–693. doi: 10.1039/b200055e.

Lutin, F., Bailly, M. and Bar, D. (2002) 'Process improvements with innovative technologies in the starch and sugar industries', *Desalination*, 148(1–3), pp. 121–124. doi: 10.1016/S0011-9164(02)00664-1.

Lye, G. J. and Woodley, J. M. (1999) 'Application of in situ product-removal techniques to biocatalytic processes', *Trends in Biotechnology*, 17(10), pp. 395–402. doi: 10.1016/S0167-7799(99)01351-7.

Mak, X. Y., Laurino, P. and Seeberger, P. H. (2009) 'Asymmetric reactions in continuous flow.', *Beilstein Journal of Organic Chemistry*, 5, p. 19. doi: 10.3762/bjoc.5.19.

Malmali, M., Stickel, J. J. and Wickramasinghe, S. R. (2014) 'Sugar concentration and detoxification of clarified biomass hydrolysate by nanofiltration', *Separation and*

Purification Technology, 132, pp. 655–665. doi: 10.1016/j.seppur.2014.06.014.

Marshall, S. A. *et al.* (2003) 'Rational design and engineering of therapeutic proteins', *Drug Discovery Today*, 8(5), pp. 212–221. doi: 10.1016/S1359-6446(03)02610-2.

Martínez, M. *et al.* (2010) 'Kinetic assessment on the autohydrolysis of pectin-rich by-products', *Chemical Engineering Journal*, 162(2), pp. 480–486. doi: 10.1016/j.cej.2010.05.048.

Matcham, G. *et al.* (1999) 'Enzyme and reaction engineering in biocatalysis: synthesis of (S)-methoxyisopropylamine (=(S)-1-Methoxypropan-2-amine)', *Chimia*, 53, pp. 584–589.

Mathew, S. *et al.* (2016) 'Biochemical characterization of thermostable ω-transaminase from Sphaerobacter thermophilus and its application for producing aromatic β- and γ-amino acids', *Enzyme and Microbial Technology*, 87–88, pp. 52–60. doi: 10.1016/j.enzmictec.2016.02.013.

McMillan, J. D. and Boynton, B. L. (1994) 'Arabinose utilization by xylose-fermenting yeasts and fungi', *Applied Biochemistry and Biotechnology*, 45–46(1), pp. 569–584. doi: 10.1007/BF02941831.

Mehtiö, T. *et al.* (2015) 'Synthesis and characterization of copolyanhydrides of carbohydrate-based galactaric acid and adipic acid', *Carbohydrate Research*, 402, pp. 102–110. doi: 10.1016/j.carres.2014.07.009.

Mes-Hartree, M., Dale, B. E. and Craig, W. K. (1988) 'Comparison of steam and ammonia pretreatment for enzymatic hydrolysis of cellulose', *Applied Microbiology and Biotechnology*, 29(5), pp. 462–468. doi: 10.1007/BF00269069.

Mesbahi, G., Jamalian, J. and Farahnaky, A. (2005) 'A comparative study on functional properties of beet and citrus pectins in food systems', *Food Hydrocolloids*, 19(4), pp. 731–738. doi: 10.1016/j.foodhyd.2004.08.002.

Metzner, A. B. and Otto, R. E. (1957) 'Agitation of non-Newtonian fluids', *AIChE Journal*, 3(1), pp. 3–10. doi: 10.1002/aic.690030103.

Modenbach, A. A. and Nokes, S. E. (2012) 'The use of high-solids loadings in biomass pretreatment-a review', *Biotechnology and Bioengineering*, 109(6), pp. 1430–1442. doi: 10.1002/bit.24464.

Mok, W. S. L. and Antal, M. J. (1992) 'Uncatalyzed solvolysis of whole biomass hemicellulose by hot compressed liquid water', *Industrial & Engineering Chemistry Research*, 31(4), pp. 1157–1161. doi: 10.1021/ie00004a026.

Moloney, A. P. *et al.* (1983) 'Enzymic Saccharification of Sugar Beet Pulp', *Biotechonlogy and Bioengineering*, 26, pp. 714–718.

Morin, C. (2003) 'Iodomethyl Group as a Hydroxymethyl Synthetic Equivalent : Application to the Syntheses of D - manno -Hept-2-ulose and L -Fructose Derivatives The elongation of carbohydrates from the reducing end allows a net aldose to ketose homologation ; 1 we now show', (19), pp. 4100–4103. doi: 10.1021/jo0342166.

Morjanoff, P. J. and Gray, P. P. (1987) 'Optimization of steam explosion as a method for increasing susceptibility of sugarcane bagasse to enzymatic saccharification.', *Biotechnology and bioengineering*, 29(6), pp. 733–41. doi: 10.1002/bit.260290610.

Morton, D. W. and Kiely, D. E. (2000) 'Evaluation of the film and adhesive properties of some block copolymer polyhydroxypolyamides from esterified aldaric acids and diamines', *Journal of Applied Polymer Science*, 77(14), pp. 3085–3092. doi: 10.1002/1097-4628(20000929)77:14<3085::AID-APP90>3.0.CO;2-7.

Mosier, N. *et al.* (2005) 'Features of promising technologies for pretreatment of lignocellulosic biomass.', *Bioresource technology*, 96(6), pp. 673–86. doi: 10.1016/j.biortech.2004.06.025.

Mosier, N. S., Ladisch, C. M. and Ladisch, M. R. (2002) 'Characterization of acid catalytic domains for cellulose hydrolysis and glucose degradation.', *Biotechnology and bioengineering*, 79(6), pp. 610–8. doi: 10.1002/bit.10316.

Neto, W. *et al.* (2015) 'Immobilisation of ω-transaminase for industrial application: Screening and characterisation of commercial ready to use enzyme carriers', *Journal of Molecular Catalysis B: Enzymatic*, 117, pp. 54–61. doi: 10.1016/j.molcatb.2015.04.005.

Ng, M. Y. T. *et al.* (2006) 'Heat treatment of unclarified Escherichia coli homogenate improved the recovery efficiency of recombinant hepatitis B core antigen', *Journal of Virological Methods*, 137(1), pp. 134–139. doi: 10.1016/j.jviromet.2006.06.016.

Norton, J. E. and Sokatch, J. R. (1970) 'Cultural methods The strain of Pseudomonas aeruginosa used in this study is the same one used in', *Biochimica et biophysica acta*, 6, pp. 261–269.

O'Sullivan, B. *et al.* (2012) 'Modular microfluidic reactor and inline filtration system for the biocatalytic synthesis of chiral metabolites', *Journal of Molecular Catalysis B: Enzymatic*, 77, pp. 1–8. doi: 10.1016/j.molcatb.2011.12.010.

Oosterveld, A. *et al.* (2000) 'Characterization of arabinose and ferulic acid rich pectic polysaccharides and hemicelluloses from sugar beet pulp', *Carbohydrate Research*, 328(2), pp. 185–197. doi: 10.1016/S0008-6215(00)00095-1.

Otten, L. G. and Quax, W. J. (2005) 'Directed evolution: selecting today's biocatalysts.', *Biomolecular engineering*, 22(1–3), pp. 1–9. doi: 10.1016/j.bioeng.2005.02.002.

Palmqvist, B. *et al.* (2016) 'Scale-up of high-solid enzymatic hydrolysis of steam-pretreated softwood: the effects of reactor flow conditions', *Biomass Conversion and Biorefinery*, 6(2), pp. 173–180. doi: 10.1007/s13399-015-0177-3.

Palmqvist, E. and Hahn-Hägerdal, B. (2000) 'Fermentation of lignocellulosic hydrolysates. II: inhibitors and mechanisms of inhibition', *Bioresource Technology*, 74(1), pp. 25–33. doi: 10.1016/S0960-8524(99)00161-3.

Pareek, V. K. *et al.* (2001) 'Particle residence time distribution (RTD) in three-phase annular bubble column reactor', *Chemical Engineering Science*, 56(21–22), pp. 6063–6071. doi: 10.1016/S0009-2509(01)00270-6.

Patchett, M. L. *et al.* (1989) 'Heat treatment purification of thermostable cellulase and hemicellulase enzymes expressed in E. coli', *Enzyme and Microbial Technology*, 11(2), pp. 113–115. doi: 10.1016/0141-0229(89)90069-0.

Patil, M. D. *et al.* (2018) 'Recent advances in ω-transaminase-mediated biocatalysis for the enantioselective synthesis of chiral amines', *Catalysts*, 8(7). doi: 10.3390/catal8070254.

Paulsen, E. P., Richenderfer, L. and Winick, P. (1967) 'Suppression of Plasma Immunoreactive Insulin in Rats given D-Mannoheptulose', *Nature*, 214(5085), pp. 276–277. doi: 10.1038/214276a0.

Payongsri, P. *et al.* (2012) 'Rational substrate and enzyme engineering of transketolase for aromatics.', *Organic & biomolecular chemistry*, 10(45), pp. 9021–9. doi: 10.1039/c2ob25751c.

Pedersen, M. and Meyer, A. S. (2010) 'Lignocellulose pretreatment severity - relating pH to biomatrix opening', *New Biotechnology*, 27(6), pp. 739–750. doi: 10.1016/j.nbt.2010.05.003.

Petri, A., Colonna, V. and Piccolo, O. (2019) 'Asymmetric synthesis of a high added value chiral amine using immobilized ω-transaminases', *Beilstein Journal of Organic Chemistry*, 15, pp. 60–66. doi: 10.3762/bjoc.15.6.

Phan, A. N. and Harvey, A. (2010) 'Development and evaluation of novel designs of continuous mesoscale oscillatory baffled reactors', *Chemical Engineering Journal*, 159(1–3), pp. 212–219. doi: 10.1016/j.cej.2010.02.059.

Phan, A. N., Harvey, A. and Lavender, J. (2011) 'Characterisation of fluid mixing in novel designs of mesoscale oscillatory baffled reactors operating at low flow rates (0.3-0.6ml/min)', *Chemical Engineering and Processing: Process Intensification*, 50(3), pp. 254–263. doi: 10.1016/j.cep.2011.02.004.

Pollack, P. (2012) *Fine Chemicals: The Industry and the Business*. Second. Wiley Online Library.

Pollard, D. J. and Woodley, J. M. (2007) 'Biocatalysis for pharmaceutical intermediates: the future is now', *Trends in Biotechnology*, 25(2), pp. 66–73. doi: 10.1016/j.tibtech.2006.12.005.

Protzko, R. J. *et al.* (2018) 'Engineering Saccharomyces cerevisiae for co-utilization of d-galacturonic acid and d-glucose from citrus peel waste', *Nature Communications*, 9(1). doi: 10.1038/s41467-018-07589-w.

Purolite (2015) 'Purolite ECR Enzyme Immobilization Procedures'.

Pustelnik, P. (1986) 'Investigation of residence time distribution in Kenics static mixers', *Chemical Engineering and Processing*, 20(3), pp. 147–154. doi: 10.1016/0255-2701(86)85019-X.

R. Hobbs, G. *et al.* (1996) 'Enzyme-catalysed carbon-carbon bond formation: Large-scale production of Escherichia coli transketolase', *Journal of Biotechnology*, 45(2), pp. 173–179. doi: 10.1016/0168-1656(95)00165-4.

Richard, P. *et al.* (2003) 'Production of ethanol from L-arabinose by Saccharomyces cerevisiae containing a fungal L-arabinose pathway', *FEMS Yeast Research*, 3(2), pp. 185–189. doi: 10.1016/S1567-1356(02)00184-8.

Ringborg, R. H. and Woodley, J. M. (2016) 'The application of reaction engineering to biocatalysis', *Reaction Chemistry and Engineering*, 1(1), pp. 10–22. doi: 10.1039/c5re00045a.

Rios-Solis, L. *et al.* (2015) 'Modelling and optimisation of the one-pot, multi-enzymatic

synthesis of chiral amino-alcohols based on microscale kinetic parameter determination', *Chemical Engineering Science*, 122(June 2014), pp. 360–372. doi: 10.1016/j.ces.2014.09.046.

Roberge, D. M. *et al.* (2005) 'Microreactor Technology: A Revolution for the Fine Chemical and Pharmaceutical Industries?', *Chemical Engineering & Technology*, 28(3), pp. 318–323. doi: 10.1002/ceat.200407128.

Saari, P. *et al.* (2010) 'Study on Industrial Scale Chromatographic Separation Methods of Galactose from Biomass Hydrolysates', *Chemical Engineering & Technology*, 33(1), pp. 137–144. doi: 10.1002/ceat.200900304.

Saha, B. C. (2000) 'α-L-Arabinofuranosidases: Biochemistry, molecular biology and application in biotechnology', *Biotechnology Advances*, 18(5), pp. 403–423. doi: 10.1016/S0734-9750(00)00044-6.

Salice, P. *et al.* (2012) 'Efficient functionalization of carbon nanotubes: an opportunity enabled by flow chemistry', *Chemistry Today*, 60(6), pp. 37–39.

Sayer, C. *et al.* (2012) 'Crystal structure and substrate specificity of the thermophilic serine:pyruvate aminotransferase from Sulfolobus solfataricus', *Acta Crystallographica Section D: Biological Crystallography*, 68(7), pp. 763–772. doi: 10.1107/S0907444912011274.

Schenk, G., Duggleby, R. G. and Nixon, P. F. (1998) 'Properties and functions of the thiamin diphosphate dependent enzyme transketolase', *The International Journal of Biochemistry & Cell Biology*, 30(12), pp. 1297–1318. doi: 10.1016/S1357-2725(98)00095-8.

Schmid, A. *et al.* (2001) 'Industrial biocatalysis today and tomorrow', *Nature*, 409(January).

Schmitt, J., Hess, H. and Stunnenberg, H. G. (1993) 'Affinity purification of histidine-tagged proteins', *Molecular Biology Reports*, 18(3), pp. 223–230. doi: 10.1007/BF01674434.

Schumacher, B. *et al.* (2010) 'Life cycle assessment of the conversion of Zea mays and x Triticosecale into biogas and bioethanol', *Engineering in Life Sciences*, 10(6), pp. 577–584. doi: 10.1002/elsc.201000069.

Scott Fogler, H. (2008) *Elements of Chemical Reaction Engineering*. Upper Saddle River, NJ: Pearson Education.

Shaeri, J., Wohlgemuth, R. and Woodley, J. M. (2006) 'Semiquantitative Process Screening for the Biocatalytic Synthesis of d -Xylulose-5-phosphate', *Organic Process Research & Development*, 10(3), pp. 605–610. doi: 10.1021/op050254a.

Sheldon, R. A. (2007) 'Enzyme immobilization: The quest for optimum performance', *Advanced Synthesis and Catalysis*, 349(8–9), pp. 1289–1307. doi: 10.1002/adsc.200700082.

Sheldon, R. A. and van Pelt, S. (2013) 'Enzyme immobilisation in biocatalysis: why, what and how.', *Chemical Society reviews*, 42(15), pp. 6223–35. doi: 10.1039/c3cs60075k.

Shin, J.-S. and Kim, B.-G. (2014) 'Comparison of the ω-Transaminases from Different Microorganisms and Application to Production of Chiral Amines', *Bioscience, Biotechnology and Biochemistry*, 65(8), pp. 1782–1788. doi: 10.1271/bbb.65.1782.

Shin, J.-S., Kim, B.-G. and Shin, D.-H. (2001) 'Kinetic resolution of chiral amines using

packed-bed reactor', *Enzyme and Microbial Technology*, 29, pp. 232–239.

Shinomiya, K. and Ito, Y. (2006) 'Countercurrent Chromatographic Separation of Biotic Compounds with Extremely Hydrophilic Organic-Aqueous Two-Phase Solvent Systems and Organic-Aqueous Three-Phase Solvent Systems', *Journal of Liquid Chromatography & Related Technologies*, 29(5), pp. 733–750. doi: 10.1080/10826070500509298.

Sidiras, D. and Koukios, E. (2004) 'Simulation of acid-catalysed organosolv fractionation of wheat straw.', *Bioresource technology*, 94(1), pp. 91–8. doi: 10.1016/j.biortech.2003.10.029.

Sievers, D. A. *et al.* (2016) 'Online residence time distribution measurement of thermochemical biomass pretreatment reactors', *Chemical Engineering Science*, 140, pp. 330–336. doi: 10.1016/j.ces.2015.10.031.

Sievers, D. A. and Stickel, J. J. (2018) 'Modeling residence-time distribution in horizontal screw hydrolysis reactors', *Chemical Engineering Science*, 175, pp. 396–404. doi: 10.1016/j.ces.2017.10.012.

Da Silva, A. S. A. *et al.* (2013) 'Continuous pretreatment of sugarcane bagasse at high loading in an ionic liquid using a twin-screw extruder', *Green Chemistry*, 15(7), pp. 1991–2001. doi: 10.1039/c3gc40352a.

Silva, E. A. B. da *et al.* (2009) 'An integrated process to produce vanillin and lignin-based polyurethanes from Kraft lignin', *Chemical Engineering Research and Design*, 87(9), pp. 1276–1292. doi: 10.1016/j.cherd.2009.05.008.

Sims, R. E. H. *et al.* (2010) 'An overview of second generation biofuel technologies', *Bioresource Technology*, 101(6), pp. 1570–1580. doi: 10.1016/j.biortech.2009.11.046.

Siró, I. and Plackett, D. (2010) 'Microfibrillated cellulose and new nanocomposite materials: A review', *Cellulose*, 17(3), pp. 459–494. doi: 10.1007/s10570-010-9405-y.

Slabu, I. *et al.* (2017) 'Discovery, Engineering, and Synthetic Application of Transaminase Biocatalysts', *ACS Catalysis*, 7(12), pp. 8263–8284. doi: 10.1021/acscatal.7b02686.

Smith, M. E. B. *et al.* (2006) 'A colorimetric assay for screening transketolase activity.', *Bioorganic & medicinal chemistry*, 14(20), pp. 7062–5. doi: 10.1016/j.bmc.2006.06.008.

Smith, M. E. B. *et al.* (2010) 'A multidisciplinary approach toward the rapid and preparative-scale biocatalytic synthesis of chiral amino alcohols: A concise transketolase-/ ω-transaminase-mediated synthesis of (25,35)-2-aminopentane-1,3-diol', *Organic Process Research and Development*, 14(1), pp. 99–107. doi: 10.1021/op900190y.

Snelders, J. *et al.* (2014) 'Biorefining of wheat straw using an acetic and formic acid based organosolv fractionation process.', *Bioresource technology*, 156, pp. 275–82. doi: 10.1016/j.biortech.2014.01.069.

Spagnuolo, M. *et al.* (1997) 'Synergistic effects of cellulolytic and pectinolytic enzymes in degrading sugar beet pulp', *Bioresource Technology*, 60(3), pp. 215–222. doi: 10.1016/S0960-8524(97)00013-8.

Spagnuolo, M. *et al.* (1999) 'Fractionation of Sugar Beet Pulp into Pectin , Cellulose , and Arabinose by Arabinases Combined with Ultrafiltration', *Biotechnology and Bioengineering*, 64(6), pp. 685–691.

Sprenger, G. A. (1995) ‘Genetics of pentose-phosphate pathway enzymes of Escherichia coli K-12’, *Archives of Microbiology*, 164(5), pp. 324–330. doi: 10.1007/BF02529978.

Stickel, J. J. *et al.* (2009) ‘Rheology measurements of a biomass slurry: An inter-laboratory study’, *Rheologica Acta*, 48(9), pp. 1005–1015. doi: 10.1007/s00397-009-0382-8.

Stokes, R. L. and Nauman, E. B. (1970) ‘Residence time distribution functions for stirred tanks in series’, *The Canadian Journal of Chemical Engineering*, 48(6), pp. 723–725. doi: 10.1002/cjce.5450480612.

Stoppok, E. and Buchholz, K. (1985) ‘Continuous anaerobic conversion of sugar beet pulp to biogas’, *Biotechnology Letters*, 7(2), pp. 119–124. doi: 10.1007/BF01026682.

Subrizi, F. *et al.* (2016) ‘Transketolase catalysed upgrading of L-arabinose: The one-step stereoselective synthesis of L-gluco-heptulose’, *Green Chemistry*, 18(10), pp. 3158–3165. doi: 10.1039/c5gc02660a.

Subrizi, F., Hailes, H. and Lye, G. J. (2015) *Production of chiral, aminated compounds from sustainbly sourced sugars using transketolase and transaminase enzymes (Unpublished)*.

Suhaili, N. *et al.* (2019) ‘Potential of sugar beet vinasse as a feedstock for biocatalyst production within an integrated biorefinery context’, *Journal of Chemical Technology and Biotechnology*, 94(3), pp. 739–751. doi: 10.1002/jctb.5819.

Sun, Y. and Cheng, J. (2002) ‘Hydrolysis of lignocellulosic materials for ethanol production: a review’, *Bioresource Technology*, 83(1), pp. 1–11. doi: 10.1016/S0960-8524(01)00212-7.

Sutherland, E. (2015) *Coflore ATR1 Characterisation Studies*. University of Edinburgh.

Takagi, K. *et al.* (2001) ‘New pathway of amine oxidation respiratory chain of Paracoccus denitrificans IFO 12442’, *European Journal of Biochemistry*, 268(2), pp. 470–476. doi: 10.1046/j.1432-1033.2001.01912.x.

Takesawa, Y. *et al.* (1990) ‘Heat-induced precipitation of cell homogenates: An investigation of the recovery of thermostable proteins’, *Enzyme and Microbial Technology*, 12(3), pp. 184–189. doi: 10.1016/0141-0229(90)90036-P.

Taylor, R. T. and Jenkins, W. T. (1966) ‘Leucine aminotransferase’, *Journal of Biological Chemistry*, 241(19), pp. 4396–4405.

Thiry, M., Cingolani, D. and Thiry, M. (2002) ‘Optimizing scale-up fermentation processes’, 20(3), pp. 103–106.

Titchener-Hooker, N. J., Dunnill, P. and Hoare, M. (2008) ‘Micro biochemical engineering to accelerate the design of industrial-scale downstream processes for biopharmaceutical proteins’, *Biotechnology and Bioengineering*, 100(3), pp. 473–487. doi: 10.1002/bit.21788.

Toftgaard Pedersen, A. *et al.* (2017) ‘Characterization of a continuous agitated cell reactor for oxygen dependent biocatalysis’, *Biotechnology and Bioengineering*, 114(6), pp. 1222–1230. doi: 10.1002/bit.26267.

Torrelo, G., Hanefeld, U. and Hollmann, F. (2015) ‘Biocatalysis’, (October 2014), pp. 309–345. doi: 10.1007/s10562-014-1450-y.

Tran, D. N. and Balkus, K. J. (2011) ‘Perspective of recent progress in immobilization of enzymes’, *ACS Catalysis*, 1(8), pp. 956–968. doi: 10.1021/cs200124a.

Tufvesson, P. *et al.* (2010) 'Process considerations for the scale-up and implementation of biocatalysis', *Food and Bioproducts Processing*, 88(1), pp. 3–11. doi: 10.1016/j.fbp.2010.01.003.

Tugtas, A. E. (2011) 'Fermentative Organic Acid Production and Separation', *Fen Bilimleri Dergisi*, 23(2), pp. 70–78.

Turner, N. J. (2000) 'Applications of transketolases in organic synthesis', *Current Opinion in Biotechnology*, 11(6), pp. 527–531. doi: 10.1016/S0958-1669(00)00140-3.

Turner, N. J. (2012) 'Biocatalysis', *Catalysis Science & Technology*, 2, p. 1523. doi: 10.1039/c2cy90030k.

Venkata Mohan, S. *et al.* (2016) 'Waste biorefinery models towards sustainable circular bioeconomy: Critical review and future perspectives', *Bioresource Technology*, 215, pp. 2–12. doi: 10.1016/j.biortech.2016.03.130.

Villegas-Torres, M. F. *et al.* (2015) 'Multi-step biocatalytic strategies for chiral amino alcohol synthesis', *Enzyme and Microbial Technology*, 81, pp. 23–30. doi: 10.1016/j.enzmictec.2015.07.003.

Visuri, K. and Klibanov, A. M. (1986) 'Enzymatic production of high fructose corn syrup (HFCS) containing 55% fructose in aqueous ethanol', *Biotechnology and bioengineering*, 30, pp. 917–920.

Vlasenko, E. Y. *et al.* (1997) 'Enzymatic hydrolysis of pretreated rice straw', *Bioresource Technology*, 59(2–3), pp. 109–119. doi: 10.1016/S0960-8524(96)00169-1.

Wandrey, C., Liese, A. and Kihumbu, D. (2000) 'Industrial biocatalysis: Past, present, and future', *Organic Process Research and Development*, 4(4), pp. 286–290. doi: 10.1021/op990101l.

Ward, D. (2017) 'Scalable separation methods for the isolation of monosaccharides in a biorefinery context'.

Ward, D. P. *et al.* (2015) 'Centrifugal partition chromatography in a biorefinery context: Separation of monosaccharides from hydrolysed sugar beet pulp', *Journal of Chromatography A*, 1411, pp. 84–91. doi: 10.1016/j.chroma.2015.08.006.

Ward, D. P. *et al.* (2017) 'Centrifugal partition chromatography in a biorefinery context: Optimisation and scale-up of monosaccharide fractionation from hydrolysed sugar beet pulp', *Journal of Chromatography A*, 1497, pp. 56–63. doi: 10.1016/j.chroma.2017.03.003.

Waschke, D., Thimm, J. and Thiem, J. (2011) 'Highly efficient synthesis of ketoheptoses', *Organic Letters*, 13(14), pp. 3628–3631. doi: 10.1021/ol2012764.

Wei, F. and Zhu, J. X. (1996) 'Effect of flow direction on axial solid dispersion in gas-solids cocurrent upflow and downflow systems', *Chemical Engineering Journal and the Biochemical Engineering Journal*, 64(3), pp. 345–352. doi: 10.1016/S0923-0467(96)85016-0.

Weil, J. R. *et al.* (1997) 'Pretreatment of yellow poplar sawdust by pressure cooking in water', *Applied Biochemistry and Biotechnology*, 68(1–2), pp. 21–40. doi: 10.1007/BF02785978.

Weil, J. R., Brewer, M., *et al.* (1998) 'Continuous pH monitoring during pretreatment of

yellow poplar wood sawdust by pressure cooking in water', *Applied Biochemistry and Biotechnology*, 70–72(1), pp. 99–111. doi: 10.1007/BF02920127.

Weil, J. R., Sarikaya, A., *et al.* (1998) 'Pretreatment of corn fiber by pressure cooking in water', *Applied Biochemistry and Biotechnology*, 73(1), pp. 1–17. doi: 10.1007/BF02788829.

Wendt, L. M. *et al.* (2018) 'Techno-economic assessment of a chopped feedstock logistics supply chain for corn stover', *Frontiers in Energy Research*, 6(SEP), pp. 1–14. doi: 10.3389/fenrg.2018.00090.

Wiedemann, B. and Boles, E. (2008) 'Codon-optimized bacterial genes improve L-arabinose fermentation in recombinant Saccharomyces cerevisiae', *Applied and Environmental Microbiology*, 74(7), pp. 2043–2050. doi: 10.1128/AEM.02395-07.

Wildschut, J. *et al.* (2013) 'Ethanol-based organosolv fractionation of wheat straw for the production of lignin and enzymatically digestible cellulose.', *Bioresource technology*, 135, pp. 58–66. doi: 10.1016/j.biortech.2012.10.050.

Wiles, C., Hammond, M. J. and Watts, P. (2009) 'The development and evaluation of a continuous flow process for the lipase-mediated oxidation of alkenes', *Beilstein Journal of Organic Chemistry*, 5(1), p. 27. doi: 10.3762/bjoc.5.27.

Wuytack, E. Y., Diels, A. M. J. and Michiels, C. W. (2002) 'Bacterial inactivation by high-pressure homogenisation and high hydrostatic pressure', *International Journal of Food Microbiology*, 77(3), pp. 205–212. doi: 10.1016/S0168-1605(02)00054-5.

Yun, H. *et al.* (2005) 'Use of enrichment culture for directed evolution of the Vibrio fluvialis JS17 omega-transaminase, which is resistant to product inhibition by aliphatic ketones.', *Applied and environmental microbiology*, 71(8), pp. 4220–4. doi: 10.1128/AEM.71.8.4220-4224.2005.

Zaks, A. (2001) 'Industrial biocatalysis', *Current Opinion in Chemical Biology*, 5(2), pp. 130–136. doi: 10.1016/S1367-5931(00)00181-2.

Zhang, Y. and Chen, H. (2012) 'Multiscale modeling of biomass pretreatment for optimization of steam explosion conditions', *Chemical Engineering Science*, 75, pp. 177–182. doi: 10.1016/j.ces.2012.02.052.

Zheng, Y. *et al.* (2012) 'Integrating sugar beet pulp storage, hydrolysis and fermentation for fuel ethanol production', *Applied Energy*, 93, pp. 168–175. doi: 10.1016/j.apenergy.2011.12.084.

Zheng, Y. *et al.* (2013) 'Dilute acid pretreatment and fermentation of sugar beet pulp to ethanol', *Applied Energy*, 105, pp. 1–7. doi: 10.1016/j.apenergy.2012.11.070.

Zheng, Y. *et al.* (2014) 'Pretreatment of lignocellulosic biomass for enhanced biogas production', *Progress in Energy and Combustion Science*, 42, pp. 35–53. doi: 10.1016/j.pecs.2014.01.001.

Zhou, H. Y. *et al.* (2019) 'Enhanced L-methionine production by genetically engineered Escherichia coli through fermentation optimization', *3 Biotech*, 9(3), pp. 1–11. doi: 10.1007/s13205-019-1609-8.

Ziemiński, K. *et al.* (2014) 'Effects of hydrothermal pretreatment of sugar beet pulp for methane production', *Bioresource Technology*, 166, pp. 187–193. doi:

10.1016/j.biortech.2014.05.021.

Ziemiński, K., Romanowska, I. and Kowalska, M. (2012) 'Enzymatic pretreatment of lignocellulosic wastes to improve biogas production', *Waste Management*, 32(6), pp. 1131–1137. doi: 10.1016/j.wasman.2012.01.016.

Zykwinska, A. W., Ralet, M. J. and Garnier, C. D. (2005) 'Evidence for In Vitro Binding of Pectin Side Chains to Cellulose 1', 139(September), pp. 397–407. doi: 10.1104/pp.105.065912.1.

10

Appendix

10.1 Pump calibration

10.1.1 SBP pretreatment pump calibration

RTD study and SBP pretreatment were carried out using a Masterflex LS25 tubing in a peristaltic pump (Cole-Parmer, Vernon Hills, USA). Below are the calibration curves correlating the pump rotational speed and the flowrate for various SBP solid loadings.

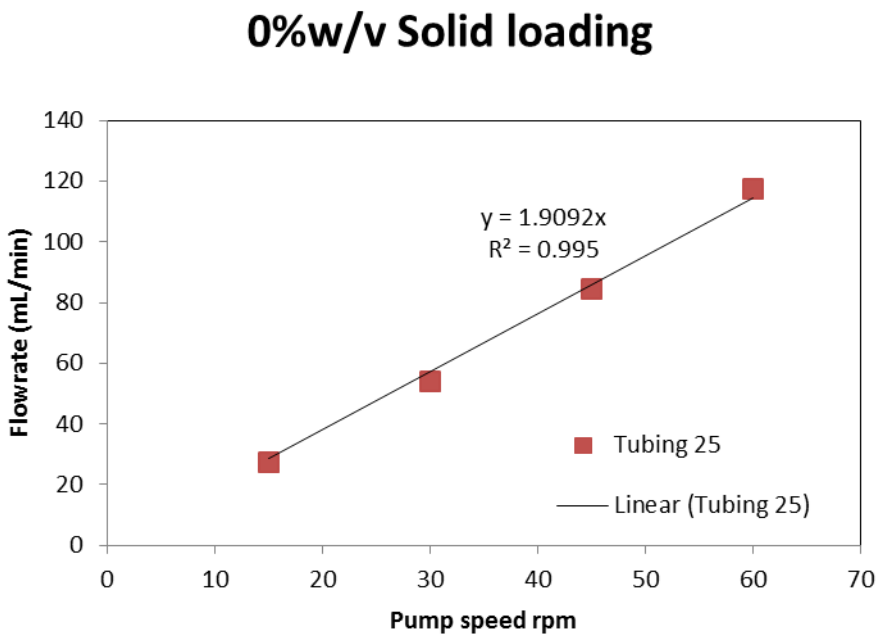

Figure A1. 1. Pump calibration curve with water

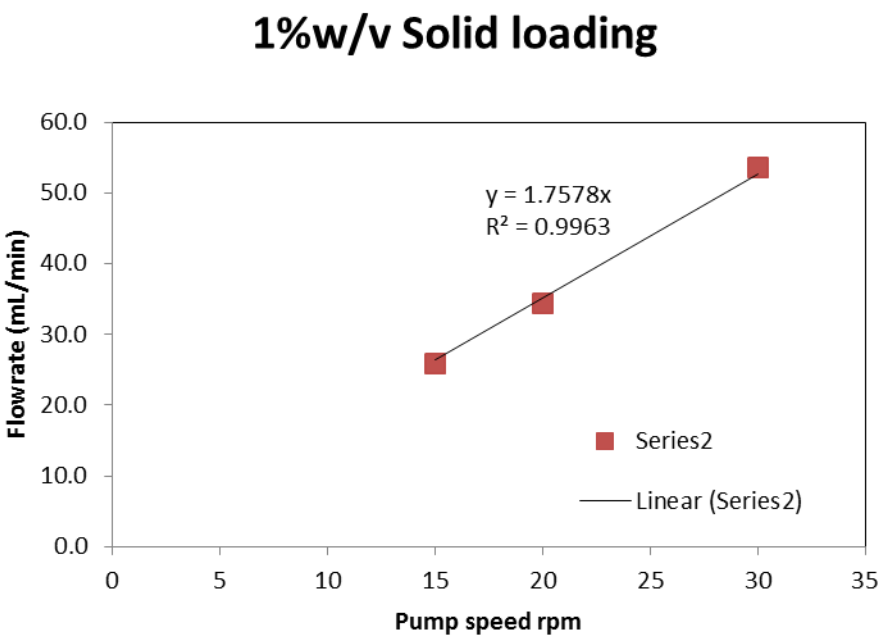

Figure A1. 2. Pump calibration curve with 1%w/v SBP slurry

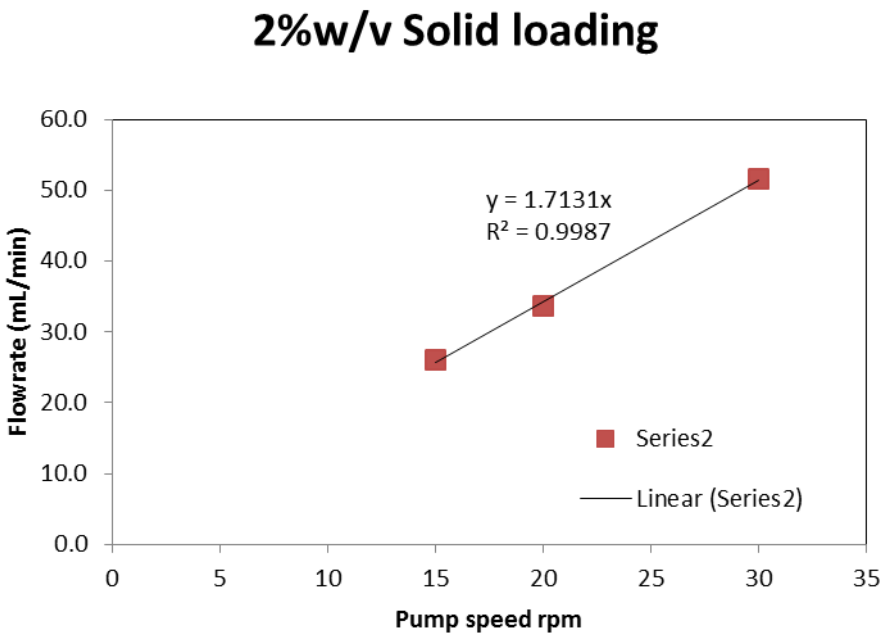

Figure A1. 3. Pump calibration curve with 2%w/v SBP slurry

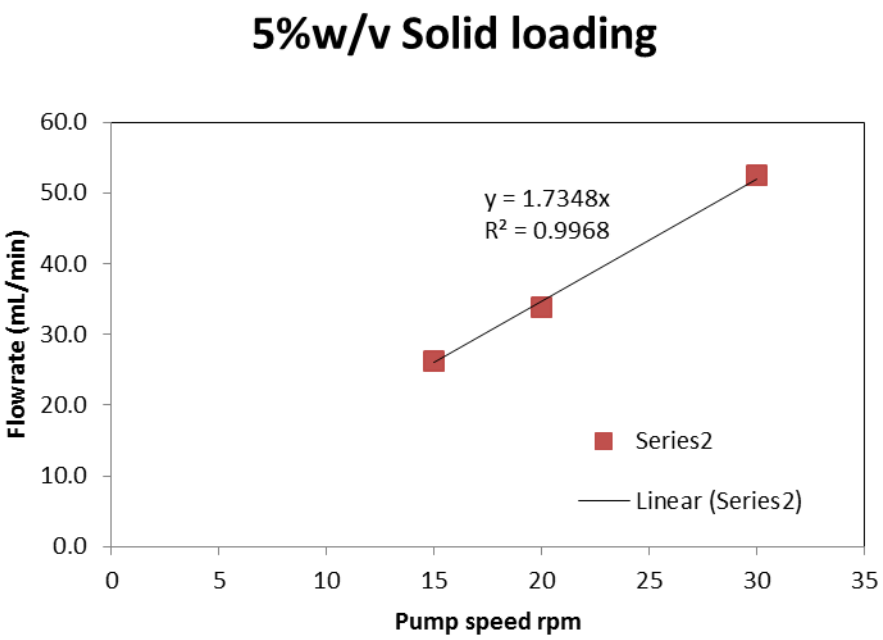

Figure A1. 4. Pump calibration curve with 5%w/v SBP slurry

10.1.2 Continuous flow biocatalysis pump calibration

The substrate stream for biocatalytic reactions in flow mode (Chapter 6) were pumped using Masterflex LS 16 tubing (Cole-Parmer, Vernon Hills, USA). The relationship between pump rotational speed and flowrate is shown in Figure A1.5. It is important to note that the calibration experiment was carried out with deionised water rather than real substrate stream. The calculations to obtain the Enzyme feed flowrate (syringe pump on side-entry port) is shown in Table A1.1.

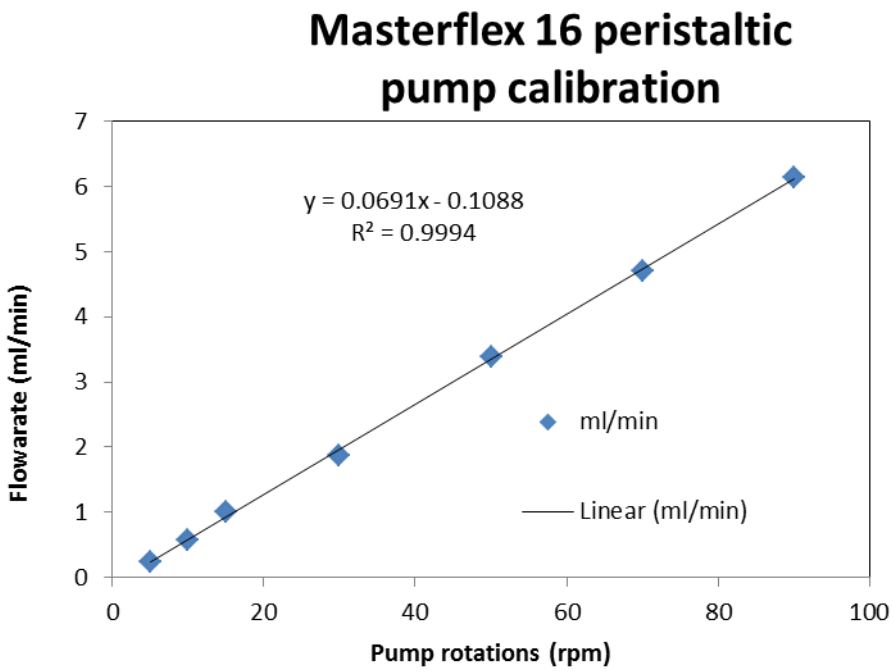

Figure A1. 5. Pump calibration curve with water, using Masteflex LS16 tubing

Table A1. 1. Values and calculations used for pump speed determination

Measure	Value	Unit
Volume of reactor	130	mL
Desired residence time	120	min
Desired total flowrate	1.08	$mL.min^{-1}$
Substrate flowrate ratio	0.7	Substrate:Total
Reagent flowrate	0.76	$mL.min^{-1}$
Reagent flowrate	45.50	$mL.hrn^{-1}$
Enzyme flowrate	0.33	$mL.min^{-1}$
Enzyme flowrate	19.50	$mL.hr^{-1}$
rpm of pump (y = a*x + b)	12.55	Rpm

12.55 rpm was rounded up to 13 rpm which was the speed used in the ACR

10.2 Bradford reagent protein assay

Total Protein content estimation was carried out with Bradford reagent assay and BSA was used as a standard protein for quantification. The calibration between protein concentration and optical density is shown in Figure A2.1.

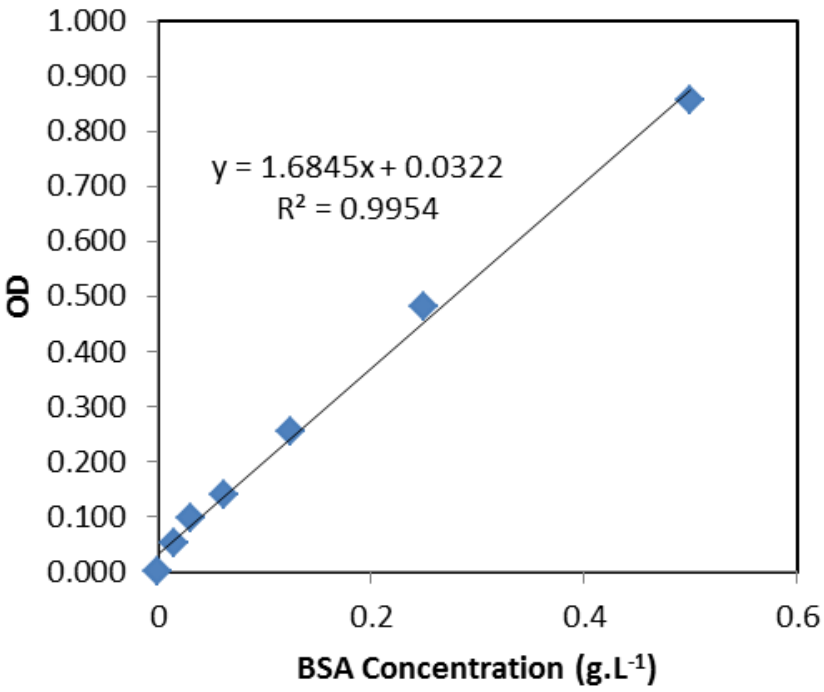

Figure A2.1. Bradford total protein calibration curve. BSA dilutions were prepared as discussed in Section 2.4.1.7.

10.3 HPAEC-PAD standards and peaks

10.3.1 Chromatograms

HPAEC-PAD was the main analytical tool to determine substrate and product concentration. The methods described in Section 2.5 were used to quantify SBP pretreatment yields (Chapter 4) and TAm and TK bioconversion yields (Chapter 5 and chapter 6). Chromatograms for the various types of injections used in this study are shown below. Quantification of acidic sugars (D-galacturonic acid) and neutral sugars for SBP pretreatment experiments are shown in Figure A3.1 and Figure A3.2. D-glucose, D-galactose, D-galacturonic acid and HPA were quantified by estimating peak height and correlating this to concentration. On the other hand, L-rhamnose, L-arabinose, L-serine and L-gluco-heptulose were estimated by area.

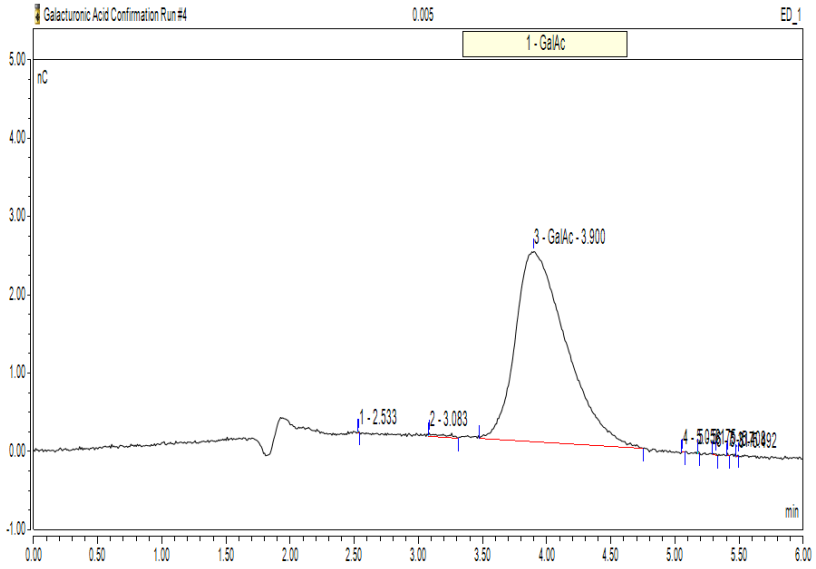

Figure A3. 1.D-galacturonic acid chromatogram

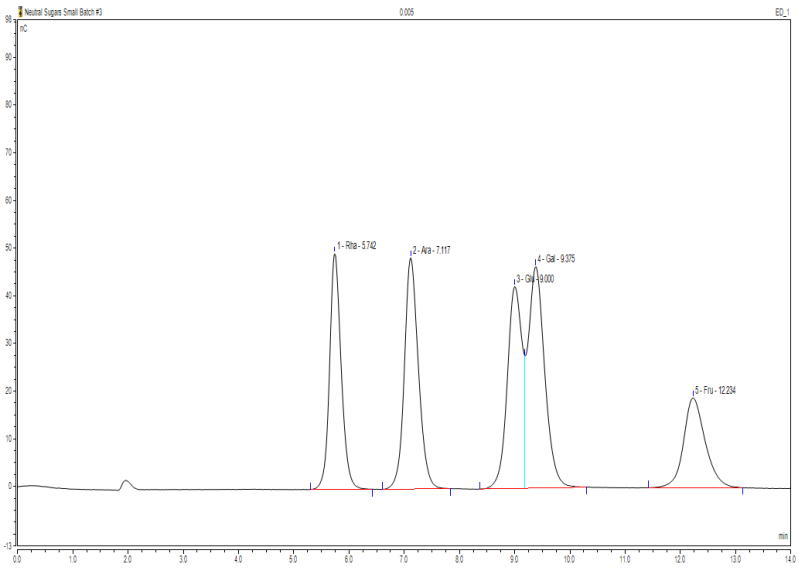

Figure A3. 2 L-rhamnose, L-arabinose, D-glucose, D-galactose and D-fructose chromatogram

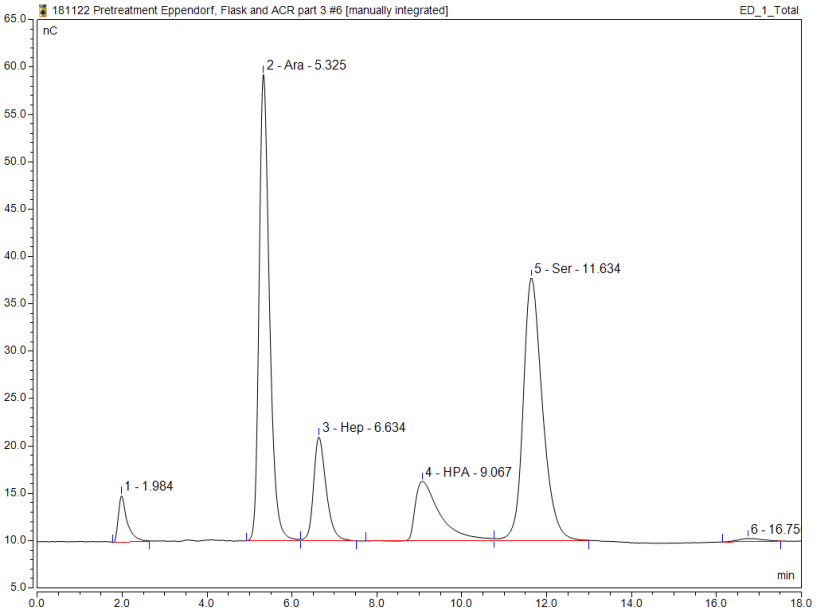

Figure A3. 3 L-arabinose, L-gluco-heptulose, HPA and L-serine chromatogram

10.3.2 Calibration curve for sugar analysis in SBP pretreatment

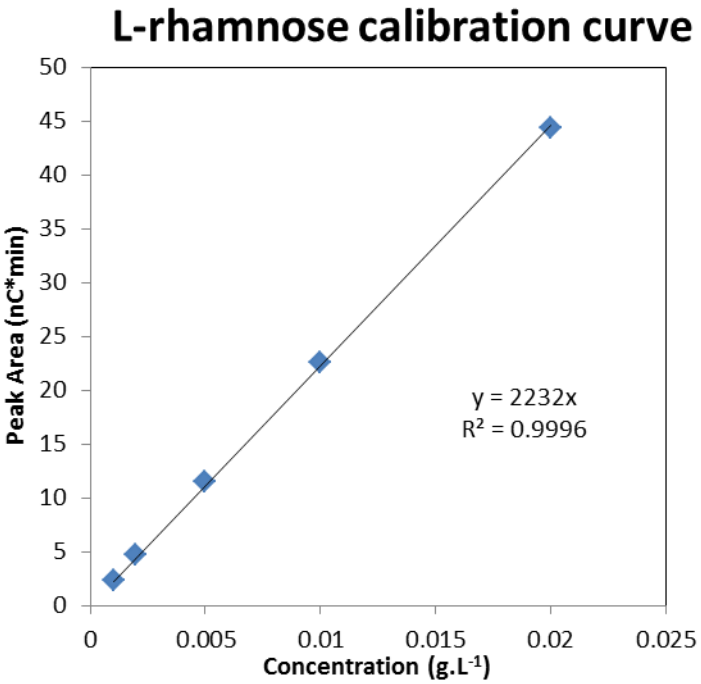

Figure A3. 4. L-rhamnose standard calibration curve

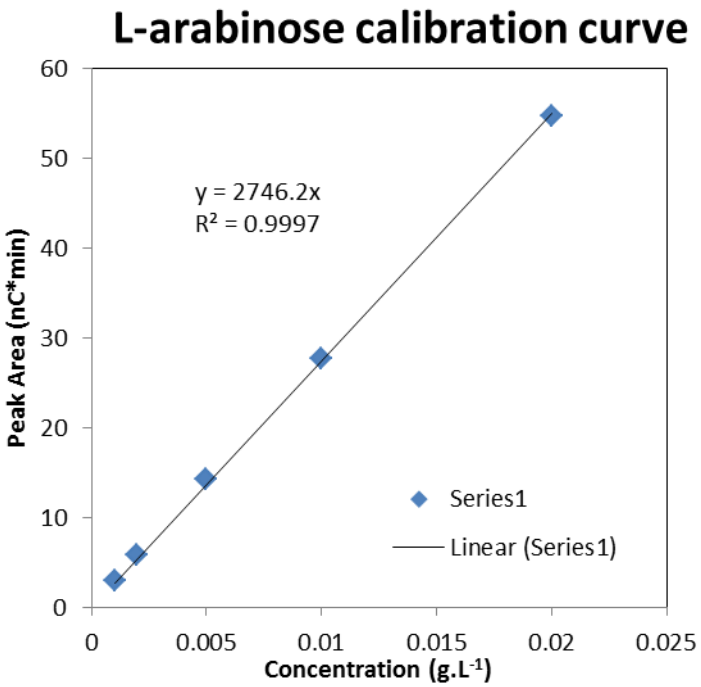

Figure A3. 5. L-arabinose standard calibration curve

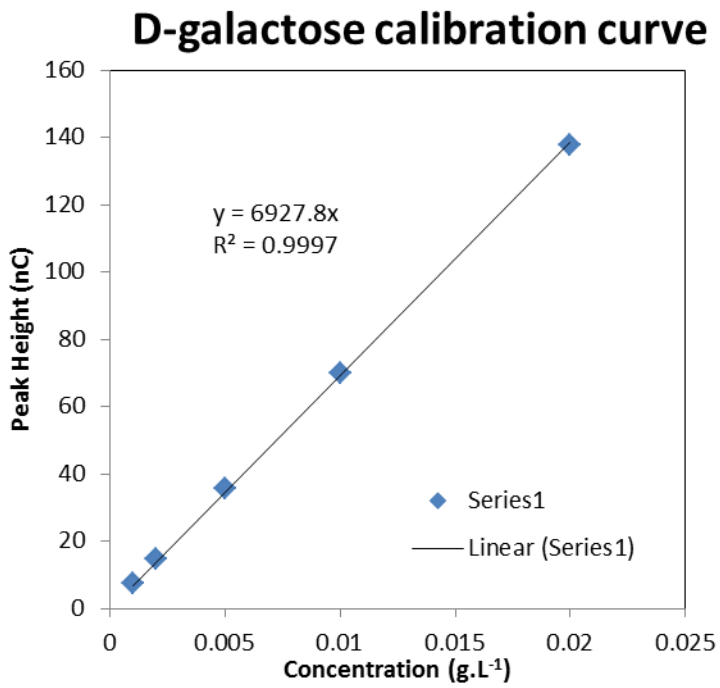

Figure A3. 6.D-galactose standard calibration curve

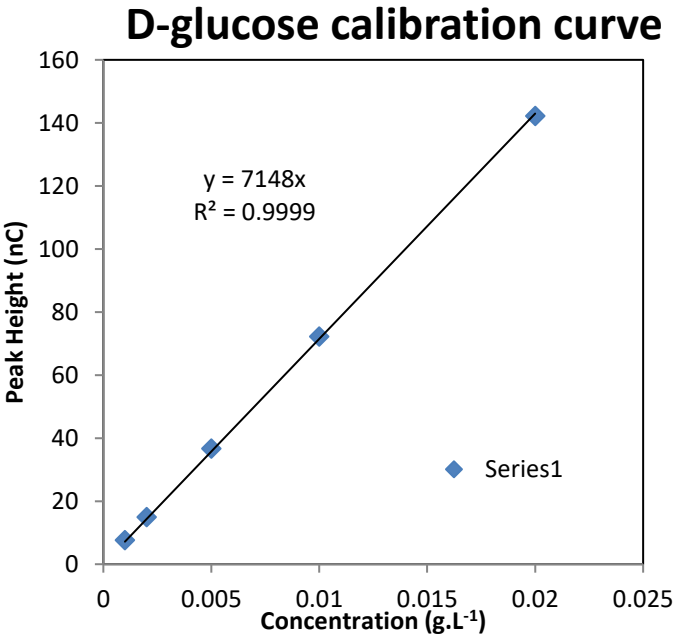

Figure A3. 7. D-glucose standard calibration curve

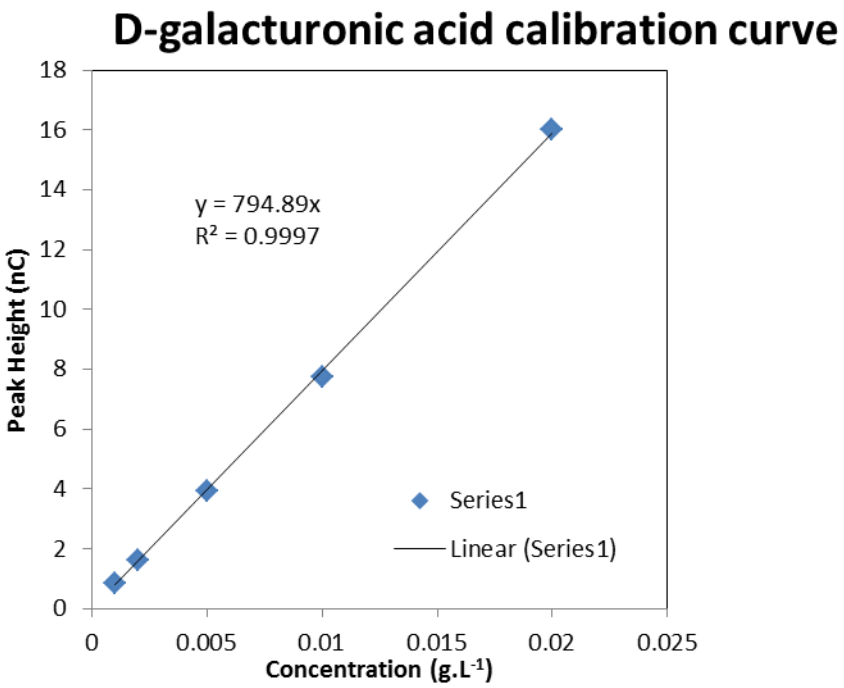

Figure A3. 8. D-galacturonic acid standard calibration curve

10.3.3 Calibration curves for substrate analysis in bioconversion reactions

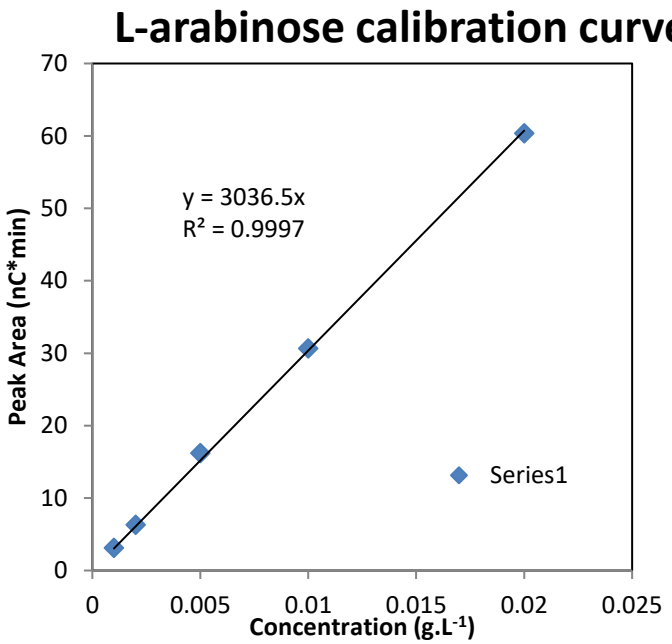

Figure A3. 9. L-arabinose standard calibration curve.

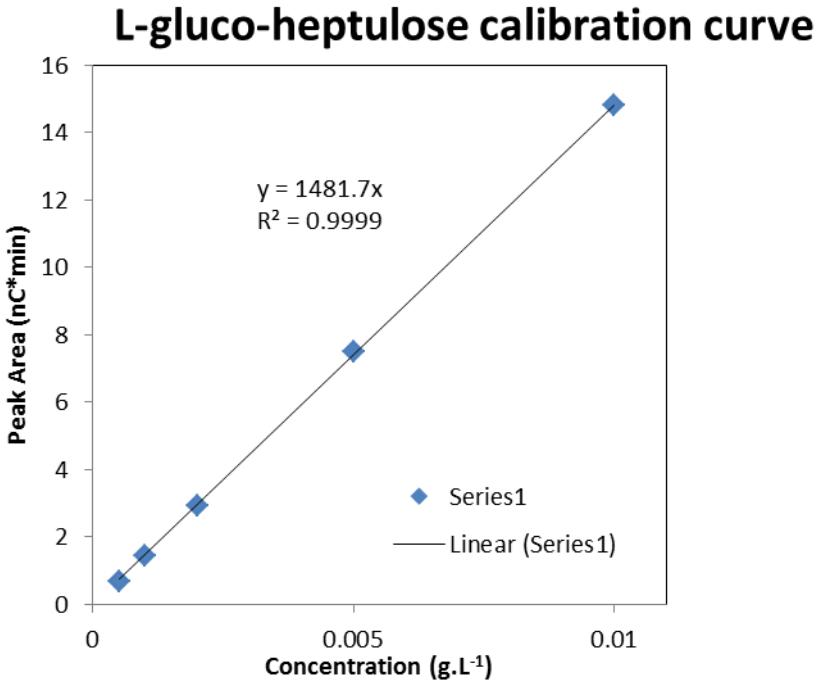

Figure A3. 10. L-gluco-heptulose standard calibration curve.

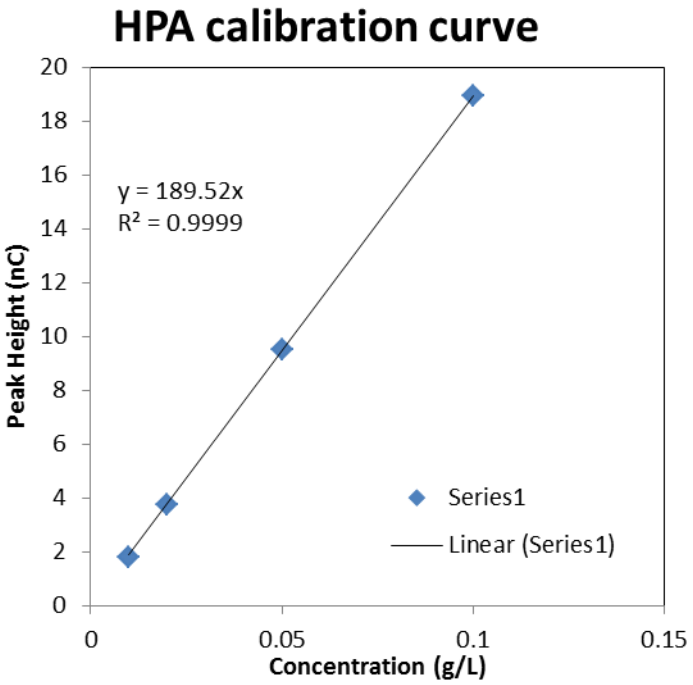

Figure A3. 11. HPA standard calibration curve.

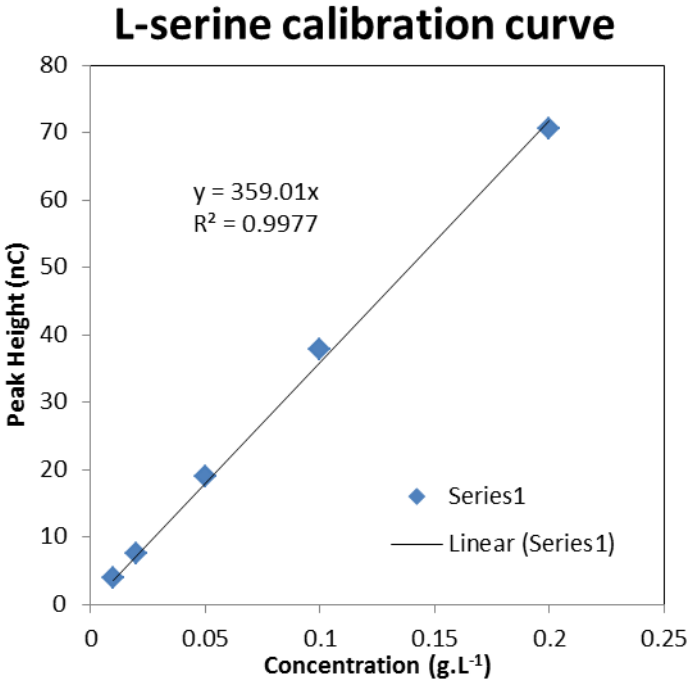

Figure A3. 2. L-serine standard calibration curve.